

Machine learning in Maritime Technology: Energy storage size reduction using load forecasting for pipelaying vessels

A. M. Menon

Delft University of Technology



Machine learning in Maritime Technology: Energy storage size reduction using load forecasting for pipelaying vessels

by

A. M. Menon

to obtain the degree of Master of Science
at the Delft University of Technology,
to be defended publicly on Monday June 17, 2019 at 09:30 AM.

SDPO.19.013.m

Student number: 4736370
Project duration: September 3, 2018 – June 17, 2019
Thesis committee: ir. K. Visser TU Delft, Chairman
Dr. A. Vrijdag TU Delft, Supervisor
Dr. ing. M. Godjevac Allseas
ir. M. Dijk Allseas
Dr. H. Polinder TU Delft, External committee member

This thesis is confidential and cannot be made public until June 17, 2024.

An electronic version of this thesis is available at <http://repository.tudelft.nl/>.

Preface

This thesis is a product of the work done over the last 10 months in collaboration with the Technical University of Delft and Allseas Engineering B.V. With the transition of the maritime industry to more green alternatives, I am glad to have been at the forefront of such innovation. The ideas developed in this thesis is one that can be applied to the world of dynamic positioning vessels. However, the ideas developed could not have been possible without a resilient team of people that have supported me throughout this journey. I would like to extend my appreciation and gratitude towards the following people:

From TU Delft:

- ir. Klaas Visser, as the chairman of my thesis committee, our early discussions about the project has been instrumental in taking the project in the right direction. He has offered valuable advice and bolstered the relationship between TU Delft and Allseas.
- Dr. ir. Arthur Vrijdag, who has supervised me through this thesis has been one of my main support structures who has been willing to take the time to offer very productive meetings with lots of useful, detail oriented feedback. Furthermore, he has supported me through the hard & stressful times and aimed to keep my morale high.

From Allseas:

- ir. Marijn Dijk, who has supervised me as the head of the naval department has always been welcoming to any questions, queries and providing the encouragement & support that I required.
- Dr. ing. Milinko Godjevac, who has supervised me at Allseas has always initiated new ideas and was the one who proposed the potential for load forecasting to be used for battery size reduction. This opened up a whole new world of machine learning to me. His knowledge and attention to detail have greatly guided me through the project.
- Dr. Nicolas Chasiotis, as an E&I inspector at Allseas has offered very practical and useful insight into the vessel operation and I would also like to thank him for his ideas on battery architectures and power management system integration.
- Panagiotis Koukouras and Christos Patsarouchas, from the technical department who have helped me understand various electrical systems onboard the *Solitaire* as well as answering my general queries.
- Serge Solntsev, as the software engineer at Allseas has helped me through tireless queries I had about the vessels datalogging system and always offered a helping hand.

Furthermore, I would like to thank:

- All my colleagues at the naval department and graduate students who have encouraged me and been willing to join me on my 3pm coffee breaks.
- Various colleagues from the Technical, Survey, Pipeline, Installation, Software, R&D departments and the second engineer of *Solitaire* Mr. Gerard Bolt for answering all my questions.
- My classmates at TU Delft who have shared their experiences working on their theses as well as their time, support and interest in energy storage systems.

Last but not least, I would like to thank my family, friends and housemates who have followed me through this journey, always cheering me on.

A. M. Menon
Delft, June 2019

Abstract

Over the last few years, a green revolution is slowly starting to take place within the maritime industry. The goal of this revolution is to improve operational efficiency and establish sustainable solutions within ships to allow a competitive edge in the market. The focus of this thesis is to develop ways in which a battery energy storage system can be integrated into the vessel. This entails the energy storage system architecture and power management system integration such that it may co-exist with the existing systems on the vessel, i.e., a retrofit option. The goal of the thesis is to use load forecasting as a tool to attempt to reduce the energy storage system size.

During dynamic positioning operations, vessels typically run with an extra generator (spinning reserve) for redundancy purposes such that no single fault will cause the vessel to lose its position or heading. As a result, all other engines on the grid share the load equally to ensure that if a failure were to occur, the remaining healthy generators would be sufficient to satisfy the total power demand. As DP vessels operate on a split-bus mode, the redundancy requirement must be satisfied across both switchboards on the vessel.

Past research has shown that significant fuel and maintenance savings can be made by eliminating the spinning reserve with a battery energy storage system. However, as Lithium-ion batteries are relatively expensive, efforts have been made in the past to attempt to incorporate a single battery system than can be connected to either switchboard in the event of a failure, however the analysis was conducted only for deep-water pipelaying operations. As the pipeline is produced in 24.4 metre sections at a time, once the production is complete, the vessel must move forward by the same distance and this event is called a 'pipe-pull'. During deep-water operations, as the pipeline is flexible, it is possible for the vessel to move forward slowly while production can continue. For shallow water operations, to prevent pipe buckling, the sequence of events must be simultaneous which results in power surges in the order of 2-4 MW. The operation continues throughout the day on average 100-150 times. Power surges were found to be a limiting factor in the battery system design.

In this research, a solution was developed as a split battery design which is arranged such that the power surges can be handled by two independent units connected to one switchboard while a tertiary unit from the secondary switchboard can be independently connected to the one switchboard wherein a failure has occurred. This allows all the battery units to be maintained at a low state of charge, which maximises the battery life.

To complement the design, two power management system integration methods were pursued. Firstly, a rule-based monitoring system was developed which allowed the power management system to make generator start-stop decisions based on a back-looking principle of measuring power demand and power surge characteristics experienced by the battery. The method resulted in daily fuel savings of 3.14 tonnes and a running hour reduction of 52.5 hours daily, which means that at minimum 2 engines can be turned off between both switchboards. Battery C-rates and depth of discharge during power surges were kept within 1.5C and 2% respectively which help prolong its calendar life. The average engine loads improved on average 10-20% in contrast to the current situation on the vessel and milder weather scenarios showing nearly a 30-40% improvement.

The second method adopted was to use a neural network based load forecasting tool in order to predict the expected loads on the vessel for the day using weather and route parameters. By doing so, generators can be scheduled to be turned on or off in advance which means that the battery can be re-sized without the power surges acting as a limiting constraint. The results suggest that in contrast to the rule-based system, the forecast model overestimates or underestimates the load which causes the fuel savings and running hour reduction to be less than the former control strategy. The neural network training was conducted on a data sample of approximately 2 million data samples which was found to be insufficient to capture all the dynamics. It is recommended to collate several years of data from the vessels datalogging systems to train the neural network model further. Due to the parallel nature of the neural net design, powerful supercomputers may be used to accelerate training on large datasets and converge to a deployable model. The potential for battery size reduction in such a scenario is 38% of the existing design size. Across both methodologies, the emission reduction opportunities are over 10 tonnes of CO_2 per day which offers a unique selling point to entities awarding pipelaying contracts.

Abbreviations

ANN	Artificial Neural Network
AVR	Automatic Voltage Regulator
AC	Alternating Current
ARMA	Autoregressive Moving Average
BESS	Battery Energy Storage System
C	C-rate
CAPEX	Capital Expenditure
DoD	Depth of Discharge
DP	Dynamic Positioning
DC	Direct Current
EOL	End of Life
ER	Engine Room
EM	Electro Motors
ESS	Energy storage system
FPSO	Floating, Production, Storage & Offloading vessel
HV	High Voltage
HSL	Higher Start Limit
HFO	Heavy Fuel Oil
IMO	International Maritime Organisation
KP	Kilometre Post
KPI	Key Performance Indicators
LV	Low Voltage
Li-ion	Lithium-Ion
LSL	Lower Start Limit
MCR	Maximum Continuous Rating
M/V	Motor Vehicle
MS	Main Switchboard
MDG	Marine Diesel Generator
MDO	Marine Diesel Oil
MGO	Marine Gas Oil
MLRA	Multiple Linear Regression Analysis
NMC	Nickel Manganese Cobalt
NN	Neural network
TDNN	Time Delay Neural Network
RNN	Recurrent Neural Network
OCV	Offshore Construction Vessel
PMS	Power Management System
sfc	specific fuel consumption
SOC	State of Charge
UPS	Uninterruptible Power Supply

List of Figures

1.1	<i>M/V Solitaire</i>	2
1.2	ESS integration option 1 [20]	2
1.3	ESS integration option 2 [20]	3
1.4	ESS integration option 3 [20]	3
1.5	Load levelling using peak shaving [43]	4
1.6	Specific fuel consumption (s.f.c): Pioneering Spirit's 11.2 MW engines[42]	5
1.7	PMS response using linear regression [42]	6
1.8	ESS applicability [16]	7
1.9	Dual and single battery arrangements	8
2.1	Chapter overview	9
2.2	DP system inputs	11
2.3	Thruster positions	11
2.4	Power distribution layout of a single switchboard	13
2.5	Integrated Automation System (IAS)	15
2.6	S-lay method	15
2.7	Firing line of the Solitaire	16
3.1	NordStream II pipeline route	19
3.2	Chapter 3 overview	20
3.3	Simplified Single line diagram of the <i>M/V Solitaire</i>	21
3.4	Vessel loads during pipelaying in shallow water	21
3.5	Average and variant DP load	22
3.6	Pipe pulls	23
3.7	Ground-speed and ancillary load correlations	24
3.8	'Rogue' power peak	24
3.9	Experimental measurements & inferences	25
3.10	Generator measures	25
3.11	Propulsion unit	26
3.12	P,Q,S on the Solitaire (Recorded on 09/01/2019)	27
3.13	Generator currents on the Solitaire	27
3.14	Power flow: Propulsion unit	28
3.15	Ideal PMS response	28
3.16	Failure scenario analysis overview	29
3.17	Normal operations with BESS (0.5PF)	29
3.18	Failure condition with BESS (0.5PF)	30
3.19	Normal operation with BESS (0.8PF)	30
3.20	Single engine failure with BESS(0.8PF)	31
4.1	Battery design steps	33
4.2	Battery life vs temperature & SOC[49]	35
4.3	Cycle life vs. DoD[44]	35
4.4	Power surges	36
4.5	Split battery design	37
4.6	Split battery sizing (4X units)	37
4.7	Split battery system layout	39
4.8	Power surge mode	40
4.9	Spinning reserve mode	40

5.1	Vessel online capacity	42
5.2	Model structure	43
5.3	Types of battery models[32]	44
5.4	General equivalent circuit cell model of an electro-chemical cell [25]	45
5.5	Equivalent circuit model with a single RC branch [25]	46
5.6	KoKam 5C datasheet discharge curves	47
5.7	SOC-OCV (Open circuit voltage) curves	47
5.8	Battery resistance at different SoC & temperatures	48
5.9	Variation of battery resistance with Temperature & SoC	49
5.10	Datasheet battery model	50
5.11	Simulink®parametrised battery model response	51
5.12	Filter delay	52
5.13	Rule based load dependent start-stop sequence	53
5.14	Peak frequency scope	54
5.15	Peak magnitude monitor & PMS response	55
5.16	New PMS response during normal pipe-laying operations	57
5.17	Simulation Dashboard on Simulink®	58
5.18	New PMS response during WoW, Pipe retrieval and pipe-laying	59
5.19	Fuel oil consumption block	59
5.20	Fuel oil consumption block	60
5.21	Specific fuel consumption of the <i>Solitaire</i>	60
5.22	Battery cycles and DoD	62
5.23	Battery cycles vs. DoD	62
5.24	Engine loads with 4 running engines	64
5.25	Cylinder block contact surfaces	65
5.26	Wear on the cylinder head & crown	65
5.27	Piston crowns	65
5.28	Engine loads under the new PMS	66
5.29	Specific pollutant emission of the <i>Solitaire's</i> Diesel engines	67
5.30	Investment return avenues	68
5.31	Savings & CAPEX	69
6.1	Chapter overview	71
6.2	Predictive algorithm overview	72
6.3	Seasonal ARMA equation [42]	72
6.4	Neural network node structure [11]	74
6.5	A simple feed-forward neural network	75
6.6	Non-linear activation functions [37]	75
6.7	Machine learning workflow overview	76
6.8	Route-plan parameters	77
6.9	Neural network design for load forecasting	79
6.10	Comparison of response from different neuron settings in the hidden layer	80
6.11	Neural network performance plot	82
6.12	Forecasted load for 19-11-2018 (MS2)	83
6.13	Forecasted load for 22-11-2018 (MS1)	83
6.14	Generator scheduling during pipelaying operations	84
6.15	Generator scheduling during downtime	85
6.16	15% reduced velocity on MS1	85
6.17	Specific pollutant emission: RBS vs Genset scheduling	87
6.18	Engine loads using the forecast model	88
6.19	Engine loads under the rule based system	89
6.20	Re-sized split battery ESS without forecasts- schematic	90
6.21	Re-sized battery ESS with forecasts- schematic	91
A.1	<i>Solitaire</i> single line diagram	102
A.2	Instantaneous power	103

A.3	0.5 power factor- no failure condition	104
A.4	0.5 power factor failure condition	105
A.5	0.8 power factor no failure condition	106
A.6	0.8 power factor failure condition	107
B.1	Discrimination diagram representing the overload and short circuit level 1 & 2 protection limits	110
B.2	MDG trip at 55% load	111
B.3	MDG trip at 85% load	112
B.4	Overshoot during heading changes	113
B.5	Cell characteristics	114
B.6	Charge, discharge & temperature characteristics	115
B.7	Voltage drop chart	116
B.8	Stateflow®Generator online capacity	117
B.9	Peak frequency monitor (Stateflow®)	118
B.10	Peak profile/magnitude monitor	118
B.11	Peak profile/magnitude monitor (Stateflow®)	119
B.12	SOC based battery control units	120
B.13	Battery mode 1 flowchart (Stateflow®)	121
B.14	Battery mode 2 flowchart (Stateflow®)	122
B.15	05/10/18 MS1 response	123
B.16	09/10/18 MS1 response	123
B.17	10/10/18 MS1 response	123
B.18	10/10/18 MS2 response	124
B.19	18/11/18 MS1 response	124
B.20	21/11/18 MS2 response	124
B.21	26/09/18 MS1 response	125
C.1	Seasonality in data [13]	127
C.2	Neural network validation check	128
C.3	Activation function with '0' bias	128
C.4	Effects of different bias values	129
C.5	Momentum term in optimisation	129
C.6	Comparison of response from different neuron settings in the hidden layer	134
C.7	18/11/18 MS1 response	135
C.8	18/11/18 MS2 response	135
C.9	19/11/18 MS1 response	135
C.10	20/11/18 MS1 response	136
C.11	20/11/18 MS2 response	136
C.12	21/11/18 MS1 response	136
C.13	21/11/18 MS2 response	137
C.14	22/11/18 MS1 response	137
C.15	22/11/18 MS2 response	137
C.16	18/11/18 MS1 response	138
C.17	18/11/18 MS1 response	138
C.18	18/11/18 MS2 response	138
C.19	18/11/18 MS2 response	139

List of Tables

2.1	ESS applicability	13
3.1	Approximate kilometres per country	19
3.2	Country KP's versus global KP's line A	20
3.3	M/V Solitaire Tensioner power consumption	22
3.4	Analysis locations	25
3.5	M/V Solitaire Grid measures	26
4.1	Li-ion cell & module characteristics	38
4.2	Battery string & rack characteristics	38
4.3	Converter & Transformer information	38
4.4	Twin units engaged	39
4.5	Three units engaged	39
5.1	Current load dependent start limits for the M/V <i>Solitaire</i>	41
5.2	Battery model types & applicability	44
5.3	Proposed load dependent start limits for the M/V <i>Solitaire</i> (per switchboard)	53
5.4	Test day descriptions	61
5.5	Fuel consumption results	61
5.6	Battery measurement results	63
5.7	Running hours measurements	66
5.8	Emission reduction opportunities for the <i>Solitaire</i>	67
5.9	Investment scenarios	69
6.1	Long term forecast requirements	73
6.2	Weather parameters	77
6.3	Route plan parameters	77
6.4	Training parameters	78
6.5	Testing parameters	78
6.6	Data partitioning	81
6.7	Testing results	82
6.8	Generator scheduling: Fuel savings results	86
6.9	Voluntary velocity reduction: Fuel consumption & savings results	86
6.10	Battery measurement results: Rule based-system (RBS)	86
6.11	Battery measurement results: Forecast based generator scheduling	87
6.12	Battery measurement results: Forecast based velocity reduction (VR)	87
6.13	Emission reduction using forecasting vs RBS (Pipe-laying scenario)	88
6.14	Running hours measurements: Rule based system vs Generator scheduling	88
6.15	Running hours measurements: Rule based system vs Velocity reduction (VR)	89
6.16	Split battery battery specifications: RBS	90
6.17	Split battery battery specifications: Forecast model	91
C.1	Numerical example results [15]	132

Contents

Abbreviations	7
List of Figures	9
List of Tables	13
1 Introduction	1
1.1 Background	1
1.2 Review of Battery Energy Storage Architectures	2
1.3 Literature Review	4
1.4 Gap analysis	7
1.5 Problem statements.	7
1.5.1 Scope	8
1.6 Research Questions	8
2 Pipelaying Operations	9
2.1 Allseas Group S.A	9
2.2 Overview	9
2.3 Case vessel characteristics	10
2.3.1 DP system	10
2.3.2 Propulsion and transmission.	10
2.3.3 Power Production	12
2.3.4 Power distribution	13
2.3.5 Power Management System	14
2.4 Pipeline production process	15
2.4.1 Methods of Pipelaying	15
2.4.2 Production process	15
2.5 DP Operational activities	17
2.5.1 DP Operations inside the 500m zone of an Offshore structure	17
2.5.2 DP operations outside the 500m zone	17
2.6 Implications on ESS.	18
3 Data analysis	19
3.1 NordStream II.	19
3.1.1 Kilometre Posts (KP's)	20
3.2 Overview	20
3.3 Vessel load components.	20
3.3.1 Level 1:DP load	22
3.3.2 Level 2 & 3: Ancillary consumers.	22
3.4 Power peak analysis.	23
3.4.1 Ground-speed & Tensioner correlation	23
3.4.2 Anomalous power peaks	24
3.5 Electrical system health analysis	25
3.5.1 Generator measurement	25
3.5.2 Thruster unit measurement	26
3.5.3 Generator measurement results	26
3.5.4 Thruster units measurement results	28
3.6 Power factor correction & assumptions	28
3.7 Failure scenarios	29
3.7.1 0.55 PF.	29
3.7.2 0.80 PF.	30

3.8	Implications on ESS.	32
4	Conceptual baseline battery design	33
4.1	Overview	33
4.2	Design requirements	33
4.2.1	Energy	33
4.2.2	Power	34
4.2.3	Battery life	34
4.2.4	Power surges	36
4.3	Baseline split battery design	36
4.4	System architecture	38
4.5	Operational conditions	40
5	Power management system integration	41
5.1	Existing rule based system	41
5.2	Overview	42
5.3	Battery	44
5.3.1	Types of battery models	44
5.3.2	Empirical model	45
5.4	Power management system	52
5.4.1	Load filtering.	52
5.4.2	Rule based control system	53
5.4.3	ESS management algorithm A: Peak frequency.	53
5.4.4	ESS management algorithm B: Peak magnitude	54
5.4.5	ESS management algorithm C: SoC control	55
5.5	Simulations & results	57
5.5.1	PMS response	57
5.5.2	Fuel reduction	59
5.5.3	Battery measurements	62
5.5.4	Engine loads & running hours	64
5.5.5	Emission reduction	67
5.5.6	Investment & Returns	68
6	Load forecasting using machine learning	71
6.1	Overview	71
6.2	Forecasting methodology	71
6.3	Neural network theory	74
6.3.1	Biologically inspired mathematics	74
6.3.2	Neural network architectures	74
6.3.3	Neural network structure	74
6.4	Neural network development	76
6.4.1	Machine learning workflow overview	76
6.4.2	Parameter selection	76
6.4.3	Data collection.	78
6.4.4	Pre-processing data	78
6.4.5	Network design	78
6.4.6	Training & Validation.	79
6.4.7	Testing	81
6.5	PMS applications	83
6.5.1	PMS response	84
6.6	Simulations & Results	86
6.6.1	Fuel reduction	86
6.6.2	Battery measurements	86
6.6.3	Emission reduction	87
6.6.4	Running hours & Engine loads	88
6.7	Implications on ESS.	89

7	Conclusions and Recommendations	93
7.1	Conclusions	93
7.2	Recommendations	95
	Bibliography	97
A	Vessel data	101
A.1	3-phase systems	103
B	ESS & PMS integration	109
B.1	ESS	110
B.2	PMS.	117
B.2.1	Stateflow ®Rule based system model (per generator)	117
B.2.2	ESS management algorithms	118
B.2.3	New PMS response.	123
C	Artificial neural network	127
C.1	Commonly used terms	127
C.2	Literature on hybrid models	130
C.3	Optimisation algorithms	131
C.4	Effects of varying number of neurons	134
C.5	Load forecast scenarios	135
C.6	Power peak forecasting	138
C.7	Neural network Matlab ®code	139

Introduction

1.1. Background

Dynamic Positioning (DP) and Dynamic Tracking (DT) are methodologies to keep a vessel at a certain position (DP) or track (DT) using thrusters instead of mooring lines. By measuring its position (and heading) and comparing it to the required position, the DP system on board can determine its position error. The control system reacts on that by determining what thruster action is needed to bring the vessel as close as possible to the required position. DP systems can be found on many types of vessels: drilling vessels, installation vessels, heavy lift vessels, cable and pipe-laying vessels and FPSO's [34].

The first vessel to fulfil the accepted definition of DP was the "Eureka", of 1961, designed and engineered by Howard Shatto. This vessel was fitted with an analogue control system of very basic type, interfaced with a taut wire reference. Equipped with steerable thrusters fore and aft in addition to her main propulsion, this vessel was about 450 tons displacement and length 130 feet. By the late 1970s, DP had become a well-established technique. In 1980, the number of DP capable vessels totalled about 65, while by 1985 the number had increased to about 150. As of 2013, the number of DP vessels worldwide stands above 3000 vessels and it is continually growing [14].

The DP system itself is a computer-controlled system employed to maintain a vessels position and heading. The operation requires a host of sensors that communicate with the mathematical model of the vessel and actuators to ensure station keeping. Due to the criticality of the operations undertaken by these specialist vessels, there are several safety and redundancy requirements set out by classification societies. One of the main redundancy requirements of DP class II and class III vessels is that the failure of a single active component must not cause the loss of position or heading of the vessel. To ensure that the requirement is satisfied-vessels always operate with an additional generator (called a spinning reserve) connected to the independent switchboards operating at very low loads. This is not an ideal scenario as the spinning reserve consumes a significant amount of fuel while operating at an inefficient point resulting in additional maintenance requirements due to extended running hours.

The solution to this problem is to use an energy storage system (ESS), which may be a battery, super capacitor, flywheels etc. to bridge the time gap between the failure of the online generator and the start-up of a new generator set. This means that the system must be robust and capable of meeting an extremely demanding power requirement during that phase. Section 1.2.1 will detail the past research conducted into this, which forms the basis for the problem statements for this research.

The project is conducted in collaboration with Allseas Group S.A. a Swiss based offshore contractor specialising in pipe lay, heavy lift and subsea construction [47]. The company, founded in 1985 by owner and President Edward Heerema, employs 3,000 people and operates worldwide [10]. They currently own and operate two multi-purpose offshore construction vessels, a heavy lift vessel (also capable of pipe laying), a trenching support vessel and four other pipe-laying vessel. Most of their assets are dynamically positioned vessels of classes DP-II or DP-III. This forms a good case to research the implementation of an energy storage system on board these vessels. The case vessel that is investigated during this research project is the '*M/V Solitaire*' (Figure 1.1).



Figure 1.1: *M/V Solitaire*

1.2. Review of Battery Energy Storage Architectures

The appropriate starting point for this research topic is with a review of the pertinent developments in the design of hybrid power and propulsion systems. In 2017, Geertsma et al [20] gauged that hybrid architectures with advanced control strategies have the potential to reduce 15-35% fuel consumption, while improving noise, maintainability, manoeuvrability and comfort.

Three main architectures exist (with their variations) to implement hybrid systems on marine vessels. The first architecture is wherein the energy storage systems is connected to the main AC bus as shown in Figure 1.2 [20].

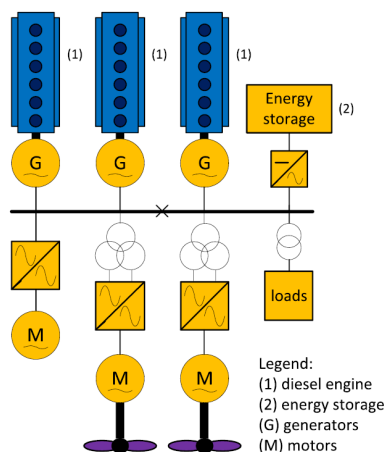


Figure 1.2: ESS integration option 1 [20]

Here, the power generation sources are:

- From diesel engines (1), gas turbines or steam turbines
- Electrochemical power supply from fuel cells; or

- Stored power supply from ESS (2) such as batteries, flywheels or super-capacitors

The paper proposes that the energy storage can be connected at various locations of the electrical system:

- At the main high voltage bus bar through an AC/DC converter;
- At the LV bus bar through an AC/DC converter;
- Directly or through a DC/DC converter to the DC link of the propulsion converter.

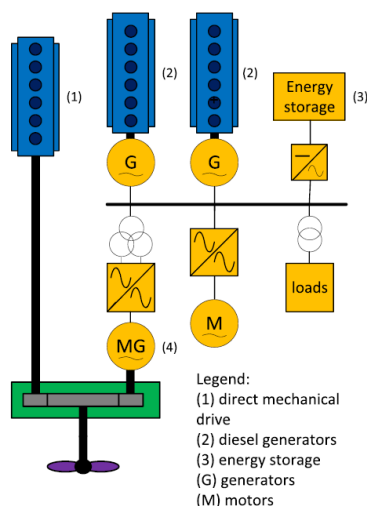


Figure 1.3: ESS integration option 2 [20]

The second arrangement is the combination of an energy storage solution with mechanically driven propeller shaft as shown in Figure 1.3

In the above case, the arrangement utilises the maximum efficiency of the direct drive mechanical propulsion system with the flexibility of the combination of combustion power from the prime mover(s) and stored power from the energy storage for electrical supply. This gives the vessel the option to operate under low loads, purely on electrical power. Lastly, the other type of system architecture would be the DC power supply, as shown in Figure 1.4. The benefits of this system is that the DC architecture allows one to run the diesel engine at variable speed, potentially leading to a reduction in fuel consumption, emissions, noise and engine mechanical and thermal loading. The network is also resilient to faults as the power electronic devices are capable in handling the faults instantaneously. The disadvantages are that for large vessels with a large number of AC loads, retrofitting may be cost prohibitive and a coordinated control strategy is required to manage stability issues.

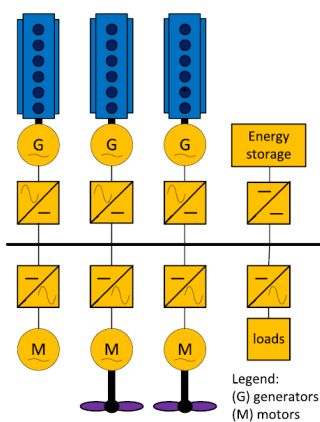


Figure 1.4: ESS integration option 3 [20]

1.3. Literature Review

Past research and literature has shown the advantages of hybridisation in the maritime sector. This review will focus more on the specific cases wherein it is possible to apply this technology by retrofitting. Furthermore, the latest developments in battery energy storage systems will be reviewed as the recent developments are more pertinent to this study.

2016/17

In 2016, Gerritsen [21] investigated the applicability of a battery for load levelling on a cutter suction dredger, the results of the research indicated that it was not a viable solution as the savings were minimal and the fluctuating power demand had the potential to reduce battery life. In 2017, Geertsma et al [20] mentions that when an engine operates close to the optimal working point from a fuel consumption perspective, load fluctuating propulsion load or other load disturbances can cause increased fuel consumption. Then, providing (a percentage of) the fluctuating load from a battery can reduce the fuel consumption increase and that dynamic engine loading can be reduced (shown in Figure 1.5). This is done by setting the engine to continuously work at, for example, 85% MCR, this would mean that the engine operates at constant load at all times. Everytime, that there exists a power demand greater than this output, that would be provided by the battery while the dip in power demand would be used to charge the battery.

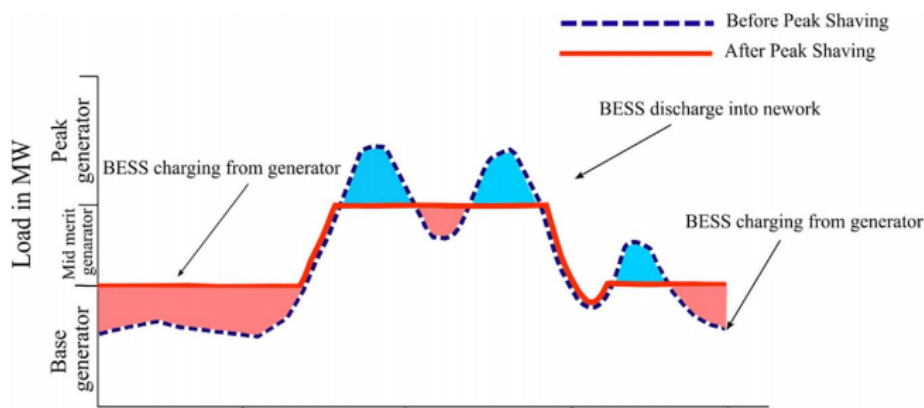


Figure 1.5: Load levelling using peak shaving [43]

However, in 2017, Godjevac et al [23] mentions that peak shaving is not particularly useful as the fuel savings made are lost due to transmission losses. The way forward would be to either reduce the size of the prime movers or turning off generators such that the remaining generators may share the total load and they operate at a more efficient operating point. Particularly in DP (Dynamic Positioning) operations, this is not the case due to the presence of a spinning reserve. The online generators in this case rarely, if ever, operate at optimal loads.

Godjevac et al also goes on to mention that the rationale behind peak shaving is to push the operating load of an engine somewhat higher to gain on the efficiency. The short bursts of power demand (i.e. the peaks in demand) actually load the engine higher for a short period of time which in turn reduces the fuel consumption at these high load as depicted by the Figure 1.6 [23, 42]. It can be seen from the s.f.c (specific fuel consumption) curve that the higher the engine load- the less fuel it would consume per kWh generated.

Godjevac Z. Lyu [31] both have demonstrated the gains that can be made in fuel savings by replacing the spinning reserve. Additionally this also reduces the corrective preventive maintenance to be conducted on the diesel engines in the long term.

2017/18

Previous research concerning this project was conducted by P. Spruijt in 2018 [42]. In this research, investigations were made using the case vessel '*M/V Pioneering Spirit*'. Spruijt explored the applicability of a single and double battery hybrid system to replace the spinning reserve. In the case of the dual battery system, it necessitated that double the required capacity were to be installed while being continuously to two switchboards separately so that they maintain their independence. This meant that the investments and space requirements double. This, in contrast with the fact that the battery would only be used in the case of a generator failure (which is a rare occurrence) - meant an unnecessary investment.

The alternative is the single battery system that can be connected to either switchboards in the case of

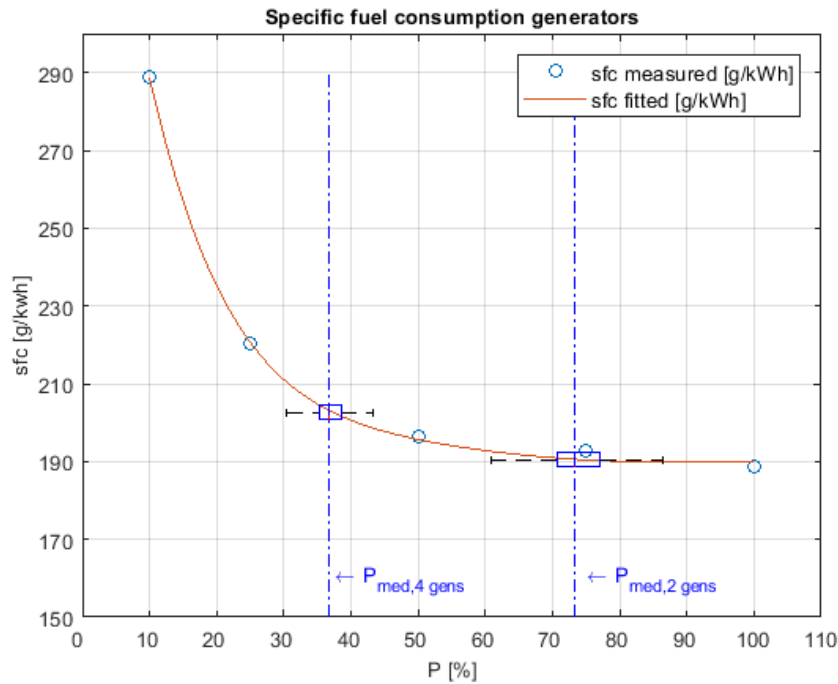


Figure 1.6: Specific fuel consumption (s.f.c): Pioneer Spirit's 11.2 MW engines[42]

a failed generator on either of the switchboards. The research focused on the concept design of the single battery hybrid system as it is practically feasible (although it does not have as much redundancy). While this design may be in breach of DP II and III regulations, the focus of the research was a smart starting decision algorithm for an additional generator. The research focuses on the initiation of a start and stop signal for an additional generator when there was a potential for the power demand to exceed the available capacity. The algorithm development was attempted using a mathematical statistical method (ARMA) - the trials proved unsuccessful as the predictions were not accurate enough to be used for generator start-stops.

The second methodology tested was the multiple linear regression analysis (MLRA) - which proved to be successful in correctly predicting the future load. In this method the regression coefficients were found by a least-square estimation based on the observations of the fuel consumption at different trips, where the predictor variables were measured. In this article, the strength of the model was analysed by examining the residuals between the model and the observations. It was stated that when the residuals are normally distributed with constant variance σ^2 the model could be considered as accurate. The input parameters were the total DP power and the significant wave height [42]. The results of this starting decision algorithm with a traditional system using a spinning reserve is shown in the Figure 1.7.

The new PMS (Power Management System) makes use of the linear regression method and as seen from Figure 1.7 is a significant improvement from the original case wherein a spinning reserve was running. Reliability studies were conducted as a follow up on both the proposed designs through the means of a fault tree analysis.

To compare the system options, the time to reach 95% reliability was compared. For the old 'no hybrid' system, this limit was reached after 200-400 days, for the single-battery hybrid system, this limit was reached after 1-3 days, for the double-battery hybrid system, this limit was reached after 1000-2700 days. In short, the reliability of the single-battery hybrid system is insufficient for this system to be used as hybrid system of a DP vessel. This poor reliability is caused by the fact that an unexpected power peak that crosses the online generator capacity causes the main event to occur directly. In other words, when the multiple linear regression model does not predict a power peak, the situation where the power generation system cannot fulfil the power demand directly occurs.

To reach the same reliability as the old 'no hybrid' system, the multiple linear regression model would have to be trained extensively and reach a confidence where an unexpected power peak would only occur once every 21 years of operation. Next to that, it is expected that the reliability could be increased by using

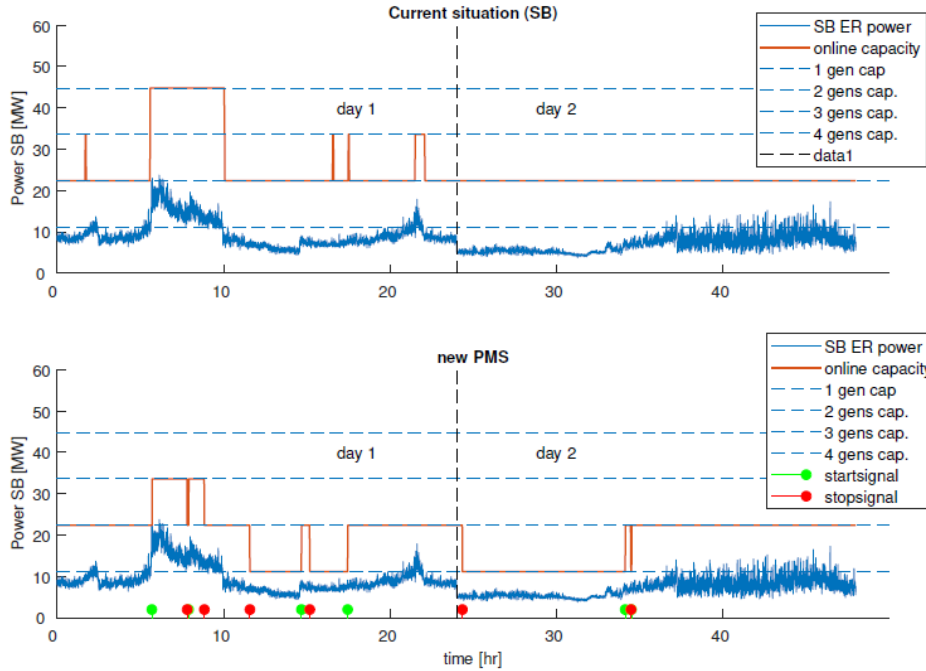


Figure 1.7: PMS response using linear regression [42]

a fast response electrical energy storage device in every engine room, where the single-battery system could still be used. These fast response electrical energy storage devices could then deal with the unexpected power peaks, where the main battery is installed for an unexpected generator failure.

2018/19

Some of the issues faced during a power outage (generator failure) is that there is a dip in the available capacity on the grid. This can cause a blackout if the demand surpasses the supply. Wetz [45], describes that in the naval vessels, with increasing electrification, the unique electrical load profiles exhibit characteristics that have not been traditionally encountered. Conventional power generation devices are unable to meet the demands of these load profiles and so must be bolstered with energy storage devices to alleviate transient loading. He proposes the use of 'active hybrid energy storage modules' that combine the use of both high-energy and high-power density units such as the use of ultra-capacitors and batteries in combination with a fuzzy logic controller to regulate them. While these are specific cases to the naval industry, in the dynamic positioning realm- the electrification is a common element shared between the two industries- the transient loads experienced by the DP vessels are far less superior to the one experienced by the naval vessels due to the use of high power weapons. Hence, the focus for DP vessels would be to use energy storage devices that are more inclined to high energy density. Further substantiation to this decision has been made with the findings of Southall et al [41] where it is mentioned that the use of ultra-capacitors would be for high power applications with duration's in the order of 3 seconds or lesser. It is mentioned that it could be used in combination with other energy storage technologies. However, in this specific case the main switchboard of the vessel is rated at 11kV, which means that for a super/ultra-capacitor to be connected to the network to handle the transient power fluctuation during a generator failure – the capacitor must be capable of maintaining this high potential difference. Farrier et al [19] notes that the key technical challenges of super-capacitor string integration is their voltage limit, currently 2kV. Capacitor banks can attain higher voltages according to Whitelegg [46], but only with significant increases in volume and weight. In the case of Farrier, an 11kV supercapacitor was used, however- it was to power a railgun. Figure 1.8 depicted by Christen [16] demonstrates the applicability of different ESS options on a Ragone plot which demonstrates which ESS is applicable for what use based on the energy density and power density.

This demonstrates that in the case for DP operations it is clear that the use of a hybrid energy storage system is useful (a combination of capacitors and batteries). However, due to the practical implementation of such an integrated system in this specific case, it would not be possible due to the sizing of the capacitors

(due to the high voltages) substantiated by Spruijt and Whitelegg. The applicability of such a system is better suited to naval vessels and smaller DP vessels that operate on lower voltage DC distribution buses [19].

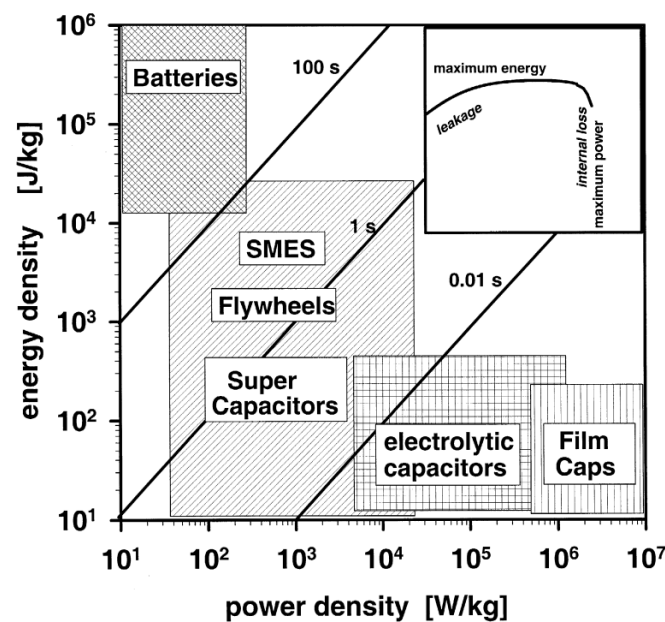


Figure 1.8: ESS applicability [16]

1.4. Gap analysis

From previous research, it is apparent that while new technologies are being explored and existing energy storage system technologies are maturing—the current state of the art in research is the combination of a variety of energy storage mechanisms to satisfy a complex load profile. No new advances have been made in regard to optimising the existing technologies to adapt it specifically for dynamic positioning operations. Much of the research has focused on the applicability of energy storage in peak shaving and hybrid operation. Factors such as reliability and redundancy have been taken into account but the solutions to these problems have been solved with doubling the required components rather than investigating alternative solutions.

Previous scenarios considered were for deepwater pipelaying by Spruijt [42], however, the shallow water conditions in pipelaying must be analysed as well before an ESS installation can be realised.

Forecasting was purposed for short forecast horizons in order to make generator start-stop decisions and proved to be unsuccessful in achieving 100% reliability. Developments of a rule-based system for generator-start-stops and non-statistical methods for long term forecasting of the load have not been explored in order to reduce the ESS sizing.

1.5. Problem statements

- The single battery system is not as reliable as the dual battery arrangement. However, the dual battery system is twice as expensive hence a different solution must be developed.
- The operational analysis conducted was exclusively on deep-water operations, however, the shallow water operations must be analysed as well before the ESS can be integrated into the vessel.
- Since no DP pipelaying vessel has been outfitted with a battery yet, it is uncertain how the operational profile of the vessel will interact with the battery. The question of power management system integration arises in this case.
- Statistical forecasting was previously used to initiate generator start-stops, however, the potential to use it for battery size reduction has not been investigated.

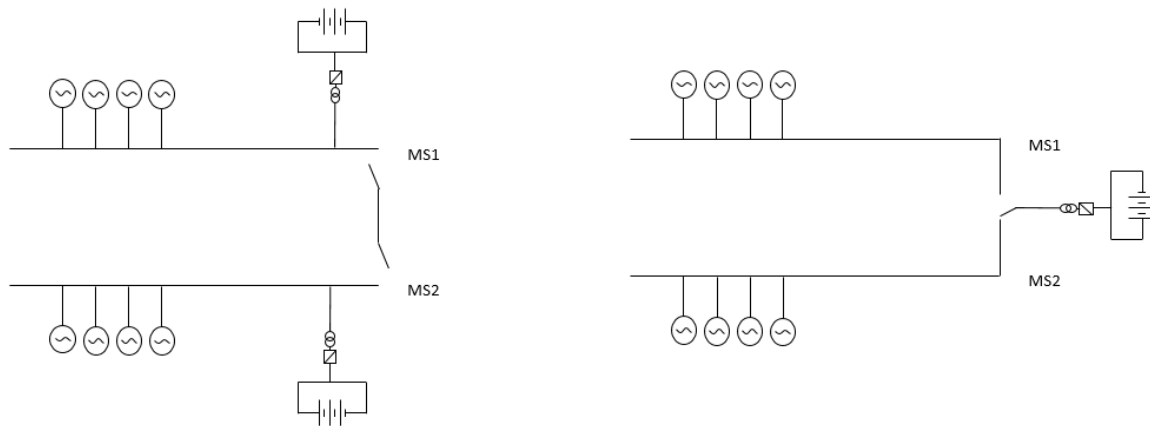


Figure 1.9: Dual and single battery arrangements

1.5.1. Scope

The scope of this research will be limited to analysing pipe laying ships during DP operations in shallow water. The operation in question that is of interest is the pipe pulls when the vessel moves from one set point to the next. The effects on the battery sizing will be analysed by using a baseline design of a split battery architecture. The key performance indicators of the vessel specific analysis will be the fuel consumption, running hour hours and emissions. Battery specific performance indicators will be the C-rates, cycle life and depth of discharge(DoD).

1.6. Research Questions

“To what extent can a smart load forecasting algorithm influence energy storage size for shallow water pipelaying DP operations?”

The main research question will be answered by answering the following sub questions:

- How does the vessels operational profile and electrical health affect the installation of an ESS?
- What kind of battery arrangement has the potential to reduce the capacity of Lithium-ion installed for split bus operations?
- How will the management of an ESS be integrated into the vessels power management system?
- How will the cycle life of the battery be influenced using load forecasting?
- How much further reduction of the ESS size is possible using load forecasting?

2

Pipelaying Operations

This chapter is structured into four distinct parts covering the case vessel characteristics, pipeline production processes, DP operational activities of pipelaying vessels and the implications of the latter three on the Energy storage system. Insight into these topics form the basis for the considerations that would be taken in the analysis and design stages of this research study.

2.1. Allseas Group S.A

The Swiss based Allseas Group S.A is a global leader in offshore pipeline installation and subsea construction. The company operates a fleet of heavy-lift, pipelay and support vessels that are all designed in house.

Founded in 1985, the company has gained worldwide experience in all types of offshore and subsea construction projects. Allseas currently possess a fleet of eight vessels in operation along with other ancillary equipment to support the main fleet. In light of the vessels life extension plan, the *M/V Solitaire* will dock in 2020 which offers a good opportunity for this research study to explore the applicability of an ESS. Hence, the case vessel for this research study is the *M/V Solitaire*. The vessel characteristics are outlined in Appendix A.

2.2. Overview

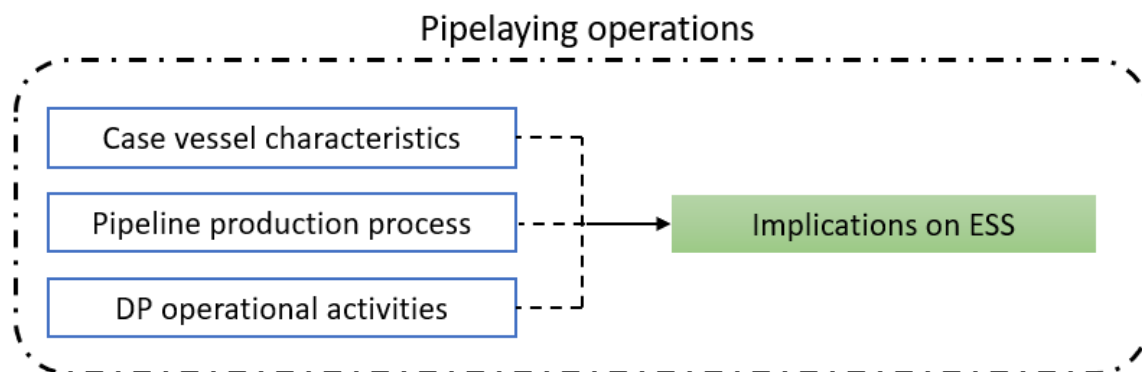


Figure 2.1: Chapter overview

The implications on the ESS are analysed on a high level by considering pertinent systems, power production & distribution characteristics of the case vessel *Solitaire* to get an understanding of sizing requirements and placement within the grid. Following this, the pipeline production process and DP operational activities are detailed to understand the different systems interacting within the vessel and how that could affect the ESS design requirements.

2.3. Case vessel characteristics

An analysis will be made of the following systems on board the *M/V Solitaire* that are pertinent to this study:

- i. DP system
- ii. Propulsion and transmission
- iii. Power generation and distribution
- iv. Power management system (PMS)

2.3.1. DP system

Solitaire has been designed to lay pipe up to a maximum 4 – 4.5 m significant wave height at a TZ of 7-9 secs (depending on the angle of attack) with an associated wind of 30-40knts. All equipment required for the pipelay process has been designed to be operational under these circumstances. Also the position keeping capability, including pipe tension, has been laid out for this situation fulfilling the requirements laid down for redundancy.

The vessel is equipped with a Kongsberg Maritime Dynamic Positioning (DP) control system K-POS32. To comply with IMO Equipment Class 3, the DP control system consists of the following components with its sensor and reference systems:

- K-Pos DP-22 (Main control system)
- K-Pos DP-12 (Backup control system)
- cJoy system (Independent Joystick system)

The K-Pos DP-22 system is an integrated and dual redundant position control system and the main control system for dynamic positioning operations. The K-Pos DP-12 system is an integrated backup position control system while the cJoy system is a stand-alone joystick system. It is physically disconnected from both of the above-mentioned control systems and has only joystick and automatic heading control functionality. It is directly wired to the thruster control cabinets. [9].

The following inputs are given to the DP system (Figure 2.2):

- a Taut wires
- b Hydro-acoustic transponders
- c Gyrocompasses for heading reference
- d Wind sensors
- e Vertical reference systems
- f Pipe tension input

2.3.2. Propulsion and transmission

The vessel consists of ten azimuthing thruster units (Figure 2.3), six of which are positioned to the vessels aft and four that are positioned toward the bow of the vessel. Pairs of thrusters are waterproof and fireproof separated. All thrusters have fixed pitch, variable speed propellers with a peak power rating of 5,500 kW. The six aft thrusters are assigned as steering devices. Each thruster drive system is supplied by two 10kV/792V transformers simultaneously. The two transformers share the same 10kV breaker.

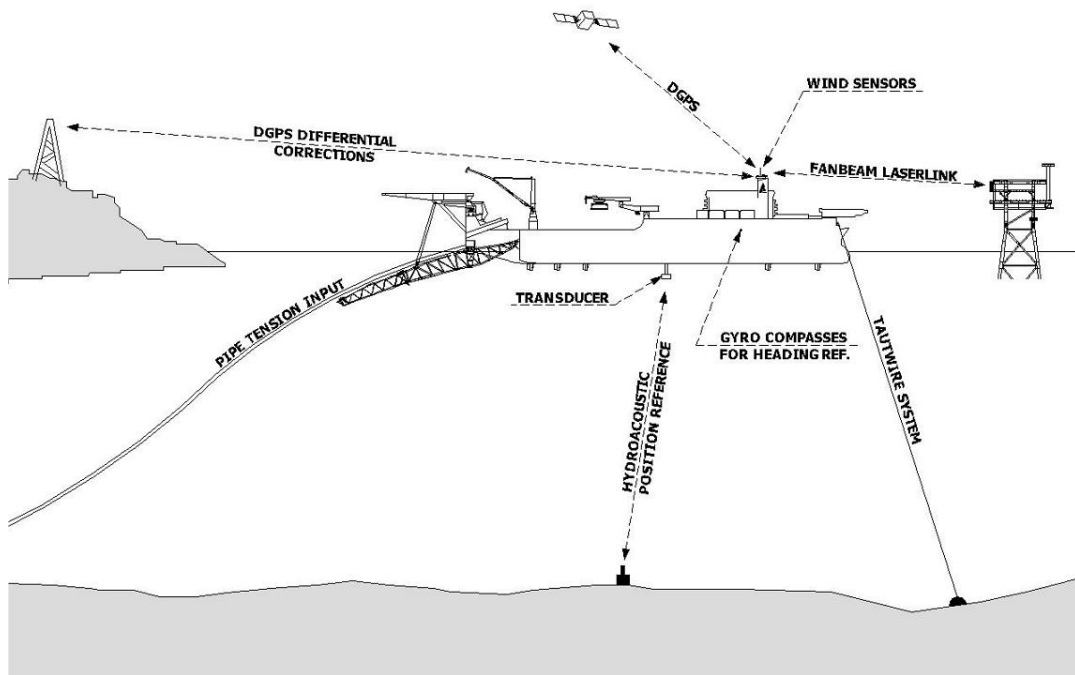


Figure 2.2: DP system inputs

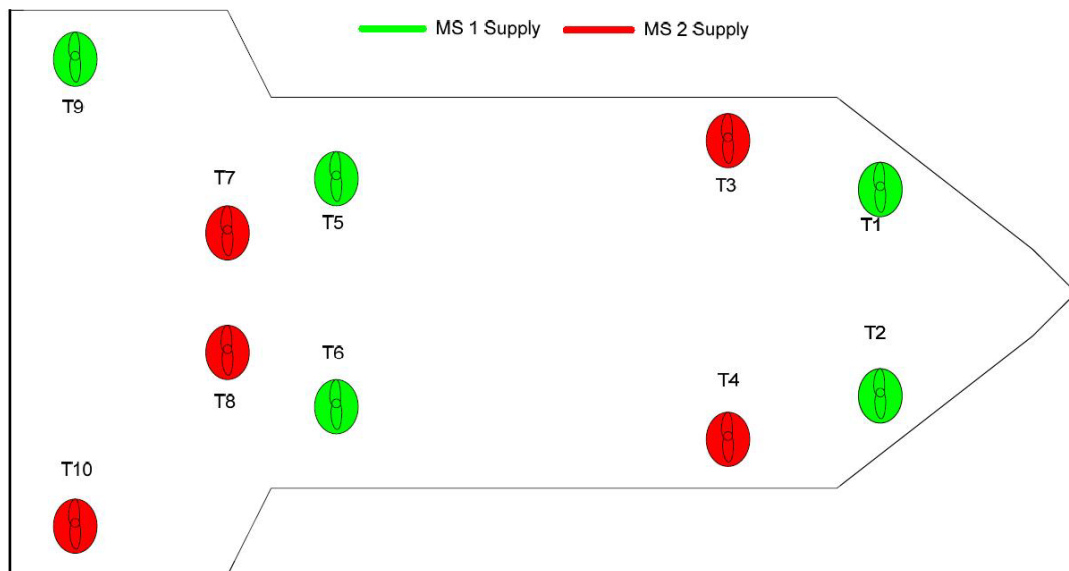


Figure 2.3: Thruster positions

2.3.3. Power Production

Main Diesel Engines

The vessel is equipped with eight diesel engines with four located in engine room 1 (ER1) and the other four in the engine room 2 (ER2). The engine type is Wärtsilä Vasa 6L46B. Maximum Continuous Rating (MCR) per engine is 5850 kW. Nominal speed is 514 rpm. The engines are suitable for a so-called pier-to-pier-operation on HFO (380 cSt/ 50°C). Besides HFO, the engines can function on MDO and MGO as well, as long as the viscosity of the fuel at the injectors remains higher than 2.8 cSt. Limited operation at 110% MCR (one hour per every twelve hours) is allowed. In case an engine is in the stand-by mode, all necessary auxiliary systems are maintaining service temperatures close to their working temperatures. This allows the engines to be loaded to full power within 48 seconds after the generator breaker is closed. Four generators supply one main switchboard. Each engine room contains one main switchboard (MS).

Main Generators

Eight AEG three-phase, synchronous, brushless generators are installed, type S 7476/14. The generators are driven by the diesel engines via a flexible coupling. The power rating is 8000 kVA, voltage 3 x 10 kV, 60 Hz at 514 rpm. The generators are enclosed and cooled by means of an air to water heat exchanger. Each generator has its dedicated cooling water pump, which is connected to the main cooling water system. In case of failure of the cooler, the generator can function as an open ventilated machine by means of opening of dedicated covers; the maximum output is in this occasion limited to 80%. The generator control and a part of the PMS are performed by the GMM (Generator management module) unit, fitted inside each generator panel.

Diesel engine modifications

L.V. Donge [18] conducted a study into the effects of installing two new thrusters on the vessel in 2009. During this study, 4 modifications were made to the engines that are still persistent. Following that study, the two thrusters were installed and a review of the effects on the power generation system have been re-investigated in this thesis as it has been over a decade since those modifications have been made. The modifications to the power generation system the findings of the study conducted by L.V Donge have been summarised below:

Modifications:

- i. Waste gate removal: The waste gate is a device that is a controllable valve that diverts exhaust gases away from the turbine in a turbocharged system to the exhaust gas pipe. This is activated when the engine operated above 85% load. This is done to prevent the over-speeding of the turbocharger and to relieve the excess pressure on the engine. Due to a malfunctioning waste gate- it was decided to remove it in 2000.
- ii. Increase in compression ratio: In order to comply with stricter environmental regulations, the decision was made to increase the compression ratio of the engine from 12.5 to 14. This was done by adding 6mm thicker shims, modifying anti-polishing rings and retarding the fuel injection by about 3 degrees crank angle. So, by effectively reducing the volume of the cylinder of the engine- the compression ratio was increased. This has consequences on the maximum power output of the engine.
- iii. Pilot injection valve removal: With the increase of the compression ratio- the effectiveness of the pilot injection valve was reduced as it was used to burn the low-quality heavy fuels well at all loading conditions.
- iv. Retarding the fuel injection timing: The fuel injection time was retarded as with an increase in the compression ratio- the induced pressure would cause the exceedance of the maximum limit of 195 bars.

Following the study conducted, the two azimuth thrusters were eventually installed on the starboard and port side sponsons.

A diesel engine simulation model was made and tested with the parameters of the Wartsila 6L46B. The model was developed by C. Dijkstra, D. Boetius, P.Baan and P. Schulten under the direction of D. Stapersma. Once the model was validated to match the diesel engine- the model was adapted to test the modified engine settings.

The results of the simulations experiments are summarised below:

As can be seen from the data, the engines have been de-rated due to the modifications made as the limiting factor has been the increased pressure in the cylinder which must not be exceeded. Consequently, this has impact on the generator output as well to the actual usable energy output totalling to a maximum of 5200 kW.

Table 2.1: ESS applicability

Parameter	Result
Engine $P_{nominal}$	5850 kW
Engine $P_{de-rated}$	5650 kW
Generator $P_{nominal}$	5650 kW
Generator $P_{de-rated}$	5200 kW
Maximum cylinder pressure	195 bar
η_{m-loss}	8%

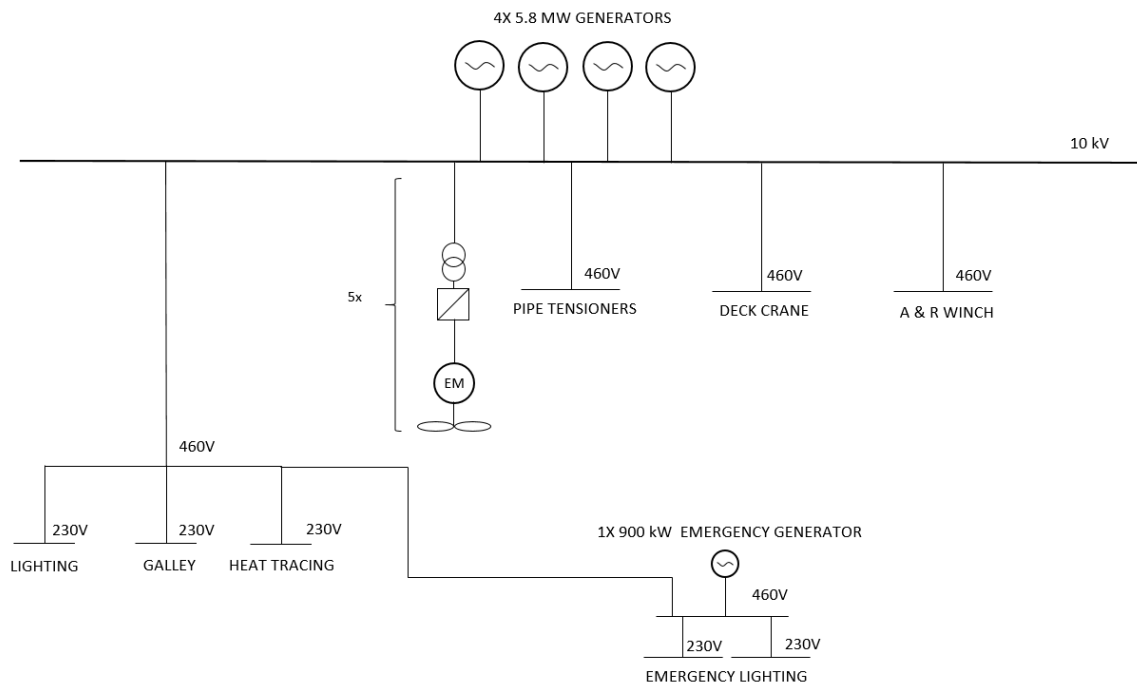


Figure 2.4: Power distribution layout of a single switchboard

2.3.4. Power distribution

The power distribution of the vessel can be classified into 3 levels (Figure 2.4):

Level 1: High voltage distribution- 10 kV Main Switchboards

Each engine room contains one main switchboard (MS). To each main switchboard, the main components are:

- Main diesel engine-generator sets (4x)
- Propulsion units (5x)
- Distribution & consumer transformer panels (3x+3x)

Generators have their dedicated generator unit for management, overload and short circuit protection (GMM10). The thruster transformers have dedicated protection modules as well (TPM10).

Level 2: Low voltage- 460V switchboards

All 460V switchboards are normally fed via 10kV/460V transformers. The individual distribution boards are installed for the following main consumers:

- i. Pipe transfer cranes & winches
- ii. Tensioners

Additionally, the vessel also has an emergency distribution (ED) board. The power supply to this switchboard comes from the emergency generator. In case one of the boards loses power, the emergency generator will receive a start signal. The generator breaker inside the ED board and one of the distribution boards is made. The allocation and distribution of each of the 460V board has been arranged to ensure that the auxiliaries associated with the main generator sets are fed from the boards inside the same compartment.

Level 3: Low voltage- 230V AC, 110V DC, 24V DC

230V distribution:

A large number of 230V switchboards are installed on board with supplies being distributed to feed the thruster back up control, process stations, battery chargers and back-up supplies to the DP UPS.

110V DC

Each high voltage (HV) switchboard has two independent 110V DC systems for powering the protection and relay circuits. Each 110V system consists of a battery charger, a battery and a distribution box. It serves half of the consumers of one HV switchboard. Loss of one 110V supply effects half a main switchboard.

24V DC

For various main systems and components, the 24V DC systems are installed. Main engines and thrusters require 24V for certain control circuits. Each 24V board is supplied by its own 230V charger and battery system.

2.3.5. Power Management System

The power management system is a part of the Kongsberg K-Chief vessel management system (VMS). It performs the following main functions:

- i. Main diesel engine (MDG) control and monitoring
- ii. Load dependent start-stop and blackout restart
- iii. Load sharing and preferential tripping
- iv. MDG load limitation
- v. Alarms and monitoring

The system is integrated with the previously mentioned DP system (K-Pos) and the thruster control system K-Thrust. The way they interface together is that DP system K-Pos collects and logs all the measurements of importance to keep the vessel in position for the operation. Based on the data- the system analyses the present state of the vessel and the ideal state it must maintain. Based on the energy requirements to position the vessel in its ideal position, K-Pos will send the necessary setpoints of the thrusters and generator outputs. These signals are received by K-Chief which controls the power management by adjusting the engines operational point and communicating the requirements to the K-Thrust system to enable the thrusters in the desired fashion i.e., controlling the required thrust output and the azimuth angle. The K-thrust system then initiates the thruster actions and relays the data back to K-Pos to complete the control loop (Figure 2.5).

The PMS shares active power and controls frequency by activating the electric governor setting of each diesel engine. Reactive power is shared by the action of the individual AVR's (Automatic Voltage Regulators) of each main diesel generator. The governor controls the fuel regulation of the diesel engine and maintains the revolutions independent of the load. The generator management module (GMM) controls the errors in the governor and protects the generator. It also controls the synchronising of the diesel generator set with the frequency of the busbar. The AVR controls the excitation of the generator and maintains the generated voltage at 10kV independent of the load; the variation in load causes variation in current.

Symmetric load sharing

The symmetric load sharing options is the usual DP operational mode. This is the case when all the online engines on a switchboard share the total load equally. The scope of this project considers only the symmetric load sharing option as it is the most relevant from an operational perspective.

The PMS will automatically start and stop main diesel generators depending on the load. Main diesel generators are started and stopped depending on the selected running order. If the selected main diesel generator starts but does not synchronize, the next selected main diesel generator should start and attempt to synchronize. The whole process from start to synchronization and connection takes 48 seconds.

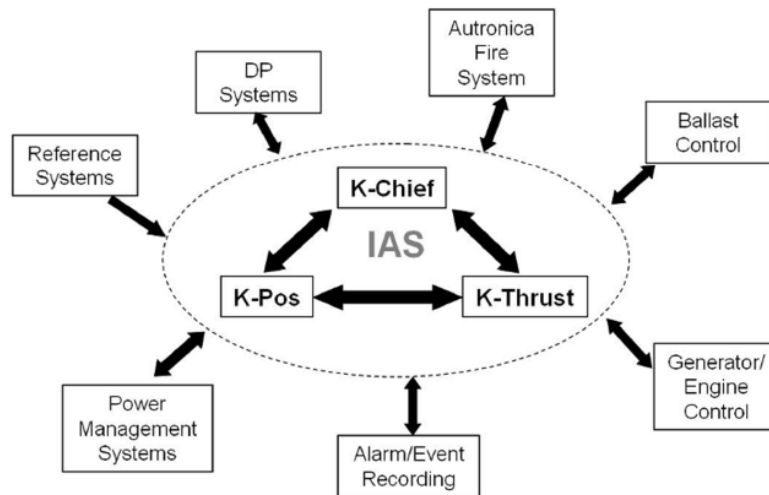


Figure 2.5: Integrated Automation System (IAS)

2.4. Pipeline production process

2.4.1. Methods of Pipelaying

Several methods of installing offshore pipelines exist; the most familiar being S-lay, J-lay, Reeling and towing.

S-lay is the method used by Allseas (Figure 2.6). This method provides fast installation for all pipe diameters over a large range of water depths. The fast installation process is possible because the onboard assembly of the pipeline can be done in a horizontal plane, the firing line. Due to the horizontal-working plane called the firing line (Figure 2.7), the pipeline leaves the vessel horizontally and has to be supported by a stinger to introduce the necessary bend to direct the pipeline to the seafloor.

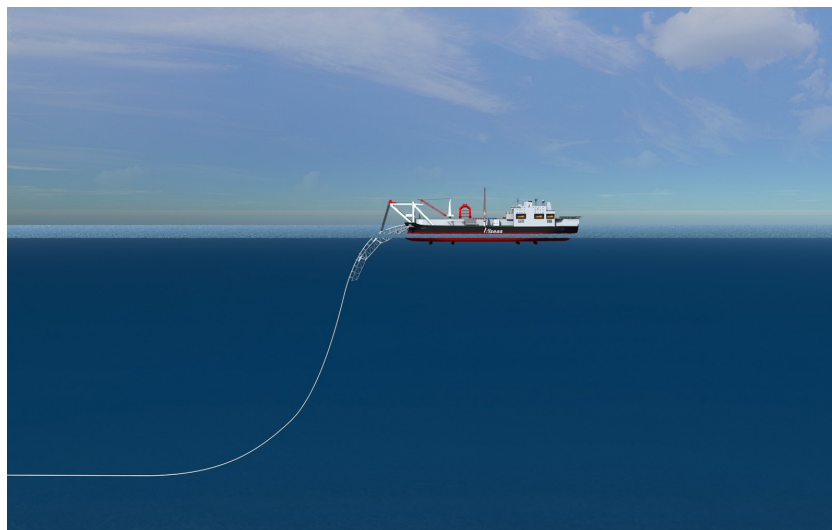


Figure 2.6: S-lay method

2.4.2. Production process

1. Transport & Onboard production:

Typically the pipes are delivered onshore by the client “coated” except for the ends that need to be bare steel for welding and in pieces of 12.2 meters. Pipe carrier vessels are chartered to transport the pipe from shore to the pipelay vessel. The preparations on the pipes are done in the firing line of the vessel (Figure 2.7). The pipe leaves the vessel’s storage holds to enter a preparatory phase after which the pipe sections move onto the firing line wherein the sections are connected together to form 24.4 metre sections. These

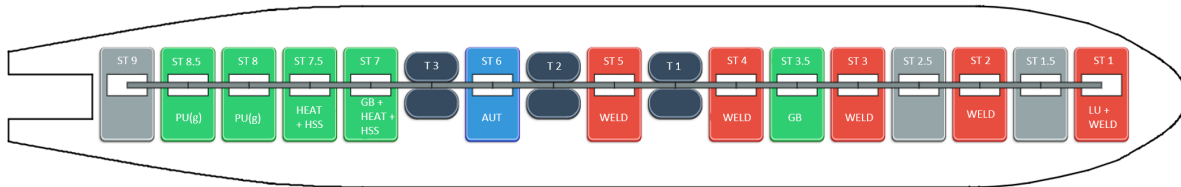


Figure 2.7: Firing line of the Solitaire

larger sections are then connected to the main pipeline to the bottom of the sea and as these sections are completed, the vessel moves forward 24.4 meters before the production of the next section continues.

Welding

The ends of the 12.2-meter-long pipe sections (joints) are bevelled by means of a beveling machine. Following the pre-heating, the pipe lengths are welded in the production line (firing line). *Solitaire* has a double joint factory which allows the joining of the two joints into one length of 24.4 meters prior to welding it to the main pipeline. This is the point where the double joint is attached to the pipeline that is suspended behind the vessel. This increases the vessel productivity, which is more economical on long distance pipelines.

The activities at the various stations are balanced out such that the average cycle time achieves an optimum time per joint of typically 5-10 minutes.

Quality control & Field joint coating

After the weld has been completed, the weld is examined by means of ultrasonic testing (UT). If the defect is larger than the permitted level, the weld must be repaired which results in a halt in pipelay operations until the repair has been completed.

The coating station is situated at the aft of the vessel. The welds and bare steel have to be provided with coating to prevent corrosion. This can be provided by epoxy which is applied to the weld after it has been grit blasted and preheated by means of (electrical) induction heating. The epoxy is then sprayed as a powder to form a thin but very strong protective layer. After coating, the joint goes into the water as the vessel moves ahead during a pull.

2. Tensioning & Stinger transition

During the pipelaying process described above, the pipeline should be kept under tension to prevent pipeline buckling. Buckling is the phenomenon that a structural element collapses under a compressive force due to out of plane bending. Buckling can occur at the point where the pipeline leaves the stinger or when the pipeline touches the seabed (touchdown point) and is caused by excessive bending in the pipeline due to its underwater weight. Tensioning reduces the bend sufficiently.

Machines called 'tensioners' perform the tensioning of the pipe. A pipelaying vessel has about 3 tensioners which clamp the pipe with a crawler that rolls fully controlled whilst the vessel is making a 24.4 metre 'pipe pull'. The weight of the pipe and depth of the water dictate the degree of tension. More weight and/or deeper water means more tension. "Tensioner forces" vary between 15 and 500 tonnes.

The pipe is fed onto an outrigger called the 'stinger', in a gentle bend (overbend). The stinger will convey the pipeline into the water on its route to the seabed in a controlled curve. Buckling can be caused by either a tensioner failure or a vessel drift-off due to a failure in the DP system, such as a thruster or generator failure.

2.5. DP Operational activities

i Normal Pipelay

In this condition, the stinger of the *Solitaire* is in the water supporting the pipe string that is being installed. The DP system is used to keep the vessel in position and to compensate the horizontal force of the pipe. After a double joint is welded to the pipe string, the vessel moves two pipe lengths (24.4 meters) forward, which is called the pull of the vessel. In the meantime, the tensioners are paying out the pipe string.

ii Abandonment and recovery

When the weather conditions deteriorate, the decision may be taken to abandon the pipe. The pipestring will be lowered to the seabed with the help of the A & R cable attached to a laydown head which is welded to the end of the pipe string. Depending on the conditions, the A & R cable can be cut and recovered, with the end of the pipe marked by a buoy allowing *Solitaire* to lift its stinger out of the water and move to sheltered waters.

iii Standby condition

Solitaire is on standby when the pipe is abandoned but remains connected to the pipe string via the A&R cable. The stinger can remain in position in the water (or raised above water), ready to resume operations when possible. In this condition the vessel can choose a favourable heading with respect to prevailing winds and waves.

iv Transit condition

In the transit condition, all thrusters are used for sailing. During transits, in which high sea states cannot be avoided, the stinger has to be rotated to its most upward position and secured to the cross over. A maximum sailing speed of 13 knots can be achieved.

2.5.1. DP Operations inside the 500m zone of an Offshore structure

DP operations within the 500m zone are carried out in compliance with the DP equipment Class III requirements. The *Solitaire* FMEA study shows that the worst-case failure design is the loss of one complete switchboard resulting in the loss of four of the generators and 5 of the thrusters. When it is not possible to comply with the DP equipment Class III regulations it could be considered to carry out the operation with a reduced level of redundancy. For instance, after a DP Class III failure it might be possible to reduce the bottom tension, leaving more thrust capacity available for station keeping.

The direction of the wind and waves can also be favourable, such that a loss of position or heading will not result in coming into contact with a facility. In these cases, a risk assessment is made where all risks of losing one switchboard section are evaluated. The redundancy level required for a particular operation should be agreed between the owner of the vessel and the client and can be based on a risk analysis. The determination of safe working limits should consider the consequences of a sudden failure of the tension load from mechanical, or control, failure so that such a failure does not risk:

- Injury to personnel working on or near the line
- The vessel coming into contact with any nearby structure (surface or sub-sea) or vessel

At all times the redundancy level should be such that a single thruster or single generator failure does not result in a loss of position or heading, and the pipe tensioning level is maintained.

2.5.2. DP operations outside the 500m zone

When operating outside the 500m zone of an offshore (subsea) structure, the consequences of a loss of position are lower than when operating within the 500m zone. A loss of position could result in damage to the pipe and pipelay equipment (stinger). The chances of injuries to personnel are very small. DP operators have standing orders to clear the firing line in case a loss of position or tension is evident.

According to the guidance note IMCA M103, DP Class III is assumed but at least DP Class II is expected. For the *Solitaire* the worst failure for both DP Class II and DP Class III is the loss of a switchboard. An evaluation of all DP related malfunctions and incidents show that the likelihood of failure of an entire switchboard itself, is small. Based on a risk analysis, it has been concluded that not being redundant against a switchboard failure is an acceptable risk for operations outside the 500m zone. All other DP Class II requirements have to be complied with.

2.6. Implications on ESS

Vessel characteristics

- The main diesel engine de-rating to 5,650 kW will have to be taken into consideration when sizing the battery.
- Only the symmetric load sharing option will be considered for this study as it is the most commonly used during DP operations.
- An insight into the vessels electrical health needs to be re-visited to understand the effects of the low power factor after the installation of the 2 new thrusters in 2009/10.
- Due to the complexity and cost associated with several battery units split throughout the ship, battery solutions connected to the main switchboard will only be considered in this study.

Production process

- The ESS will have to be able to sustain spinning reserve capabilities during all of the pipeline production phases.
- The pipe-pull scenarios need to be analysed further from the vessels power profiles to get a better understanding of its effects on the ESS.

DP Operational activities

- The ESS applicability must persist across all DP operational activities which includes pipeline loading, laying, abandonment and recovery which would need the analysis of different power profiles.
-

3

Data analysis

The data analysis chapter is divided into five main areas of interest: Vessel load components, Power peak analysis, Electrical system health analysis, power factor corrections & assumptions and failure scenarios.

3.1. NordStream II

The NordStream2 project concerns the construction of an offshore natural gas transmission system comprising two 48-inch diameter pipelines from Russia through the Baltic Sea to Germany (Figure 3.1, Table 3.1).

In general, the pipeline offshore route has been determined with the aim to achieve a line as direct as possible, but respecting or avoiding adverse natural conditions, environmentally sensitive areas, military exclusion zones, major navigation traffic lanes and special areas commissioned to other economical or recreational interests. The pipeline route is within the European Union (EU), except for the short section in Russia, as per the table below, where EEZ means Exclusive Economic Zone and TW means Territorial Waters.

Table 3.1: Approximate kilometres per country

Country	EEZ(km)	TW (km)	Total (km)
Russia	0	114	114
Finland	374	0	374
Sweden	511	0	511
Denmark	87	53	140
Germany	31	53	84

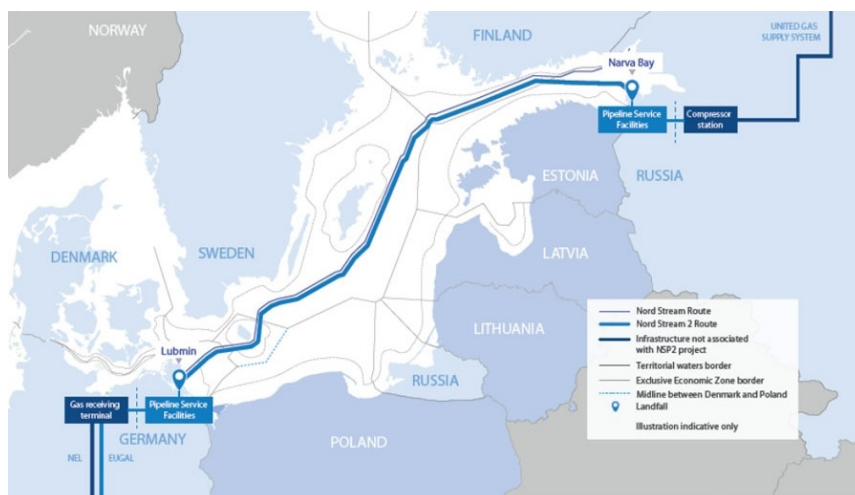


Figure 3.1: NordStream II pipeline route

3.1.1. Kilometre Posts (KP's)

The Kilometre Post (KP) values indicated in the sections to follow are measured from Russia as a starting point. They are represented in two formats i.e., the Global KP's and the Per country KP's. The global route considers the kilometre points relative to the whole pipelaying project and the 'per country' routing is relative to same starting point (Russia) but only considers the number of kilometres of pipe to be laid in that countries' waters. For this study, the analysis has been conducted only for the Finland KP's using the 'per country' KP's. The 'per country' KP's start at KP0 on the border of each country closest to Russia (Table 3.2).

Table 3.2: Country KP's versus global KP's line A

Country	Global route		Per country	
	Start GKP	End GKP	Start KP	End KP
Russia (RKP)	0	113.796	0	113.796
Finland (FKP)	113.796	448.104	0	374.308
Sweden (SKP)	488.104	999.359	0	511.255
Denmark (DKP)	999.359	1138.772	0	139.413
Germany (KP)	1138.772	1223.224	0	84.452

3.2. Overview

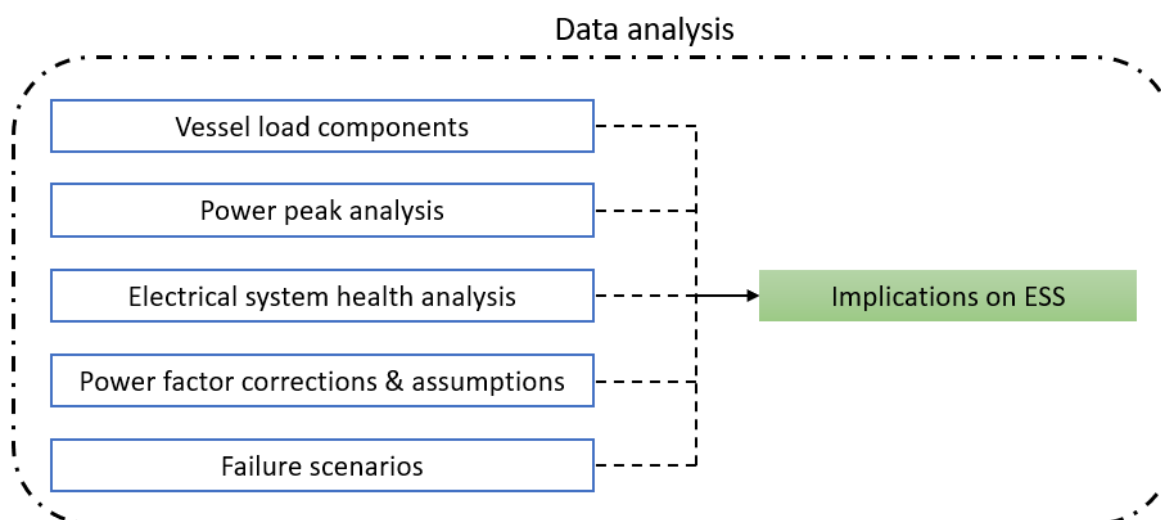


Figure 3.2: Chapter 3 overview

3.3. Vessel load components

There exists a provision for all Allseas vessels data to be logged on the vessels datalogging system. For the *Solitaire*, this consists of nearly 2500 sensors on board that record various parameters. To conduct a load analysis, the load can be split into 3 levels on review of the single line diagram attached in Appendix A.

- Level 1: 10x Thrusters (DP load)
- Level 2: Pipe tensioners, Deck cranes, A&R Winch (Ancillary consumers)
- Level 3: Lighting, RCCB panel, Heat tracing, Stabilised supply, HVAC, Galley, Laundry, Heaters (Ancillary consumers)

Using the vessels datalogging system, the active power of all the 10 thrusters on board were recorded as well as the active power output of all the generators on switchboard MS1. This gives a good representation of the total load demand breakdown on the power generation system of the vessel.

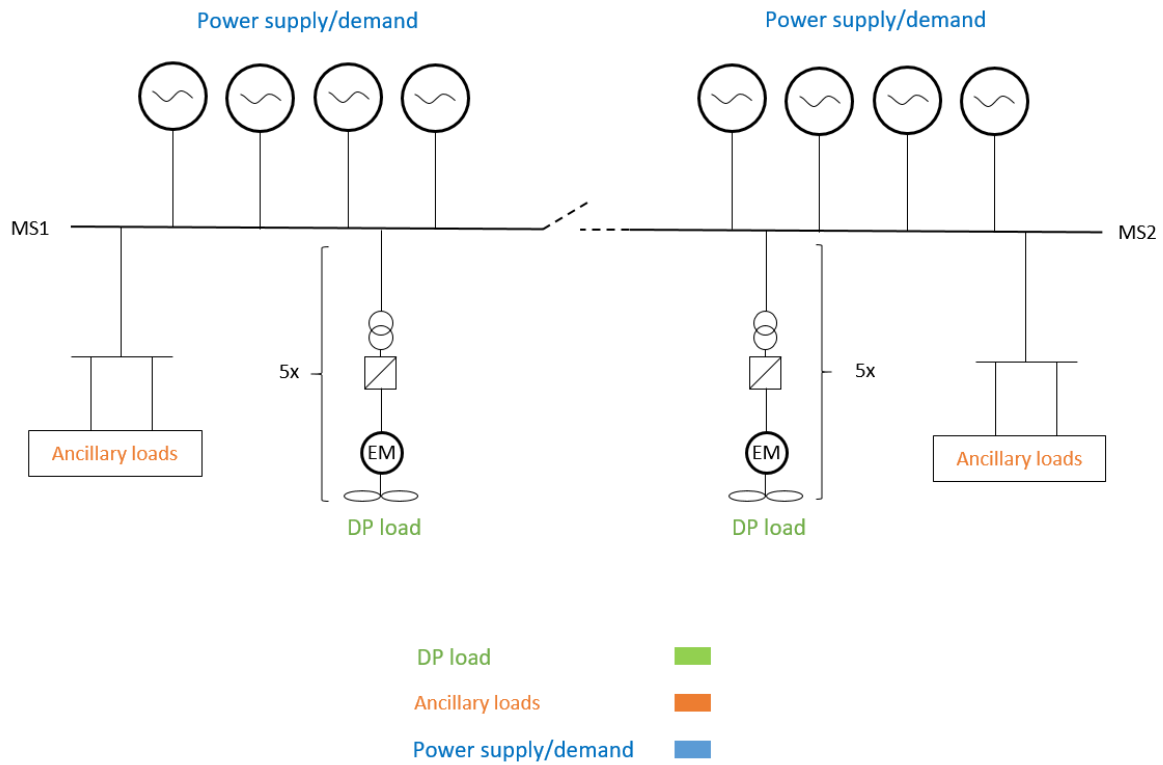


Figure 3.3: Simplified Single line diagram of the M/V Solitaire

The simplified single line diagram of the vessel depicts the two switchboards of the vessel. Onto each switchboard, the DP load component comes from the thrusters while the remaining loads are considered ‘ancillary’ loads which are required to support the primary activities of the vessel. Further in this report, the aforementioned colour coding will be used for the representation of figures (except in Section 3.5 which is characterised by its own colour coding system).

$$P_{demand} = DP + Ancillary \tag{3.1}$$

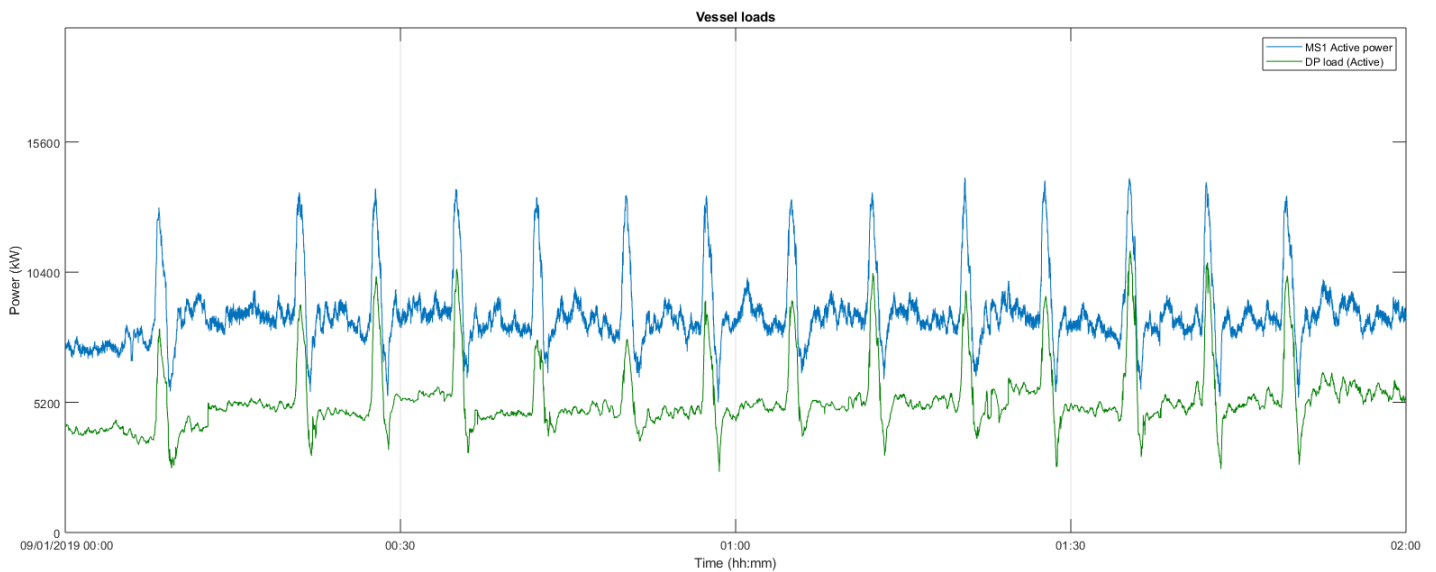


Figure 3.4: Vessel loads during pipelaying in shallow water

From Figure 3.4 it is apparent that the majority of the load experienced by the vessel is as a result of the demand from the thrusters which constitute the DP load. However, it can be seen that between 00:30 and 01:00 that although there is a slight dip in the size of the DP power peak, the size of the overall power peak is the same size. This means that there exists a relationship between the DP load as well as the ‘ancillary load component’ which seems to be compensating this load in some way. The difference between the power demand and DP load would be the remaining Level 2 and 3 consumers (i.e., ancillary load component).

3.3.1. Level 1: DP load

The DP load is consistent of two primary sub-components, namely, the moving average load which is the load the vessels thrusters must compensate due to the weather and pipe-tension effects. The variant load which is due to vessel excursions from its setpoint and the large power peaks caused due to the vessels forward motion to the next position setpoint.

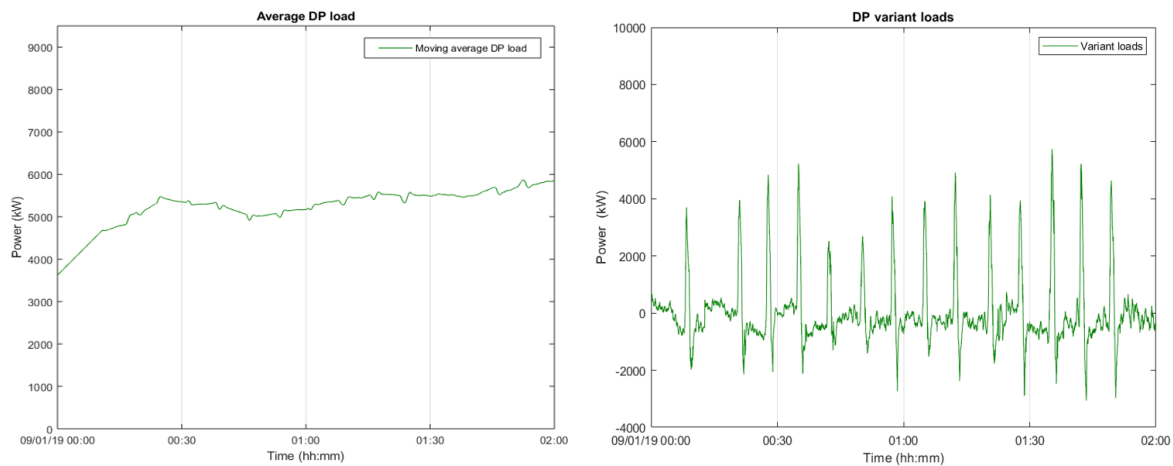


Figure 3.5: Average and variant DP load

From Figure 3.5 it is apparent that the station keeping requirements of the vessel can be satisfied by one generator while the power peaks require an additional running generator.

$$DP_{load} = DP_{average} + DP_{variant} \quad (3.2)$$

3.3.2. Level 2 & 3: Ancillary consumers

Observations were made that although the DP load exhibited the power peaks that were expected, interestingly even the ancillary load component shows these power peaks albeit to a lower extent as the amplitudes of these peaks are in the order of 1-2.5 MW. Looking at the components in the Level 2 and Level 3 hierarchy on the single line diagram it is evident that the most active components during a pipe-pull operation would be the tensioners. The vessel has three such tensioners and the capacity of each tensioner is 350 tonnes.

Table 3.3: M/V Solitaire Tensioner power consumption

Tensioner component	Power consumption (max. rated)	Per tensioner quantity
Hydraulic power unit (HPU)	200 kW	0.33
Gearbox cooling unit (GCU)	4 kW	1
Trackdrive motors (per tensioner)	360 kW	4
Total (per tensioner & per switchboard)	2195.3 kW (maximum)	

Delving into the power consumption of the tensioners shown in Table 3.3, it is evident that the operation of the tensioning systems during pipe-pulls could play a significant role in the size of the power peaks too. To further investigate this hypothesis, a power peak analysis is conducted to observe any correlations. Power supply to the tensioners come from both switchboards separately in order to ensure redundancy in the event of a complete switchboard failure.

3.4. Power peak analysis

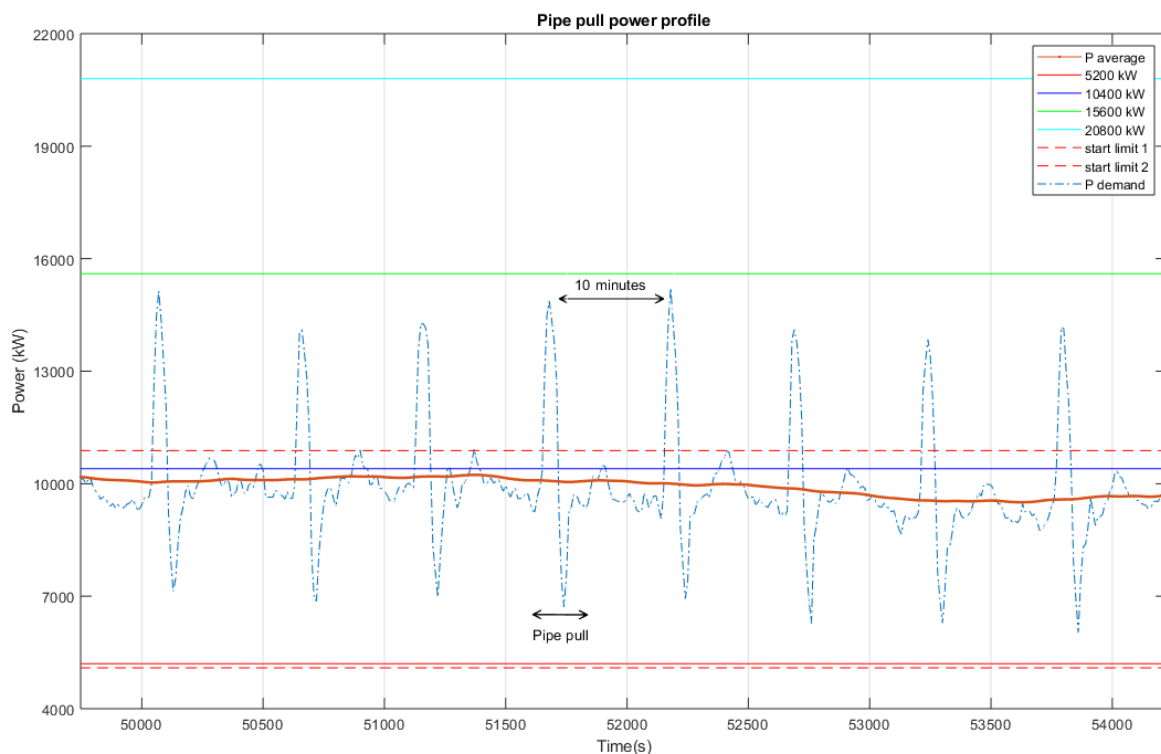


Figure 3.6: Pipe pulls

The Figure 3.6 represents a typical pipe pull power peak. The time between two consecutive pipe pulls on the Solitaire is approximately 10 minutes. This process continues throughout the day. It can be seen that around the 51,500 second mark the vessel is maintaining position, soon after once the pipeline production phase of 24.4 metre section is completed, all the 'green lights' on the vessels 'pipe-ahead' systems are activated which means that all stations have completed their tasks. When this is the case, the same information is communicated to the bridge where the DP operator/captain initiates a 'pull' which essentially moves the vessel forward by the pipe length to the next DP setpoint. The vessel begins to accelerate its thrusters to ramp up to a ground-speed that has been set (usually around 0.4 m/s). Once the vessel approaches the setpoint the thrusters ramp down to a very low load which causes a large dip in the power demand. But as the ground-speed then decreases and the vessel reaches its next setpoint location, the thrusters re-engage back to a point that is required to maintain the vessel in the new position. This operation lasts about 70 seconds.

3.4.1. Ground-speed & Tensioner correlation

Figure 3.7 shows that two types of correlations exist for the power peaks. Firstly, the increase in ground-speed causes the increase of the DP load. Secondly, the ancillary load component fluctuates with two peaks during each pipe-pull. The reason can be attributed to tensioners operating to compensate the pipe-tensions. At the 370- second mark, it can be seen that the vessel moves forward for the pipe-pull, it results in the pipe tension increasing as the tensioners consume power to restrain the pipe from moving. After this, the tensioners pay out slack to the pipeline which results in a drop in pipe-tension (until the 440 second mark). Once the pull is completed, the tensioners re-engage to restore the tension in the pipeline which results in another power-peak just after the pull.

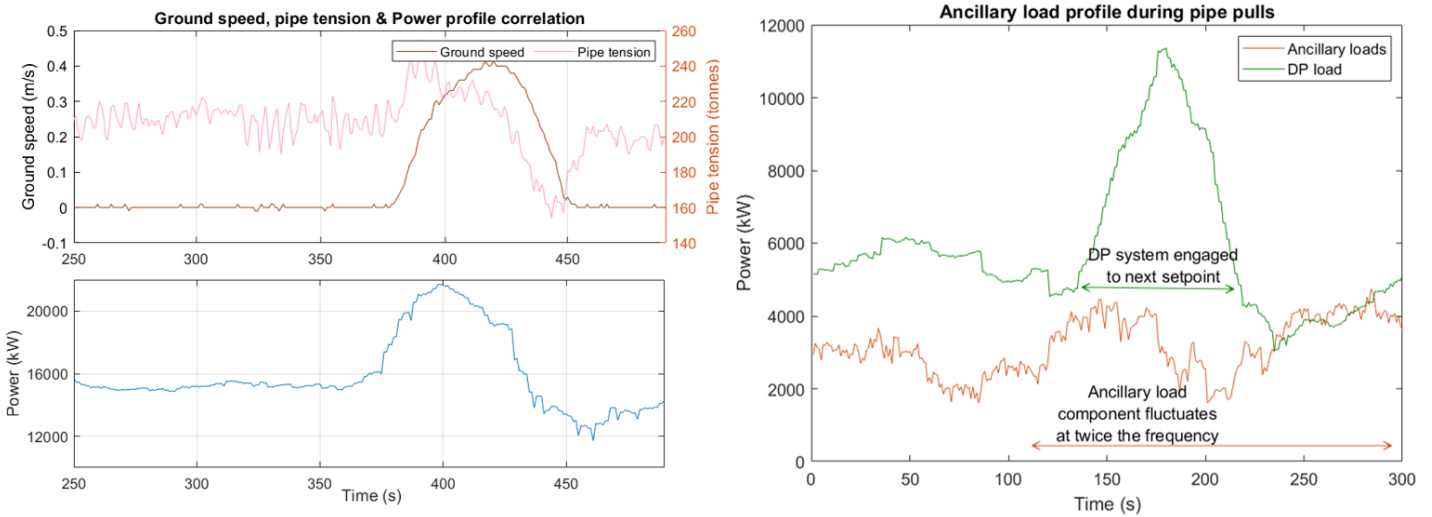


Figure 3.7: Ground-speed and ancillary load correlations

3.4.2. Anomalous power peaks

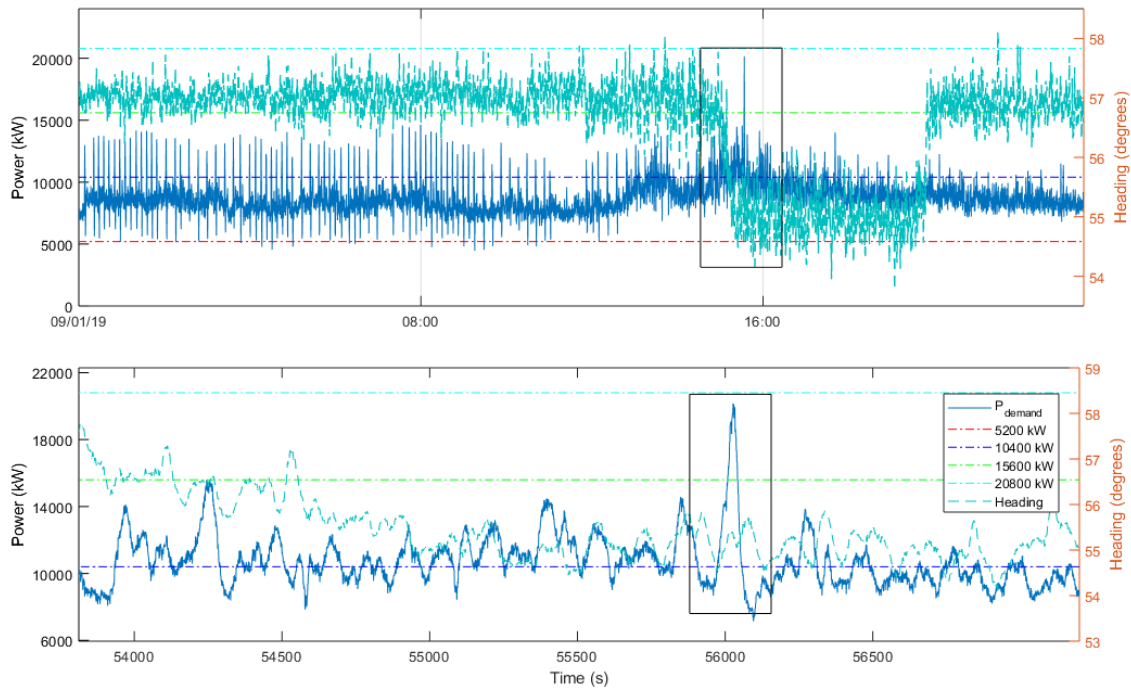


Figure 3.8: 'Rogue' power peak

Figure 3.8 shows that at the 56,000 second mark, the power peak caused is nearly the capacity of an engine (above the 15600 kW limit). This was caused due to a heading change from 57° to 55° as the vessel attempts to prevent an overshoot. Such scenarios although rare, occur when vessel orientation is changed during pipelaying. From the size of the power peak (nearly 5 MW), it is similar to an engine failure scenario. To prevent an unnecessary generator start-up during such a scenario, the thrusters could be phased back in order to reduce the load. Alternatively, the ESS could supply power for this one-off event.

3.5. Electrical system health analysis

On analysing the online capacity in use during DP operations, it was noted that more insight into the vessels electrical system was required. The peak analysis gives insight into the battery sizing requirements but not the reason for the additional generators ($n + 2$) running on the *Solitaire*. The findings of L.V Donge [18] had brought up issues of the vessels poor power factor, however since that analysis was done in 2009 for a thruster upgrade- it was ascertained that a similar analysis must be done to understand the implications on the energy storage system. Measurements were recorded on the power generation and thruster unit side.

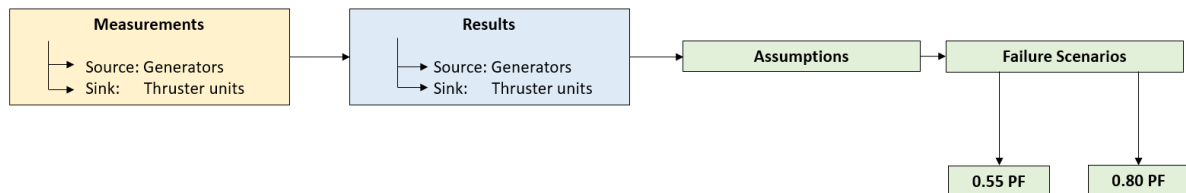


Figure 3.9: Experimental measurements & inferences

3.5.1. Generator measurement

The electrical measurements were conducted for all 8 generators across MS1 and MS2. This entailed the logging of the currents and voltages. Additionally, the real power produced was also recorded in kilowatts for the generators.

The required power for DP operations are determined by the DP model of the vessel. These requirements are sent to the power management system that translates these requirements as setpoint commands to the diesel engine. The engine throttle is set based on the active power measures taken on the generator output side. This setpoint is the desired value of the induced electrical power. In general the actual value fluctuates around the setpoint [18]. The electrical measurements on the exit side of the generator (Figure 3.10) gives a clearer picture of the state of the electrical health of the system grid.

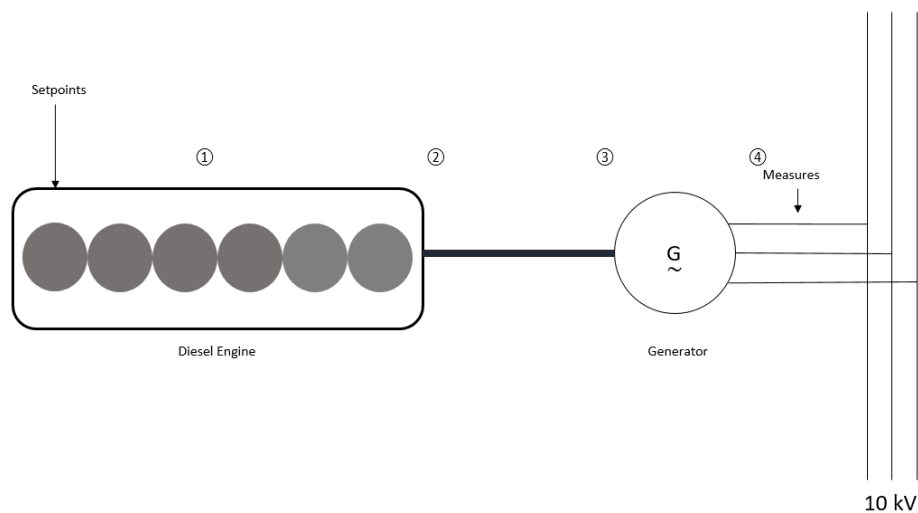


Figure 3.10: Generator measures

Table 3.4: Analysis locations

1	Diesel engine induced power
2	Diesel engine brake power
3	Brake power- generator input
4	3-phase output (I_{line}, V_{line})

3.5.2. Thruster unit measurement

The second set of measurements were taken at the thruster unit breaker (numbered '11' in this example) (Figure 3.11), which includes a step down transformer with two secondary windings which allow for 12 pulse rectifying for the propulsion drives. The propulsion transformers, supplying the frequency converters of the thruster drives, are constructed with double secondary windings with phase shifts. In this way, the secondary side will be a 24-pulse system and the 5th, 7th, 11th and 13th harmonics from the secondary side will be deleted on the primary side [9].

The purpose of these transformers are to reduce the total harmonic distortion (THD) of the AC wave entering the VFD (Variable Frequency Drive). Although the motor requires a 3-phase AC sinewaves to operate the thruster control is employed by maintaining a 3-phase supply but at different frequencies and not 60Hz. The peak frequency at 110% load for these thrusters are 35 Hz and the continuous rating is specified at 31 Hz 3-phase AC [18].

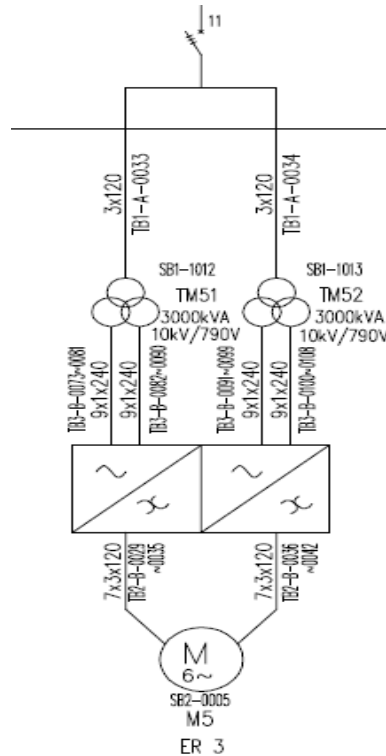


Figure 3.11: Propulsion unit

3.5.3. Generator measurement results

The measures taken for this analysis are:

Table 3.5: M/V Solitaire Grid measures

Parameters	Symbol	Units
Line currents	I_{L-grid}	A
Bus voltage	V_{bus}	V
Active Power	P_{grid}	kW

Using the measurements, the Active, Reactive and Apparent power are plotted to give an overview of the vessels grid power factor (Formulas attached in Appendix A).

From the Figure 3.12 it can be seen that in the first 800 seconds, the vessel engages in one pipe-pull. During the pipe-pull the maximum available capacity comes from 3 engines. These are all that is required to satisfy the active power requirement. Since 3 engines are online, 24000 kVA generator capacity is available. In the

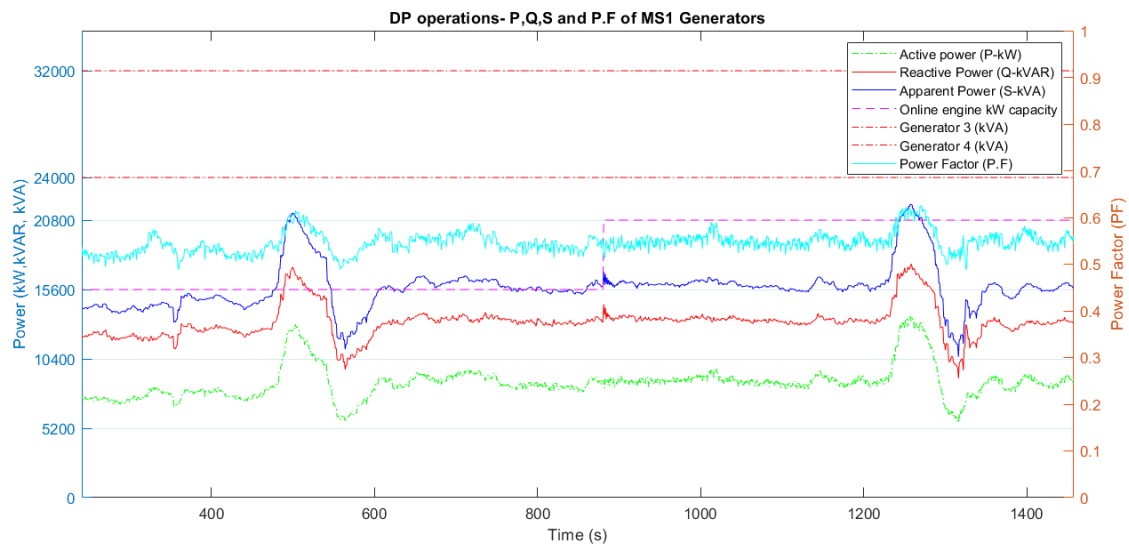


Figure 3.12: P,Q,S on the Solitaire (Recorded on 09/01/2019)

scenario that a pipe pull takes place- the vessel seemingly does not have redundancy¹, because the failure of an engine would mean that the active power capacity would reduce to 10,400 kW and the generator capacity, correspondingly to 16,000 kVA. The vessel has a mean power factor of 0.55 during DP operations which means that the reactive power requirement is significant.

The presence of large amounts of reactive power result in the conductor capacity to allow real power to flow through it to reduce as well as limits the engine from fully inducing its maximum continuous rating. i.e., the full capacity of $P_b = 5,650kW$ of the engine cannot be utilised [18]. This is because of the limit on the generator line currents to $I_{Line} = 465A$ for normal operations and $I_{Line} = 555A$ as the overload trip current.

It can be seen from Figure 3.13 that when 3 generators are online initially, the peak currents reach closer to the generator trip limit during the first pipe pull. Due to high currents during a pipe pull - the fourth engine-generator unit is turned on around the 800 second mark. The presence of high currents have been known to cause damage to equipment on board as the equipment has nearly reached its end of useful life.

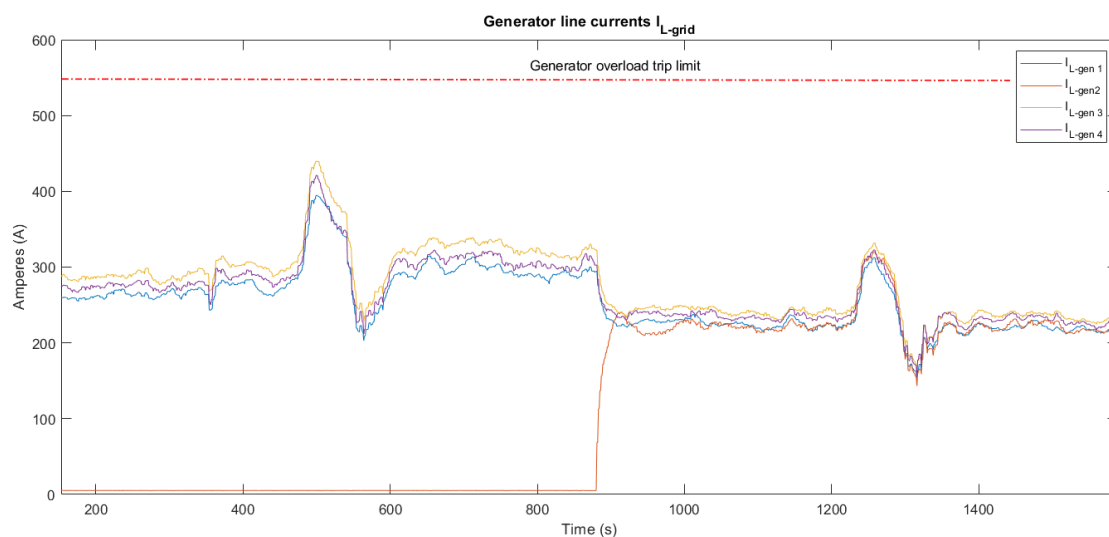


Figure 3.13: Generator currents on the Solitaire

¹The vessel is equipped with protection systems for the generators which allow an overload current of 555A for upto 10 seconds and two levels of short circuit protection. This gives enough time for the thruster control system to phase back the thrusters in order to reduce the power demand in the event of a failure (See discrimination diagram in Appendix B)

3.5.4. Thruster units measurement results

Thruster measurements were taken according to Section 3.5.2 and the source of the poor power factor can be seen in Figure 3.14. The inductive effect of the electromotors, transformers and the VFD contribute to an average power factor of 0.45 on the load side.

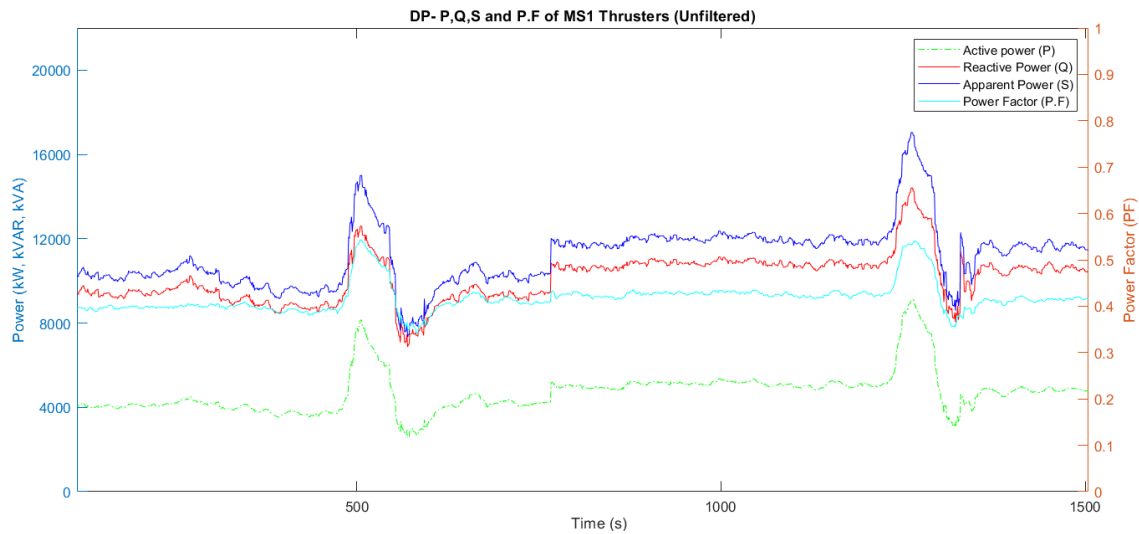


Figure 3.14: Power flow: Propulsion unit

3.6. Power factor correction & assumptions

For this research, the assumption is being made that the vessel would undergo upgrades in order to achieve a grid power factor of 0.8. Power factor correction options have been documented well in the master thesis of L.V Donge [18]. A power factor function was built in order to simulate what would happen if the power factor were to be 0.8 (Figure 3.15). This was done by capturing the existing power factor fluctuations with respect to different thruster loads and augmenting the profile to PF=0.8.

Power factor function

$$PF = -1.8227 \times 10^{-17} \times x^4 + 8.1961 \times 10^{-13} \times x^3 - 1.2878 \times 10^{-8} \times x^2 + 9.929 \times 10^{-5} \times x + 0.47339 \quad (3.3)$$

$$x = P_{switchboard} [\text{kW}] \quad (3.4)$$

Resulting power profile

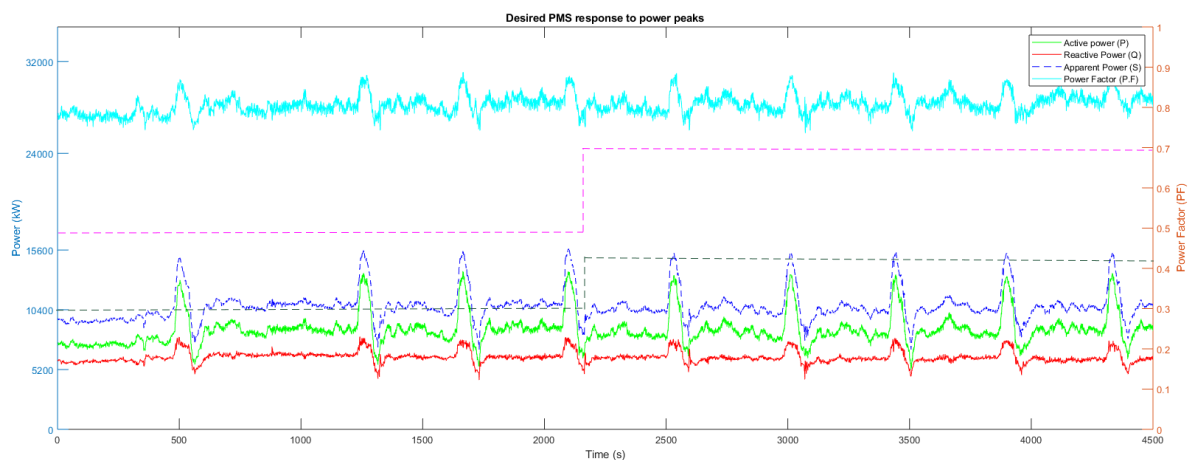


Figure 3.15: Ideal PMS response

Figure 3.15 shows that in a desirable scenario, the PMS must allow the battery to be used to shave off power surges. If the power surges get too large, the PMS must initiate a generator start-up to prevent damage or overuse of the ESS. Hence this gives rise to a mode of operation of the ESS called the ‘power surge shaving mode’.

3.7. Failure scenarios

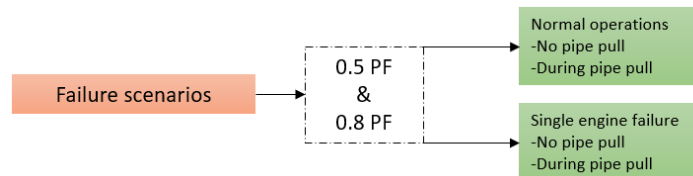


Figure 3.16: Failure scenario analysis overview

Using the measured and augmented power factor scenarios, scenarios of normal pipelaying operations and a scenario of the event of a single engine failure will be considered. Within these two conditions, the effects of the ESS will be considered during station keeping (no-pipe pull) and the pipe-pull condition (power surge).

3.7.1. 0.55 PF

Normal operations

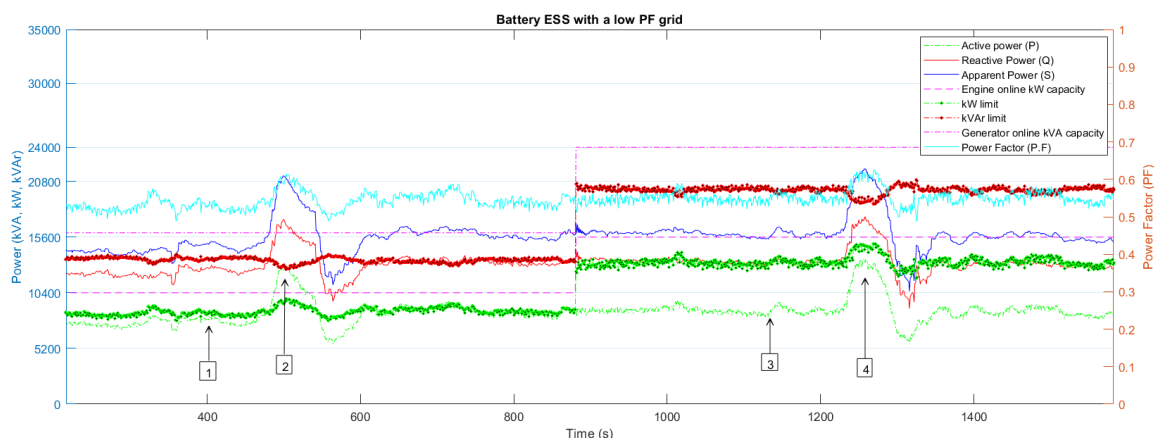


Figure 3.17: Normal operations with BESS (0.5PF)

The normal operational scenario of the *Solitaire* analysed here is representative of the existing condition of operation with one less engine running, no failure occurrence & that a battery is installed.

Such a scenario is represented in Figure 3.17. Due to the poor power factor, the active power limit of the engine is depicted as the ‘kW limit’² is seen that this does not match with the rated capacity of 5200 kW of electrical output (per engine). In region 1, this is not an issue as the apparent power requirement can be met by the existing set of generators. In region 2, i.e., during a pipe-pull, it can be seen that the apparent power exceeds the maximum output of two generators. This ESS must supply the apparent power above this limit which dictates that the ESS must have an inverter capable of 8000 kVA output per switchboard³. The ESS would not have to be active in region 3 & 4 as the engines & generators can handle the load requirements.

²The kW limit was calculated by using the measured power factor profile & reducing the online capacity by 8000 kVA to simulate a situation with a battery & one less engine running

³Same as the existing generators coupled with the main diesel engines

Single engine failure

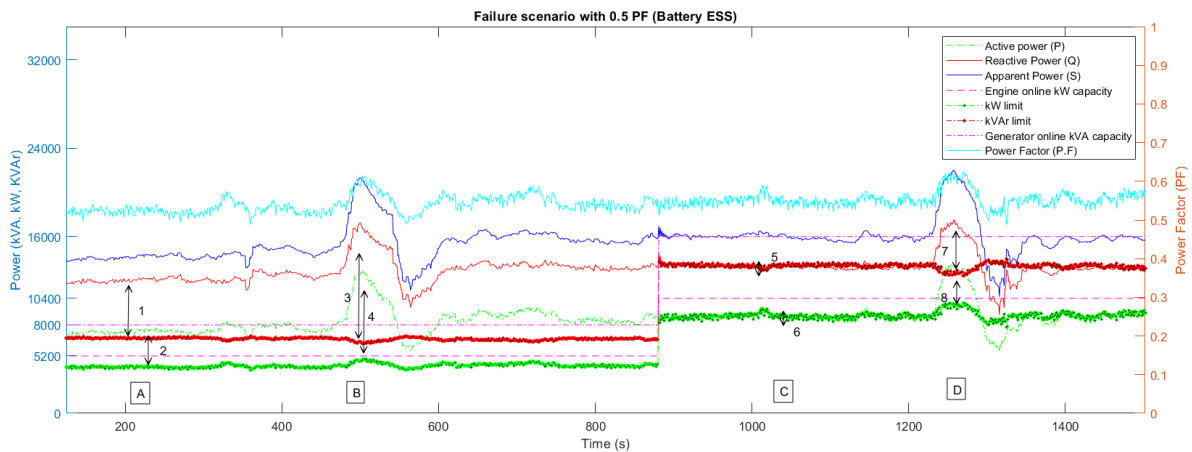


Figure 3.18: Failure condition with BESS (0.5PF)

From Figure 3.17, if the online capacity is reduced by 5200 kW, it presents the case of a single engine failure as shown in Figure 3.18. In region A (Figure 3.18), it can be seen that the available active power capacity from the generators is limited which means that the BESS will have to compensate for a larger range of power demand. The requirement to supplement the additional reactive power necessitates an inverter with the capability to supply 8000 kVA (as is the case with the diesel generators). However, on analysing the region B, it is evident that during a pipe-pull, if an engine were to fail, the apparent power to be compensated exceeds 8000 kVA.

As the *Solitaire* is equipped with protection systems to prevent a blackout in such scenarios⁴, the vessel would reduce thrust to reduce the power demand. However, after the pipe-pull (600-800 second mark), the load still hovers around the 16000 kVA limit which means that a battery inverter of 8000 kVA would not suffice as there is a risk of loss of position if the vessel reduces its thrust capabilities (or the inverter trips due to an overload). In this case, a solution would be to add a power factor compensation device or to over-size the inverter. Region C would require minimal battery support as the existing supply nearly meets the demand. In region D, the ESS would operate in a similar way to region A.

3.7.2. 0.80 PF Normal operations

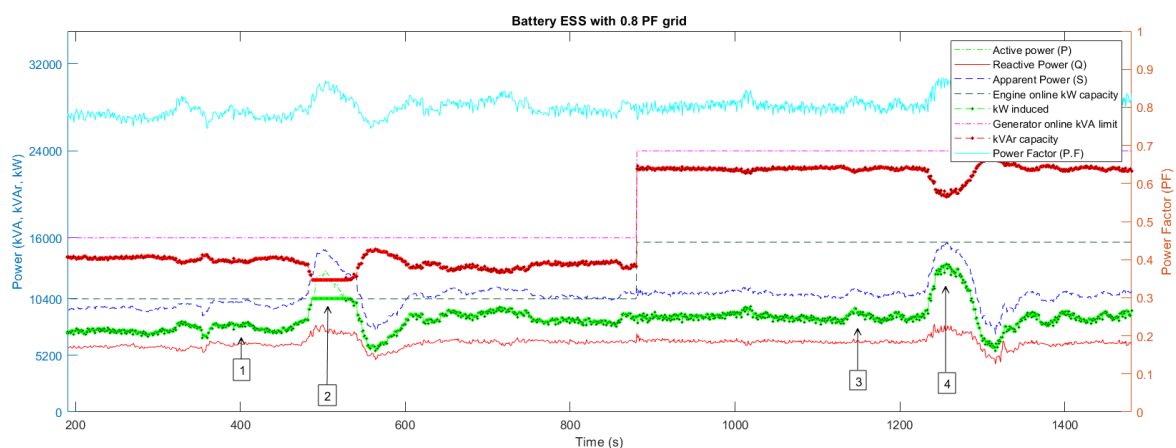


Figure 3.19: Normal operation with BESS (0.8PF)

⁴Discrimination diagrams attached in Appendix B which shows the overload, short circuit level 1 and short circuit level 2 limits

Using the power factor augmentation function (Equation 3.3), the analysis of the vessels grid is done under the scenario wherein the power factor is 0.8.

In the situation wherein the vessel operates at a higher power factor (0.80) it is evident from Figure 3.19 that the battery system would be used to power only the active power demand during pipe pulls (Region 2). This is advantageous, in that the inverter need not have large reactive compensation units and/or need not be oversized⁵. This is done by using the online generators capability to compensate the required increase in apparent power. This could be done by ensuring the AVR (Automatic Voltage Regulator) of the generator is overexcited in order to produce the required reactive power to the grid rather than allowing a battery inverter to do the same. In all other regions, the ESS is not used. Furthermore, the engine and generators capabilities can be fully utilised in the event of a higher power factor as the reactive power is not high enough to cause significantly large currents through the electrical system and saturate the generator output current.

Single engine failure

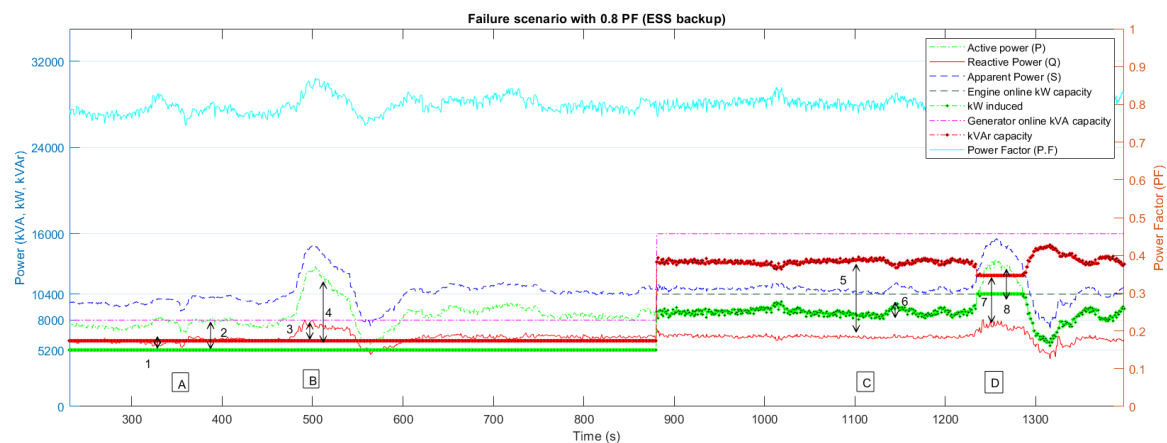


Figure 3.20: Single engine failure with BESS(0.8PF)

Figure 3.20 is the same as Figure 3.19 with one less running engine to depict a single engine failure.

Region B shows that since a generator has failed (during the a pipe-pull), the online engine and generator both work at full capacity, the remaining apparent power must be provided by the ESS. So an 8000 kVA inverter (or lower) would be sufficient to satisfy this load requirement (per switchboard).

Region A & C do not pose an issue to the ESS. In this failure condition, the remaining capacity would be able to handle the power requirement. In region D, despite having lost a generator, the remaining generator capacity is capable of compensating for the apparent power, while the active power above the 2nd engines limit is supplied by the ESS.

 Note: Up-scaled figures for all scenarios are attached in Appendix A for closer inspection

⁵Downsizing the inverters is possible to the point which the kVA capacity will still be able to sustain position keeping- however the pipe-pull will have to be terminated mid-way if the vessel is engaged in the operation. For sizing characteristics, refer to Chapter 4

3.8. Implications on ESS

Vessel loads & power peaks

- It is observed that the moving average DP load during pipe-laying is usually within one or two of the engines output capacity (Figure 3.5) which means that a single engine failure criteria is sufficient to ensure that the station keeping abilities are maintained.
- The correlations suggests that the power peak profile is a combination of the moving average DP load, ground-speed induced DP load and the pipe tension compensating action of the tensioners during a pull.
- If the ESS were to supply the power demand during these peaks, the maximum allowable limit would be set by the manufacturer of the ESS. This limit would allow the battery to be cycled in an unlimited way so long as the C-rates are kept within this constraint. Typically, for medium power air-cooled batteries, this limit is 1.5C [17].
- In order to ensure that the anomalous power peaks are handled by the ESS as one-off events, the inverter sizing must be such that it allows a full engines power rating to be extracted from the ESS (i.e., 5,650 kW of electrical power output) per switchboard.

Electrical health analysis & Failure scenarios

- It is observed that the vessel has a mean power factor of 0.55 based on the measurements logged on the vessel. This results in high line currents at the generator output. The maximum allowable line current is calculated to be 465A notwithstanding the overload and short-circuit limits.
- For this study, an assumption is made that the vessel operates on a 0.8 power factor during DP operations. This assumption is made in light of uncertainty in regard to future vessel upgrades pertaining to new drives, electromotors and/or power factor correction equipment.

Power factor=0.5

- In the scenario of low power factor, it is observed that in the event of a single engine failure, the battery inverter must be oversized or power factor compensation must be present to prevent a potential loss of DP capability.
- Alternatively, a battery inverter rated to the same as the existing generators (8000 kVA) must be capable of handling an overload for a few minutes without causing the inverter to trip (per switchboard).

Power factor=0.8

- In the scenario that the vessel operates with a 0.8 power factor, the battery inverters can be sized such that 7000 kVA is available for each switchboard. This will allow 5650 KW of electrical power output for spinning reserve, power surges caused due to pipe-pulls and anomalous power peaks.
-

4

Conceptual baseline battery design

4.1. Overview

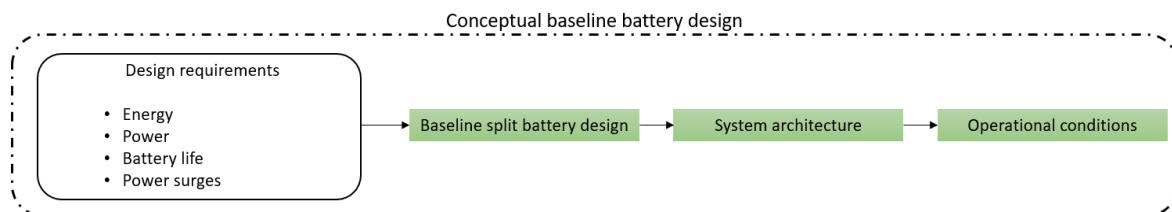


Figure 4.1: Battery design steps

Based on the findings made in Chapters 1-3, implications of the vessel characteristics and pipe-laying operations on the energy storage system were analysed. The energy storage system can be split into the battery and the power conversion components. Design requirements of energy, power, battery life and power surges dictate the battery sizing while the operational characteristics affect the remaining system architecture. For this case study, a 5C discharge rate battery is considered.

4.2. Design requirements

The design requirements are dependent on the following four primary parameters:

- Energy
- Power
- Battery life
- Power surges

4.2.1. Energy

The basis of the battery design is to ensure that there exists a spinning reserve in event that an engine fails during DP operations. This means that the nominal power to be delivered by the energy storage system should be $5,650kW$ in line with the rating of the engine. The time that this power must be delivered is dependent on the new generator start-up time of 48 seconds. However, if the generator fails to synchronise with the grid, a secondary generator start-up is initiated by the power management system. Additionally, it must be noted that the new generator start-up would only be initiated once a failure is detected and it begins to affect the power production capabilities of the vessel. The total bridging time of 3 minutes (180 seconds) is deemed to be appropriate in order to ensure enough redundancy in the scenarios outlined and a safety margin.

Based on the aforementioned deductions on the energy requirement for the bridging time the battery size for the spinning reserve can be calculated as:

$$E_{ef} = P_{nom} \times \frac{t_1}{t_2} [\text{kWh}] \quad (4.1)$$

Where: E_{ef} : Effective energy required [kWh]
 t_1 : Bridging time [s]
 t_2 : Number of seconds in one hour [s]

$$5650 \text{ kW} \times \frac{180}{3600} = 282.5 [\text{kWh}] \quad (4.2)$$

4.2.2. Power

This energy can only be extracted at a discharge rate of 20C from a battery. Few commercial batteries exist with such capabilities, however they have poor cycle & calendar life characteristics. Hence, another aspect that has to be taken into account for sizing are the C-rates¹ of the available battery, end of life (EOL) capacity and reduction in capacity due to high discharge rates. The typical batteries available commercially for maritime applications range between discharge rates of 1C-10C. For this case study, a battery of the discharge rate of 5C is being considered as this offers a good balance between high energy density and high power. Therefore, the sizing requirements are dominated by the power production requirements. This capability must be met even at the end of life (EOL) of the battery which is taken to be when the battery capacity degrades to 80% of the newly installed capacity. Additionally, the battery must not be depleted below the 20% SoC (State of charge). Taking these requirements into account, the new energy requirement based on power as a limiting constraint can be calculated as:

$$E_{sp} = P_{nom} \times \frac{1[h]}{C - rate \times p_1} \quad (4.3)$$

Where: E_{sp} : Spinning reserve energy [kWh]
 p_1 : EOL parameter=0.8 [-]
 $C - rate$: 5C [-]

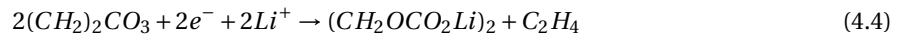
The calculated power requirement in this case is found to be 1412 kWh. This ensures that at end of life (EOL), the remaining capacity of the battery is 1130 kWh. This ensures that the power requirement is satisfied even at EOL.

4.2.3. Battery life

Calendar life

$$L_{cal} = f_t(\bar{\sigma}, \bar{T}_c, t)$$

Calendar ageing is a phenomenon caused by the battery not being used i.e., when the battery is not undergoing charging or discharging. In this situation, the lithium ions begin to react with the electrode to produce irreversible chemical compounds called Solid Electrolyte Interfaces (SEI's). As the SEI grows larger over time, it begins to degrade the battery. The chemical equation is represented as [12]:



The model by Bolun Xu [49] considers a model with the SOC (State of charge($\bar{\sigma}$)) and the Temperature effects on a Lithium ion NMC type batteries. The results clearly show that maintaining the battery at an elevated temperature has a more detrimental effect on the battery degradation than the SOC (Figure 4.2). From a practical perspective this would mean that the battery room in a vessel would have to have ambient temperature control & measurements at the cells to ensure it does not heat up during operation or otherwise. It is evident that by maintaining the battery at a low SOC, the calendar life of the Lithium-ion cells can be prolonged well past the manufacturer prescribed calendar life².

¹The C-rate of the battery is the discharge rate of a battery. For example, a 100 Ah battery discharges at a nominal rate of 1C would imply that the battery is fully discharged in 1 hour while it can be discharged in 30 minutes if the current drawn from it is 50 amperes. However, in reality the time taken would be around 25 minutes due to a reduction in capacity at higher than nominal discharge rates

²This varies from manufacturer to manufacturer but is usually quoted as 10-15 years- although in reality the battery would last longer than the prescribed time provided it is operated under a low SoC & reasonably low temperatures

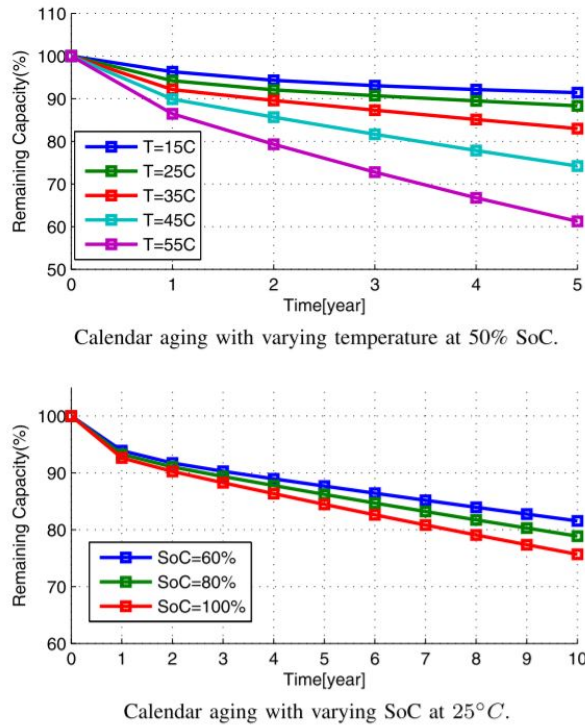


Figure 4.2: Battery life vs temperature & SOC[49]

Cycle life

$$L_{cyc} = f_t(\text{charge - discharge cycles}, DoD, C - \text{rate})$$

Cycle ageing of batteries refers to the degradation of the batteries due to the charge and discharge cycles it undergoes. It has a strong dependence on the depth of discharge (DoD) and number of iterations of charging & discharging (Figure 4.3). The C-rate experienced by the battery also affects the cycle life of the battery although, to a lower extent than the DoD. The battery will be able to throughput lower cycles if the battery is discharged to a greater extent. For example, for a spinning reserve situation (either an failure or test situation), this would mean a deep discharge, however, such a situation is not common. During combating the power surges, the battery will undergo several smaller cycles which the battery will be able to sustain for an exponentially longer period of time.

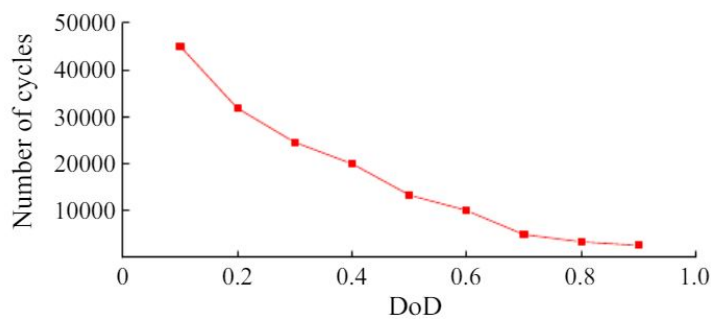


Figure 4.3: Cycle life vs. DoD[44]

4.2.4. Power surges

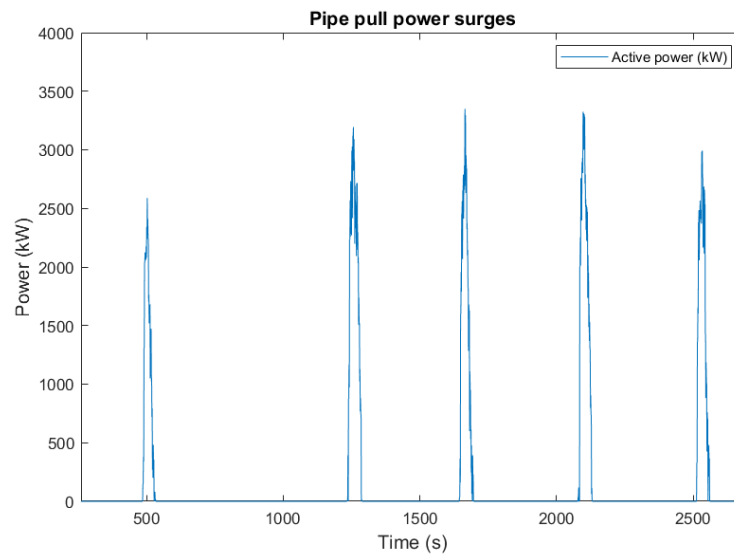


Figure 4.4: Power surges

Figure 4.4 shows the typical magnitude of the power peaks above the capacity of the engines. Based on the data analysis, the magnitude of these peaks are in the order 1.5-4 MW depending on the weather. Typically each thruster consumes between 0.5-1.5MW of power for position keeping which means the total DP load on the switchboard amounts to 2.5-7.5 MW (5 thrusters). The remaining load is the ancillary component. From this it can be deduced that to the original battery sizing calculated at 1412 kWh, an additional reserve of 120 kWh for the power surge can be incorporated. Approximately 100 kWh corresponds maximum energy required per power peak of 4 MW.³

4.3. Baseline split battery design

Now that the battery sizing has been calculated, the architecture of the system can be arranged in a new novel way to maximise the calendar life of the battery by maintaining it at a low SoC. As the battery is essentially a collection of cells, they may be split up and reorganised in a different way to achieve the necessary objectives. Two battery units can be used to supplement the power surging on a single switchboard while allowing an interconnection of a tertiary battery unit from the other switchboard in the event of a failure. This means that the energy between the units need only be shared in the event of a failure. Due to the inherently poor calendar life of high power batteries, this arrangement allows the use of higher power batteries which can share the energy for spinning reserve. Maintaining a low SoC on high power batteries can maximise its calendar life without compromising on performance with this system architecture. Additionally, such an arrangement allows the inverter to be sized smaller.

The schematic of this design is depicted in Figure 4.5. This design will be referred as the 'split-battery' design. Figure 4.6 shows the ranges within which the split battery units can be operated. This architecture enables the individual units to be maintained at a relatively low SoC than a dual battery arrangement by allowing 3 individual units to share the energy requirement in the event of a failure. Given an operational profile different from a pipelayer and that of a traditional DP vessel, this design has the potential to make a 33% reduction in battery size.

³During the supply of power for the power surges, a manufacturer prescribed 1.5C discharge limit is advisable for continuous charge-discharge operation of the battery. Hence with a 1532 kWh battery a maximum allowable peak size can be calculated as $1.5 \times 1532 \text{ kWh}$. This signifies that peaks upto 2.35MW and 1.87MW at EOL can be supplied by the battery. The EOL power surge handling can be improved to match the newly installed capabilities using better cooling technologies. This aspect is out of the scope of this research study. Additionally, rather than installing new cooling systems- the battery sizing could be augmented by 300kWh later in its operational life

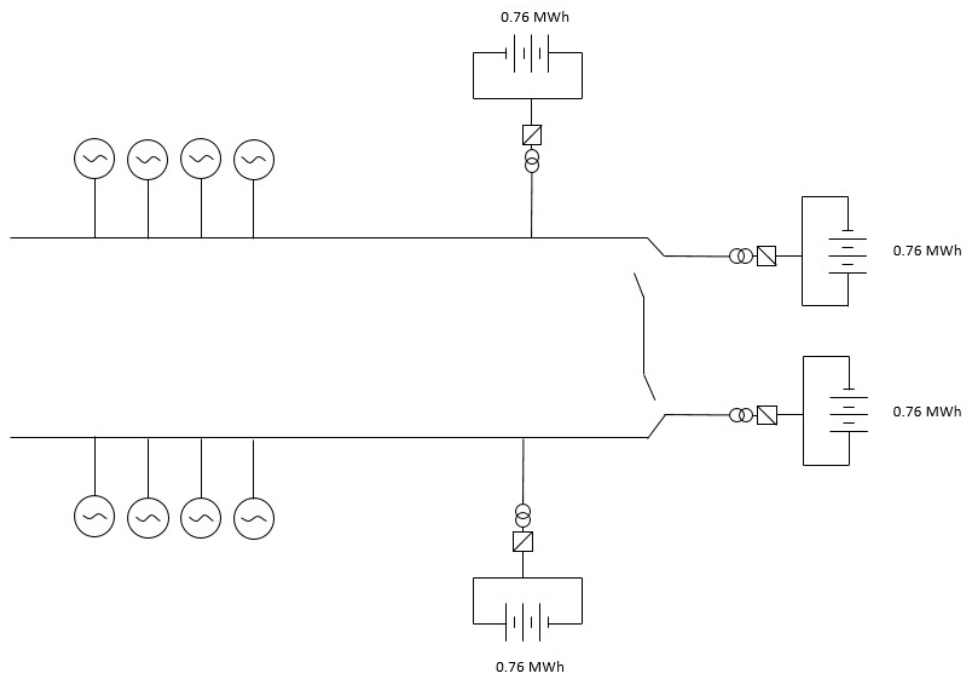


Figure 4.5: Split battery design

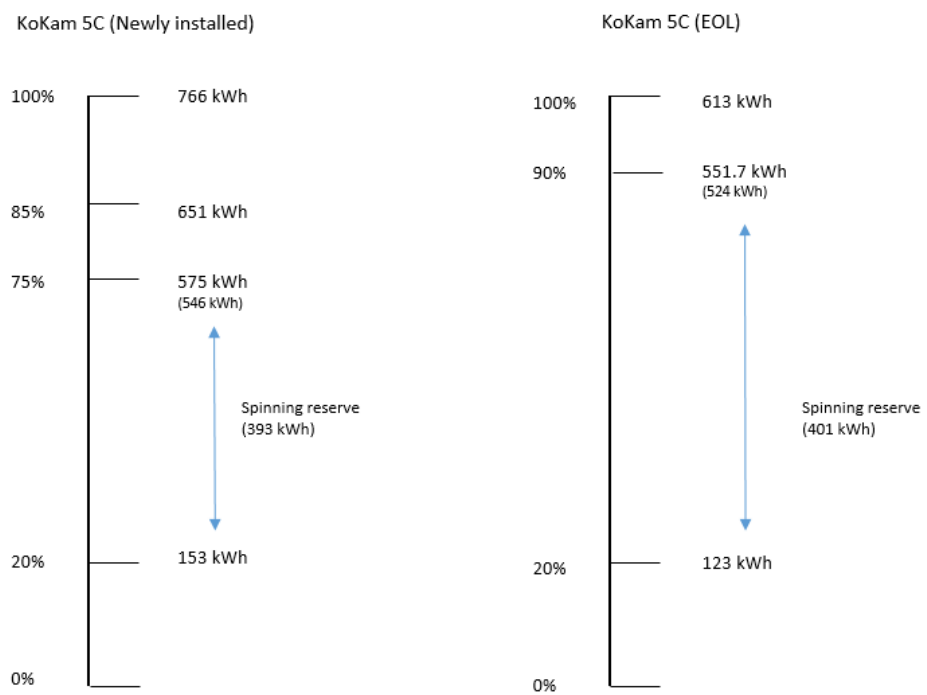


Figure 4.6: Split battery sizing (4X units)

4.4. System architecture

Cells & Module characteristics

The selection of the Lithium-ion battery has been made to demonstrate an example of a battery with a balance of high energy & high power. Following are the Kokam 5C (100Ah) cell & module characteristics:

Table 4.1: Li-ion cell & module characteristics

Characteristics	
Pouch cell capacity	100 Ah
Maximum cell Voltage	4.2 V
Minimum cell voltage	2.7 V
Nominal cell voltage	3.7 V
C-rate (Continuous)	5C
Peak C-rate (10 sec)	6C
Energy per cell	0.37 kWh
No of cells in module	14
Module Nominal voltage	51.8 V
Energy per module	5.18 kWh

Strings & racking arrangement

For the purposes of power conversion, the modules must be arranged such that the appropriate DC voltage is created to build a rack of Lithium ion modules. In this case, the desired DC input voltage is determined to be 1139V based on the requirement to have sufficient redundancy for the racks in case of an individual rack failure. Moreover, this value is chosen as commercial converters have a DC input of a maximum value of 1500V DC. The nominal operating range of the converters are 875V-1300V, hence at the peak charge of the Li-ion cell of 4.2V, the DC voltage is 1298V DC which is still within the nominal range.

Table 4.2: Battery string & rack characteristics

Characteristics (Per unit)	
Desired DC voltage	1139 V
Modules in series	22
Capacity (per rack)	113.95 kWh
Total installed capacity	766 kWh
Number of strings	7
Total number of Lithium-ion cells	2156

Power conversion: Converters & Transformers

For the purposes of power conversion, decisions have to be made on the sizing based on the size of the power peaks desired to be handled by the battery. The power peaks to be handled by the battery must fall within the range of 0.1-1.5C of the installed capacity for continuous charging and discharging during power surges [4]. This must be true even at the end of life of the battery. A 2298 kW limit on power surge peak value allowance ensures that the average C-rate is kept under 1.5C. This means that if an engine failure were to occur during a pipe pull, the required output for station keeping would still only be 5650 kW at maximum. To satisfy this power demand during a worst case scenario of a failure, a 3500 kVA ($\cos\phi = 0.8$)⁴ converter *per* battery unit would ensure that three such units of the split system would satisfy the worst case power demand.

Table 4.3: Converter & Transformer information

Characteristics (Per unit)	
Converters required	1 per unit
Assumed grid power factor	0.8 lagging
Desired power surge limit	2298 kW
Converter rating	3500 kVA
Voltage range for nominal power	875 V-1300 V

⁴For 0.55 PF, the inverter would have to be sized to approximately 4.8 MVA each

System Layout

Based on this conceptual design, the system layout can be visualised below: (per switchboard)

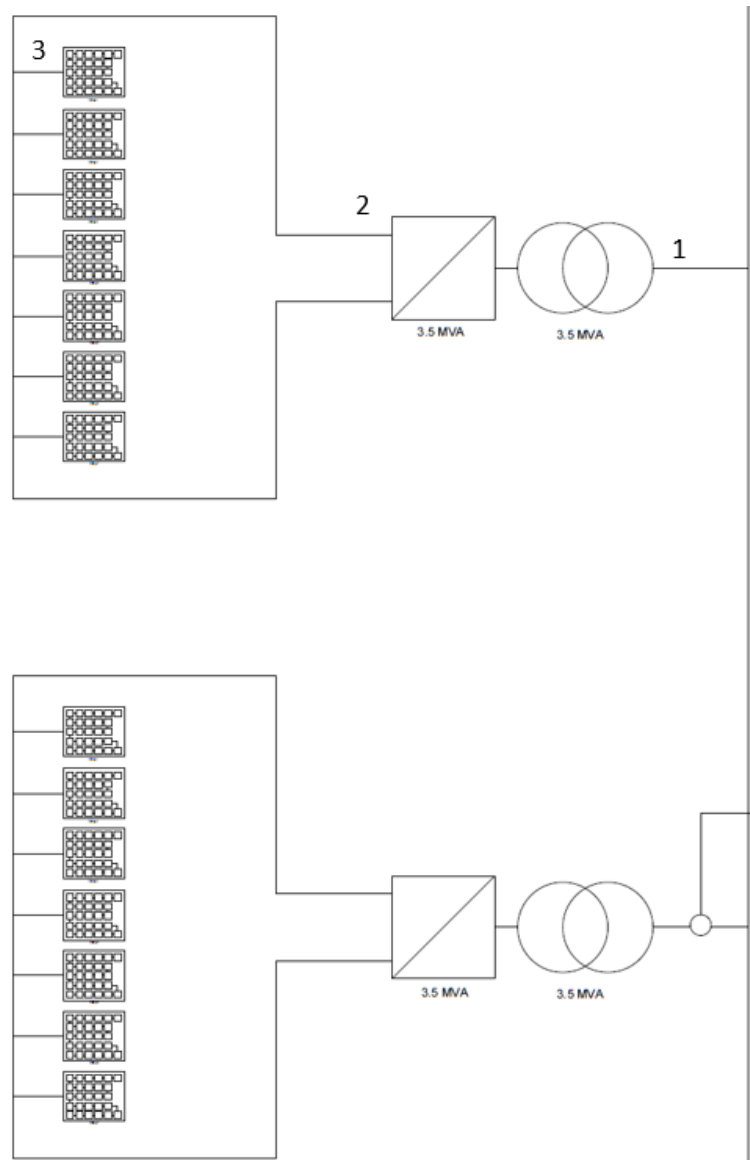


Figure 4.7: Split battery system layout

The calculations for the currents in the table below is the worst case scenario wherein the vessel engages in a pipe pull and the generator set fails in the power surge shaving mode. The vessels protection will ensure that the thrusters are phased back to prevent a blackout and the station keeping load requirements only will be used up from the ESS. Table 4.4 shows the currents when the two units are online and Table 4.5 shows the system currents once the tertiary unit has connected to the switchboard where the failure has occurred. In both cases the minimum voltage of 1010 V has been considered as this causes the maximum current.

Region	Voltage	Current
1	10000 V	$I_{line} = 203 A$
2	1010 V	2825 A
3	1010 V	404 A

Table 4.4: Twin units engaged

Region	Voltage	Current
1	10000 V	$I_{line} = 136 A$
2	1010 V	1883 A
3	1010 V	269 A

Table 4.5: Three units engaged

4.5. Operational conditions

Power surge mode

In the power surge shaving mode, two units of the split architecture are independently connected to each switchboard (Figure 4.8). As each unit is 766 kWh, they are capable of ideally handling power peaks in the order of 2298 kW (within 1.5C of the battery). Larger power peaks can be handled by the battery but it is not recommended to cycle the battery at higher C-rates often. Typically, a 2-3 MW peak would cause a 1-2% DoD which means that an allowance of 2% DoD can be made before the battery is recharged after a power peak. The minimum SoC that each of the split units can be maintained at to still ensure 3-minutes of spinning reserve is at SoC= 35%.

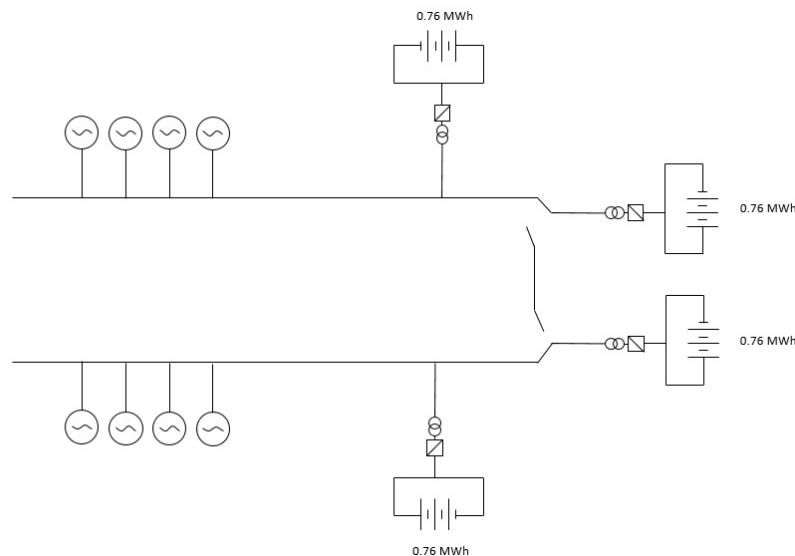


Figure 4.8: Power surge mode

Spinning reserve mode

In the event of an engine failure on either of the switchboards, three units will connect to that switchboard (Figure 4.9). This ensures that there is an availability of 3 minutes of support to the switchboard to start a new engine.

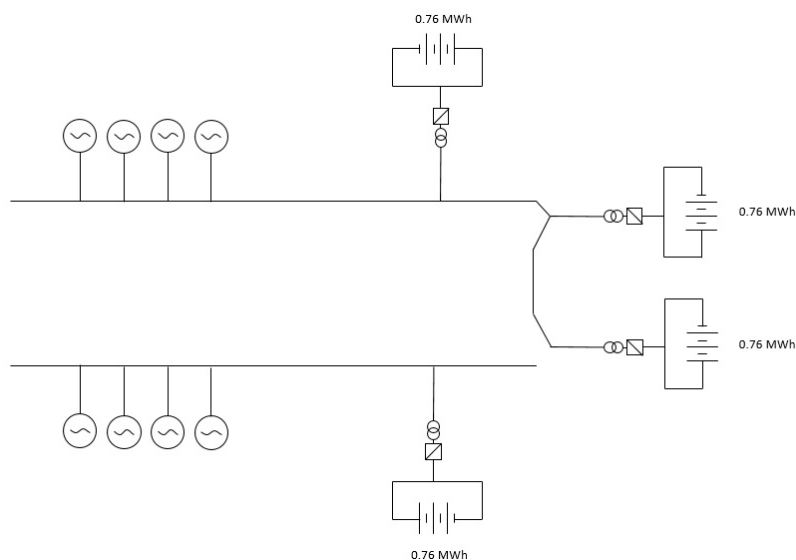


Figure 4.9: Spinning reserve mode

5

Power management system integration

For the implementation of an energy storage system on the Solitaire, it is important to develop a method in which such a system would be integrated into the power management system of the vessel. This chapter reviews the existing system which the vessel uses to ensure that the vessel has a level of redundancy in the case of a single engine failure. Following which, a new set of elements are designed to be integrated into the existing PMS which will allow an ESS to operate. Simulations are conducted on Simulink® to verify the fidelity of the algorithm by measuring key performance indicators (KPI's) as cycle life, C-rates, depth of discharge for the battery and the fuel and running hour measurements in different operational conditions.

5.1. Existing rule based system

To match the power demand of the vessel, the power management system of the vessel has a rule based generator start stop sequence (Table 5.1). The settings prescribed by these rules are based on experience and can be changed based on operational conditions manually. For example, if the vessel has a power demand at 7400 kW with two engines supporting the load, the system does not engage another engine to start but if the load were to increase to 7900 kW for a period of over 25 seconds then the PMS automatically initiates the start-up of the third diesel engine. The time taken to start up this engine and synchronise it to the grid takes it approximately 48 seconds. If the synchronisation fails- a new MDG start-up is initiated. Similarly, for an engine shutdown procedure, the PMS monitors whether the load has dropped to below the stop limit for the past 24 minutes. If so, then a generator shutdown is initiated.

Table 5.1: Current load dependent start limits for the M/V *Solitaire*

MDG's*	$P_{nom}(kW)$	LSL (kW)	Delay time	HSL (kW)	Delay time	Stop limit [kW]	Delay time (min)
1	5200	3900	25s	4160	2s	-	-
2	10400	7800	25s	8320	2s	4160	24
3	15600	11700	25s	13260	2s	8286	24
4	20800	-	-	-	-	12480	24

*The new generator capacity of 5200 kW is considered here (Section 2.3.3)

DP III regulations as stated in Section 2.4 requires that the vessel needs to have redundancy in case of a generator failure. Which means that if ' n ' generators are require to satisfy the load, then $(n + 1)$ generators must be available. Observing the data recorded on 27/09/18 (Figure 5.1), it can be seen that despite the load conditions not necessitating an additional generator to be turned on, the DP operator on board the vessel initiates a generator start-up. So in this case there seems to be $(n + 2)$ generators running during some portions of the day. The reasons for this are due to the power factor issues which warrant additional generators to keep running to satisfy the reactive power requirement as found in Chapter 3-these starts are manually initiated.

Figure 5.1 shows that available capacity (displayed by the blue line) at all times is maintained above the power demand such that should a failure were to occur, it would not cause the vessel to lose position or cause a blackout. The day is characterised by a waiting on weather condition followed by a pipeline recovery from the seabed. Once this is completed, the pipelaying operations begin at about 18:00. The vessel does not

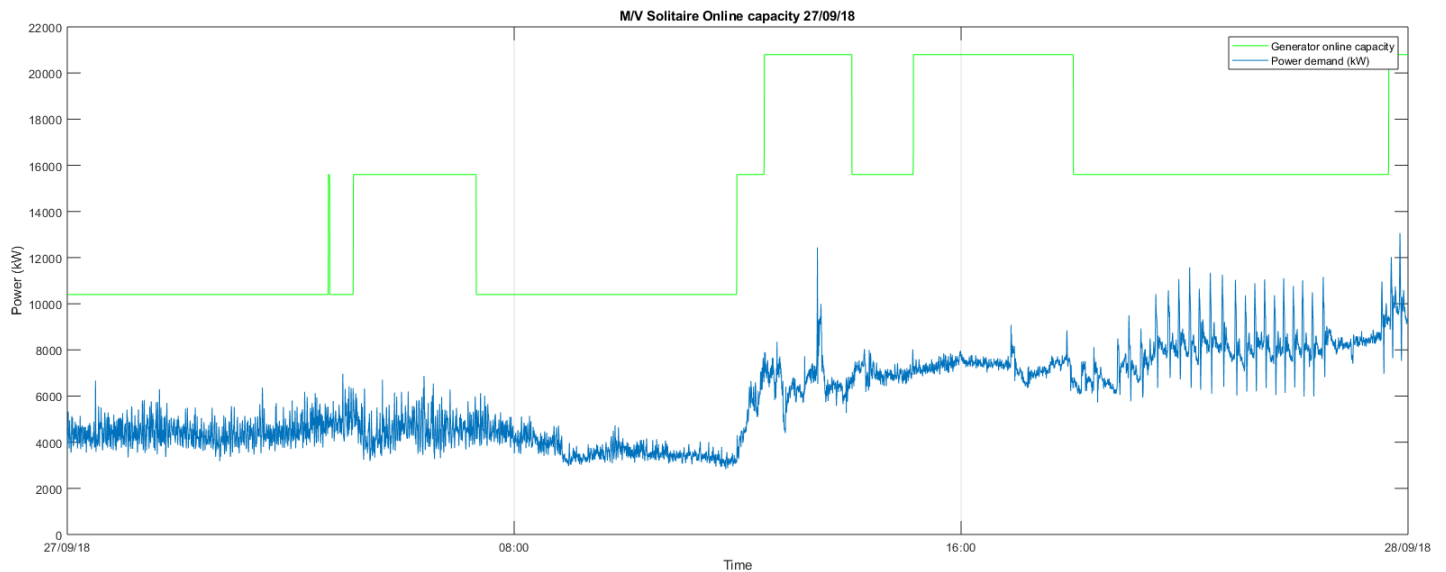


Figure 5.1: Vessel online capacity

appear to be following the prescribed rule-based start-stop system as there is a lot of manual control involved. The reason for this is not very clear. During pipe-laying operations, the reasoning for the manual starts are that the currents induced are large due to the excessive reactive power in the network.

5.2. Overview

Based on the requirements, a new PMS decision making process has to be developed and tested. During the testing phase, the viability of the system will have to be compared against the pre-existing system through the use of key performance indicators.

PMS Requirements

1. Ensure that the additional generator can be turned off for more efficient operations with the ESS acting as the backup power supply
2. The new PMS can make decisions about generator start-stops based on the following characteristics of the power peaks
 - Magnitude and Frequency of the power surges
 - State of charge and runtime of the battery

Key Performance indicators

To test if the battery and power management system design are appropriate, performance indicators will have to be used to measure and compare their performances. They are classified into three types of indicators:

1. Vessel parameters: Fuel consumption, Running hours, Emissions
2. Battery measures: Cycle life, DoD, C-rates
3. Feasibility: Investment costs

Model Structure

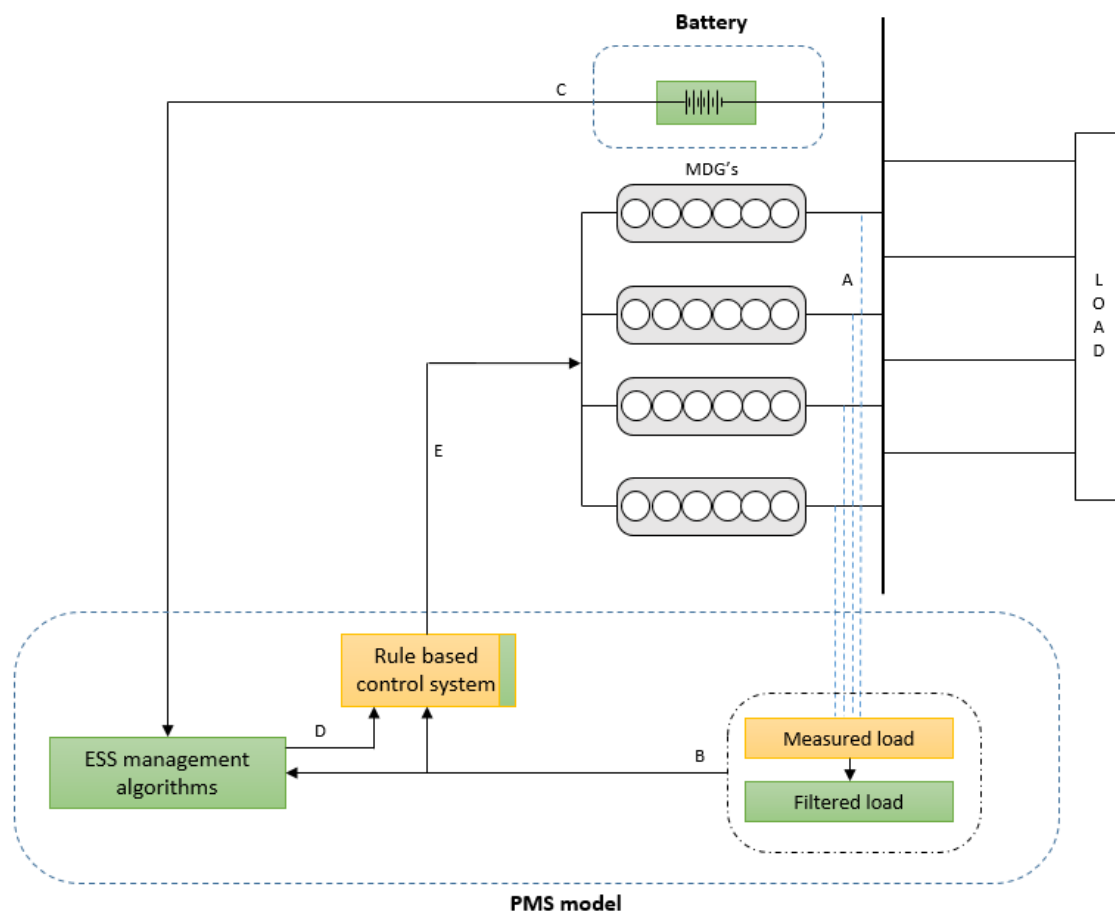


Figure 5.2: Model structure

Figure 5.2 depicts the structure of the model which consists of the PMS model and the battery. The green blocks are the new elements developed in this research study to allow the battery to be integrated into the vessel. Additional to the new elements, the old table based start-stop system would have to be updated in order to integrate it with the new elements.

The signals transferred between the blocks are summarised as:

- A. Total measured active power (kW)
- B. Moving average filtered load (kW)
- C. Battery Current (A), Voltage (V), Power (kW) and SoC (%)
- D. Binary signal [Trigger=On/Off]
- E. Generator online capacity command

As the generators are running, the output is regarded as the power demand as the generators match whatever the powering requirement is from the load side. In the current PMS of the *Solitaire*, the load is measured and is intended to follow the load dependent start-stop sequence (Table 5.1). For example, if the load were to exceed the lower start limit for 25 seconds, a new generator would start up. In the new model, this measured load is filtered out using a moving average filter with a 900 second time window and this load is used instead to determine generator start-stops. The highly variant loads are allowed to be absorbed by the battery. As the battery absorbs the highly variant loads, the battery monitoring algorithm monitors the usage of the battery and makes decisions on whether it is appropriate to start a new generator or not.

5.3. Battery

5.3.1. Types of battery models

There exists different levels of modelling of batteries depending on the purpose of the model. Maheshwari [32] summarises the developments in mathematical models of batteries developed in the last years (Figure 5.3).

The simplest model is the Empirical model which are regarded as low accuracy models. Linear, polynomial, exponential or other commonly used functions are used to fit the experimental data directly to obtain the parameters for the model. The simplicity of the model allows one to rapidly develop them and test them in simulations as they are computationally non-intensive. The uses of empirical models are to test it on real world applications such as power management, battery management systems etc. Their extrapolation from the usual operational conditions is poor.

The next two levels of modelling are the single particle model (SPM) and the pseudo two dimensional model (P2D). These models take into account the kinetics and diffusion phenomenon in the electrolyte and the electrodes using partial differential equations [32]. Finite element methods are employed to solve these coupled equations.

The most advanced models are used to simulate the battery response down to the atomic/molecular level. These models are called the Kinetic Monte Carlo (KMC) models and can help predict thermodynamic properties of materials & mobility of lithium inside the crystal structure [32].

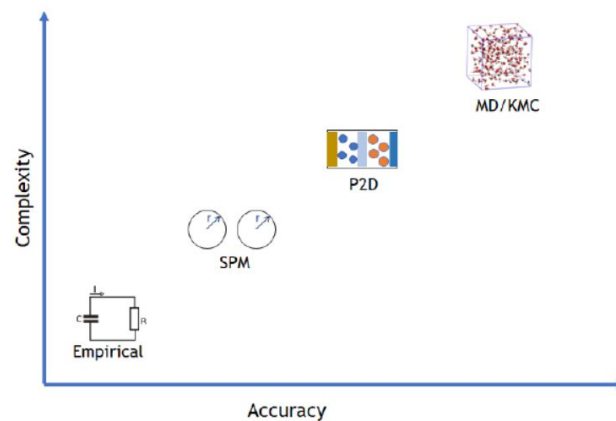


Figure 5.3: Types of battery models[32]

Table 5.2: Battery model types & applicability

Battery models	Description	Purposes
1. Empirical model	Simple but not as the most accurate	Real world applications for BMS/PMS
2. Single particle model (SPM)	Models kinetics and diffusion (use of FEM)	Works well for modelling low current & thin electrode type cells
3. Pseudo two dimensional model (P2D)	Models kinetics and electrolyte & solid electrode diffusion (use of FEM)	More accurate than SPM. Computationally intensive.
4. Kinetic Monte Carlo model(KMC)	Simulation at the molecular level	Restricted to studying one specific process taking place in over a fraction of a second

Model selection

The SPM model is not relevant as it is more suited to the study of thinner electrodes and low current conditions. KMC and P2D models are used to analyse specific processes within the lithium-ion cell and are not suited to fast applications such as BMS/PMS testing as they are inherently computationally intensive. A typical empirical model works on the principle of an equivalent circuit but faces some issues with accuracy. The reason for the lack of accuracy with time is due to the effects of current integration. Current integration is

the method used to determine the energy discharged from the Li-ion cell and determine the SoC. With time the errors accumulate and the accuracy drops. To alleviate this problem, a method prescribed by Huria T & Jackey is being used to build an empirical model. In this model the effect of current integration is minimised by using Open Circuit Voltage (OCV) values of the cell at different SoC's and temperatures. This means that the current integration only has to be done for short durations after which the cell voltage is updated periodically with its OCV at that SoC. For the current application of use in the PMS, this improved version of a traditional empirical model is deemed to be the relevant choice for analysis.

The analysis involves using the parameter estimation methods developed by Huria T & Jackey combined with the datasheet information from KoKam. The data is extracted from the datasheet and the parameters are determined to develop a working model of the battery. In this study, the improved empirical model of Huria T & Jackey will be used.

5.3.2. Empirical model

Electrical model with thermal dependence

The model prescribed in the analysis is based on Huria T & Jackey [25]. The model is built using an equivalent circuit model (ECM) as it is the most common approach for battery numerical analysis. The complexity of such a model can be built up using several RC branches. For lead acid batteries, due to parasitic discharge effects the model must include a parasitic branch. However, for the Lithium-ion type batteries, this parasitic effect is not present and hence is not required to be modelled. Additionally, depending on the type of Lithium-ion battery- the decision to choose the number of RC branches must be made. For chemistry's of Lithium Iron Phosphate ($LiFePO_4$), Lithium Titanate ($Li_4Ti_5O_{12}$) and more complex chemistries- multiple RC branches must be used to model it correctly (as in Figure 5.4). In the case of this analysis, the selected battery for analysis is Lithium Nickel Manganese Cobalt Oxide ($LiNiMnCoO_2$ or $Li - NMC$). The model was developed and validated using the NMC chemistry and it was found that using a single RC branch is sufficient.

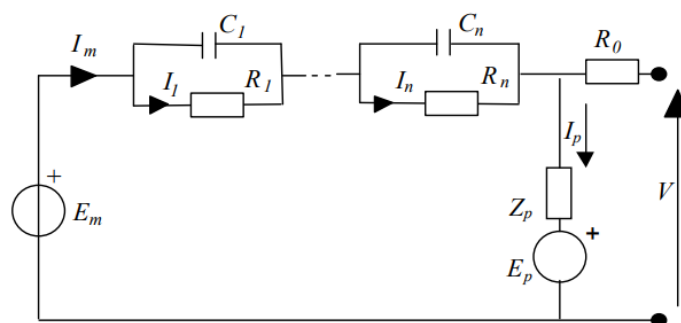


Figure 5.4: General equivalent circuit cell model of an electro-chemical cell [25]

Where:

E_m :	Cell voltage[V]
E_p, Z_p, I_p :	Parasitic branch elements
R_1, C_1, I_1 :	Branch 1 elements
R_n, C_n, I_n :	Branch n elements

According to Huria & Jackey [25], it is sufficient to reduce the general ECM with 'n' RC blocks to an ECM with just a single RC block (Figure 5.5), which is sufficient to account for all dynamic characteristics of the cell including nonlinear open-circuit voltage, average discharge current and inner cell temperature. During the model development, it was found that there exists dependencies between the state of charge and the temperature which were then implemented as lookup tables. An extremely complex equivalent circuit model would fit experimental data well, however, would come at a cost of computational effort. Using more than two RC blocks will not produce any significant improvement in model accuracy.

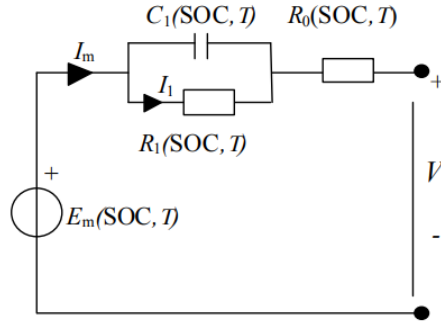


Figure 5.5: Equivalent circuit model with a single RC branch [25]

For short duration of analysis, the cell capacity can be limited to observing the effects if average discharge current, discharge time and inner cell temperature [25].

$$C_q = C_q(I, T) \quad (5.1)$$

$$Q_e(t) = \int_0^t I_m(\tau) d\tau \quad (5.2)$$

Then the state of charge can be given as:

$$SOC = 1 - \frac{Q_e}{C_q} \quad (5.3)$$

Where:

- C_q : Total capacity
- Q_e : Extracted charge
- τ : Time(s)
- T : Temperature(K)
- I_m : Current in main branch (A)

Most models in literature determine the SOC based on the ‘Coulomb counting’ method outlined- this is usually inaccurate as time progresses as the errors build up. This model designed by Hurian & Jackey [25] alleviate that issue by periodically compensating this error using an SOC-OCV (open circuit voltage) correlation curve.

Datasheet battery & Parametrisation

To parametrise the model to simulate a real battery, the discharge curves of the KoKam 5C battery were obtained from the datasheet (See Appendix B). The discharge curves were present for a nominal discharge rate of 0.5C for a range of different temperatures which enabled the battery to be modelled from -20°C to 55°C. However, during parametrisation, the inclusion of very low temperatures for the parameter estimation led to incorrect results to be obtained so these datasets were excluded for further analysis. The problem of simulating Li-ion at very low temperatures have been investigated by Ji et al [26] which shows that model estimations at high discharge rates for sub-zero temperatures. Since the interest in this case is room temperature i.e., 25°C, this has been pursued for the modelling purposes.

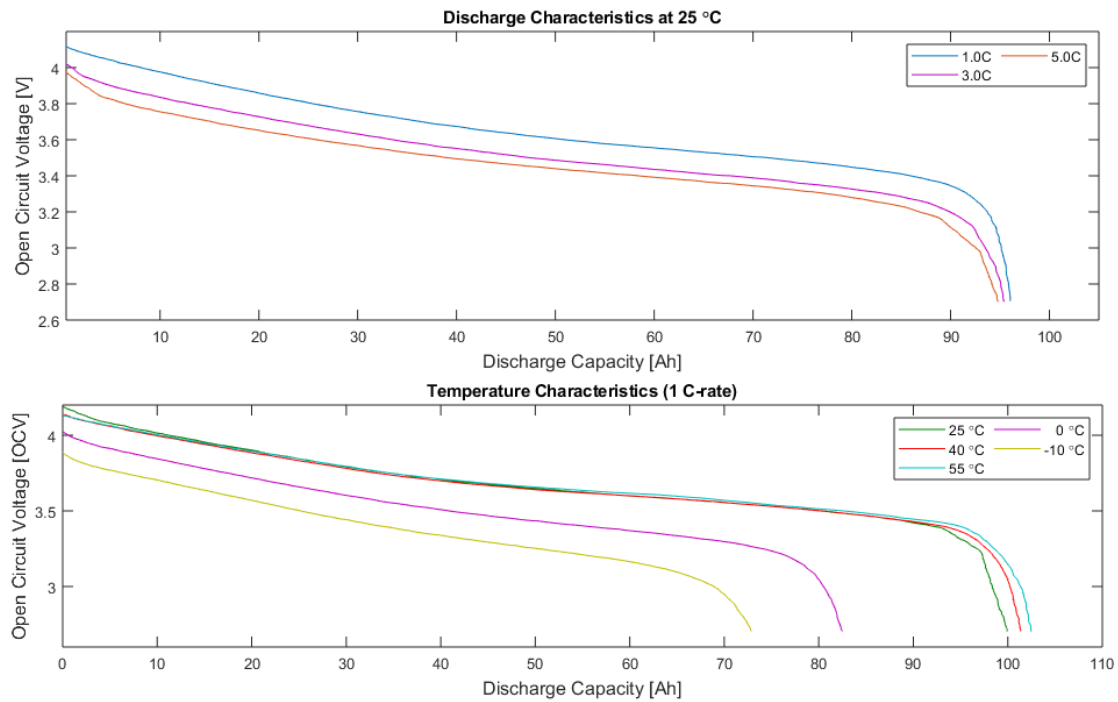


Figure 5.6: KoKam 5C datasheet discharge curves

In the Figure 5.6 the discharge characteristics of the Li-ion cell at 25°C temperature and different discharge rates ranging from 0.5C (i.e., 50A) to 5C (i.e., 500A) are shown. The second subfigure shows the discharge characteristics of the same cell discharged at 1C but at different temperature conditions. Both figures show the voltage drop as the cell is discharged. The relative capacity is shown on the x-axis. It is interesting to note that during high discharge rates i.e., 5C, the relative capacity of the cell reduces by about 5% (from 100Ah to 95Ah). This effect is also seen as a result of low temperatures wherein the Li-ion cell has significantly lower capacity available to discharge.

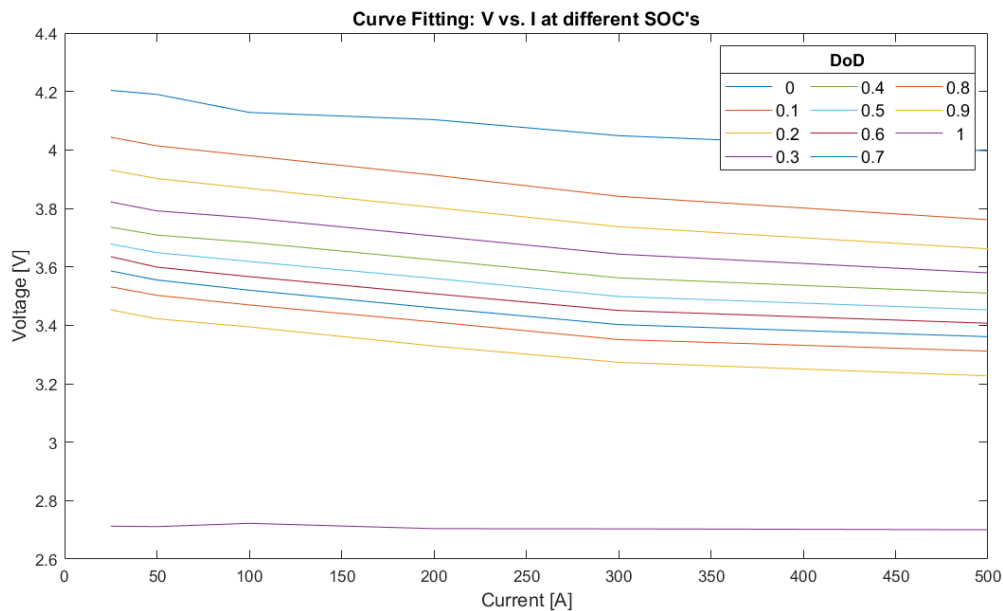


Figure 5.7: SOC-OCV (Open circuit voltage) curves

To alleviate the problems caused by the current integration i.e, Coulomb counting method of calculating remaining capacity of the Li-ion battery, the Figure 5.7 is obtained by noting the cell voltage at different discharge rates at different DoD. The correlation between cell voltage and relative capacity ensures that, for example, if a battery were to be discharged from 100% SoC to 90% SoC, the capacity of the battery would have to be ascertained at 90% SoC for the next discharge event (for low discharge rates, this SoC value would increase to, for example 92%). This will depend on the current integration of the previous cycle i.e., at what discharge rate the battery was discharged at until 90% SoC and what the effective capacity would be available in the next discharge cycle. These curves allow the model to continuously update itself for the errors that would otherwise develop using the Coulomb counting method.

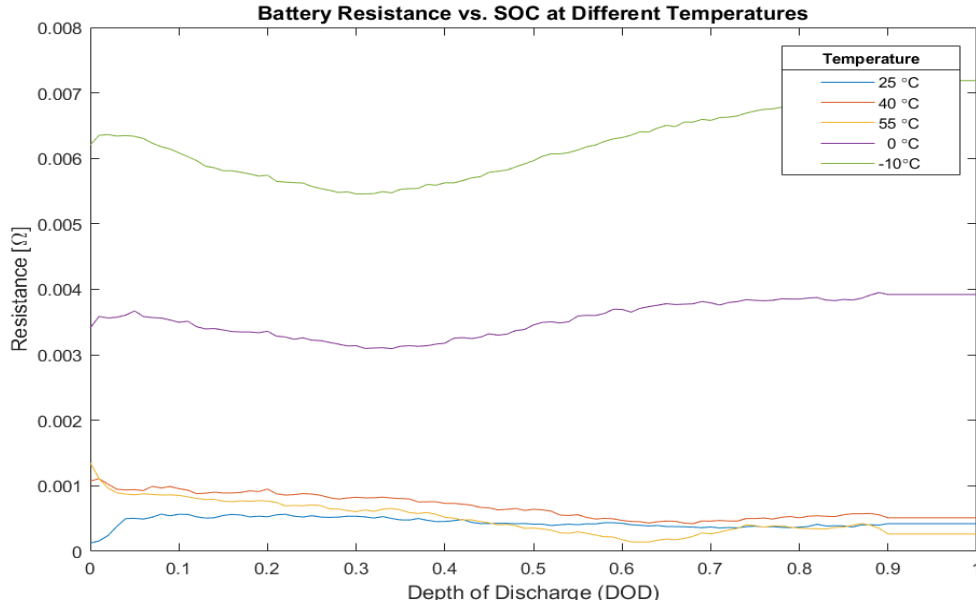


Figure 5.8: Battery resistance at different SoC & temperatures

The resistance is computed by taking 100 unique breakpoints between 0 & 100% SOC as (Ohm's law):

$$R_0 = \frac{\Delta V}{I} = \frac{V_{bkpt1} - V_{bkpt2}}{I} \quad (5.4)$$

Where:

R_0 :	Resistance	Ω
ΔV :	Change in Voltage between breakpoints	V
I :	Current	A

From the Figure 5.8 it can be seen that the battery has lower resistance when the SoC of the battery is in the range of 0.3-0.5. A more significant effect is seen with the battery resistance when the temperature is lowered. Ji et al [26] states that at low temperatures, the operation of Lithium ion is inherently linked to thermal effects wherein increased internal resistance and very strong dependency of kinetic and transport properties can cause significant increase in internal heat generated. The implication that this has on the ESS is that it must be ensured that when the ESS is installed on the vessel, that the ambient temperature of the cell must be maintained at room temperature (in this reference case=25°C).

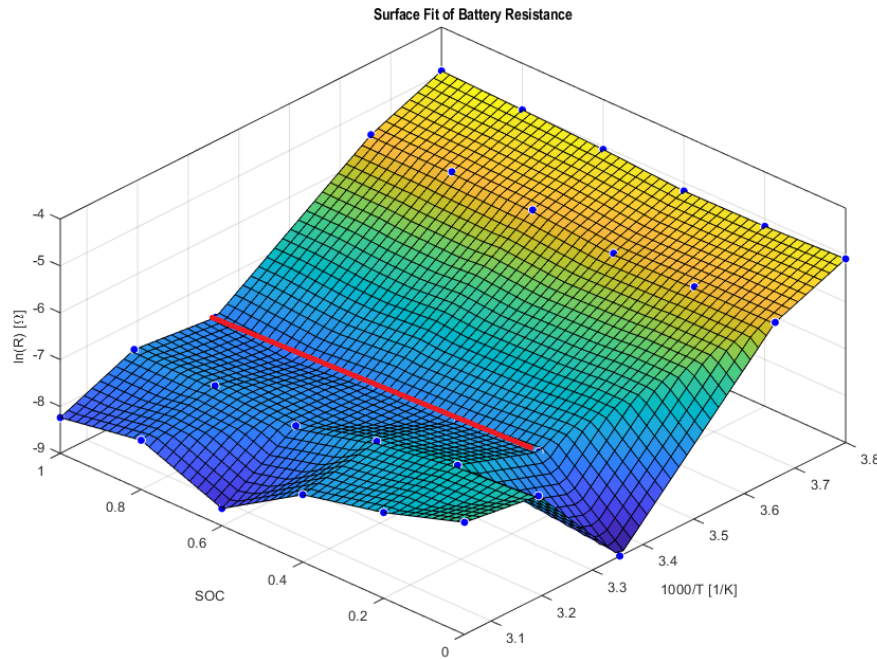


Figure 5.9: Variation of battery resistance with Temperature & SoC

The same procedure is adopted for all the temperature ranges available in order to generate a surface plot showing the variation in resistance with respect to the temperature change and the SoC (Figure 5.9). For further modelling purposes of the power management system, the event of the battery being used at 25 degrees will only be considered, represented along the red line. This assumption is made as the commercial battery systems rarely operate at sub-zero temperatures or even at elevated temperatures such as at 55°C. Commercial battery rooms are outfitted with sufficient HVAC systems to ensure the temperature is maintained at room temperature. The fitting parameters of the curve that must fit the discharge curve are obtained by using a curve fitting function on Matlab which yields the resistance parameters at different temperatures.

$$R_{int} = \begin{pmatrix} 0.000124158 & 0.001072211 & 0.001349884 & 0.003412431 & 0.006206476 \\ 0.000527221 & 0.000952374 & 0.000768588 & 0.003360786 & 0.005743599 \\ 0.000455232 & 0.000732818 & 0.000519449 & 0.003177671 & 0.005627788 \\ 0.000428557 & 0.000472347 & 0.000178489 & 0.003694026 & 0.006317822 \\ 0.000369124 & 0.000510414 & 0.000353655 & 0.00385164 & 0.006786517 \\ 0.000422848 & 0.000511938 & 0.000264812 & 0.003921262 & 0.007188454 \end{pmatrix}$$

$$T_{batt} = (263.15 \quad 273.15 \quad 298.15 \quad 313.15 \quad 328.15)$$

The parameter estimation yields the resistance and the temperature breakpoints which are fed as inputs to the battery model along with other tunable characteristics such as the capacity, open circuit voltage table, cells in series and parallel to build a battery bank. For the baseline case, the cells in series are 308 to build up a voltage of 1139V and the cells in parallel during the power surge shaving mode are 14 units. This is inline with the split battery design wherein only two units are connected to a single switchboard during operation. Only in the situation of a failure will the tertiary unit connect to the switchboard which will then result in 21 units in parallel to be connected.

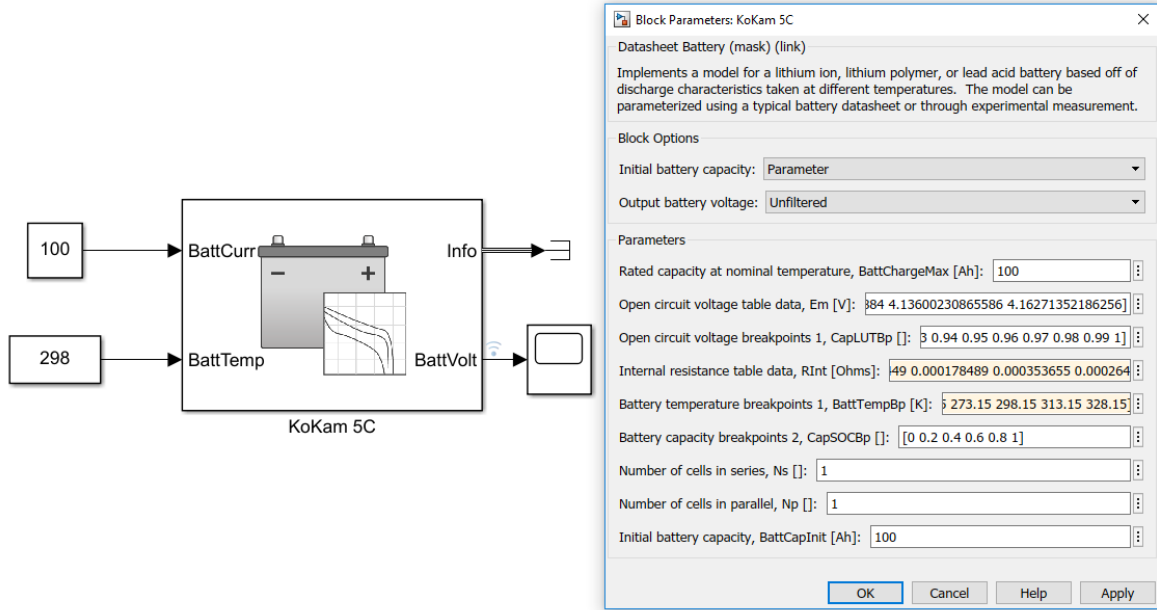


Figure 5.10: Datasheet battery model

During the simulation, the input to the model is the current demand and the output is the battery voltage, state of charge and energy output. For the simulation, the state of charge will be used by the PMS and the corresponding voltage of the battery will be used to determine the current input to the ESS based on the power demand that exceeds the online capacity of the generators.

$$i_{in} \rightarrow \left\{ \begin{array}{l} i_{batt} = \frac{i_{in}}{N_p} \\ V_T = E_m + I_{batt} \cdot R_{int} \\ V_{out} = N_s \cdot V_T \\ SOC = \frac{1}{Cap_{batt}} \int_0^t I_{batt} dt \\ Ld_{Amphr} = \int_0^t I_{batt} dt \end{array} \right\} \rightarrow SOC, V_{out}$$

Where:	i_{in} :	Combined current flowing into the battery network	A
	N_p :	Number of cells in parallel	–
	I_{batt} :	<i>per</i> module battery current	A
	E_m :	Battery open circuit voltage	V
	R_{Int} :	Battery internal resistance	Ω
	V_T :	<i>per</i> module battery voltage	V
	N_s :	Number of cells in series	–
	V_{out} :	Combined voltage of battery network	V
	Cap_{batt} :	Battery capacity	Ah
	Ld_{Amphr} :	Battery energy	Ah

Model Verification

To verify the model, three tests were conducted on the Simulink model. As the cell is a 100Ah cell, tests were conducted at three different C-rates i.e., 1C, 3C, 5C. The voltage drops and runtimes were checked to determine if it accurately represented the battery from the datasheet.

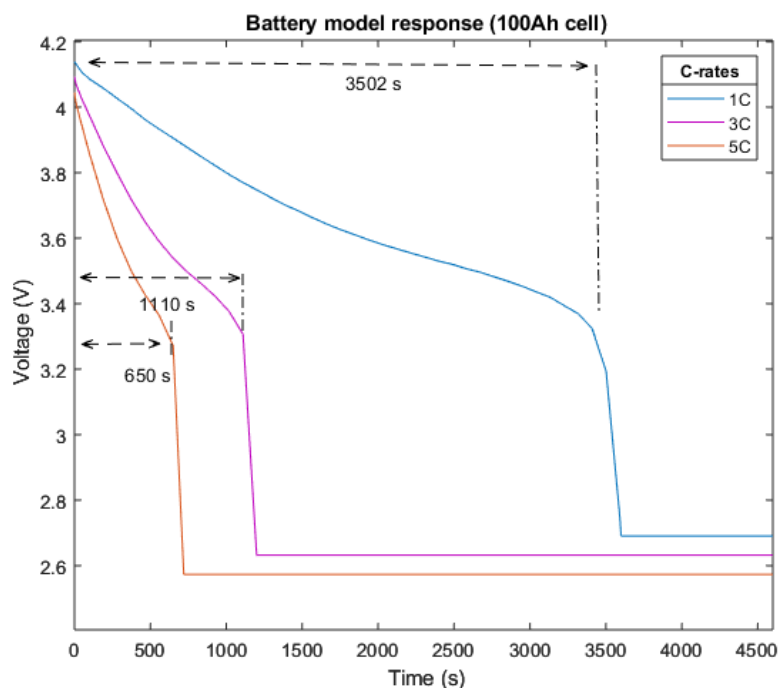


Figure 5.11: Simulink@parametrised battery model response

Figure 5.11 shows that for the nominal discharge rate of 1C the runtime is approximately 3500s which is consistent with a 100Ah cell which should supply 100A for 3600 seconds. Similarly, in the cases of 3C and 5C, the battery runs for the expected timescales. For 5C it would be expected to run for approximately 720 seconds. In this case, the voltage drops rapidly after 650 seconds which is consistent with the discharge curves of the battery wherein the voltage drops off at about 3.2V. The starting voltage drops of the 1C and 3C are consistent with the discharge curves. However, for the 5C case the model suggests a starting voltage slightly over 4V but the discharge curves suggest a voltage slightly under 4V. On testing the same parametrization procedure on another battery dataset (KoKam 20C discharge rate Li-ion cell), it was found that the model does not accurately capture very high discharge rates. As the model is not being tested under the failure condition and only as a part of the PMS integration, this error is deemed acceptable. Furthermore, the runtime for all cases are accurate enough to be used for BMS/PMS purposes. The implications of this initial starting voltage drop error (approx. 0.2V) only has an effect on the discharge current, in this case due to a slightly higher prediction of the cell voltage, the currents experienced by the battery would appear to be lower than according to the datasheet values. This is a trade-off for this model as it is not intended to be tested at 5C and only within the 1-2C range during the power surge operation (Section 4.5).

5.4. Power management system

The power management system consists of the load filtering, rule based start-stop table and battery algorithms. The battery algorithms consist of the peak frequency, magnitude monitoring components as well as the battery state of charge controllers. It must be noted that all the algorithms run in parallel and the decision making of each algorithm is independent. The setting of the trigger variable (either 0 or 1) is dependent on any one of the algorithms causing the variable to activate to a '1' state.

5.4.1. Load filtering

The filtering method employed is a moving average filter. Based on tests conducted with the measured power signals, a window size of 900 seconds was found to capture the moving mean well and ensuring the delay induced is small enough for the battery to handle any eventualities. Normally during pipe-laying operations, the mean value of the load does not fluctuate rapidly which means that the effect of the filter delay is not significant for the battery. The most significant delay seen was in a situation when the vessel switches from a non-DP to DP mode.

$$y(n) = \frac{1}{w} \cdot (x(n) + x(n-1) + \dots + x(n-(w-1))) \quad (5.5)$$

Where:

$y(n)$:	Filtered response	kW
w :	Window size	–
x :	Past observations	kW
n :	1:w	–

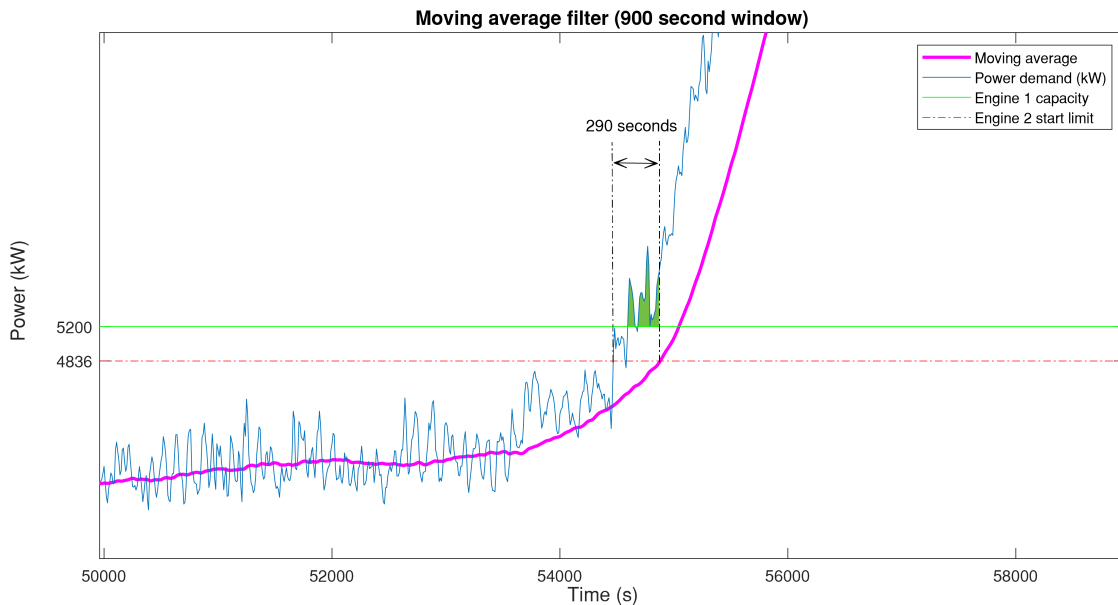


Figure 5.12: Filter delay

The effects of the filter delay in such a scenario (non-DP to DP switching) are of little consequence to the battery as it can be seen from Figure 5.12 that as the start limit for the engine is lower than 100% of the engine's full capacity- the delay in this case is approximately 290 seconds. The region above the start limit is also available to supply the load increase which allows the moving average to 'catch-up' to the actual load. The discharge of the battery is at a relatively low power for a duration that the baseline battery is capable of withstanding. The green-shaded area represents the battery discharge before the start limit is triggered for a new engine start-up by the moving average.

As the battery is designed with power as a constraint, the baseline battery will be able to provide up to 12 minutes of runtime at the nominal rated load (5650kW) under a fully charged condition.

5.4.2. Rule based control system

Table 5.3: Proposed load dependent start limits for the M/V *Solitaire* (per switchboard)

MDG's*	P_{nom}	LSL	Delay time	HSL	Delay time	Stop limit [kW]	Delay time	Trigger
1	5200 kW	4524 kW	5s	4836 kW	2s	-	-	[0,1]
2	10400 kW	9672 kW	5s	9880 kW	2s	4524 kW	24min	[0,1]
3	15600 kW	14508 kW	5s	14820 kW	2s	9672 kW	24min	[0,1]
4	20800 kW	-	-	-	-	14508 kW	24min	[0,1]

*The new generator capacity of 5200 kW is considered here

In contrast to Table 5.1, it can be seen in Table 5.3 that the limits for the start-up have been raised to 0.87-0.93 (of nominal power) from the pre-existing case of 0.7-0.85 (of nominal power). This, coupled with the new method of logging the moving average over a long period of time (filtered power demand) will ensure that the engines will operate at higher partial loads during DP operations. The trigger column would be the new addition to the existing rule based system. In addition to the LSL and HSL conditions, this would be the tertiary 'OR' condition which is controlled by the battery algorithms. This variable is used to notify the PMS that an additional generator must start-up even though the moving average load does not necessitate a generator start up. The instruction given by this variable to the table is dependent on a few other algorithms that will be explored in the following sections.

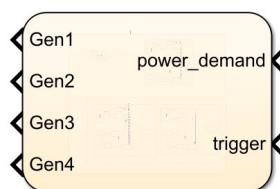


Figure 5.13: Rule based load dependent start-stop sequence

The decision making model receives the filtered active power demand and decides whether it breaches wither the lower or higher start limits. Depending on the scenario, the delay time before a start up of the generator is either 5 seconds or 2 seconds respectively. Additionally, for the generator to be able to fully produce power on the grid, a 48 second delay has been implemented using Stateflow's temporal logic capability which allows time delays to be implemented in the code. This simulates a realistic scenario & works in line with the time domain simulations. The full decision making process for a single generator has been represented in Appendix B. The model includes four such generators running simultaneously as a decision making process in parallel with their individual lower and higher power limit settings according to Table 5.3.

5.4.3. ESS management algorithm A: Peak frequency

The peak frequency algorithm 1 receives the total power '*demand*' which is the sum of the measured power output from the generators and the battery power output. The '*supply*' variable signifies the online capacity available from the generators (i.e., 5200 kW, 10,400 kW,...). Each time the total power demand crosses this supply limit, it means that the vessel experiences a power peak. These instances are counted over a time window (in this case, 900 seconds). If the number of peaks within the time window exceeds the threshold ¹ '*limit*', then the algorithm sets the '*trigger*' variable to '1' which initiates a generator start-up. Figure 5.14 shows the scope viewer on Simulink @wherein the sliding 900 second time window checks whether the limit has been exceeded at any given time.

¹If a battery is capable of 1,000,000 cycles for instance (at low DoD) with a 10 year lifespan, this means that *per* day the vessel may undergo 400 small discharge cycles (assuming 250 days of DP *per* year). If a monitoring window of 900 seconds were to be implemented, this would mean that the number of power peaks allowable would be upto 5 cycles during that single watch window.

Algorithm 1 Peak frequency Pseudo-code

```

start:
if demand > supply then
  peak → active
  k → 1
  if peak=active then
    sum = sum + k;
    if sum ≥ 15 then
      break;
      trigger → 1
    end if
  end if
end if
end if
after(900,seconds)
reset: sum=0;
goto(start)

```

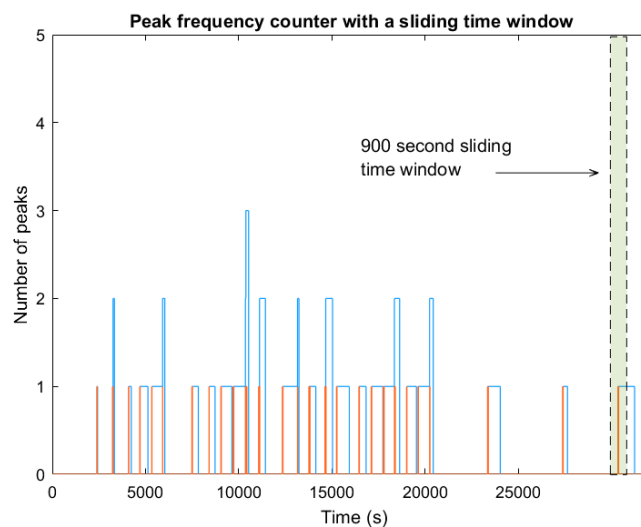


Figure 5.14: Peak frequency scope

5.4.4. ESS management algorithm B: Peak magnitude

The peak magnitude algorithm (Algorithm 2) consists of a generator starting and shutdown decision maker. The algorithm Stateflow® charts are available in Appendix B.

Generator start-up: Upperbound monitoring

The total power demand² is compared against the online capacity (*supply*) available³ and if it exceeds the online capacity, the peak magnitude *demand-supply* value is recorded. Additionally, the algorithm counts the number of power peaks within a watch window (in this case 3600 seconds). Using these two values, the average size of the power peaks are calculated within the watch window. If this exceeds the threshold value 'limit', a generator start-up is initiated by setting the trigger variable to '1'. The threshold value is dependent on the ideal C-rate for continuously charging and discharging the battery, which in this case is 1.5C of the battery. Based on the baseline battery specification, this value is about 2.3MW.

Generator shutdown: Lowerbound monitoring

In a similar method as the upperbound monitoring technique, the generator shutdown mechanism continuously checks the same conditions to check if the power surge limits would be breached if a generator would be turned off.

²The total power demand is the sum of the generator power output and battery power measurements

³The online capacity corresponds to the total load acceptable by the generators. For example, if two engines are running then the value of online capacity is 10,400 kW

Algorithm 2 Peak magnitude Pseudo-code

```

start:
upperbound:
if  $demand > supply$  then
     $peak_{average} = peak_{max}/(count)$ 
    if  $peak_{average} > limit$  then
         $trigger \rightarrow 1$ 
    else
         $trigger \rightarrow 0$ 
    end if
end if
lowerbound:
if  $demand < supply$  then
     $peak_{L-average} = peak_{max}/(count)$ 
     $k \rightarrow 1$ 
    if  $peak_{L-average} > limit$  then
         $trigger \rightarrow 1$ 
    else
         $trigger \rightarrow 0$ 
    end if
end if
after(3600,seconds) goto(start)

```

From Figure 5.15, it can be seen that at the 61250s mark, the 3600 second watch window has expired and at the end of this time period, the average value of the power peak exceeds the limit. In this case, an additional generator start up is initiated. The lowerbound monitoring window begins once the generator has been started-up. This lower bound monitoring checks the average of the power peaks in the event that a generator has been turned off once again. This is done in order to make a decision as to when it is appropriate to turn off a generator. In this case, it can be seen that after the generator start-up, the average power of the power peaks is still above the power peak limit (represented by the 'lowerbound peak average' line = approx. 3.5MW). The initiation of a generator is done by setting the trigger variable to 1 which as can be seen from the PMS response causes the additional generator to start-up.

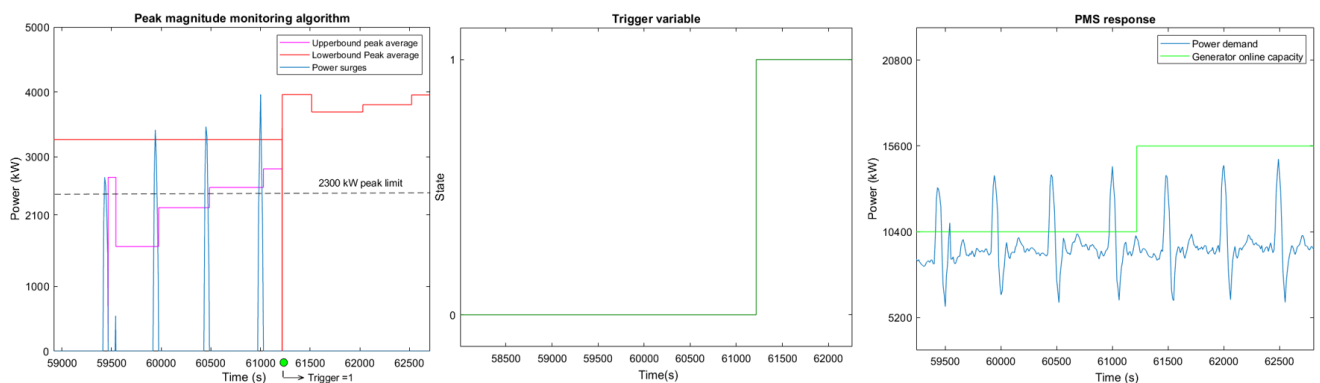


Figure 5.15: Peak magnitude monitor & PMS response

5.4.5. ESS management algorithm C: SoC control

State of charge control of the battery is consistent of two distinct processes i.e., charge and discharge. These processes occur in two scenarios: (Stateflow @diagrams are attached in Appendix B)

Reality

In reality, the battery will be discharged automatically without any prompt as any load requirement above the generators capabilities will be drawn from the battery. Algorithm 3 and 4 both would work in the same way except that the $i_{discharge}$ would not be required to be sent as a signal to the battery.

Model

In the case of the model, the physical battery model works by sending an input signal of the discharge current ($i_{discharge}$). During the time domain simulations, the pre-recorded timeseries of the load signal is the measured load. Using the measured load, any load above the online capacity is divided by the battery voltage which results in the discharge current experienced by the battery.

Mode 1: Pulse mode

The pulse mode of battery charge (Algorithm 3) is programmed such that the battery will be charged at 0.2C of the battery rating after every battery discharge event. One complete charge and discharge event is considered a single cycle. In this case the SoC setpoint has been defined as 85%, however, this setpoint may be increased or lowered. The energy consumed when charging the battery has not been included as a feedback to the total load as this value is negligible. Additionally, the i^2R losses at low charge rates (0.2C in this case) is negligible compared to the gains made by preventing a generator start-up.

Algorithm 3 Pulse mode operation pseudo-code

```

start:
inputs: SOC; battvolt;
supply % Online capacity;
demand % total power demand;
if demand > supply then
     $i_{discharge} = (demand - supply) / battvolt;$ 
end if
after: demand < supply
cycle ++;
charge:
if SOC < 85% then
     $i_{charge} = 0.2C;$ 
    if SOC >= 85% then
         $i_{charge} = 0;$ 
    end if
end if
goto(start)

```

Mode 2: Limit mode

The limit mode works such that the battery has an upper and lower SOC setpoint. The battery is allowed to then shave power surges within these limits. In Algorithm 4 the upper limit is taken to be 60% and the lower limit is taken to be 50%. Within this 10% band the algorithm allows the shaving of power surges. Once the battery SOC reaches 50%, the battery is recharged to the original SOC.

Algorithm 4 Limit mode operation pseudo-code

```

start:
inputs: battsoc; battvolt;
supply % Online capacity;
demand %Power demand;
if demand > supply && SOC > 75% then
     $i_{discharge} = (demand - supply) / battvolt;$ 
    trigger → 0
end if
if SOC <= 75% then
     $i_{charge} = 0.2C;$ 
end if
goto(start)

```

5.5. Simulations & results

The simulations are conducted on Simulink and Matlab 2018b. A model simulation dashboard (shown in Figure 5.17) is developed to test the various algorithms and visualise the data in realtime. The key performance indicators are measured for the baseline battery to gain insight. Based on the results, the potential to reduce the battery size is determined in Chapter 6.

5.5.1. PMS response

Scenario 1: Pipe-laying

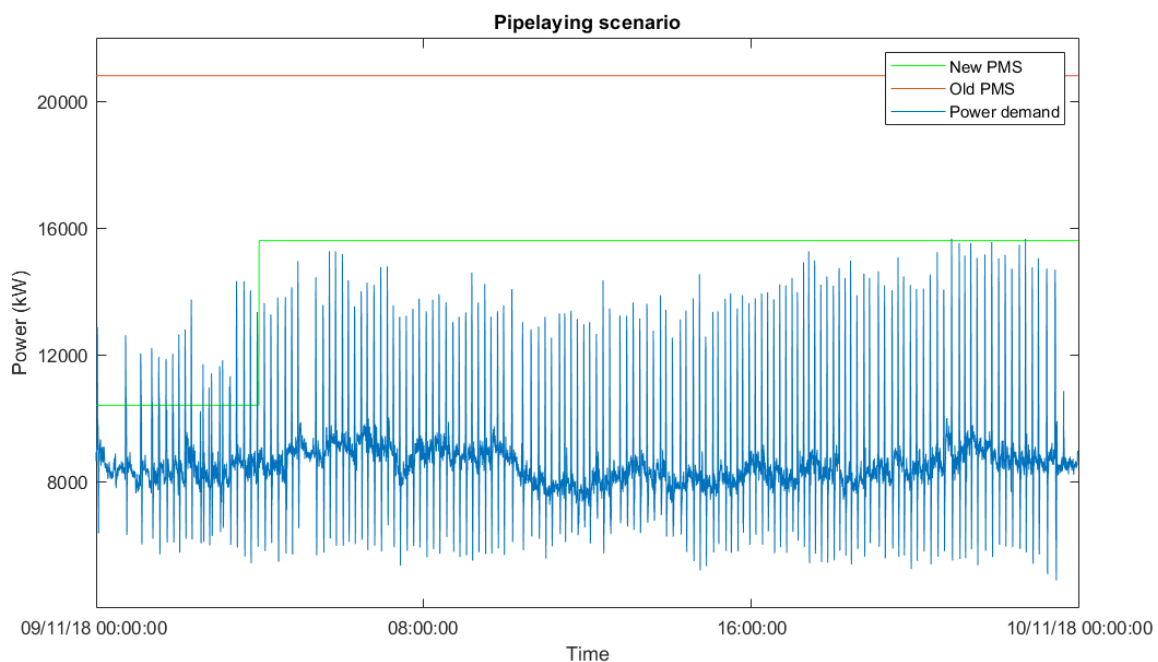


Figure 5.16: New PMS response during normal pipe-laying operations

Discussion

In the first scenario, the response of the newly developed peak monitoring algorithm can be seen in a normal pipelaying condition of the vessel. Initially, 2 generators are running to satisfy the loads and the battery ESS is being used to supply any energy that exceeds the supply from the generators. Around the 04:00:00 mark in Figure 5.16, the algorithm registers that the magnitude of the power peaks have grown too large, i.e., above the limit setpoint. At this moment, a new generator start-up is initiated. In contrast to the old PMS, the vessel runs on either one or two generators less throughout the day. For this particular day, the new PMS algorithm & an energy storage system would have saved the vessel 3.81 tonnes of fuel. Additionally, the reduction in total running hours for the engines (across both switchboards) was found to be 61 hours. The battery underwent 54 cycles on the MS1 switchboard and 23 cycles on the MS2 switchboard. The imbalance between the two has to do with the thrusters that are specifically connected to the MS1 & MS2 switchboards. Depending on the orientation of the vessel, some thrusters have to work more than the others. This imbalance is present on most days and alternates between the switchboards depending on the weather conditions the vessels relative orientation. The mean DoD (depth of discharge) on both switchboards was measured to be 1.2%. Additional PMS response examples are attached in Appendix B.

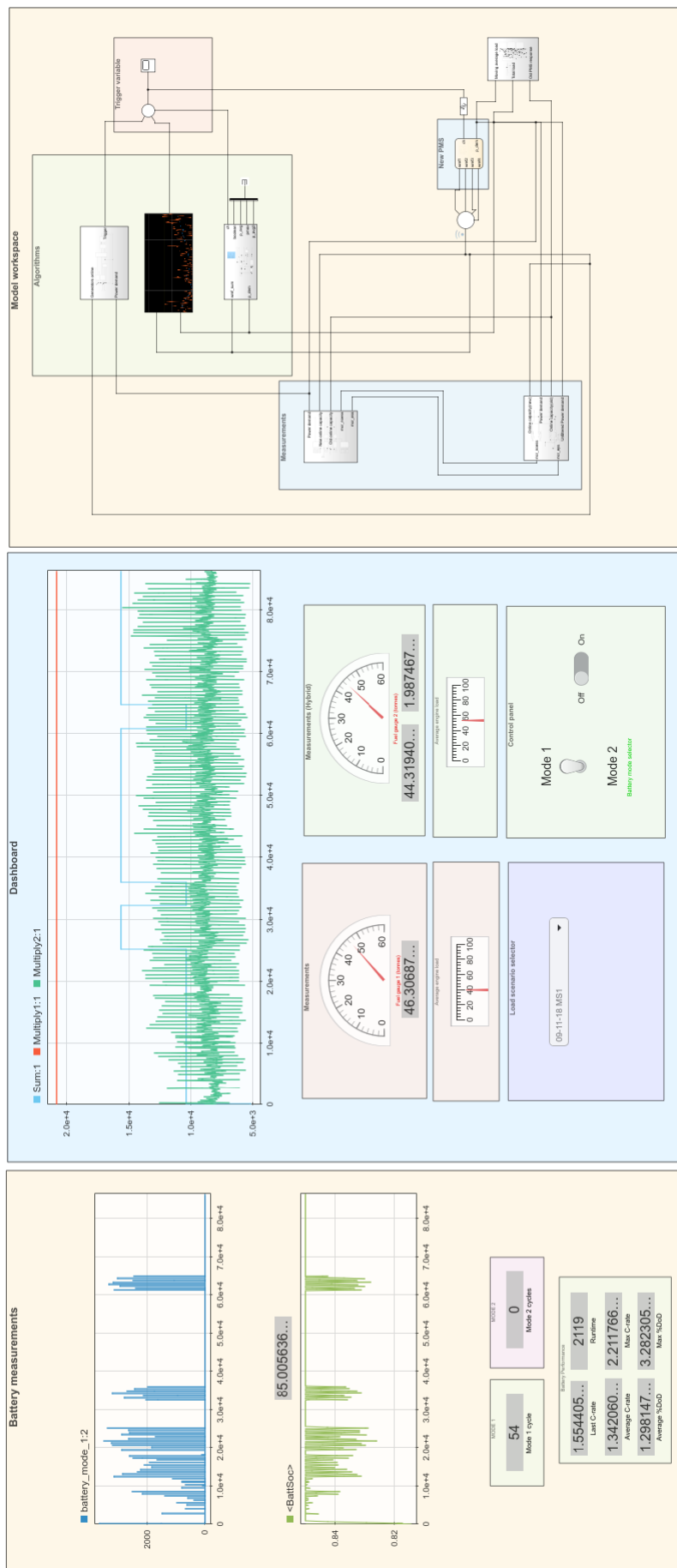


Figure 5.17: Simulation Dashboard on Simulink®

Scenario 2: WoW, pipeline recovery & pipe-laying

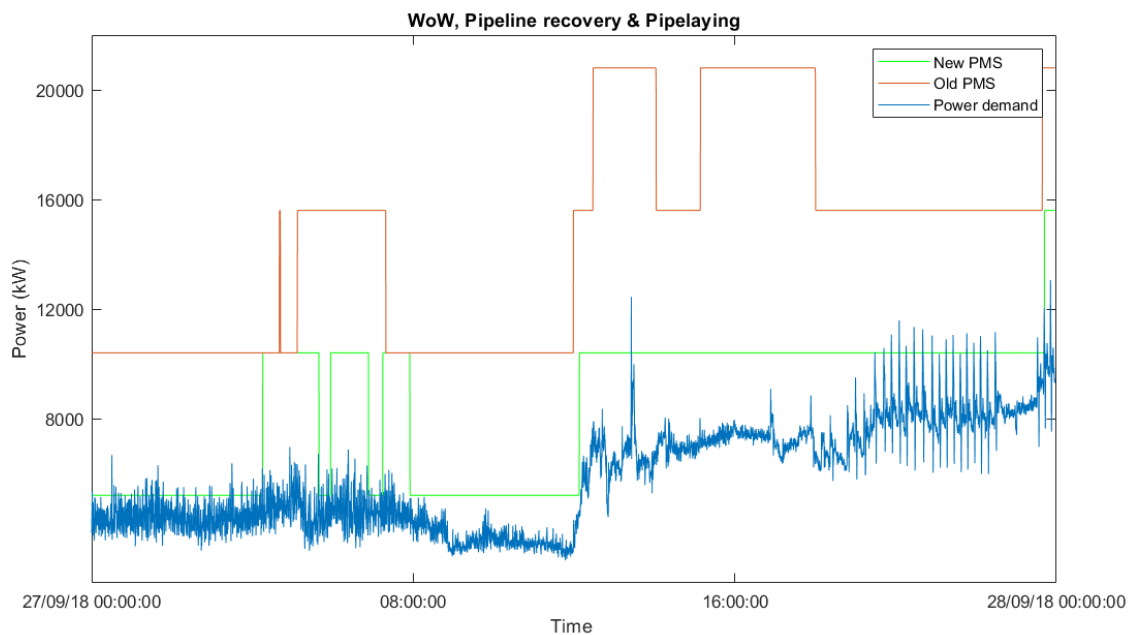


Figure 5.18: New PMS response during WoW, Pipe retrieval and pipe-laying

Discussion

In this scenario, the progress report of the vessel indicates that the vessel was in a 'Waiting on weather' (WoW) condition which means that the vessel was waiting for better weather condition before pipe-laying operations are continued. At 14:45, the pipeline recovery is initiated and as can be seen from Figure 5.18, it is depicted by a load increase. The generator start-up at this point is caused by the moving average load increasing as the peaks at this point are not significant. At 19:00 the vessel resumes pipe-laying which is seen by the power peaks that are present at this point of the day. The power peaks in this case are not significant enough to warrant an extra generator so the PMS's peak monitoring algorithm ensures to keep the generator turned off. At the end of the day, there is an increase in the load which necessitates an additional generator and the PMS performs the necessary start-up. Throughout the day it can be seen that in contrast to the old PMS, the vessel always operates on one generator less and on some occasions, even 2 generators less. In this particular case, the fuel savings were measured to be 3.14 tonnes with the MS1 connected battery unit undergoing 62 cycles and the MS2 battery undergoing 26 cycles. The reduction in running hours in this case was found to be 50.5 hours across both switchboards.

5.5.2. Fuel reduction

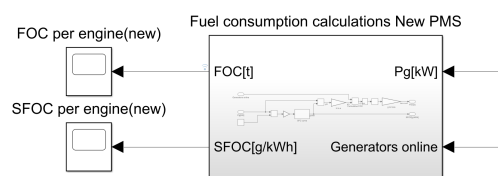


Figure 5.19: Fuel oil consumption block

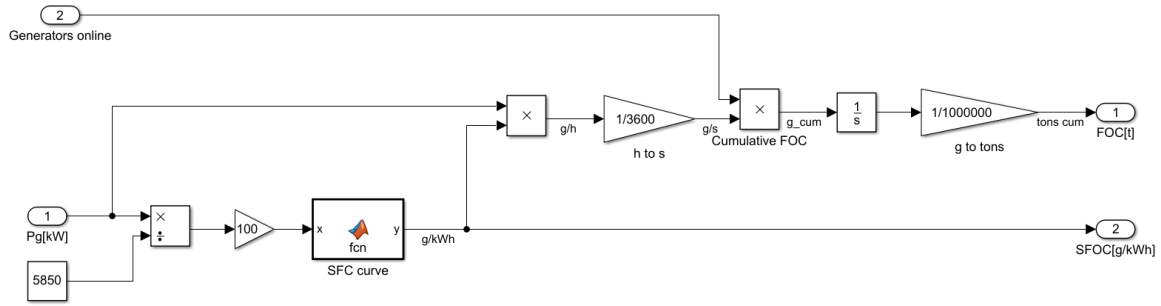


Figure 5.20: Fuel oil consumption block

The fuel oil consumption block calculates the fuel consumed during the operations based on two cases, the old PMS and the New PMS case. The input to the block is the power demand and the number of running generators. The efficiency losses due to the generator and the shaft have been adapted from L.V Donge [18] to produce an augmented power demand which is the real power demand that must be used in order to calculate the actual brake power induced in the engines. This is used to determine where along the sfc (specific fuel consumption) curve the load point exists at every simulation timestep. This is then integrated throughout the whole simulation to determine the total fuel consumed through the day by the vessel.

$$\%MCR = \frac{P_g}{5850} \cdot 100 \tag{5.6}$$

$$foc = \frac{P_g \cdot sfc}{3600} \tag{5.7}$$

$$FOC(tonnes) = \int_0^t foc \cdot ndt \div 1,000,000 \tag{5.8}$$

- Where:
- $\%MCR$: Load point as a function of MCR (maximum continuous rating) –
 - P_g : Brake power kW
 - foc : Fuel consumed g/s
 - sfc : Specific fuel consumption g/kWh
 - FOC : Fuel consumption $tonnes$
 - n : Number of running generators –

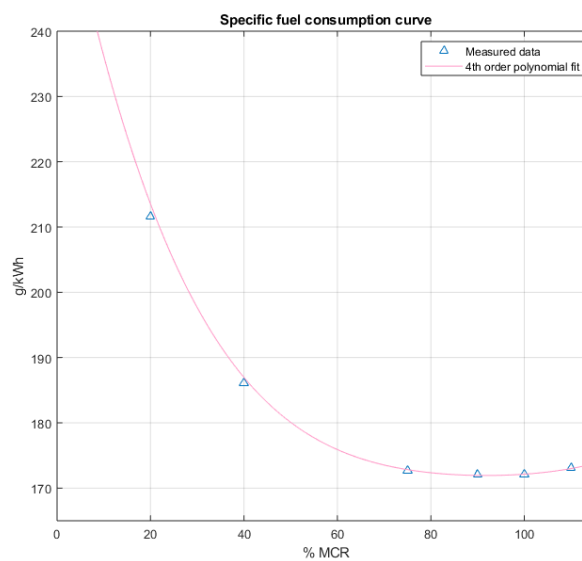


Figure 5.21: Specific fuel consumption of the Solitaire

In order to use the sfc curve⁴ in the simulation, a continuous function was created using a 4th order polynomial fit described by the following equation:

$$y = (9.8978 \cdot (10^{-07}) \cdot x^4) - (0.00036066 \cdot x^3) + (0.052167 \cdot x^2) - (3.5166 \cdot x) + (2.6386 \cdot 10^2) \quad (5.9)$$

Where: x : % MCR
 y : Specific fuel consumption g/kWh

Table 5.4: Test day descriptions

Day	Activity
21/11/2018	Pipelaying
18/11/2018	Pipelaying
09/11/2018	Pipelaying
10/10/2018	WoW, Pipeline recovery & Pipelaying
09/10/2018	WoW
05/10/2018	Pipelaying & partial downtime
27/09/2018	WoW, Recovery of pipeline & Pipelaying
26/09/2018	Pipeline abandonment & WoW

Table 5.5: Fuel consumption results

Test day	Old PMS (MT)			New PMS (MT)			Fuel savings(MT)
	MS1	MS2	Total	MS1	MS2	Total	
21/11/2018	48.91	51.1	100.01	47.15	49.57	96.72	3.29
18/11/2018	49.4	53.61	103.01	47.88	52.33	100.21	2.8
09/11/2018	46.31	45.79	92.1	44.32	43.97	88.29	3.81
10/10/2018	38.07	38.52	76.59	36.69	37.2	73.89	2.7
09/10/2018	20.97	22.13	43.1	19.29	20.62	39.91	3.19
05/10/2018	39.49	42.77	82.26	37.86	41.49	79.35	2.91
27/09/2018	31.13	32.51	63.64	29.41	31.09	60.50	3.14
26/09/2018	24.88	25.41	50.29	23.17	23.83	47.00	3.29
Mean value							3.14 tonnes

Discussion

From the simulation results, it is apparent that average fuel savings of 3.14 tonnes can be made *per* day which is approximately 4.11% of the *Solitaires* daily fuel consumption. On the days that the vessel is engaged in pipe-laying, the fuel consumption seems to be marginally greater than when the vessel is not pipelaying. The marginally greater values are attributed to the power peak energy being supplied by the battery. This means that sizing the battery even larger results in the possibility to save even more fuel without having to start up a new generator; although this option may be cost prohibitive. In the case of the Old PMS, on the pipe-laying days, there were 4 running engines on each switchboard while with the new PMS, it was 2-3 engines *per* switchboard. On the days that the vessel was not pipelaying, activities such as a pipeline recovery, repair downtime and waiting on weather were in progress. During these days, the vessel was still on DP which means that despite the vessel being considered on 'downtime', there is a potential to save fuel on such days.

⁴The sfc curve used is prior to the engine de-rating. As no further tests were conducted on the engine, the most recent sfc curve wherein the vessel has a de-rated engine is not available

5.5.3. Battery measurements

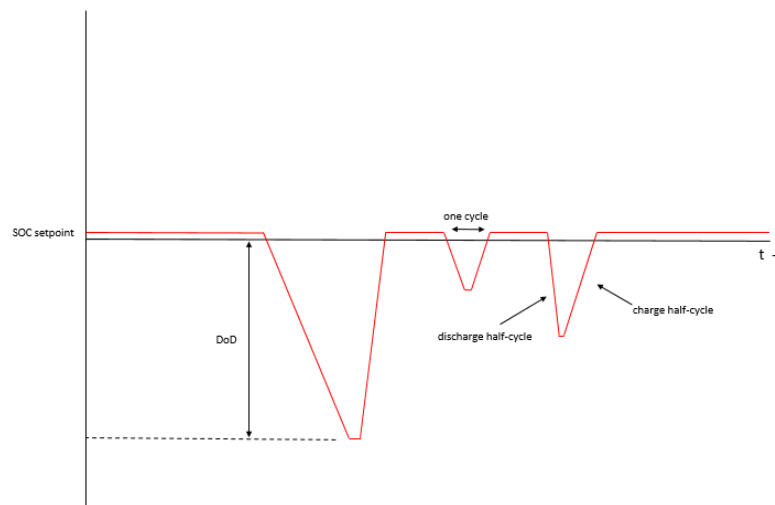


Figure 5.22: Battery cycles and DoD

The cycles of the battery are calculated after each discharge and charge half cycles. A single cycle therefore consists of both types of cycles. A setpoint SOC of 85% is defined for the test cases to determine just how much of a DoD would be produced by the power peaks according to the battery model.

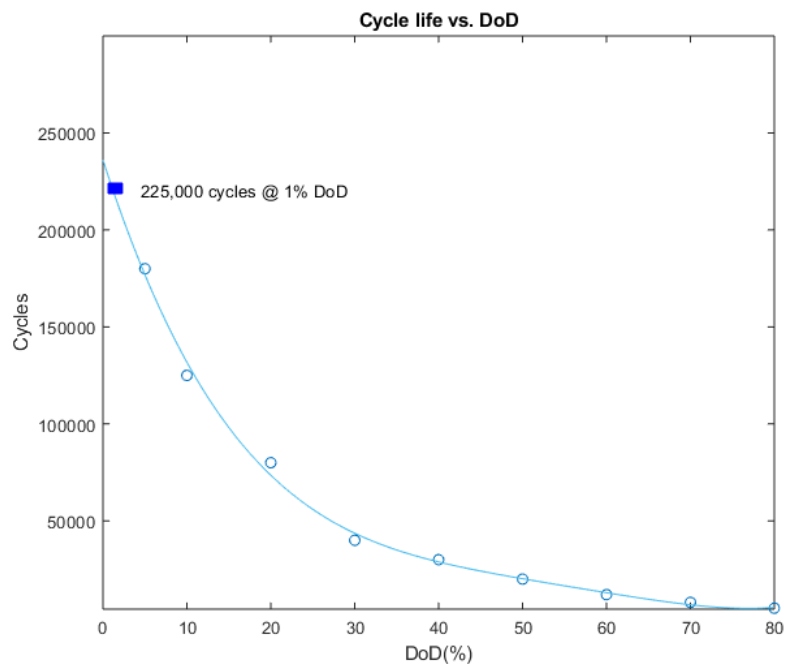


Figure 5.23: Battery cycles vs. DoD

It can be seen from the battery cycle life vs DoD curve that at very low discharge rates, it is possible to achieve exponentially large number of charge-discharge cycles out of the battery. Keeping it within this range will ensure that the battery lasts several years. A conservative assumption of 225,000 cycles at 1% DoD (Figure 5.23) results in about 15,000 times that the battery can be cycled *per* year. Assuming the vessel operates on DP for 250 days, this would result in the batteries being capable of 60 cycles *per* day. The results from the simulation are displayed in the table below.

Table 5.6: Battery measurement results

Test day	Runtime (min)		Average C-rate		Average DoD(%)		Cycles	
	MS1	MS2	MS1	MS2	MS1	MS2	MS1	MS2
21/11/2018	19	4	1.52	1.54	1.59	1.37	27	8
18/11/2018	8	11	1.43	0.54	1.28	0.4	15	39
09/11/2018	35	12	1.34	1.14	1.3	1.1	54	26
10/10/2018	34	43	0.51	0.59	0.35	0.38	52	66
09/10/2018	1	3	0.21	0.14	0.1	0.03	5	16
05/10/2018	21	58	0.39	0.58	0.29	0.61	40	73
27/09/2018	29	17	0.31	0.39	0.13	0.28	62	26
26/09/2018	7	21	0.47	0.46	0.32	0.54	17	46

Discussion

From the results, it can be seen that the average DoD during power surge shaving is in the range of 0.1-2%. The average C-rates that have been logged is the average of all the peak values of the power surges throughout the day. The C-rate measurements suggests that the algorithm has successfully ensured to keep the battery operating at the nominal discharge conditions of the battery (i.e., within 1.5C of the battery). There have been instances where the power demand has exceeded the limit on few occasions (i.e., >2300 kW power peaks). During this scenario, the battery may either be allowed to supply energy or else a power output limit may be set. In the latter case, this will have an effect by limiting the thrusters power consumption.

On almost all days, the number of cycles *per* day are lower than the limit 60 cycles using the pulse mode of charging. Further improvements to this charging can be made by incorporating a limit before a re-charge is employed which can reduce the cycles even further.

Reducing the battery size, however, will result in higher C-rates and a reduced power peak handling capacity. Either the decision to select a higher power battery must be made or the capabilities of the battery must be reduced. Reducing the capabilities of the battery means that it comes at a cost of reduced fuel savings. The runtime of the batteries on both switchboard's are relatively low meaning they are not being used as much. However, this is an advantage as the presence of the batteries prevent an additional generator start-up which has the potential to reduce the running hours on the *Solitaires* engines and enabling the remaining engines to operate at a more efficient working point.

5.5.4. Engine loads & running hours

To demonstrate the improvement in engine loading conditions, a pipelaying scenario (See Figure 5.16) will be reviewed. The vessel operates on symmetrical load sharing during DP operations which means that all the engines share the load demand equally.

Old PMS

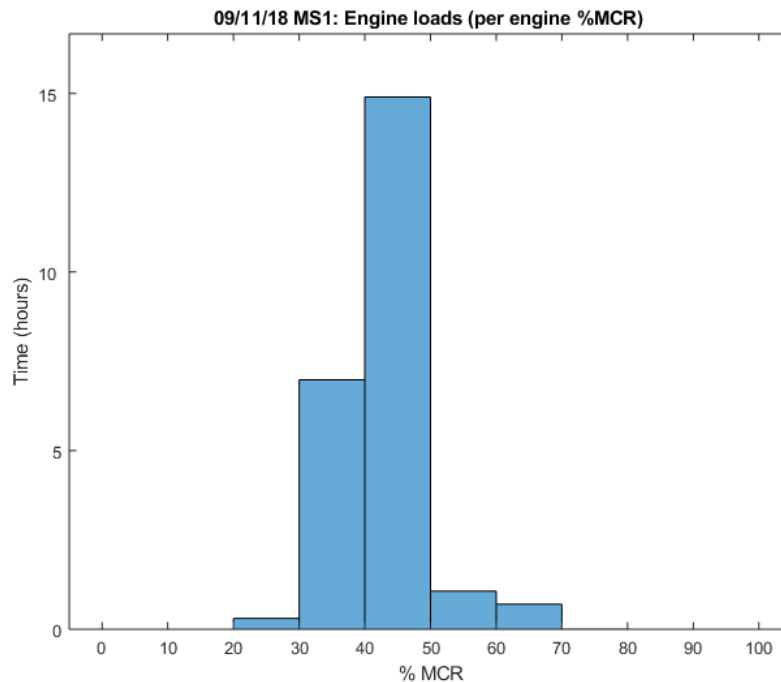


Figure 5.24: Engine loads with 4 running engines

In the case of the existing PMS (referred to as 'Old PMS'), the vessel operates with 4 running engines throughout the day. This results in the average load on the engine to be between 40-50% (Figure 5.24). The time spent within this range of operation is nearly 15 hours by each of the 4 engines. The instances attributed to the vessel reaching loads of upto 60-70% is due to the pipe-pulls wherein the power demand is large but the duration is short. Based on the existing rule based limit that has been set to turn on another engine should the load exceed 70% is the reason why no load beyond that point is experienced by the engine. The existing rule set cannot be increased to a higher start limit due to redundancy requirements of DP class III regulations. While most DP vessels operate with an average load of upto 35%, in the case of the *Solitaire*, these limits have been raised in contrast to the *Pioneering Spirit* which means that the engines on the *Solitaire* operate marginally more efficiently than with the traditional settings.

The implications of low load operation is significant for the vessel from a maintenance perspective. Based on the overhaul done on the *Solitaire's* marine diesel engines in 2018 prior to the inception of Nordstream II, several maintenance issues were identified which required the replacement of parts. From the testimonial from the engine room engineer, it was identified that common issues were the carbon deposits in the combustion spaces, cylinder heads, inlet valves, exhaust valves and injector tips. The exhaust side of the turbochargers also had significant carbon deposits due to the low load operation. The piston crown sides were relatively clean due to the use of anti-polishing rings. The maintenance scheduling of the vessel is based on running hours.



(a) Cylinder block contact surface crack



(b) Contact surface to the cylinder block

Figure 5.25: Cylinder block contact surfaces



(a) Cylinder head wear



(b) Worn out threads of the piston crown

Figure 5.26: Wear on the cylinder head & crown



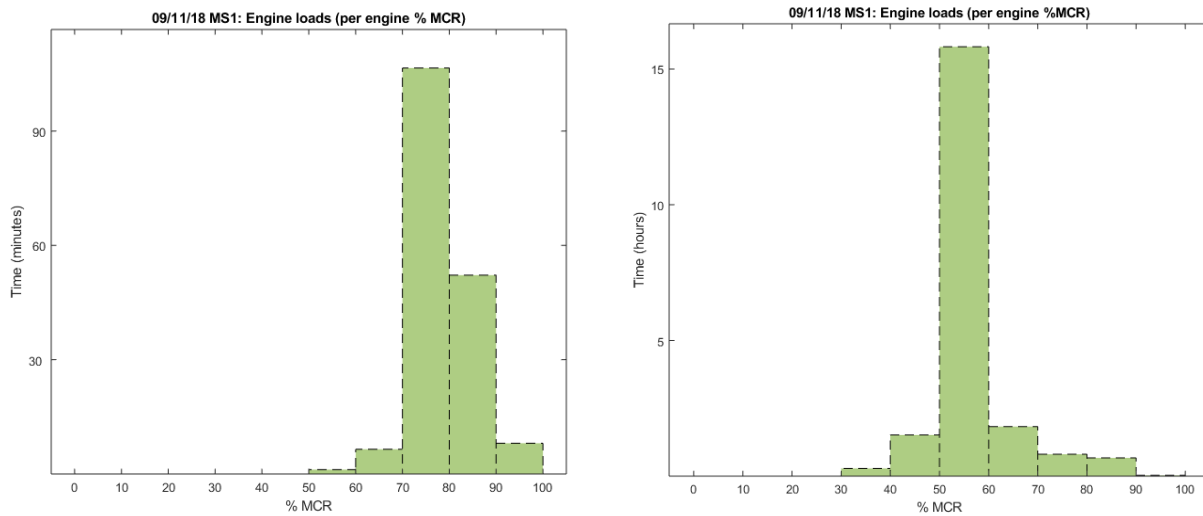
(a) Crown condition



(b) Fretting of the piston crown

Figure 5.27: Piston crowns

New PMS



(a) Engine loads with two engines operating

(b) Engine loads with three engines operating

Figure 5.28: Engine loads under the new PMS

With the implementation of the new PMS based on peak monitoring, there is a significant improvement in performance. During this particular operational scenario, the vessel operates for 1.5 hours at a load of 70-80% MCR (Figure 5.28b) which is ideal to burn off carbon deposits. When the PMS initiates an engine startup, the average load on the engine drops to between 50-60% (Figure 5.28a). This is still a 10-20% improvement in loading conditions in contrast to the old case and also has an effect on fuel consumption as previously found. The combination of having better loading on the engines and total running hours have a profound effect on maintenance costs.

Running hours

Table 5.7: Running hours measurements

Test day	Running hours (No ESS)		Running hours (with ESS)		Total reduction (hours)
	MS1	MS2	MS1	MS2	
21/11/2018	96	96	64.62	69.59	57.79
18/11/2018	96	96	71.02	71.08	49.9
09/11/2018	96	96	62.75	67.87	61.38
10/10/2018	71.89	71.89	47.91	48.77	47.1
09/10/2018	50.33	50.33	24.86	26.32	49.48
05/10/2018	76.23	76.23	47.91	50.16	54.39
27/09/2018	66.8	66.8	39.07	44.03	50.5
26/09/2018	59.43	59.43	34.19	35.23	49.44
Mean value					52.5

Discussion

The running hour measurements have shown that the mean reduction in total running hours is 52.5 hours- which is a 35% reduction in running hours compared to the existing case. However, it must be observed that on the days that the vessel is not partaking in pipelaying operations, the running hour reduction is lower than in the case of pipelaying. This means that the vessel downtime must be reduced in order to maximise running hour reduction. Additionally it can be seen that on 18/11/18, the running hour reduction is 49.9 hours while on 21/11/18 & 09/11/18 they are higher. This depends on the magnitude of the power peaks as having larger power peaks and relatively greater DP load which can be attributed to harsher weather would mean that the running hour reduction would not be as much due to the requirement to start up an

additional generator. However in all cases, the vessel would operate with one less engine compared to the existing PMS. This means that the minimum running hour reduction would be 48 hours (taking into account both switchboards).

5.5.5. Emission reduction

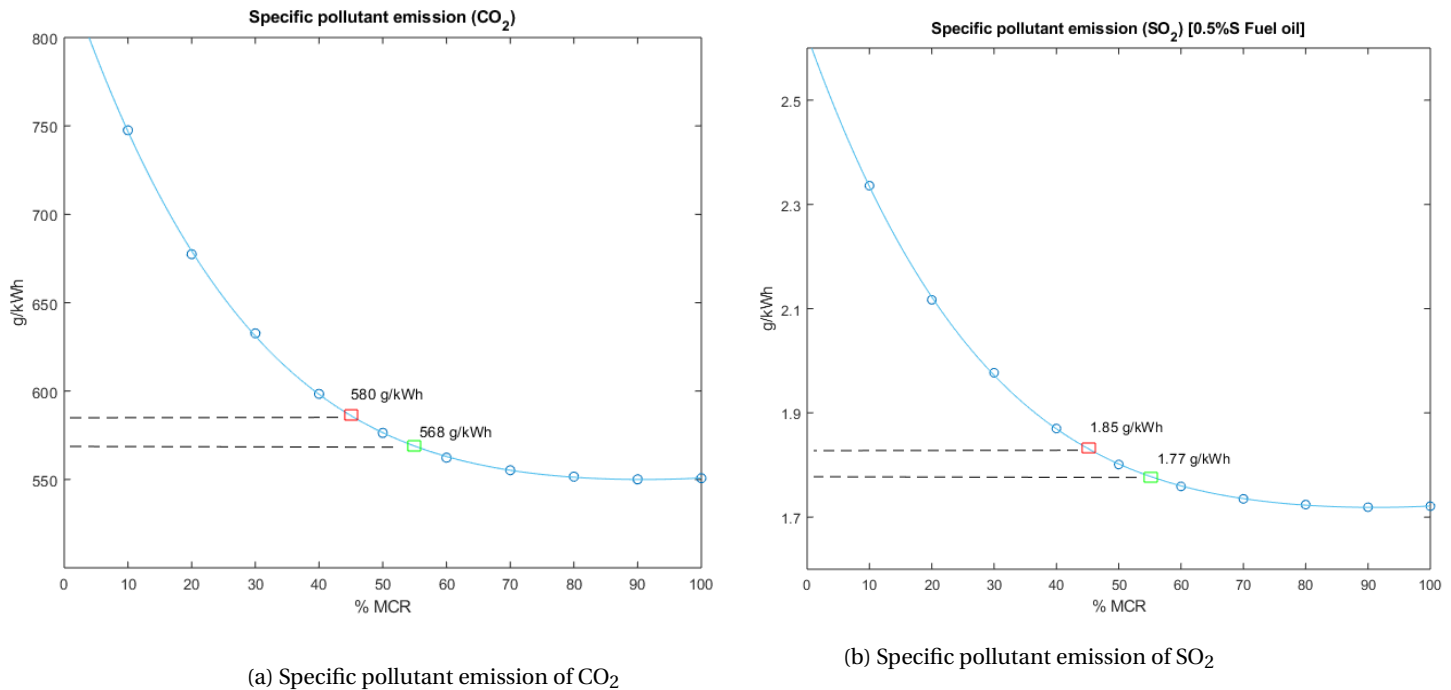


Figure 5.29: Specific pollutant emission of the *Solitaire*'s Diesel engines

Table 5.8: Emission reduction opportunities for the *Solitaire*

	Daily savings	Annual savings
CO ₂ reduction	10,048 kg	2512 tonnes
SO ₂ reduction	31.4 kg	7.85 tonnes

*250 DP days assumed for calculations

Discussion

The specific pollution emission is analogous to the specific fuel consumption curve in that it shows the potential reductions in emissions possible with an increase in engine loads. The average car in the EU emits 1.8 tonnes of CO₂ annually as reported by the European Federation for Transport & Environment [5]. When making a comparison to the CO₂ emissions of the *Solitaire*, it is evident that the potential to save over 2500 tonnes annually. Over the course of 10 years of operation, this would be the equivalent of having 14,000 less vehicles on the road. While this may seem like an opportunity that may not be an avenue to earn revenue (as Carbon taxes are not yet implemented), testimonials from multinational oil corporations such as Shell and Equinor have suggested a move towards more energy efficiency, sustainability & reduction of Carbon emissions [6] [7]. Companies that move forward towards energy efficiency and low carbon operations could be positively disposed during contract negotiations as it would produce a positive impact on both parties. The emergence of such 'green contracts' imply that a single such contract awarded to any company that has invested in an energy storage system would then result in an instant payback of the investment.

5.5.6. Investment & Returns

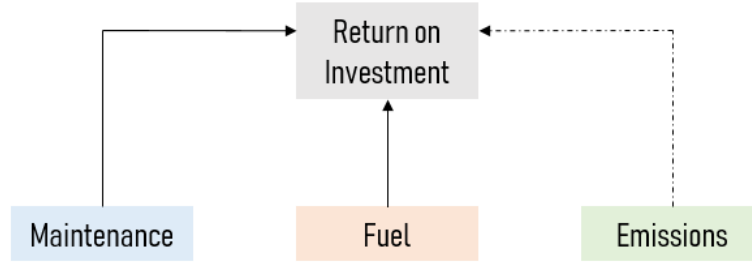


Figure 5.30: Investment return avenues

Fuel

The most important factors to calculate the returns from fuel savings would be the fuel saved *per day*, fuel cost and the time the vessel spends on the DP mode in a year. The spread for the DP days in the calculations were taken for a range of 0-365. '0' signifying that the vessel has no work and '365' signifying that the vessel is busy throughout the year. The mean fuel savings were taken from the simulations to be 3.14 metric tonnes and the fuel cost was taken from a range of \$200-\$950 (USD).

$$DP = [0 \quad 10 \quad 20 \quad \dots \quad 365]' \quad (5.10)$$

$$FP = [200 \quad 250 \quad 300 \quad \dots \quad 950] \quad (5.11)$$

$$S_f = DP \cdot FP \cdot 3.14[\text{USD}] \quad (5.12)$$

Where:

DP :	Days spent on DP	–
FP :	Bunker prices	USD/MT
S_f :	Fuel price payback	USD

Maintenance

Maintenance costs are the second most significant savings one can obtain from the installation of an ESS. The engines of the *Solitaire* are manufactured by Wartsila. The maintenance programmes that take place are based on a major overhaul that is to be performed for every 12000 hours the engines are running. Additionally, within this 12000 hour period, there are checks to be made every 2000, 4000, 6000 hours periodically. When the engine reaches some major 'milestones' such as the 24000, 36000, 72000 hour marks- there are more significant maintenance works that must be performed on the vessel. Based on measurements taken from another vessel from the Allseas fleet (*M/V Audacia*) which is equipped with a 6.2 MW engine- the costs associated with maintenance are about 28 USD *per hour* of engine operation. Extrapolating this to the *Solitaires* 5.8MW engine, this would amount to approximately 26 USD *per hour* of operation. Based on the reduction in the running hours ascertained from the PMS simulaitons, we can calculate the daily mean savings from a maintenance perspective. This works out to be \$1360 *per day*. This value is significant and nearly as much as the fuel savings *per day* that amount to \$1570. Once again, these savings are directly correlated to the time spent on DP by the *Solitaire*. Hence the savings can be calculated as:

$$S_m = DP \cdot rh \cdot c_{rh}[\text{USD}] \quad (5.13)$$

Where:

S_m :	Running hour cost savings	USD
DP :	Days spent on DP	–
rh :	Reduction in running hours (52.49)	hours
c_{rh} :	Cost <i>per</i> running hour (25.8)	USD

The total payback *per year* that can be calculated that are correlated with the fuel cost and DP days are:

$$TP = S_f + S_m [USD] \quad (5.14)$$

Using this, we can gain a good insight into the different options subject to changes in fuel prices & operational conditions of the vessel. If the payback period were to be pinned at 5 years, this would also give us an idea of what the maximum permitted CAPEX investments (i.e., CAPEX budget) are depending on the vessel & market conditions.

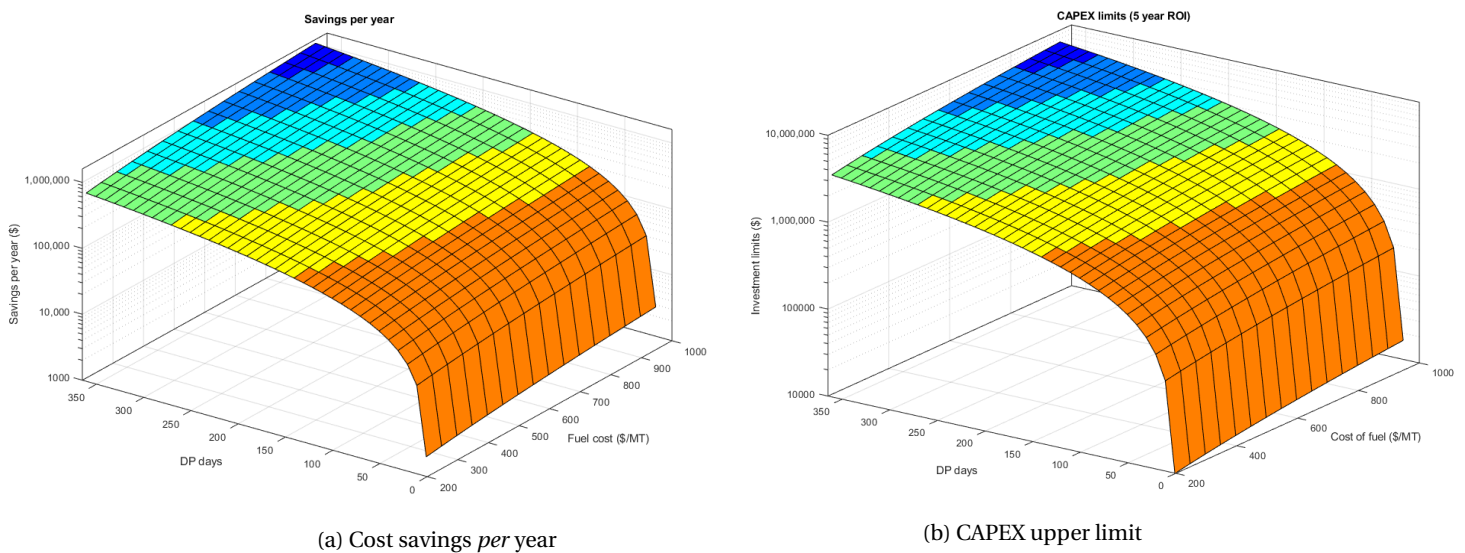


Figure 5.31: Savings & CAPEX

Discussion

Table 5.9: Investment scenarios

Scenario	DP days	Fuel cost (\$/MT)	Savings <i>per year</i> (\$)	CAPEX budget
A	250	550	\$773,400	\$3,867,000
B	250	450	\$694,000	\$3,470,000
C	180	450	\$500,900	\$2,504,500
D	180	700	\$643,000	\$3,215,000
E	270	650	\$920,100	\$4,600,000
F	365	550	\$1,112,000	\$5,560,000

The results on the surface plot show all possible cross combinations of DP days and movements in global bunker prices. Figure 5.31a shows the returns on investments per year year, using this data, Figure 5.31b shows the limit on CAPEX based on a 5-year payback period. Table 5.9 depicts a few investment scenarios using the represented cross-combinations.

In previous research, the assumptions of 365 day operational conditions are deemed to be too optimistic as the apparent savings in that case are very high which results in potentially unrealistic payback periods. While it is true that the operational efficiency of the vessel increases, the returns from fuel and maintenance alone may not be enough to warrant a battery installation from a realistic perspective. The emission aspect of batteries in that reduced CO_2 emissions are a positive impact for the environment would be a good reason to invest in batteries. Alternatively, either the payback period must then be assumed to be longer, i.e., about 10 years. In such a case, the batteries must have a longer calendar life.

Since the battery is one of the most expensive components of an ESS installation, the following chapter explores the opportunity to attempt to reduce the size of the battery using load forecasting. By being able to schedule generator start-stops and/or determine an optimal vessel velocity during pipe pulls, there could be a potential to reduce the battery size even further with the split battery design. The forecasting model could then be used to supplement the rule based algorithm.

6

Load forecasting using machine learning

Based on the results from Chapter 5, it is apparent that although the advantages of battery ESS systems have been outlined for fuel savings, running hours and emission reduction, there exists opportunities to further reduce the installed capacity as the limiting factor seems to be the investment cap. The rule based system is one that works on data recorded in the past operation of the vessel using a back looking principle. As this is advantageous from an operational perspective, it would be insightful to understand the load conditions in the future which will allow decision making processes to be made in advance. This would eliminate or reduce the watch window that is required before a generator shutdown is initiated on the rule based power management system. The added benefit is that then, the battery may be re-sized to handle smaller power peaks and still provide sufficient spinning reserve for position keeping.

6.1. Overview

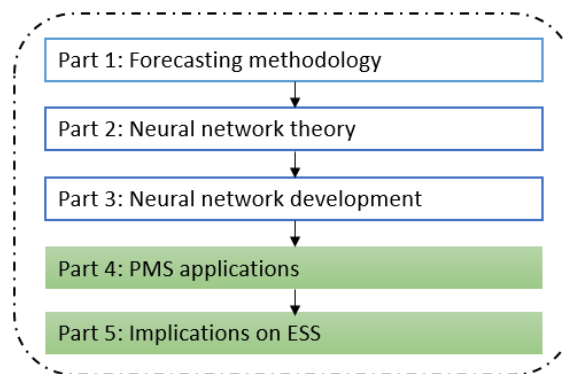


Figure 6.1: Chapter overview

The first part of this chapter discusses the various options available to conduct forecasting as well as the selected model for the application of load forecasting. Following this, the background theory of neural networks are reviewed before the development process is outlined for this study. The final step is to understand how the forecasts can be implemented into the power management system of the vessel and the corresponding simulation, results and implications on the ESS design.

6.2. Forecasting methodology

Predictive algorithms

A variety of methodologies exist for forecasting, in this study however, only quantitative forecasting methodologies are analysed as the qualitative methods are not applicable to load forecasting purposes. Among the quantitative methods of forecasting, we can generally classify them as shown in Figure 6.2:

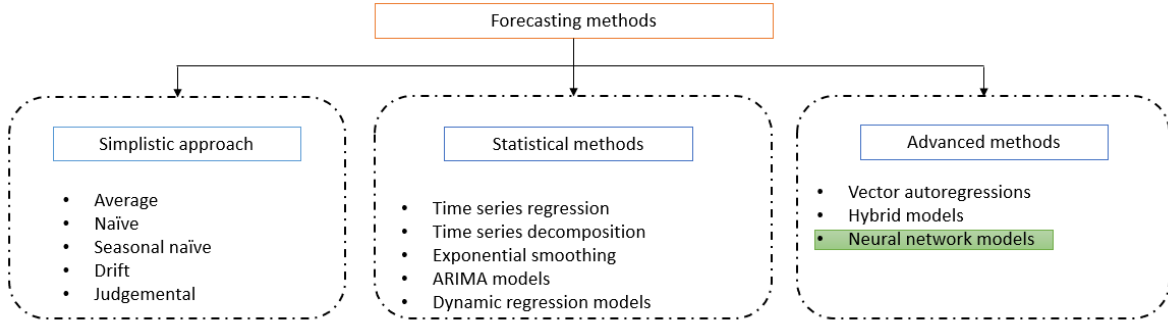


Figure 6.2: Predictive algorithm overview

i Simplistic approach

Simple approaches are classified due to their relatively straightforward forecasting techniques. Typically they are useful only for forecasting single time step ahead which is not particularly useful for decision making in the case of vessel loads. The average approach uses past data available in a time series to predict the next time-step ahead as the average of all the past observed values.

$$\hat{y}_{T+h|T} = y_T + \frac{h}{T-1} \sum_{t=2}^T (y_t - y_{t-1}) = y_T + h \left(\frac{y_T - y_1}{T-1} \right) \quad (6.1)$$

For the purposes of vessel load forecasting, there is no added value in knowing the information of a single time-step hence this method is not appropriate for the intended application within the PMS.

ii Statistical methods

In a causal statistical approach, one does not rely on any future inputs into the model i.e., the model makes forecasts based on the past inputs and response of the system in the past. Methods of causal forecasting that are predominantly used are linear regression and ARMAX models (Auto-regressive moving average with exogenous inputs). In these models, the forecasts take account of past relationships between variables. For example, if one variable has been linearly related to another for a long period of time, it may be appropriate to extrapolate such a relationship into the future without necessarily understanding the reasons for the relationship [3].

Other time series models are moving average, weighted moving average, auto-regressive moving average, auto-regressive integrated moving average, linear prediction, trend estimations and more. No literature was found apart from Spruijt [42] for the use of electric load prediction on DP pipelaying vessels using a seasonal ARMA model (forecasts dependent on past values of the variables being forecasted and past prediction errors).

$$x_t = \phi_1 x_{t-1} + \dots + \phi_p x_{t-p} + \theta_1 \epsilon_{t-1} + \dots + \theta_q \epsilon_{t-q} + \underbrace{\phi_p x_{t-T} + \theta_q \epsilon_{t-T}}_{\text{seasonal}} + \epsilon_t$$

Figure 6.3: Seasonal ARMA equation [42]

iii Advanced methods

Advanced forecasting methodologies are primarily known as artificial intelligence methods. The tools for artificial intelligence to solve problems in computer science can be classified into search & optimisation, logic programming, probabilistic methods, classifiers and artificial neural networks [1]. While the tools for AI are used for data mining, pattern recognition and classification of inputs, neural networks are a branch of artificial intelligence that can be used for forecasting linear or non-linear relationships between the inputs and outputs. This is done by a method of system identification wherein a model is fed in with input and target data and over the course of the training, the model understands and 'learns' these relationships through trial and error as opposed to step-by-step coding [33].

Problem requirements

The model must be able to capture the moving average total load which is a sum of the moving average DP load and the ancillary load component. The pipe-pull induced power peaks and any loads caused as an effect of the vessels heading changes need to be accounted for. Furthermore, these requirements need to be met over a long forecast horizon in the order of at least an hour or more. This is to ensure that the forecasts do not cause frequent generator start-stops.

Table 6.1 outlines the capabilities of the different forecasting methods to capture these phenomenon over a long term forecast.

Table 6.1: Long term forecast requirements

Requirement	Statistical methods	Advanced methods
Moving average total load (non-stationary)	✗	✓
Pipe-pull induced loads (stationary)	✓	✓
Sudden heading change induced loads	✗	✓

Model selection

The simplistic approach is not applicable for PMS decision making as it can only offer a single time step ahead prediction. The time window required to efficiently schedule generator start stops would have to be in the order of hours. Of the time series approaches, in previous research by Spruijt [42], a ARMA model was used to predict the load using a statistical approach based on the data recorded in the past with a time window of one hour as the ‘observation window’ and the prediction horizon of 90 seconds. The disadvantage of this method is that it can only predict the load for 90 seconds which was designed for a single battery system in order to make a decision as to which switchboard the battery must connect to in order to satisfy the failure/power surge. However, as seen from the rule based system of monitoring, it would be advantageous to know the forecasted load for atleast an hour in advance. This would allow decisions to be made whether it is appropriate to use the generator to satisfy the power demand or to use the battery. As none of the statistical methodologies of forecasting can predict over a long horizon, the approach to be adapted would be more advanced forecasting techniques.

As the *M/V Solitaire* is equipped with a datalogging system recording over 2000 parameters daily, it is possible to use this data to build a model using a data driven approach that employs machine learning¹.

Adhikari et al demonstrates that as practical time series often exhibit trends and seasonal patterns, traditional statistical methods are limited in its capabilities in forecasting such series. Artificial neural networks (ANN’s) have shown the ability to recognize and forecast strong seasonal patterns without removing the seasonality from the raw data [8]. In the paper, ANN’s outperformed other traditional statistical methodologies, viz. SARIMA (Seasonal-ARIMA), SVM (Support vector machines) and Holt-Winters (HW) models. In the case of load prediction for a DP vessel, it is apparent that as weather conditions change, the DP load will change as well which is analogous to a trends, seasonalities & cyclic patterns. This is compounded with the pipelaying process that produces large power peaks due to ground speed correlation. Hence, the feedforward artificial neural network is deemed to be the appropriate model for the application as it offers the capabilities to capture all the requirements².

¹Artificial neural networks are a subset of the advanced modelling method also referred to under machine learning or artificial intelligence

²Another potential model candidate would be to use hybrid models. The literature on how hybrid models are used and why it is not necessarily better than a neural network are outlined in Appendix C: Section C2

6.3. Neural network theory

6.3.1. Biologically inspired mathematics

A neural network is a computing model for information processing. It is modelled after a biological neuron. The underlying principle is that the neurons receive input signals in the form of ‘synapses’. As these synapses collectively sum up, they pass a threshold value after which the neuron fires a signal as the output to more neurons.

From a mathematical perspective, the interest lies in attempting to capture the behaviour of these neurons in the form of equations. Each node of a neural network is modelled as shown in Figure 6.4.

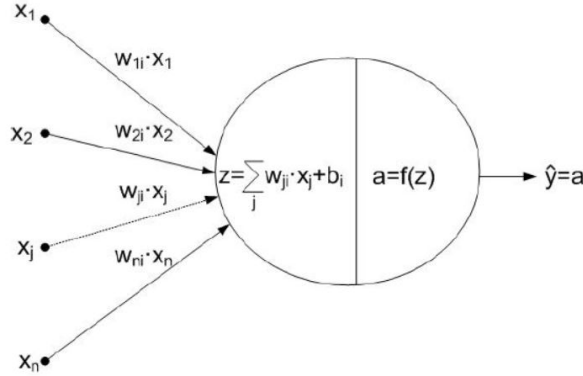


Figure 6.4: Neural network node structure [11]

$$\hat{y}_i = f \left(\sum_{j=1}^N w_{ji} \cdot x_j + b_i \right) \quad (6.2)$$

Where:

- \hat{y}_i : Predicted value
- w_{ji} : Weights
- x_j : Inputs
- b_i : Per-layer biases
- f : Activation function

6.3.2. Neural network architectures

There exist several neural network architectures that are suited to purposes such as speech recognition, image classification and control system design. In the case of forecasting, the two types of neural networks that are most prevalent are the Recurrent neural network (RNN) and the Feed-forward neural network (FNN). The most widely used type of network in literature was found to be the feed-forward type network with a single hidden layer due to its relatively straightforward design and capability to model a wide variety of non-linear functions according to the universal approximation theorem [24]. Recurrent neural networks work by having additional inputs as feedback signals which can generate past error patterns. In this way, RNN's can model richer dynamics however, their superiority over feed-forward type neural networks has not been established. Furthermore, some of the problems suffered by the RNN's are that RNN's can assume a variety of architectures and it can be difficult to specify appropriate model structures to experiment with. It is also more difficult to train RNN's due to the unstable nature of the training algorithms [50]. Hence for multi-step timeseries forecasting, the most appropriate architecture would be the feed-forward type neural network with a single hidden layer.

6.3.3. Neural network structure

General structure

Figure 6.5 is a simplified structure of a feed-forward neural network. It consists of an input, hidden and output layer. The input variables are fed into individual nodes of the input layer after which mathematical

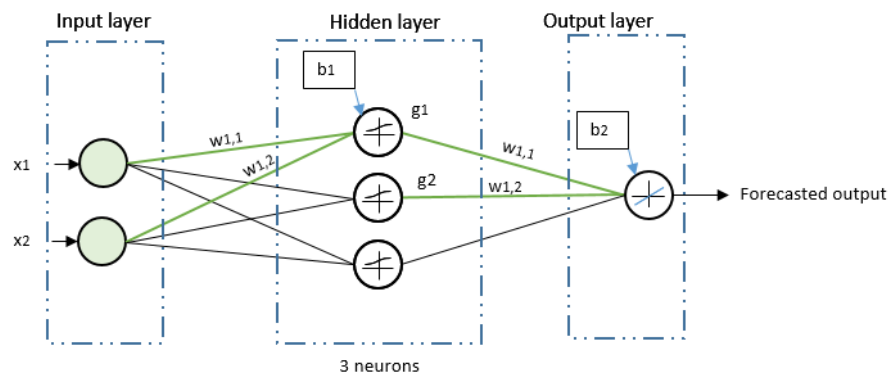


Figure 6.5: A simple feed-forward neural network

transformations transmits these values through the network in order to produce a forecasted response. Following the 'green' set of paths, an understanding of the path of the individual variables can be better grasped.

Input layer & biases

The input layer corresponds to the layer in which the variable inputs are made. These inputs are multiplied by a set of weights that are randomly assigned at the start of a 'training' procedure. Once, multiplied by these weights, the sum of those products (along with bias³ values) are introduced into a layer called the hidden layer. Using Figure 6.5, mathematically, the input layer can be represented as:

$$z_1 = \{x_1 w_{1,1} + x_2 w_{1,2} + \dots\} + b_1 \quad (6.3)$$

Hidden layer & activation functions

This layer consists of an activation function which is analogous to the 'threshold' of a neuron. The capability of a neural network to capture the system non-linearity's are due to the presence of this non-linear activation function. The input into the hidden layer node will ensure that the input is 'squashed' within the limits of this activation function which lies between the range $[-1, 1]$ or $[0, 1]$ depending on the function.

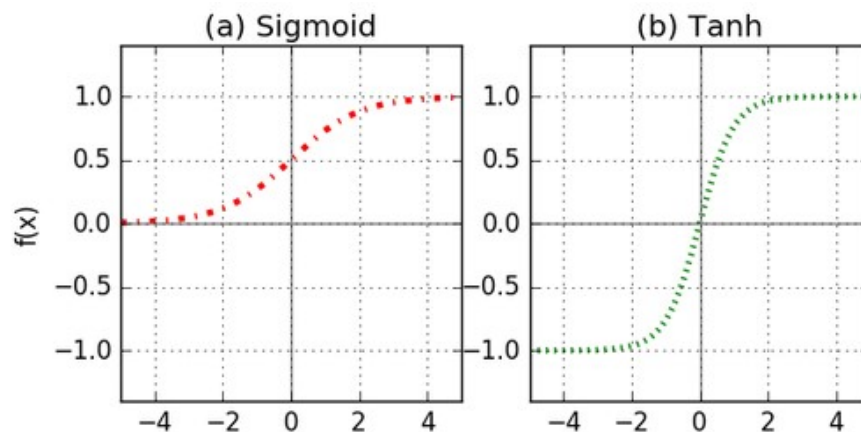


Figure 6.6: Non-linear activation functions [37]

The sigmoid and hyperbolic tangent activation functions (Figure 6.6) can be represented mathematically as:

$$g_1 = f(z_1) = \frac{1}{1 + e^{-z_1}} \quad (6.4)$$

³The bias is analogous to the 'y-intercept' of linear system. It allows the activation function in the hidden layer to shift left or right. See Appendix C1 for figures representing the effects of the bias variable

$$g_1 = f(z_1) = \frac{e^x - e^{-z_1}}{e^x + e^{-z_1}} \quad (6.5)$$

The choice between the functions is arbitrary and can be tested to ascertain if the neural network performance improves. The advantage of a ‘smooth’ activation function as opposed to a classifier type step function is that it can be differentiated- this is a useful feature when optimisation is used in the training phase. This is a method that will be used during the ‘training’ phase of the neural network development.

Output layer

The output layer consists of the combined inputs of the nodes of the hidden layer. The output also contains an activation function, however, in the case of classification problems, the output is set to a function that allows a ‘0’ or ‘1’ output (binary classifier) but while in the case of forecasting real values such as the electric load or house prices etc., we use a linear output activation function which maps the output of the hidden layer into a forecast value [39]. This is represented as:

$$\hat{y}_j = \{g_1 w_{1,1} + g_2 w_{1,2} + \dots\} + b_2 \quad (6.6)$$

6.4. Neural network development

6.4.1. Machine learning workflow overview

The machine learning workflow is a series of steps used to develop the neural network for the purposes of load forecasting (Figure 6.7). The steps begin with selecting & collecting the input and target parameters followed by a pre-processing stage. Once the data has been prepared, the next task is to design the neural network structure. Training ensues from this point wherein a training optimisation algorithm must be implemented in order to allow the model to identify the input-output (target) relationships. The last step is to test the network performance on a testing dataset. Using the response from the testing phase, one may re-design the network iteratively until the necessary performance goals are reached.

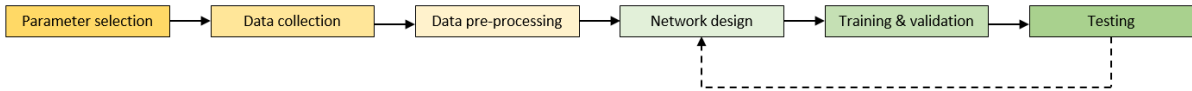


Figure 6.7: Machine learning workflow overview

6.4.2. Parameter selection

One of the first steps to developing a neural network is to select the parameters responsible for the target process. According to May et al, the difficulty of selecting input variables is exacerbated during ANN development, since the task of selecting inputs is often delegated to the network itself. Due to the non-linearity, inherent complexity and non-parametric nature of ANN regression- it makes it difficult to apply many existing analytical variable selection methods. The notion is that neural networks are capable of understanding the salient input variables while ignoring the redundant parameters [35]. However, steps can be taken to improve the performance by considering a few important factors that affect the network development.

The steps taken are to gauge the relevance of the input variables to the output, consider the computational effort required of potentially redundant variables and the availability of the required input parameters. In this case, all the available variables that link the vessel to the environment have been considered.

Inputs: Weather parameters

Realistically, the model must be trained to the real weather recorded on the vessel but during the testing phase, it must be tested on the forecasted weather as this will be the only available data in order to make power demand forecasts. From the vessel’s data-logging system- the parameters of wind speed, wind direction and significant wave height (recorded on the WAVEX system) were used as input variables for weather. Additionally, it would be useful to incorporate the effects of currents, however, as this data is rarely available for forecasting within Allseas- the decision was made not to include this parameter as there is a lack of availability of this data. As the vessels position with respect to the currents do not change significantly, it is

expected that the neural network will understand this relationship automatically- however, it may also result in larger than usual forecast errors unless the currents are included.

Table 6.2: Weather parameters

Parameter	Units	Normalised
Wind speed	m/s	✓
Wind direction	degrees	✓
Significant wave height	cm	✓

Inputs: Route plan parameters

While the weather data is sufficient to determine the moving average DP load, it does not completely capture the bindings between the vessel and the environment. As the vessel moves forward during each pipe-pull, the power peaks are caused by the vessels forward motion. This is a result of the vessels ground speed profile. While it is not possible to receive ground speed forecasts, the real ground speed profile can be input into the neural network as a forecast of the number of pipe pulls planned for the day. For instance, if the ground-speed setpoint is 0.35 m/s and a route plan is made such that the vessel is expected to complete 120 pipe pulls in a day, the input ground-speed profile can be an input stream of data that represents 120 instances of the vessels' ground speed profile throughout the day. The vessel always follows a pre-determined track, therefore it is then possible to plan (Figure 6.8) for the day ahead as to how many kilometres of pipe to lay. This gives rise to a profile of the vessels heading throughout the day. These two parameters can be regarded as the 'vessel centric parameters'.

Another system binding the vessel to the environment is the pipeline and the effect of the ground acting on the vessel. To take this effect into account, the required pipe-tension setpoints for the day and depth at any given time were taken as the 'pipelaying processes' related parameters. Collectively, the route plan parameters are summarised in Table 6.3.

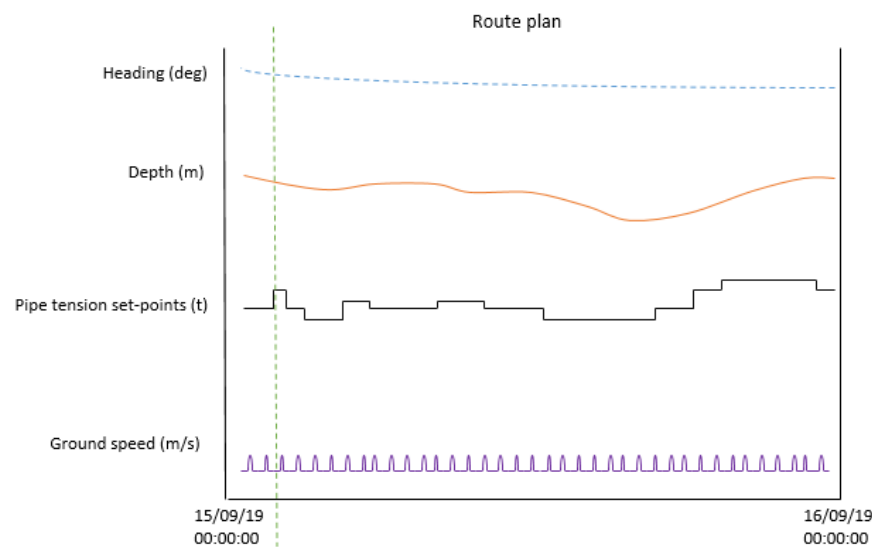


Figure 6.8: Route-plan parameters

Table 6.3: Route plan parameters

Parameter	Units	Normalised
Ground speed	m/s	✓
Heading	degrees	✓
Pipe tension	tonnes	✓
Depth	m	✓

Targets

The neural network learns input-output(target) relationships using trial and error. In this case since the load is the variable of interest to be forecasted, the pre-recorded generator output measurements have to be fed in as 'target' values.

6.4.3. Data collection

For neural network training purposes, the collected data are measured values on the vessel while for testing purposes- only the forecasted parameters are used.

Table 6.4: Training parameters

Parameter	Source
Ground speed	Vessel datalogger
Heading	Vessel datalogger
Pipe tension	Vessel datalogger
Wind speed & direction	Vessel datalogger
Significant wave height	Vessel WAVEX system
Depth	Pre-lay survey

Table 6.4 shows the parameters used for training the neural network. In all instances the data used are real measured values.

Table 6.5: Testing parameters

Parameter	Source
Ground speed	Developed profile
Heading	Pipe route
Pipe tension	Pre-determined setpoints
Wind speed & direction	Weather forecast
Significant wave height	Weather forecast
Depth	Pre-lay survey

In the case of the testing parameters (Table 6.5), to forecast the load, one will not be able to use measured values to make forecasts. For the weather parameters, the latest weather forecasts received at Allseas are used. The depth and pipe-tension setpoints have been pre-determined based on measurements & calculations respectively. The vessels heading is determined by taking the general direction that follows the pipe-route which is known in advance. As for the groundspeed, the measured groundspeed is filtered (to remove any noise) to obtain a smooth & regular profile in order to allow the measured and forecasted values to be compared.

6.4.4. Pre-processing data

Once the inputs and targets have been selected, the next task is to pre-process the data. The pre-processing stage involves filling in the missing data-points and normalising the data. Most parameters had little to no missing data (<5%), however due to the nature of significant wave height measurements wherein the WAVEX system measures data over a 300 second period, the information is updated only every 300 seconds. In order to alleviate this problem when building a time-series at a sampling rate of 1 second, the nearest neighbour interpolant was used. The advantage of this method is that it does not create any new data points but merely connects all the available data-points in the form of steps that accurately captures the trend in which significant wave height varies throughout the day. Following the filling of missing data-points, all the input parameters were normalised within the [0 – 1] range.

6.4.5. Network design

The final neural net consists of 7 input parameters into an input layer followed by a single hidden layer consisting of 25 neurons and sigmoid activation functions (Figure 6.9). The output layer consists of a linear activation function in order to map the output values as power demand forecast (in kW). The selection of the number of neurons in the hidden layer is through a trial and error estimation. Several tests were conducted

on small and larger datasets by varying the number of neurons and the best responses of the target power profile was obtained when using 25 neurons. Effects of varying neuron numbers are outlined in Appendix C.

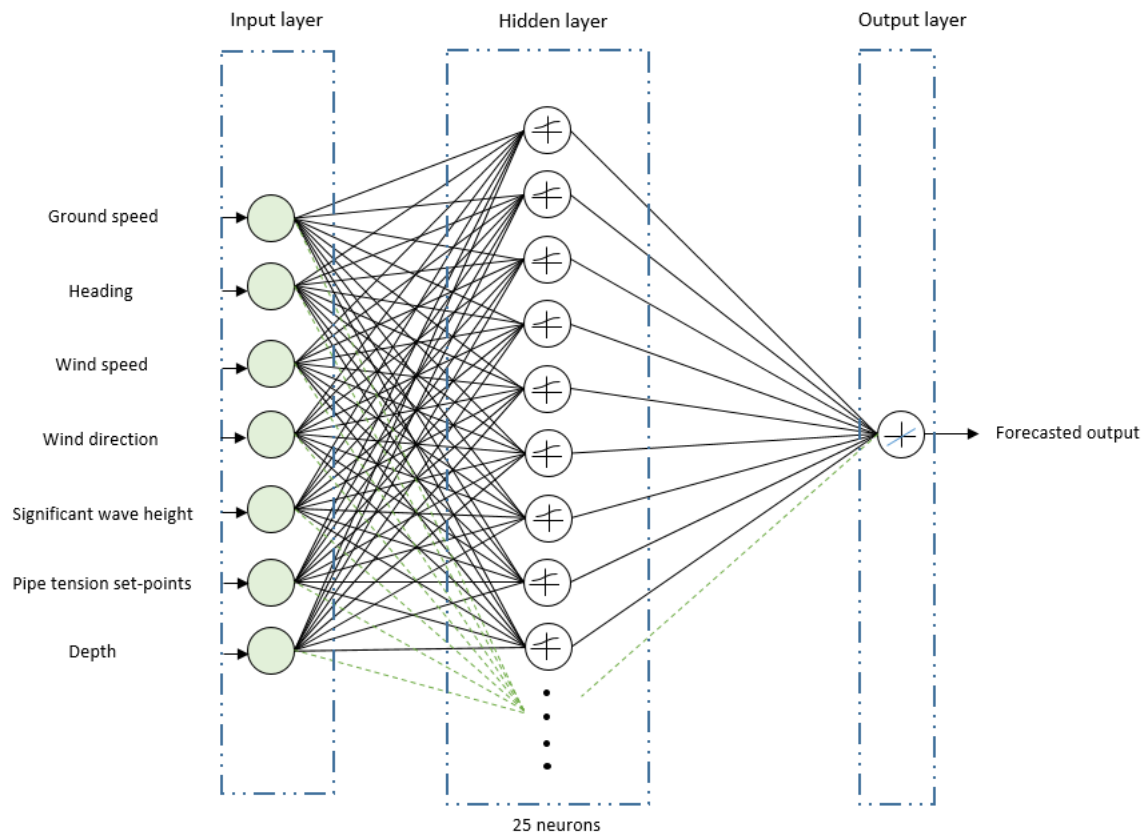


Figure 6.9: Neural network design for load forecasting

6.4.6. Training & Validation

Training is the process of teaching the neural network how to adapt itself to perform system identification. It is done by a process of trial and error wherein the network predicts an outcome and this is compared to the actual outcome in the form of a performance function. This performance function is then used to readjust the weights and biases within the network in order to improve its prediction capabilities. This type of training has a feedback element involved in the training process (Figure 6.10). A deployable version of this neural network can be built once the training process is complete and the feedback loop is removed in order to produce the required feed-forward neural network. The process of training is essentially an optimisation process wherein the cost function is the error which must be minimised. A variety of optimisation algorithms exist that are suited to different types of problems. While the optimisation strategy remains the same, the methods employed to make the optimisation strategies more efficient are dependent on the size of problem, accuracy required and computational power available. In this case, the goal is to be able to handle a large datasets as the recorded data consists of approximately 2 million datapoints for the seven input parameters and their corresponding target values of the same size.

In the training phase, at each iteration, the error 'E' is computed. This error is fed back into the neural network model and depending on the magnitude of the error, the weights in the network are readjusted in order to make a slightly better prediction in the next iteration. This process continues until either the performance goals are met or the 'validation checks' are complete.

Optimisation strategy

The general optimisation strategy comprises of a forward pass wherein the error is computed (performance measuring parameter). In this case, the performance function is the mean square error (MSE). The reason for taking the square of the error is that it is mathematically convenient. If the error were to be taken as the

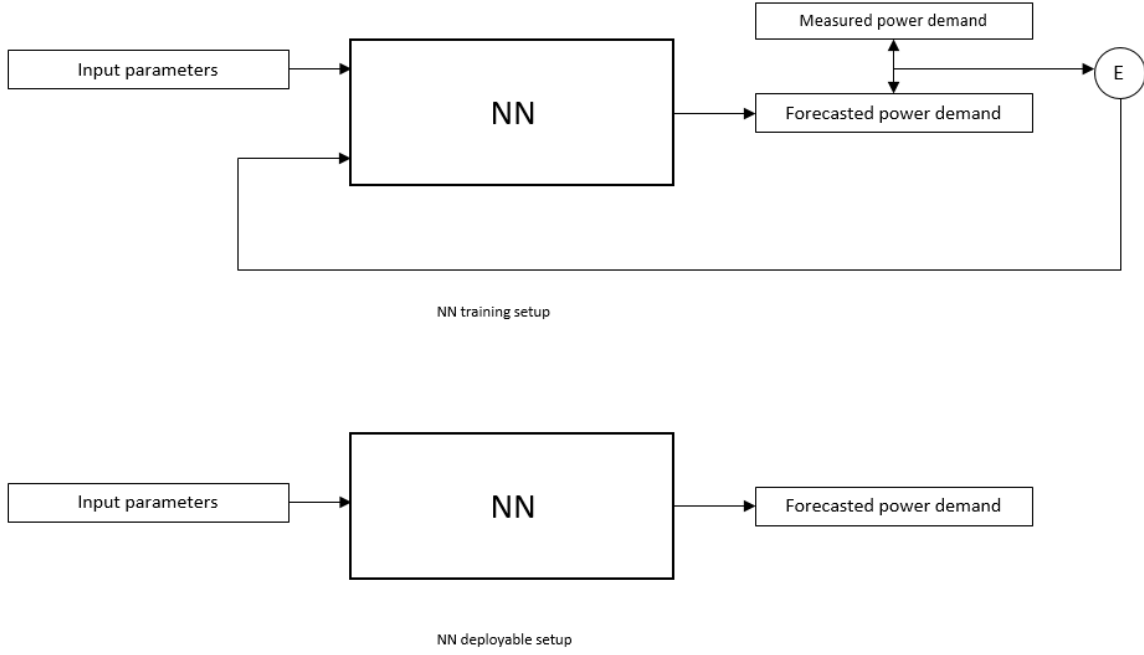


Figure 6.10: Comparison of response from different neuron settings in the hidden layer

absolute value, when calculating gradients (which are required for the optimisation process), the resulting differential would result in a constant value which would be the slope the performance function (straight line). By taking the square of the error, we solve this problem by being able to obtain a curve which can be differentiated to give a better insight into the error surface. Following this computation in the first iteration, the backward pass is used in order to re-adjust the weights within the network.

$$E_i = \sum_{j=1}^N \frac{(y_j - \hat{y}_i)^2}{n} \quad (6.7)$$

Where: E : Mean squared error
 y_j : Target value
 \hat{y}_j : Predicted value
 n : Samples

If we consider a system with a weight vector represented by [36]:

$$\hat{w} = (\dots, w_{ij}^{(l)}, w_{i+1j}^{(l)}, \dots, w_{Nj}^{(l)}, \theta_j^{(l+1)}, w_{ij+1}^{(l)}, w_{i+1j+1}^{(l)}, \dots) \quad (6.8)$$

Where: $w_{ij}^{(l)}$: Weight from unit number i in layer number l to unit number j in layer $l+1$
 N_l : Number of units in layer l
 $\theta_j^{(l+1)}$: Bias for unit j in layer $l+1$

The error during this optimisation process is calculated in a forward pass as $E(\hat{w})$. The gradient is calculated in a single forward and backward pass $E'(\hat{w})$. The gradients vector is represented as:

$$E'(\hat{w}) = \left(\dots, \dots, \sum_{p=1}^P \frac{dE_p}{dw_{ij}^{(l)}}, \dots, \sum_{p=1}^P \frac{dE_p}{dw_{i+1j}^{(l)}}, \dots, \dots, \sum_{p=1}^P \frac{dE_p}{dw_{Nj}^{(l)}}, \dots, \sum_{p=1}^P \frac{dE_p}{d\theta_j^{(l+1)}}, \dots, \sum_{p=1}^P \frac{dE_p}{dw_{ij+1}^{(l)}}, \dots, \dots \right) \quad (6.9)$$

where P is the number of patterns presented to the network and E_p is the error associated with the pattern 'P' [36].

Now assuming the first iteration has been completed, we reach a stage in which the decision must be made as to proceed to re-adjust the weight vectors in order to reduce the global error. A traditional approach to this would be to use the popular gradient descent based back propagation algorithm [22]. In this algorithm, we decide the direction (\hat{p}_k) to take the next step by computing the steepest gradient ($-E(\hat{w})$) is chosen as the direction in which the weights will be re-adjusted. The step to the next point is based on a fixed step size of α_k . One of the disadvantages of this optimisation strategy is that the error at a point ($\hat{w} + \hat{y}$) given by $E(\hat{w} + \hat{y})$ is linearly estimated as $(E(\hat{w}) + E(\hat{w})^T y)$ which leads to poor convergence. Furthermore, parameters such as the step size are selected manually, hence, the convergence either takes too long or too short with poor results. In order to alleviate this problem, Rumelhart et al introduced a ‘momentum’ term which helps the algorithm escape local minimas.

Algorithm 5 General optimisation strategy [36]

start: $k = 0$

1: Choose initial weight vector \hat{w}_i and set $k=k+1$.

2: Determine a search direction \hat{p}_k and step size α_k so that $E(\hat{w}_k + \alpha_k \hat{p}_k) < E(\hat{w}_k)$.

3: Update weight vector: $\hat{w}_{k+1} = \hat{w}_k + \alpha_k \hat{p}_k$.

4: If $E''(\hat{w}_k) \neq \hat{0}$ then set $k = k + 1$ and go to Step 2 else return \hat{w}_{k+1} as the desired minimum.

The complete optimisation strategy is outlined in Appendix C: Section C.3.

Validation

During the training phase, the data fed into the model amounted to 2,056,320 data points. The partitioning of the data is represented in Table 6.6.

Table 6.6: Data partitioning

Type	Samples	%
Training	1,439,424	70%
Validation	308,448	15%
Testing	308,448	15%

The validation step is an important step in determining whether the model is overfitting the data or not. The way this works is by conducting validation checks throughout the training process i.e., while the model is training, some inputs are fed in as ‘test inputs’ to check if the performance of the model matches that of the target values without producing large errors. A sign that the model is overfitting is when the error reduces on training but rapidly increases as it is trained even further. The moment this threshold of validation checks have been satisfied, the model stops training.

In the validation performance plot it can be seen that the green line slowly diverges away from the training error which means that the model is slowly beginning to overfit. The training process is then terminated at epoch 2166 and the weights from the best performance epoch is saved to the neural network model.

6.4.7. Testing

In the previous section, the model was trained using the feedback set-up which means that it only performed one step ahead predictions and an MSE of 8810 (=93 kW) was recorded at epoch 2160 (Figure 6.11). This error rate is quite small given that it is being used for system identification of the vessel. However, to deploy such a tool to be used in the power management system or to use it remotely for forecasting would require it to perform multi-step predictions. This is done by removing the feedback element and creating the feed-forward structure of the neural network. The model will only receive the exogenous inputs i.e., the weather forecasts, depth, pipe tension setpoints and ground speed profiles. Based on this the neural network will forecast the total load for the day to come.

For the purposes of testing, another dataset was assigned which the neural network had never ‘seen’ i.e., a set of data that has not been associated with any past use for model development. This is done so that the model uses its new found capabilities to generalise well enough to make load forecasts rather than having ‘memorised’ past input-output relationships. The test set contains data from 18-11-2018 to 22-11-2018 (5 days in total). While the responses of the neural network are available in Appendix C, two instances have been highlighted here- one wherein the network performs well and the case where the performance is poor. A

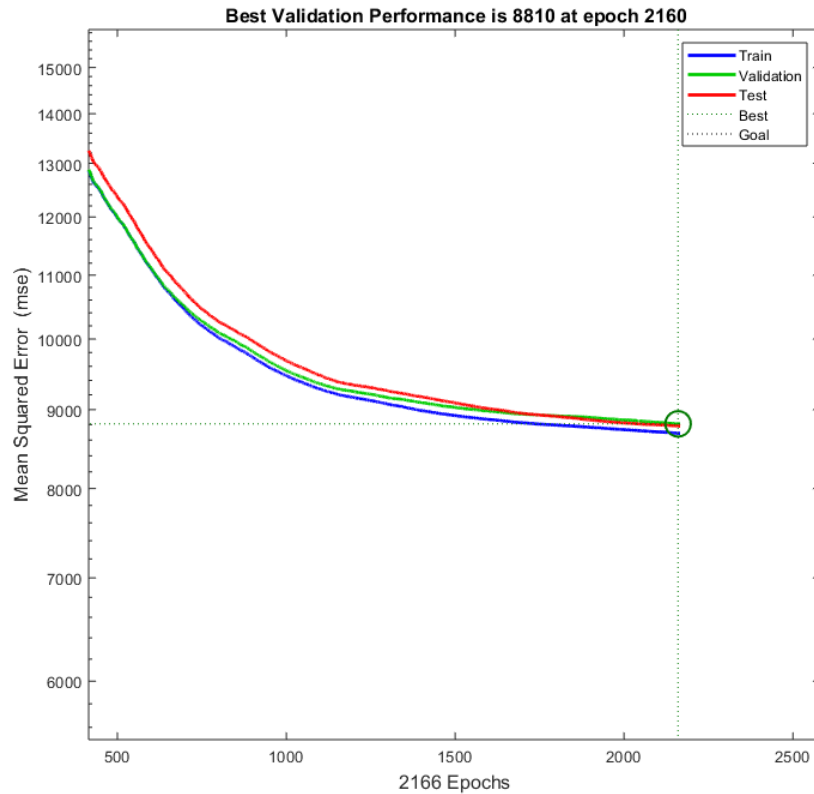


Figure 6.11: Neural network performance plot

summary of the test days are outlined using MAPE (Mean absolute percentage error) in Table 6.7 to compare this with the performance of the AMRA model used by Spruijt (2018).

$$MAPE = \frac{1}{N} \sum_{t=1}^N \left| \frac{\hat{y}_t - y_t}{y_t} \right| \quad (6.10)$$

Where:

- $MAPE$: Mean absolute percentage error
- y_j : Measured value
- \hat{y}_j : Predicted value
- N : Total samples

Table 6.7: Testing results

Test day	MAPE(%)		Remarks
	MS1	MS2	
18/11/2018	9.13 %	14.57%	Imbalance between switchboards
19/11/2018	6.90%	7.98%	No significant trends
20/11/2018	9.40%	8.03%	No significant trends
21/11/2018	13.07%	16.99%	Load changes due to vessel heading changes
22/11/2018	14.49%	14.40%	Load changes due to vessel heading changes

Good forecast performance

The forecasted response of the MS2 switchboard on 19-11-2018 shows good agreements between the forecasted and measured response (MAPE=7.98%). As the day progresses, at around 10 am, the forecasts overestimates the load despite the load actually reducing. The magnitude of the peaks are captured well throughout the day.

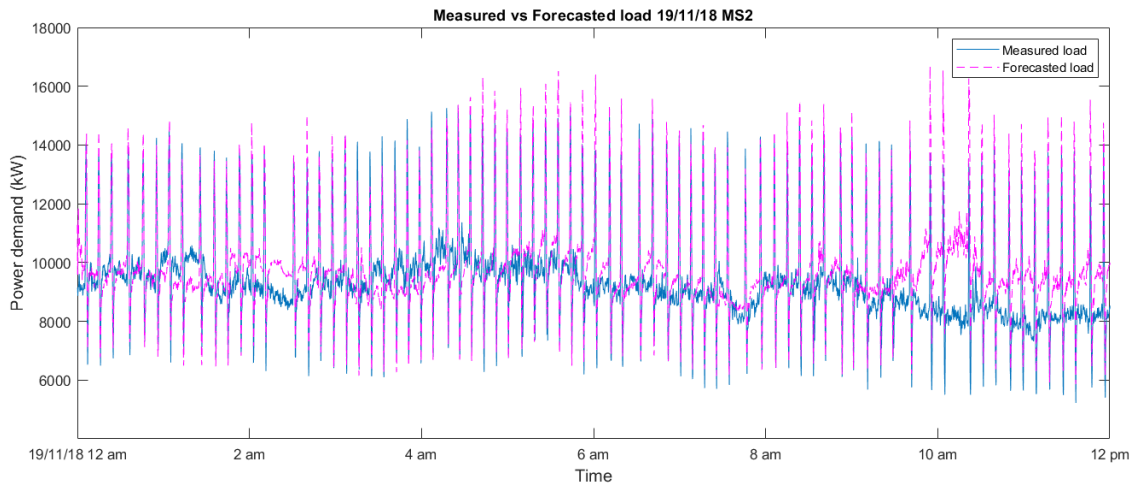


Figure 6.12: Forecasted load for 19-11-2018 (MS2)

Poor forecast performance

The forecasted response from 22-11-18 shows that around approximately 11:45 am, the load has a sudden increase. This was due to a vessel heading change as noted from the input parameters. The neural network then struggles to cope with understanding the new condition as it has not had enough training on a sample size large enough to incorporate such instances.

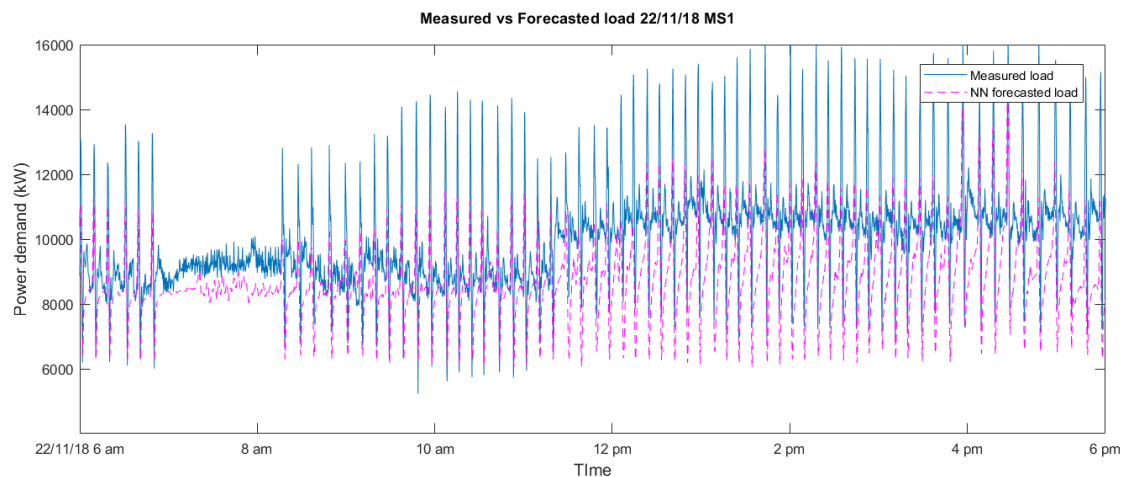


Figure 6.13: Forecasted load for 22-11-2018 (MS1)

6.5. PMS applications

Based on the forecasting capabilities of the neural network, it will now have to be determined as to how these forecasts can be used in order to reduce the size of the battery installed for spinning reserve. Given that the baseline design of the battery experiences on average 1.5C discharge during the power surge shaving mode on pipe-laying operations, if the profile of the power demand can be forecasted in advance, a generator can be started up instead of using the battery while the rule based system works on the back looking principle.

This means that the battery can be sized smaller and still ensure that it has a sufficiently long enough cycle life. This method of employing the forecasts to reduce the battery size will be referred to as the ‘generator start-stop scheduling’ method.

As the size of the power peaks are highly correlated with the magnitude of the power peaks, it can be said that reducing the ground speed setpoint could reduce the magnitude of the power peaks. This would mean that an additional generator need not be turned on as the power peaks would be smaller. The C-rate experienced by the battery would also be lesser in this case while it is on the power surge shaving mode. The battery size can be reduced in this case as well. In the further sections, this method will be referred to as the ‘voluntary velocity reduction’ method.

In both approaches, the rule based system works concurrently to offer a backup/safety-net to the power management system which will not be completely reliant on the forecasts.

6.5.1. PMS response

Method 1: Generator start-stop scheduling

For the generator start-stop scheduling method, two types of scenarios have been considered. One scenario looks at a day that is characterised primarily by pipe-laying. The second scenario was one in which the vessel had a partial downtime that lasted approximately half the day. To determine the load profile, latest weather forecasts available to the *Solitaire* were fed into the neural network (NN) model along with the route plan.

Scenario 1: Pipe-laying operations

In the pipe-laying scenario (Figure 6.14), the *Solitaire* spends the day laying pipe with no downtime. Certain portions of the day, such as, just before 10 am and after 4 pm, the forecast suggests that the magnitude of the power peaks would be low enough to warrant a generator shutdown. Once the shutdown is initiated, the rule based system continues to monitor the power peaks. It can be seen that the actual measured power demand (blue line) indeed is larger than the forecasted values which causes the rule based PMS to initiate a generator start-up at a little after 12 pm in the first case and similarly in the second case, before 6 pm. In this case, there seems to be a constant battle between the rule based system and the forecast model as the neural network model underestimates the load while the measurements have shown otherwise. This would mean that the installed battery would suffer more usage as long as the load predictions are underestimations and hence a size reduction of the battery is not recommended. A reduction in size implies that the battery is cycled at higher C-rates during these generator shutdown phases.

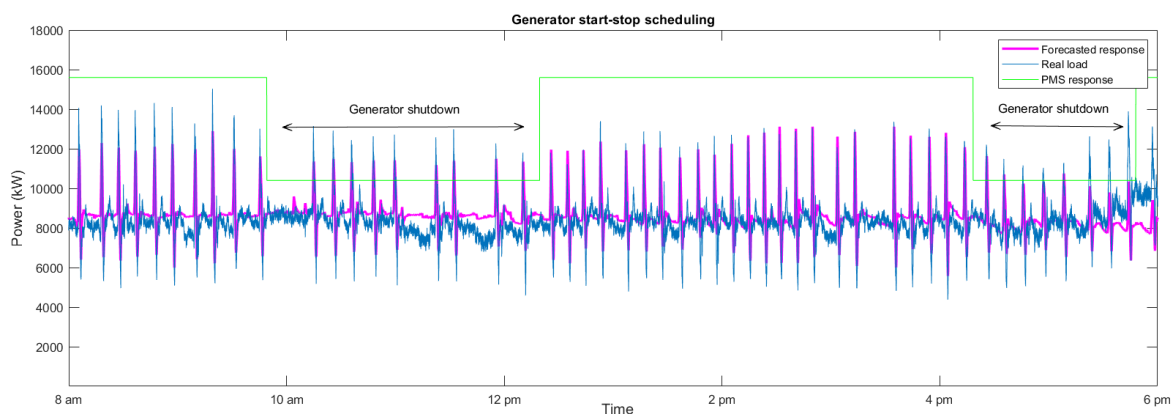


Figure 6.14: Generator scheduling during pipelaying operations

Scenario 2: Pipe-laying & downtime

In the scenario that the vessel has a partial downtime (Figure 6.15), it can be seen that the forecast model overestimates the load that would be experienced by the vessel. The rule based system would have initiated a generator shutdown around the 8 am mark however, the forecast model has predicted a larger load. This discrepancy results in the PMS not shutting down an engine due to an overestimation of the load. The results are that the battery is not used at all for the power surges and can indeed be sized smaller as overestimations or accurate predictions in loads do not result in any significant usage of the battery and a generator is kept running instead. The implications of this would be that while the battery sizing can be reduced, the savings in the form of fuel consumption, running hours and emissions would also reduce. On test days 19/11/18

and 20/11/18 (see Appendix C), the forecast was accurate enough that the scheduling of generators could be done and that a battery size reduction could be made in such scenarios.

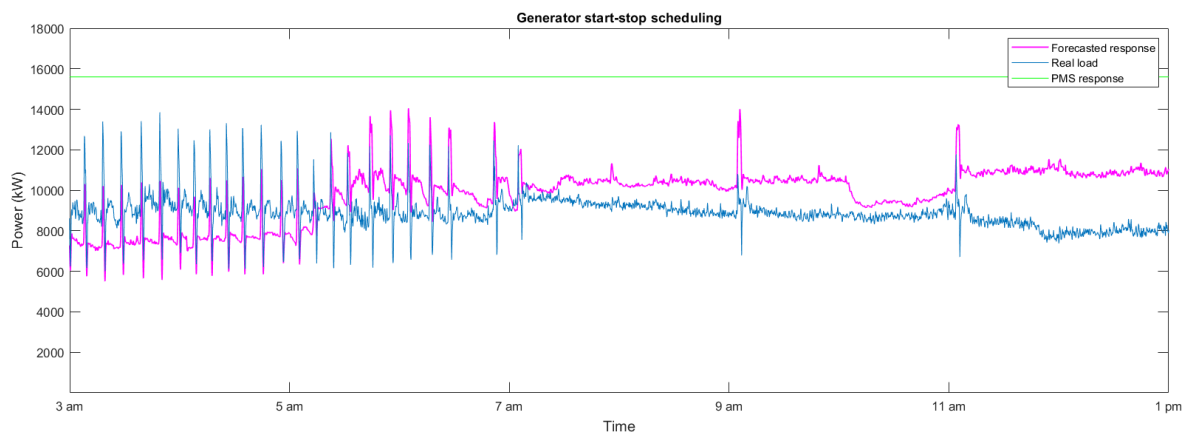


Figure 6.15: Generator scheduling during downtime

Method 2: Voluntary velocity reduction

As the size of the power peaks is correlated with the ground speed of the vessel, a case can be made for reducing the peak speed set-point during a pipe-pull. By voluntarily reducing the velocity, the size of the power peaks could be reduced such that the batteries can handle these peaks without exceeding the power surge limit of allowing the battery to work within 1.5C. As the agreement between the forecasted and measured response was most accurate on 19/11/18, the input ground-speed profile of this day was selected to test the forecasted load in the event that the velocity would be reduced by 15%.

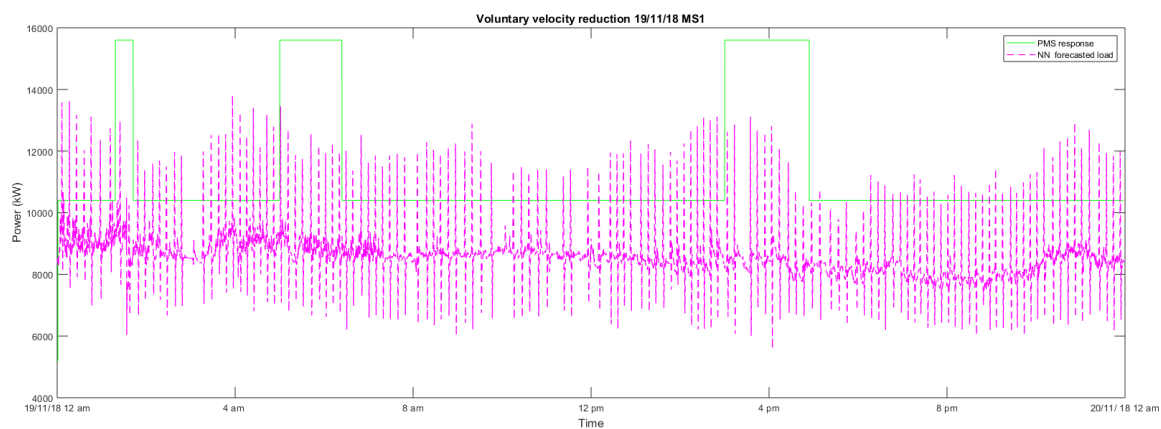


Figure 6.16: 15% reduced velocity on MS1

On 19/11/18 (Figure 6.16), the forecast suggests that a 15% reduction in velocity would significantly change the power profile such that the batteries could be used for large portions of the day to shave off the power surges. The relatively smaller power peaks imply that technically, a smaller (re-sized) battery could be used to shave off these power surges. The rule based system was used in this case to initiate generator start-stops, however, using the forecasts even the three instances of the generator start being initiated (at 1 am, 5 am and 3 pm) could be prevented if the vessel reduces its velocity in those cases by more than 15%. As a consequence of reducing the velocity, the time taken to complete a pipe-pull would increase. The influences of this are considered in Section 6.6.1.

6.6. Simulations & Results

6.6.1. Fuel reduction

For fuel reduction calculations, the quantification approach is using the same model as prescribed in Chapter 5. Based on the output of the forecast model, the measurements were tabulated under the two methods and compared against the response of the rule-based system.

Table 6.8: Generator scheduling: Fuel savings results

Operation	Rule-based model (MT)			Forecast model (MT)			Fuel savings(MT)
	MS1	MS2	Total	MS1	MS2	Total	
Pipe-laying	1.49	2.02	3.51	1.59	1.71	3.3	-0.21
Pipe-laying & Downtime	1.94	2.14	4.08	1.88	1.69	3.57	-0.51

Table 6.9: Voluntary velocity reduction: Fuel consumption & savings results

Velocity setting	Velocity reduction (MT)			No velocity reduction (MT)			Fuel savings(MT)
	MS1	MS2	Total	MS1	MS2	Total	
15% velocity reduction	43.23	42.63	85.86	43.56	44.55	88.11	2.25

Discussion

In the case of the generator-scheduling method (Table 6.8) the results suggest that using the forecasts results in lower than expected fuel savings. This is consistent with the PMS response previously seen wherein the forecasts tend to make over-estimations which result in an additional generator running when it is not necessary. In the event that the forecasts make an under-estimation, the rule based system then engages in order to protect the batteries from over-use. However, as the generator is running, this implies that a battery is not necessary at this point to shave the power surges. This creates a paradox in that one may decide to rely on the forecast model and size the battery smaller- consecutively receiving lower savings or else, sizing the battery larger and reaping the benefits of a larger battery with its better capabilities.

As the power peaks are correlated with the ground-speed, a 15% reduction in ground-speed was made in order to reduce the power peaks and allow a potentially smaller battery supply the power peaks. The average speed is reduced from the existing 0.340 m/s to 0.249 m/s (as the ground speed input-parameter). The fuel savings in this case compared to the rule-based system operating without velocity reduction shows that there is a significantly larger savings in fuel (Table 6.9). However, the time taken to complete the pipe-pull increases from approximately 70 seconds to 82 seconds. This 12 second increase in time means that in a day with approximately 100 pipe-pulls, there would be a reduction in 14 pipe pulls (each at 24.4 meters) that could be completed. Approximately every 10 days, this distance adds up to 3.4 kilometres- which means that the vessel will have to lay pipe for an additional day. This negates any fuel savings made in the 10 day period.

6.6.2. Battery measurements

Battery measurements were collated across two main scenarios i.e., using the rule based system (Results: Table 6.10) and the forecasting mode. Additionally, the two sub-categories of generator scheduling and velocity reduction methods were considered under the forecasting mode to understand the effects on the batteries. Across all analyses the rule based system was used as a backup system in the event that the forecasts failed to capture the load sufficiently well.

Table 6.10: Battery measurement results: Rule based-system (RBS)

Test day	Runtime (min)		Average C-rate		Average DoD(%)		Cycles	
	MS1	MS2	MS1	MS2	MS1	MS2	MS1	MS2
Pipe-laying	5.66	2.8	0.86	0.75	1.01	1.16	11	15
Pipe-laying & Downtime	16.9	8.5	0.94	0.78	0.98	0.77	76	13

Table 6.11: Battery measurement results: Forecast based generator scheduling

Test day	Runtime (min)		Average C-rate		Average DoD(%)		Cycles	
	MS1	MS2	MS1	MS2	MS1	MS2	MS1	MS2
Pipe-laying	4.33	0.3	0.37	0.19	0.39	0.1	17	4
Pipe-laying & Downtime	6.6	0	0.61	0	0.67	0	48	0

Discussion

Comparing the rule-based system and the generator scheduling method (Table 6.11)- it can be seen that the battery is not used as much in the latter case. The cycles experienced by the battery is also lower than in the case of the rule-based system. All measured parameters suggest that there is a case to be made for reducing the batteries as the nominal conditions of operating the battery at 1-1.5C during power surge has not been met in the scheduling case. This is due to an additional generator running based on the forecast. These measurements further corroborate the paradox that a smaller battery can be used as long as the limited capabilities & smaller savings of the re-sized battery arrangement is acceptable.

Table 6.12: Battery measurement results: Forecast based velocity reduction (VR)

Test day	Runtime (min)		Average C-rate		Average DoD(%)		Cycles	
	VR	RBS	VR	RBS	VR	RBS	VR	RBS
19/11/18 MS1	80	30.16	0.91	1.01	0.77	1.04	109	41
20/11/18 MS2	88.8	42.96	0.72	0.74	0.54	1.17	129	76

Discussion

The velocity reduction method results (Table 6.12) has shown that this is the best option from a re-sizing perspective. In this case the battery usage is significantly greater as it will be used for large portions of the day, however as the DoD and C-rates are lower, it is possible to reduce the size to an extent that the new battery would produce C-rates in the range of 1-1.5C during power surges. The limiting factor in this case is the number of cycles that the battery experiences per day which is relatively larger than in all other options considered. This would mean that a battery with a very high cycle life is required for this application.

6.6.3. Emission reduction

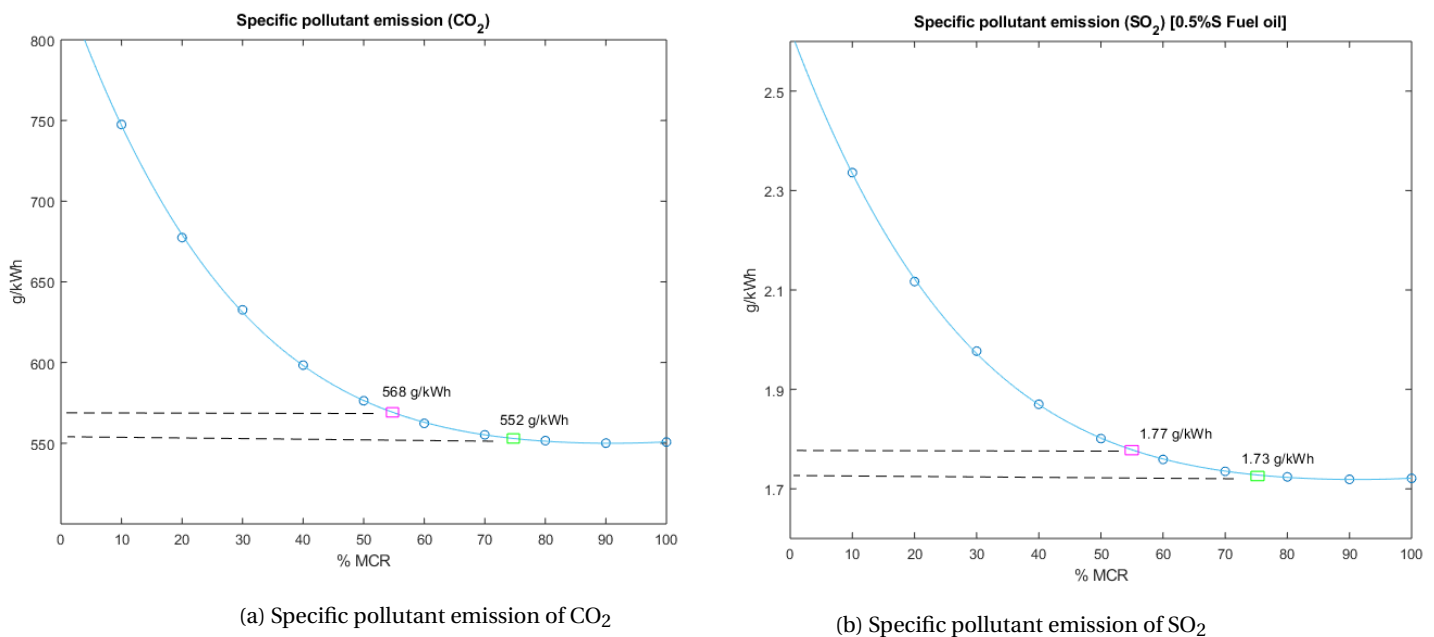


Figure 6.17: Specific pollutant emission: RBS vs Genset scheduling

Table 6.13: Emission reduction using forecasting vs RBS (Pipe-laying scenario)

Test day	Daily emission reduction	
	CO ₂	SO ₂
RBS	12,160 kg	38 kg
Genset scheduling	11,008 kg	34.4 kg
Velocity reduction	17,248 kg	53.9 kg

Discussion

Between the generator scheduling and rule based system- the forecast model has a higher pollutant emission (Table 6.13) as it is generally working at lower operational loads (Figure 6.17a and Figure 6.17b). As can be seen, if the battery sizing were to be made small such that it would then necessitate a generator start-up, the pollutant emission would be larger. The velocity reduction option is not regarded as a viable solution to the problem as the reduction in velocity implies additional operational days of the vessel.

6.6.4. Running hours & Engine loads

Engine loads for the RBS as well as the scheduling method were compared during pipelaying operations. The results show that in the case of the rule-based system, using the baseline battery design, the vessel operates for about 7 hours under 50-60% and 70-80% MCR load on the engines (Figure 6.19). This is clearly the superior choice compared to the forecast model which, due to over-estimations in the load results in an additional generator running rather than allowing the battery to absorb the power peaks. Furthermore, in the case of the generator scheduling, if the battery were to be resized to a smaller arrangement, even if the forecast correctly made the load estimations- it would not always allow the battery to shave off those power peaks as the magnitudes would be too large to do it within the batteries power surge shaving C-rate range of 1.5C.

The generator scheduling option keeps the engines running in the 50-60% range for the most part of the day (12-13 hours) while allowing only about 2 hours for the engine to operate at 70-80% load (Figure 6.18).

Running hours

Table 6.14: Running hours measurements: Rule based system vs Generator scheduling

Test day	Rule based system		Generator scheduling		Total reduction (hours)
	MS1	MS2	MS1	MS2	
Pipe-laying	69.66	60.92	68.78	71	-9.2
Pipe-laying & Downtime	64.79	59.86	67.54	71.46	-14.35

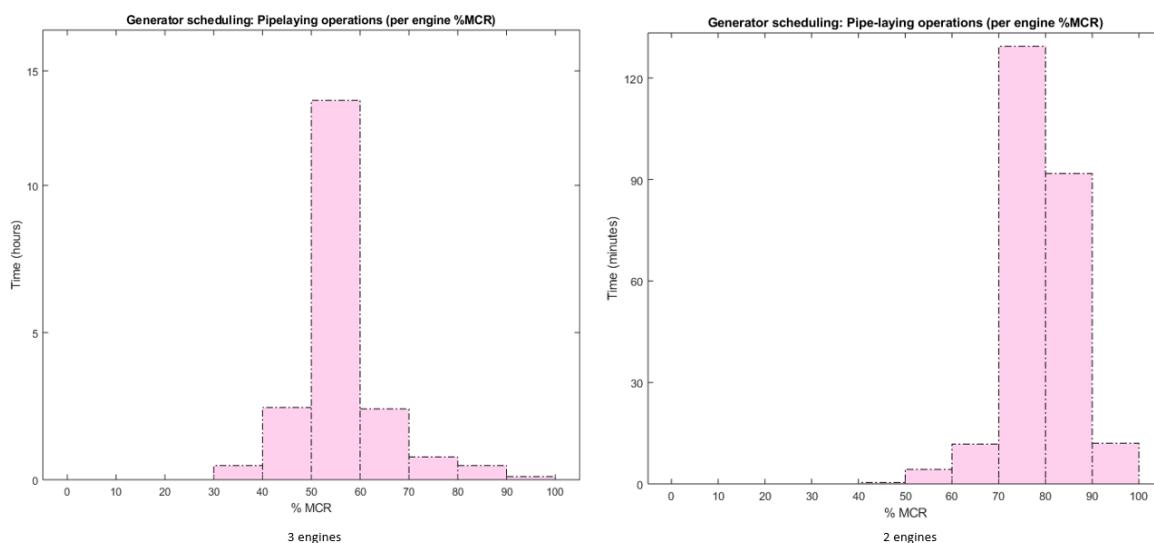


Figure 6.18: Engine loads using the forecast model

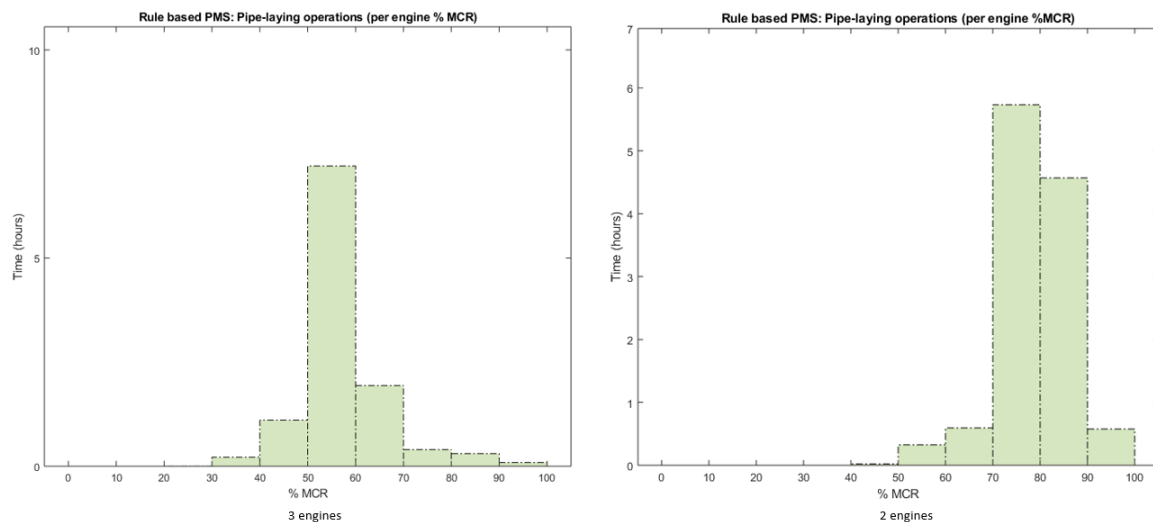


Figure 6.19: Engine loads under the rule based system

Table 6.15: Running hours measurements: Rule based system vs Velocity reduction (VR)

Test day	Total running hours		Total reduction (hours)
	RBS	VR	
19/11/18	118.32	103.22	15.10
20/11/18	110.44	96.62	13.82

Discussion

While engine loading conditions have improved in the case of using the rule based system as well as the forecast model, reduction in running hours shows that in the case of the generator scheduling (Table 6.14), due to the nature of the forecast, it keeps additional engines running to avoid the eventuality that the load is higher than the measured values in the future. This prediction keeps the engines running despite the actual not exceeding this value. Hence the greater number of running hours and lower fuel savings in this case offset any savings made by reducing the battery size marginally. The velocity reduction option (Table 6.15) makes significant savings in the number of running hours of engines but the advantages of this are offset by the fact that the slower lay speeds will require an additional day of work. The additional fuel expenses of this additional day of work offset any significant savings made by running hour reduction.

6.7. Implications on ESS

Based on the inferences from Chapter 5 and Chapter 6 results it is apparent that the forecasting model has the potential to reduce the battery size only if the predictions made by the model are near perfect. Any over-estimations or under-estimations of the load would result in either the smaller re-sized battery being over used or keep additional generators unnecessarily running. In the event that the model can be trained on several years of data, in theory, it would still have troubles accurately predicting the load due to the fact the the exogenous inputs into the neural network model are weather forecasts rather than actual weather conditions. The weather forecasts are reliant on a variety of forecasters at Allseas and the dependency of the the model output on another forecast would mean that there is a likelihood of the errors compounding if the weather forecasts are not as accurate as desired.

Scenario 1: Battery re-sizing without forecasts

Based on the simulations from Chapter 5 using the rule based control system, it was found that the average C-rate experienced by the battery throughout the day is typically lower than 1.5C as the battery is subjected to large as well as small power peaks. The previously set 120 kWh (to account for the maximum energy under a 4 MW power peak) may be reduced to obtain a smaller sized battery. The upper limits of the battery's operational capabilities are shown in Table 6.16. In the fully charged condition, the re-sized battery may be used in the 85%-83% range for power surge shaving and the remaining reserve for spinning reserve requirements. At the end of life condition, the top 5% may be used for power surge shaving and the 75% for spinning

reserve. The lowest SoC that all the units can be maintained is at 42% (54% at EOL) to ensure that there is sufficient energy for spinning reserve (for at-least 3 minutes) and for power surges.

Table 6.16: Split battery battery specifications: RBS

	Baseline split battery		Re-sized split battery	
	New	EOL	New	EOL
Total battery size	3064 kWh	2451 kWh	2816 kWh	2252 kWh
Nominal power rating	7830 kW	6127 kW	7040 kW	5632 kW
1.5C power surge limit	2298 kW	1838 kW	2112 kW	1690 kW
Spinning reserve power rating	11490 kW	9191 kW	10560 kW	8445 kW
Run-time	3+ minutes		3+ minutes	
CAPEX*	\$1,991,600		\$1,830,400	

* only the Lithium-ion is considered here (=650 US\$/kWh- Corvus Energy Orca ESS)[2]

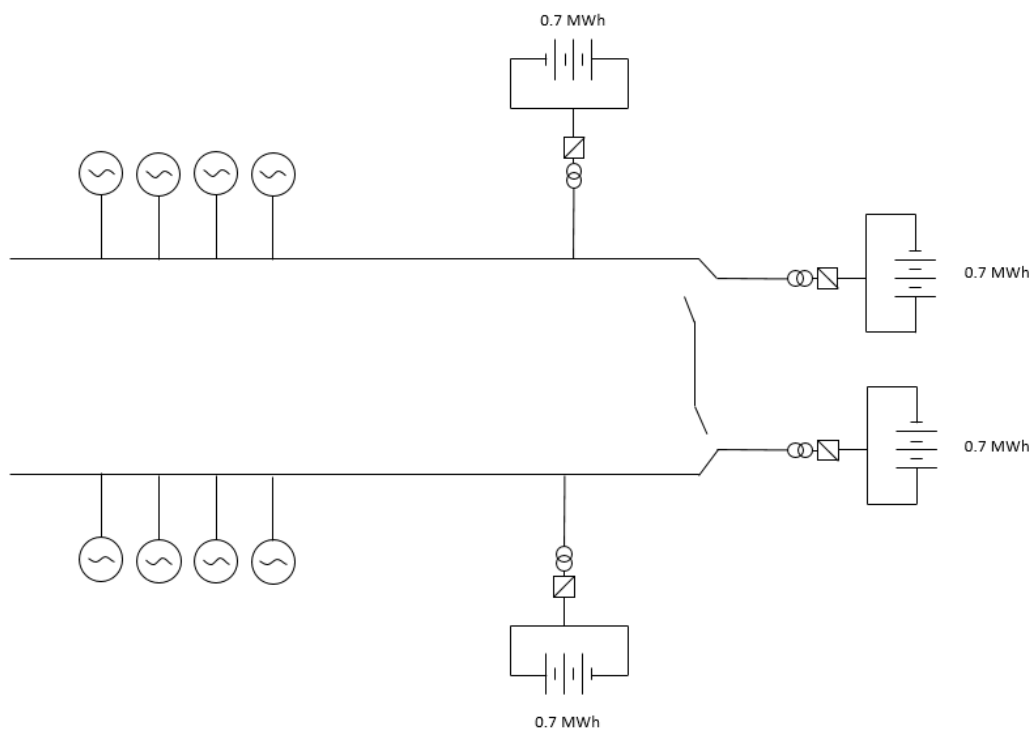


Figure 6.20: Re-sized split battery ESS without forecasts- schematic

Scenario 2: Battery re-sizing with accurate forecasts

In the scenario that the forecasts are successful in predicting the power demand of the vessel throughout the day with the fidelity to capture the DP load and changes in load due to heading changes, there exists a possibility to reduce the battery size. However it must be noted that this reduction in battery size will come at the cost of running generators in order to satisfy the excess power demands that surpass the batteries capabilities. Over-using the batteries due to inaccurate forecasts could harm battery life in the event that the forecasts underestimate the load. The savings obtained by installing the batteries would not be significant if the generators were to continue to run in order to satisfy the load demand. The advantage of this system is that under conditions that the power peaks are within 1-1.5MW, the system will be able to reap the maximum benefits with a lower CAPEX. Table 6.17 outlines the comparison between the re-sized split battery design and the split battery design with forecasts. The sizing of the 'split battery with forecast model' have been quantified by designing the spinning reserve requirement to 93% of the rated capacity of 5,650 kW.⁴ The

⁴This is because 0.93 is the new start limit for the next generator.

reduction in Lithium-ion capacity used in the event that the forecasts are accurate are a reduction of 37.8% compared to the re-sized split battery design.

Table 6.17: Split battery battery specifications: Forecast model

	Re-sized split battery		Split battery with forecast model	
	New	EOL	New	EOL
Total battery size	2816 kWh	2252 kWh	1751 kWh	1400 kWh
Nominal power rating	7040 kW	5632 kW	4377 kW	3500 kW
1.5C power surge limit	2112 kW	1690 kW	1313 kW	1050 kW
Spinning reserve power rating	10560 kW	8445 kW	6566 kW	5250 kW
Run-time	3+ minutes		3+ minutes	
CAPEX*	\$1,830,400		\$1,138,000	

* only the Lithium-ion is considered here (=650 US\$/kWh- Corvus Energy Orca ESS)[2]

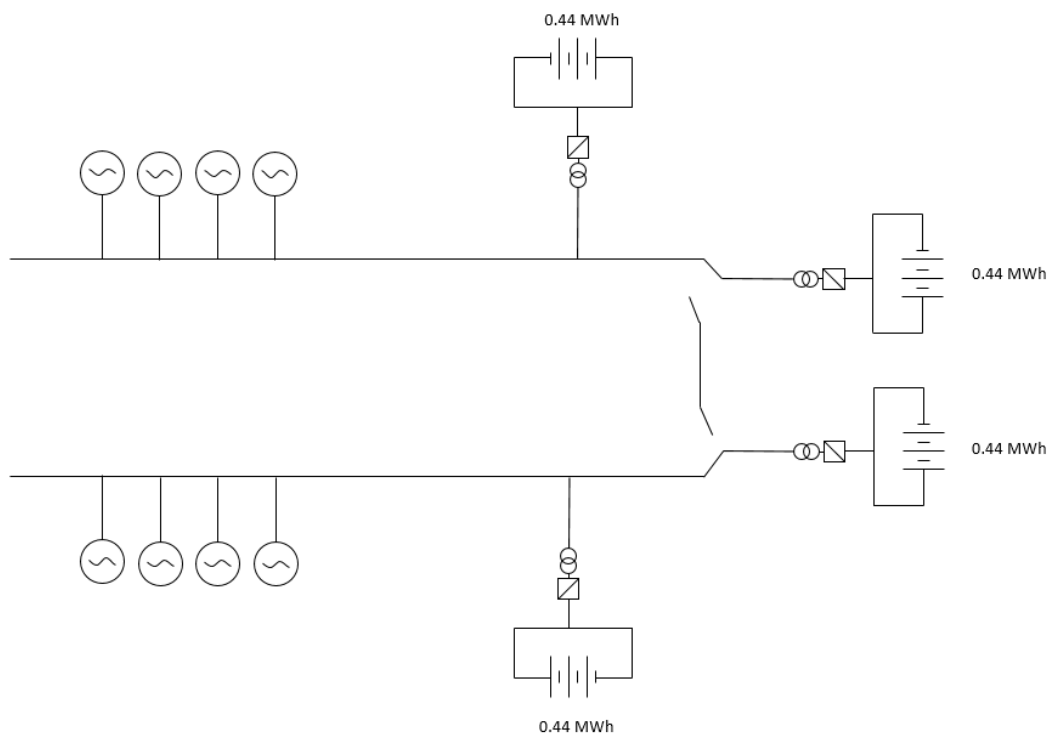


Figure 6.21: Re-sized battery ESS with forecasts- schematic

Conclusions and Recommendations

This research study has focused on the integration of a battery energy storage system with the electrical grid of a pipelaying vessel. The scope of analysis has been primarily shallow water operations which is characterised by pipe-pull actions i.e., the simultaneous movement of the vessel forward while the pipeline from the vessel is being payed out from the aft of the vessel. This characteristic operation in shallow water produces power surges in the order of megawatts. In previous research, the analysis was limited to deep-water operations but in this study it was found that power surges in shallow water operations are the main design consideration to be made for ESS sizing. Insight into the health of the electrical grid was gained through the help of measurements on board. Using these measurements, a better understanding of the implications of a battery installation under different failure scenarios were gauged. Following this analysis, the design criteria were identified as a result of the vessels operational profile and a new 'split-battery' design was developed.

Alongside the new system architecture, ESS management methods were developed to work in tandem with the existing power management setup. To further explore the potential for battery size reduction from the developed baseline design, a machine learning approach was used to forecast loads in order to gauge the possibility to reduce the battery size.

7.1. Conclusions

The research study is underpinned by the main research question formulated as:

“To what extent can a smart load forecasting algorithm influence energy storage size for shallow water pipelaying DP operations?”

To answer this, the sub-questions are re-visited to formulate a complete picture of the research study:

- *“How does the vessels operational profile and electrical health affect the installation of an ESS?”*

Statement: The operational profile has shown that the power surges caused due to pipe-pulls are a limiting factor when it comes to the ESS sizing. The poor electrical health of the Solitaire suggests that the inverters of the ESS must be oversized if no power factor compensation is conducted.

Reasoning: The operational profile of the pipelaying vessel *M/V Solitaire* was analysed during the Nord-Stream II project in 2018. In contrast to the previous research conducted on deep-water operations, in shallow water it is seen that the simultaneous pipeline deployment and forward motion of the vessel results in large power surges that occur periodically that must be supplied by the battery throughout the day. Hence the battery was designed to handle not only the spinning reserve requirement but also to handle power surges. As a design requirement to keep the power surges within 1.5C of the batteries capabilities, the maximum allowable peak size was determined to be in the 2-2.5MW range which resulted in the final battery sizing.

Based on the data analysis it was found that under the circumstances that the vessel continues to operate with a low power factor (0.55PF) and a battery energy storage system, the consequences of a generator failure could be more detrimental which requires an oversized inverter to compensate for the excessive apparent power demand during such a scenario.

- *“What kind of battery arrangement has the potential to reduce the capacity of Lithium-ion installed for split bus operations?”*

Statement: The developed split battery design allows a 33% reduction in lithium-ion for spinning reserve requirement, however as the power surges are a limiting factor in ESS sizing, the split units had to be oversized to handle the surges within 1.5C of the battery’s discharge capabilities. The architecture allows energy sharing between the split units which prolongs battery calendar life.

Reasoning: With the split architecture, the minimum spinning reserve requirement energy can be shared with 3 units of the architecture which allows all the individual units to be maintained at a low SoC as they are sharing the energy requirement during a failure event. This prolongs the calendar life of the battery and design is applicable across both open and closed bus. The design maintains the independence between the two switchboards under all operational scenarios and satisfies DP III regulations.

- *“How will the management of an ESS be integrated into the vessels power management system?”*

Statement: To integrate a battery ESS to the vessels grid, it was determined that a traditional rule-based power management system would not be sufficient as the benefits of the battery must be reaped by allowing the battery to handle the power surges. To do this, the moving average of the measured load must be taken over a 900 second time window in order to filter out the highly variant loads. In addition to the filtered load, the existing rule based table is augmented to include a new condition that must be met to initiate a generator start-up. These conditions are determined by a set of algorithms that monitor the usage of the energy storage system.

Reasoning: The setting of the new On/Off (trigger) variable is determined by a set of ESS management algorithms that monitor the magnitude and frequency of the power peaks to gauge whether they lie within the nominal operating conditions of the battery for power surge shaving. If they fall out of this region, it initiates the start up a new engine.

- *“How will the cycle life of the battery be influenced using load forecasting?”*

Statement: The improvements made in the cycle life of the battery suggest that marginal improvements could be made using a generator scheduling approach according to Table 6.10 and Table 6.11. In the case of the velocity reduction, the cycle life worsened (Table 6.12) which necessitates a battery with high cycle life to be used in the scenario.

Reasoning: The results suggests that the cycle life was improved using forecasting however the reason for this was that on occasion the neural network would overestimate the load which resulted in the PMS leaving a generator on when it was not required. The effect of an underestimation in the load would result the battery being used as per the conditions set by the rule based system (as it operates as a ‘safety-net’) and so no improvements were seen in cycle life in that scenario. The cycle life was influenced such that as the accuracy of the forecasts improve, the cycle life improves and as the accuracy reduces, the improvements are marginal to none in contrast to the rule-based system.

Using an alternative approach of reducing the forward velocity of the vessel by 15% during pipe-pulls resulted in the cycle life worsening as the battery was being used for nearly all pipe pulls throughout the day. This would suggest that the use of a battery with a high cycle life is required for long term operation.

- *“How much further reduction of the ESS size is possible using load forecasting?”*

Statement: Due to the effects of load underestimation and overestimations, the neural network based load forecasting has not yet achieved the capability to forecast the load with a high enough confidence to allow any reduction in the ESS size. However, with the ability to train the model on several years of data, it could be possible to obtain the forecasted results to be in close agreement with measured results or near perfect. In such a scenario, the battery may be resized to only the spinning reserve requirement & consequently downsized. Along with the split architecture, this offers the capability to reduce the battery size by 38%.

Reasoning: In the neural network model, one of the deficiencies observed was the inability for the model to capture the vessels heading changes and how the load on the vessel changes with respect to that action. The reason the model was unable to capture this phenomenon was that such instances

in the training dataset were far too few for the model to understand the relationship. Given more data from several months/years and more computational power- it would be possible for machine learning models such as the neural network to accurately capture the trends in the data.

However it must be noted that the response of the neural network is based on training done on actual weather conditions but the only available input data during the testing phase are the weather forecasts. Due to the inherent nature of the inputs themselves being forecasts, the error in weather forecasts would imply that an error in the neural network forecast would persist.

Based on the sub-questions, the main research question can now be addressed by comparing the two methodologies of ESS integration:

Base case: The new rule based system with a 2.8 MW split battery has been capable of reducing on average 3.14 tonnes of fuel oil per day of DP operations and a total running hour reduction of 52.5 hours per day. In addition to the monetary savings offered- the reduction of CO_2 and SO_2 emissions are approximately 10 tonnes and 32 kg respectively. These emission reductions have a profound effect on potential new contracts that could be pursued in the maritime market as there is a shift to more 'green contracts'. The implication of this is that although the economic viability of a battery is debatable from a savings and payback point of view, a contract award due to the 'green' status of the vessel would imply that the capital expenses of such an installation would ultimately be covered by the entity awarding the contract to the vessel operator due to the aforementioned reasons.

Forecast case: For shallow water operations, the extent to which the battery size can be reduced is upto 38% compared to the re-sized split battery design in the scenario that the forecasts and measured values are near perfect. The capability to reduce the capacity by such a large extent is due to the battery having to be re-sized only keeping the spinning reserve requirement in mind. The strengths of the split architecture in size reduction are more prevalent when the battery is designed only to the spinning reserve requirement. The power surge handling capabilities of such a battery will be limited but by using load forecasting, it is possible to allow the generators to handle large power peaks beyond the capabilities of the battery. In the event that the forecasts are not accurate enough to quantify the load correctly, it is not possible to make any size reductions of the battery as the incorrect forecasts can have negative effects on the health of the battery.

7.2. Recommendations

This research study has explored the vessels operational profile, electrical grid health, alternative design architectures to maximise battery calendar life and power management system integration using a rule-based and forecast-based system. Further areas of work that could be pursued following this study are:

Energy storage system

- One of the areas of future work would be to analyse the calendar life of the batteries- as this varies from manufacturer to manufacturer, it would be an area wherein the effects of different operational profiles of vessels could be incorporated in the battery calendar life prediction.
- For this study, the manufacturer prescribed 1.5C limit was used as the baseline for continuous charging and discharging. This limit is prescribed for air-cooled batteries. However, with liquid cooling, the battery may be cycled at higher C-rates for power surges which gives the opportunity to reduce the battery size. However the effectiveness of liquid cooling on Lithium-ion pouch cell is an area of research that could be pursued.
- A failure mode effect analysis could be conducted on the effects of low power power factor operation on the energy storage system as well as tests on thruster phase back at 100% load on the generators. Currently such tests have been performed on 55% and 85% load on the generators, however during pipe-pulls, situations will exist where the generators are loaded to 100%.

System architecture

- Recent developments within Allseas signal towards the vessels operating on a closed bustie with the necessary protection systems to be installed in 2020 (AGS- Advanced Generator Supervisor). This would mean that a large single battery is likely sufficient so long as the vessel operates on closed bustie. As the power peaks are characteristic for each switchboard- their combined effect on a single battery must be analysed in this event to size the single battery correctly for long life operation.

Load forecasting

- The neural network developed for this research could be trained further with larger datasets spanning years which would allow it to capture the effects of heading changes on the total load. Additionally, several more parameters could be incorporated such as the non-DP to DP mode switching signals, crane On-Off signals as all of these large equipment have an effect on the load changes seen when non-pipelaying. By identifying all the parameters that are responsible for the load changes, a neural network with more hidden layers could be used which would be able to capture even more complex relationships. Spanning a large dataset from several years would ensure that the model is not over-fitted and the neural net can also then be safely allowed to perform 'on-line' learning as opposed to batch learning techniques.
- A statistical model could be used in conjunction with the neural network in order to offer 'medium-term' forecasts that could allow the strengths of both models to be used in synergy.

Business outlook

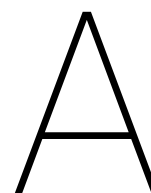
- Due to the nature of battery design having to incorporate energy and power as design requirements- it is seen that with current day Lithium-ion technology, the limiting factor is the battery life. To maximise the battery life- a relatively low power and higher energy battery is selected for the design when in reality it would be desirable to use a high power battery that has long calendar life. Since another constraint is battery power, it would make a case for analysing the business case for other smaller vessels in the Allseas fleet. For instance, OCV's such as *M/V Oceanic* and *Fortitude*. The reason for this is that due to the lower power rated engines- a spinning reserve requirement for these vessels could make a better business case. The operational profile of pipe-layers have shown that the large power peaks have to be addressed when designing the battery while this would not be the case for the offshore support vessels. Furthermore, the suitability of the split architecture to reduce Lithium-ion capacity is more attuned to vessels with only spinning reserve as a requirement.
 - Based on the testimonials from crew aboard the *Solitaire*, it is understood that sometimes during quay-side operations, the vessel engages its DP system as the mooring arrangement is poor- perhaps the battery could be used in such circumstances to power a part of the power needed for station keeping. Another use of the battery that could be investigated is its potential for use during loading or unloading using cranes at shore.
 - The economic viability of such an investment is dependent on how many days the vessel spends on DP. Given that the *Solitaire* has not been scheduled for any major project post NordStream II, it would possibly be more financially viable to install a battery in the near future rather than immediately. As batteries have limited shelf life and depreciating value year on year it would be better to design the infrastructure and integration techniques in advance, however, the battery installation itself is one that could be carried on later. The lowest cost of implementation of such a system would be a deck placement which requires no additional structural work.
 - A market analysis of the potential shallow and deep-water projects could be analysed in order to gain a better understanding of whether the *Solitaire* would engage in more shallow or deepwater projects in the future. It would also be interesting to determine what water depth would be regarded as 'deepwater' such that the operation of paying out the pipe and forward motion could be de-coupled. By doing so, the power surges would not affect the battery in those scenarios.
-

Bibliography

- [1] Artificial intelligence. URL https://en.wikipedia.org/wiki/Artificial_intelligence.
- [2] Electric and Hybrid Propulsion Leaders Recognized. URL <https://www.maritime-executive.com/article/electric-and-hybrid-propulsion-leaders-recognized>.
- [3] Forecasting- Wikipedia. URL <https://en.wikipedia.org/wiki/Forecasting>.
- [4] High ESS Discharge/Charge Rates are Key to Fuel-Efficiency with Variable Loads | Corvus Energy. URL <https://corvusenergy.com/high-ess-dischargecharge-rates-are-key-to-fuel-efficiency-with-variabl>
- [5] CO 2 EMISSIONS FROM CARS: the facts A report by Transport & Environment Acknowledgements. Technical report, 2018. URL www.transportenvironment.org.
- [6] Batteries on board: offshore vessels setting the course - DNV GL, 2019. URL <https://www.dnvgl.com/expert-story/maritime-impact/Batteries-on-board-offshore-vessels-setting-the-course.html>.
- [7] Climate change, 2019. URL <https://www.equinor.com/en/how-and-why/climate-change.html>.
- [8] Ratnadip Adhikari and R K Agrawal. Forecasting Strong Seasonal Time Series with Artificial Neural Networks Market Mix Modeling (MMM) using BBN View project IT Growth Driver Analysis using Bayesian Belief Network (BBN) View project Forecasting strong seasonal time series with artificial neural networks. Technical report, 2012. URL <https://www.researchgate.net/publication/230583150>.
- [9] Allseas Engineering B.V. Technical Description- M/V Solitaire. 2018.
- [10] Allseas Group S.A. Allseas.com. URL allseas.com/company/.
- [11] Itziar Alonso-González, David Sánchez-Rodríguez, Carlos Ley-Bosch, and Miguel A. Quintana-Suárez. Discrete indoor three-dimensional localization system based on neural networks using visible light communication. *Sensors (Switzerland)*, 18(4), 4 2018. ISSN 14248220. doi: 10.3390/s18041040.
- [12] Bharat Balagopal, Cong Sheng Huang, and Mo-Yuen Chow. Effect of calendar aging on li ion battery degradation and SOH. In *IECON 2017 - 43rd Annual Conference of the IEEE Industrial Electronics Society*, pages 7647–7652. IEEE, 10 2017. ISBN 978-1-5386-1127-2. doi: 10.1109/IECON.2017.8217340. URL <http://ieeexplore.ieee.org/document/8217340/>.
- [13] Jason Brownlee. How to Decompose Time Series Data into Trend and Seasonality. URL <https://machinelearningmastery.com/decompose-time-series-data-trend-seasonality/>.
- [14] Alexander Castro. Training and competence session DP Emergency Drills. Technical report.
- [15] M. V. K. Chari and S. J. (Sheppard Joel) Salon. *Numerical methods in electromagnetism*. Academic Press, 2000. ISBN 9780126157604.
- [16] Thomas Christen and Martin W Carlen. Theory of Ragone plots. Technical report, 2000. URL www.elsevier.com/locate/jpowsour.
- [17] Corvus Energy. Corvus energy At 6700 Li-ion cell. Technical report. URL https://corvusenergy.com/wp-content/uploads/2016/03/AT6700-Module_-CORVUS-ENERGY_Specifications-Brochure-_Mar2016.pdf.
- [18] L van Donge. Analysis of the power management system on board the Solitaire. Technical report, TU Delft, 2009.

- [19] Farrier. Investigating the faulted performance of warship power systems with integrated energy storage. *INEC/iSCSS 2018 Conference Proceedings 2-4 October 2018*, pages 318–332, 2018.
- [20] R. D. Geertsma, R. R. Negenborn, K. Visser, and J. J. Hopman. Design and control of hybrid power and propulsion systems for smart ships: A review of developments, 2017. ISSN 03062619.
- [21] J L S Gerritsen. The Hybrid Cutter Dredger a study on technical and economical feasibility. Technical report.
- [22] Murray Gill and Michael Wright. Methods for Large-scale Nonlinear Optimisation. Technical report, Stanford University, Stanford, California, 1980. URL <https://pdfs.semanticscholar.org/653b/9fe0ddf23fe3d444ad2ba90bb5bfbf8f28d1.pdf>.
- [23] M. Godjevac, K. Visser, E. J. Boonen, C. Malikouti, B. T.W. Mestemaker, Z. Lyu, and F. Van Der Veen. Electrical energy storage for dynamic positioning operations: Investigation of three application case. In *2017 IEEE Electric Ship Technologies Symposium, ESTS 2017*, 2017. ISBN 9781509049448. doi: 10.1109/ESTS.2017.8069278.
- [24] Boris Hanin. Universal Function Approximation by Deep Neural Nets with Bounded Width and ReLU Activations. 8 2017. URL <http://arxiv.org/abs/1708.02691>.
- [25] Tarun Huria, Massimo Ceraolo, Javier Gazzarri, and Robyn Jackey. *High Fidelity Electrical Model with Thermal Dependence for Characterization and Simulation of High Power Lithium Battery Cells*. ISBN 9781467315616. URL <https://www.mathworks.com/content/dam/mathworks/tag-team/Objects/i/71900-ieee-2012-high-fidelity-lithium-battery-model-with-thermal-effect.pdf>.
- [26] Yan Ji, Yancheng Zhang, and Chao-Yang Wang. Issue 4, Pages A636-A649. *J. Electrochem. Soc*, 160, 2013. doi: 10.1149/2.047304jes. URL <http://ecce.mne.psu.edu/Pubs/047304JES%202013.pdf>.
- [27] Murat Kankal and Ergun Uzlu. Neural network approach with teaching-learning-based optimization for modeling and forecasting long-term electric energy demand in Turkey. *Neural Computing and Applications*, 28:737–747, 12 2017. ISSN 09410643. doi: 10.1007/s00521-016-2409-2.
- [28] Mehdi Khashei and Mehdi Bijari. An artificial neural network (p, d, q) model for timeseries forecasting. *Expert Systems with Applications*, 37(1):479–489, 1 2010. ISSN 09574174. doi: 10.1016/j.eswa.2009.05.044.
- [29] Denis Kwiatkowski, Peter C.B. Phillips, Peter Schmidt, and Yongcheol Shin. Testing the null hypothesis of stationarity against the alternative of a unit root. *Journal of Econometrics*, 54(1-3):159–178, 10 1992. doi: 10.1016/0304-4076(92)90104-Y. URL <https://linkinghub.elsevier.com/retrieve/pii/030440769290104Y>.
- [30] Chunshien Li and Tai Wei Chiang. Complex neurofuzzy ARIMA forecasting - A new approach using complex fuzzy sets. *IEEE Transactions on Fuzzy Systems*, 21(3):567–584, 2013. ISSN 10636706. doi: 10.1109/TFUZZ.2012.2226890.
- [31] Zelan Lyu. Concept Design of Hybrid Crane Vessel Feasibility study of utilizing electric energy storage technology. Technical report. URL <http://repository.tudelft.nl/>.
- [32] A Maheshwari. Modelling, aging and optimal operation of lithium-ion batteries. Technical report.
- [33] Spyros Makridakis, Evangelos Spiliotis, and Vassilios Assimakopoulos. Statistical and Machine Learning forecasting methods: Concerns and ways forward. *PLoS ONE*, 13(3), 3 2018. ISSN 19326203. doi: 10.1371/journal.pone.0194889.
- [34] MARIN. Dynamic Positioning. URL <http://www.marin.nl/web/Research-Topics/Manoeuvring-DP/Dynamic-Positioning.htm>.
- [35] Robert May, Graeme Dandy, and Holger Maier. Artificial Neural Networks- Methodological advances and biomedical applications. pages 19–22.

- [36] Martin Fodslette Møller. A scaled conjugate gradient algorithm for fast supervised learning. *Neural Networks*, 6(4):525–533, 1993. ISSN 08936080. doi: 10.1016/S0893-6080(05)80056-5.
- [37] Daisik Nam, Hyunmyung Kim, and R Jayakrishnan. A Model Based on Deep Learning for Predicting Travel Mode Choice Persistent Traffic Cookies View project. Technical report, 2017. URL <https://www.researchgate.net/publication/317913178>.
- [38] R V Rao, V J Savsani, and D P Vakharia. Teaching-learning-based optimization: A novel method for constrained mechanical design optimization problems. *Computer-Aided Design*, 43:303–315, 2011. doi: 10.1016/j.cad.2010.12.015. URL www.elsevier.com/locate/cad.
- [39] Muhammad Rizwan. How to Select Activation Function for Deep Neural Network. URL <https://engmrk.com/activation-function-for-dnn/>.
- [40] Murray Smith. *Neural networks for statistical modelling*. Van Nostrand Reinhold, New York, 1993.
- [41] Martin Southall and K Ganti. Battery and Ultra-capacitor based energy storage vessel integration, capabilities, considerations and challenges. *INEC/iSCSS 2018 Conference proceedings 2-4 October 2018*, pages 342–352, 2018.
- [42] P Spruijt. Investment Costs Reduction of Marine Energy Storage using Smart Power Generation Control. Technical report, TU Delft, 2018. URL <http://repository.tudelft.nl/>.
- [43] Moslem Uddin, Fakhizan Romlie, Mohd Faris Abdullah, Abd Halim, Ab Halim, Abu Bakar, and Tan Chia Kwang. A review on peak load shaving strategies. 2017. doi: 10.1016/j.rser.2017.10.056. URL <http://dx.doi.org/10.1016/j.rser.2017.10.056>.
- [44] Ying WANG, Zhi ZHOU, Audun BOTTERUD, Kaifeng ZHANG, and Qia DING. Stochastic coordinated operation of wind and battery energy storage system considering battery degradation. *Journal of Modern Power Systems and Clean Energy*, 4(4):581–592, 10 2016. ISSN 2196-5625. doi: 10.1007/s40565-016-0238-z. URL <http://link.springer.com/10.1007/s40565-016-0238-z>.
- [45] David A. Wetz, Isaac J. Cohen, and John M. Heinzl. Active control of a hybrid energy storage module (HESM) driving transient loads. *INEC/iSCSS 2018 Conference proceedings 2-4 October 2018*, pages 333–352, 2018.
- [46] I Whitelegg. Power system design considerations when integrating electromagnetic railguns with electric warships. In: *INEC 2016, Bristol: IMarEST*.
- [47] Wikipedia. Allseas. URL <https://en.wikipedia.org/wiki/Allseas>.
- [48] Wai Keung Wong, Enjian Bai, and Alice Wai Ching Chu. Adaptive time-variant models for fuzzy-time-series forecasting. *IEEE Transactions on Systems, Man, and Cybernetics, Part B: Cybernetics*, 40(6):1531–1542, 12 2010. ISSN 10834419. doi: 10.1109/TSMCB.2010.2042055.
- [49] Bolun Xu, Alexandre Oudalov, Andreas Ulbig, Goran Andersson, and Daniel S. Kirschen. Modeling of Lithium-Ion Battery Degradation for Cell Life Assessment. *IEEE Transactions on Smart Grid*, 9(2):1131–1140, 3 2018. ISSN 1949-3053. doi: 10.1109/TSG.2016.2578950. URL <http://ieeexplore.ieee.org/document/7488267/>.
- [50] G. Peter Zhang. Neural Networks for Time-Series Forecasting. In *Handbook of Natural Computing*, pages 461–477. Springer Berlin Heidelberg, Berlin, Heidelberg, 2012. doi: 10.1007/978-3-540-92910-9_14. URL http://link.springer.com/10.1007/978-3-540-92910-9_14.



Vessel data

Name	<i>Solitaire</i>
Type	Pipelay vessel
Port of registry	Valletta
Gross tonnage	94,855
Net tonnage	28,456
Deadweight	31,500 t
Lightship weight	52,215 t
Dimensions	<i>L_{oa}299.85m : L_{pp}248.65m X B_{mld}40.6m X D_{mld}24.0m</i> (excl. stinger)
Transit draught	8.50 m (excl. thrusters), 13.64 m (incl. thrusters)
Max. draught	11.15 m (16 m incl. thrusters)
Air draught	70.64 mast up, 60.98 m mast lowered (at 8.5 m draught)
Service draught	6.50 - 9.23 m (excl. thrusters), 14.37 m (incl. thrusters)
Maximum speed	13.5 knots
Bunker capacity	HFO (6,438m ³) MDO (1,179m ³) MGO (62m ³)
Quarters	420 persons in 1 and 2 berth cabins
Cranes	Huisman special purpose crane: 300t at 17 m, whip hoist 40 t at 57 m 2x Liebherr pipe transfer cranes each at 35 t at 33 m, whip hoist 18 t at 42 m 5x 35 t Liebherr overhead cranes, single joint 2x 65 t Liebherr overhead cranes, double joint 2x 35 t Liebherr overhead cranes, equipment handling
Pipelay	Double-joint working stations: 2x 4 (each with 3x welding and 1 NDT) Main firing line welding stations: 8 Polyurethane field joint coating stations: 2 Pipeline diameter: 60" max Total pipe capacity: 14,625 t- 22,000 t (depending on pipe properties) Tension capacity: 1,050 t (3x 350 t) A&R winch capacity: Electrical, 400t / hydraulic four cable system, 1,000 t (4x 250 t) Stinger: 140 m adjustable stinger (3 sections)
Engines	(a) Main engines: 8x Wartsila Vasa 6R46B, 514 rpm, 5,850 kW (b) Emergency diesel: Cummins KTA 50G2, 1800 rpm, 900 kW
Thrusters	10x 5,550 kW peaks Lips azimuth thrusters
DP	NMD Class 3, LR DP (AAA), fully redundant Kongsberg K-Pos DP-22, K-Pos DP-12 and 3x cJoy system
Navigation	1x GMDSS, Fleet 77, Private satellite line VSTA, Autopilot, 3x Gyros, 2x Echosounder, Doppler Log, ((3)+1)x (D)GPS, VHF's, 2x Radar (X&S-band), 3x DWTW, 2x Fanbeam, DWTP, PHINNS

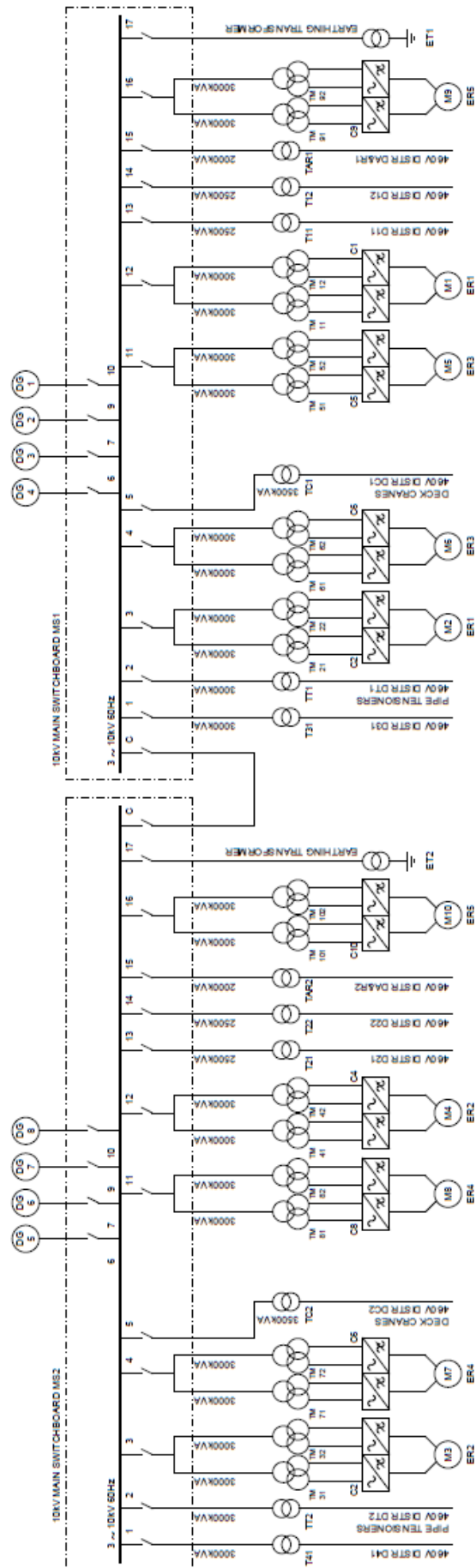


Figure A.1: Solitaire single line diagram

A.1. 3-phase systems

The nature of reactive power is that it uses up the conductor capacity and moves between the inductive elements in the network (load) and source. The energy is stored in the inductors' magnetic fields and fluctuates between the load and source instantaneously. The phenomenon is better described with the following equations:

$$V_{inductor} = \frac{d\phi}{dt} = \frac{dLi}{dt} = -L \frac{di}{dt} [V] \quad (A.1)$$

$$Power_{inductor} = V_{inductor} \times i = L \frac{di}{dt} \times i = \frac{1}{2} L \frac{di^2}{dt} = \frac{d}{dt} \left(\frac{1}{2} Li^2 \right) [W] \quad (A.2)$$

$$E_{Stored} = \int_0^t P dt = \int_0^t \frac{d}{dt} \frac{1}{2} Li^2 dt = \frac{1}{2} Li^2 [J] \quad (A.3)$$

From the Equation A.1 we can see that the voltage across the inductor depends on the rate of change of magnetic flux which in turn depends on the rate of change of current. In an AC current, the inductor is constantly storing and releasing energy. The released energy is sent back to the source during the cycle wherein there is negative power. To understand this, the Figure A.2 represents the instantaneous power flow in AC systems.

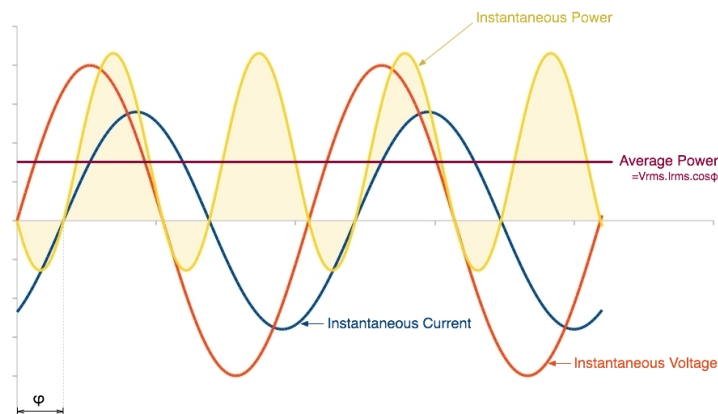


Figure A.2: Instantaneous power

Due to the current lagging the voltage in an inductive network, the product of the voltage and current will be negative in some parts of the AC wave form. The greater this negative power is, the greater the reactive power within the network and hence a lower power factor. Capacitive elements (leading power factor) are used to offset this issue normally to attempt to achieve a power factor as close to 1 as possible. In this case, since the Solitaire has a power factor of 0.55, the reactive power traversing through the conductors is higher than the active power that is capable of being delivered. The high line currents flowing through the network are a consequence of this as the inductive elements draw large currents during pipe-pulls.

In order to keep the grid voltage constant, the AVR of the generators control the excitation of the generators in order to regulate the reactive power.

Formulae:

$$S_{grid} = I_{L-grid} \times V_{bus} \times \sqrt{3} [kVA] \quad (A.4)$$

$$\cos \phi = \frac{P_{grid}}{S_{grid}} \quad (A.5)$$

$$Q_{grid} = I_{L-grid} \times V_{bus} \times \sqrt{3} \times \sin \phi [kVAR] \quad (A.6)$$

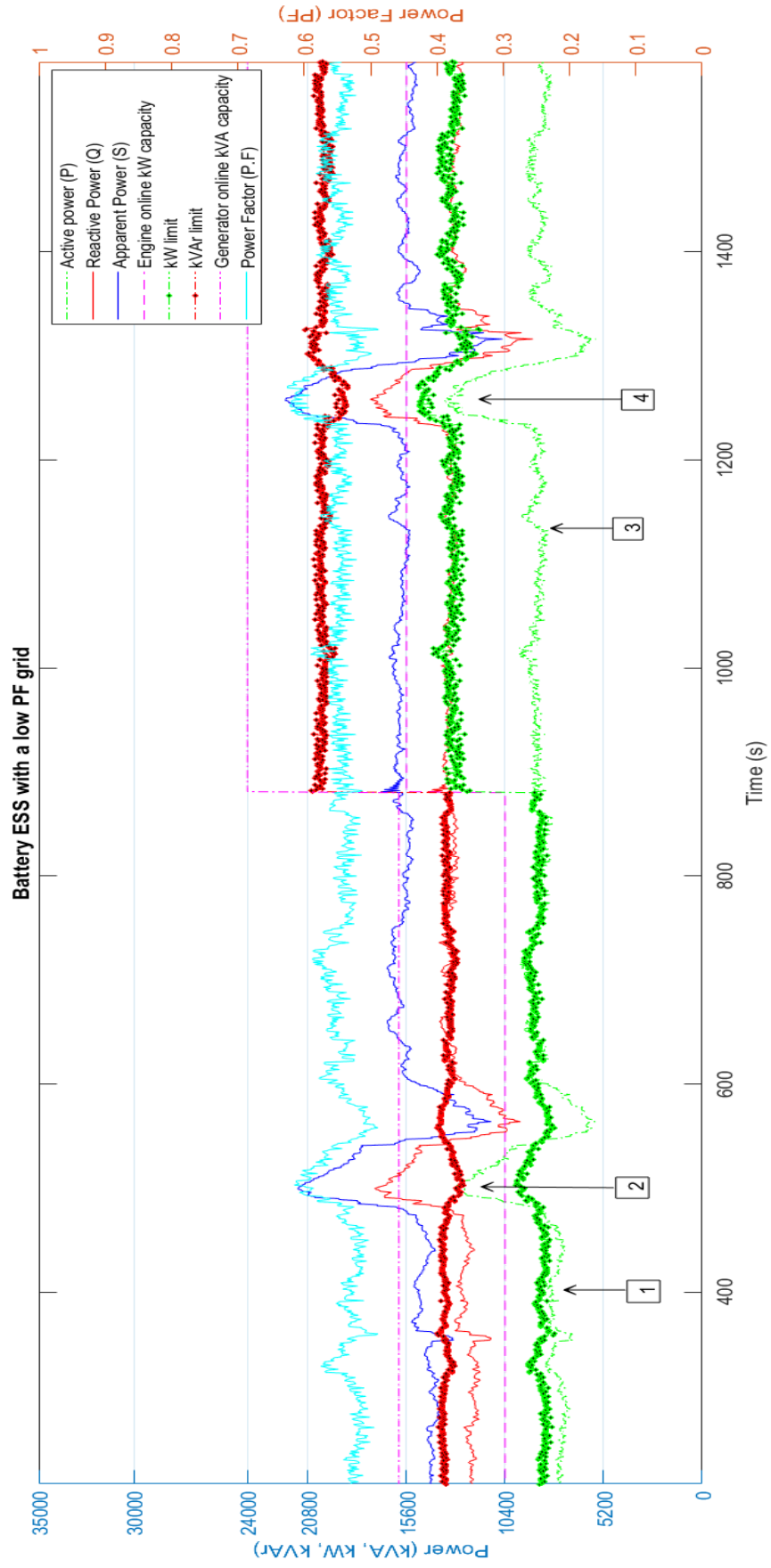


Figure A.3: 0.5 power factor- no failure condition

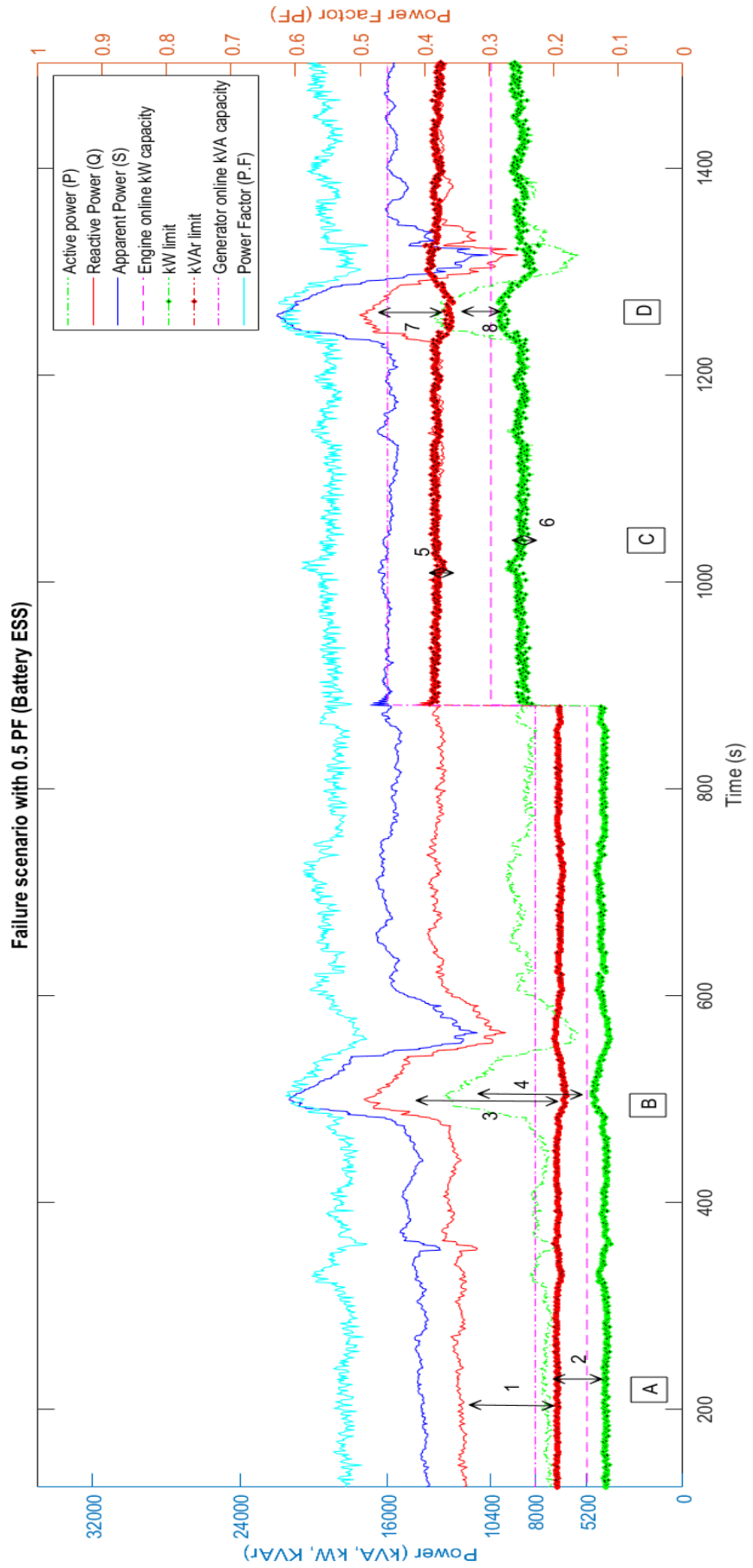


Figure A.4: 0.5 power factor failure condition

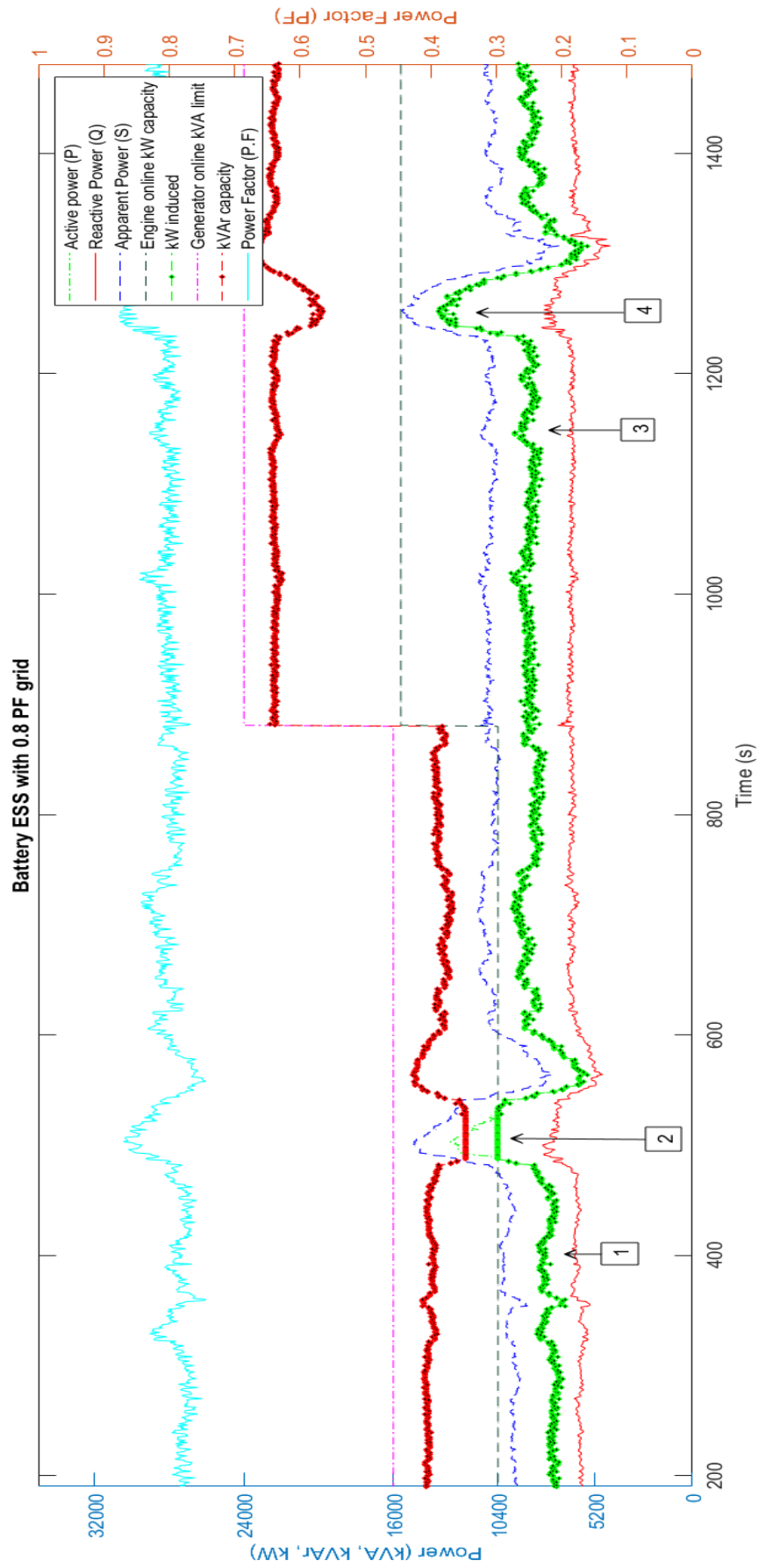


Figure A.5: 0.8 power factor no failure condition

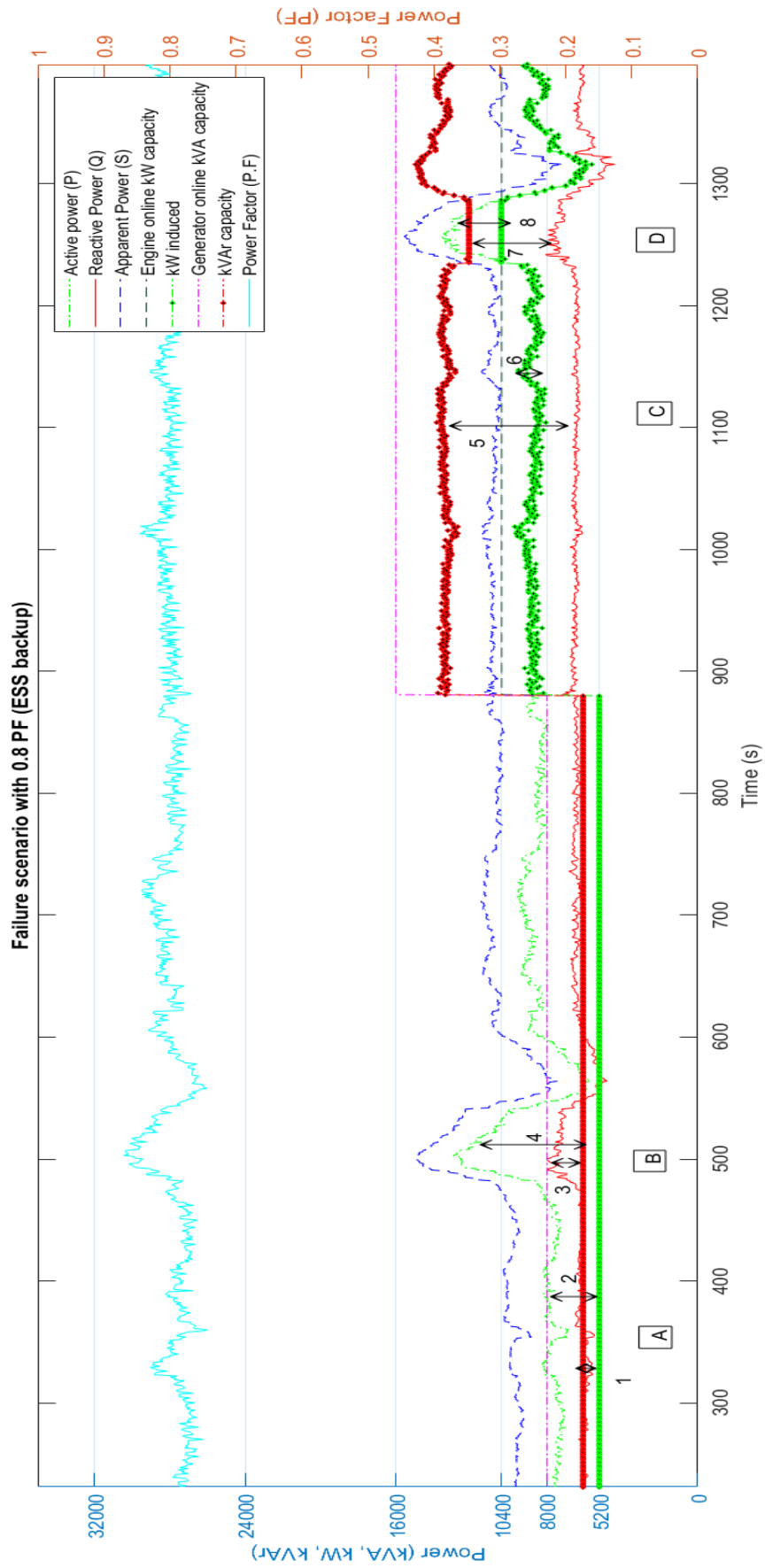


Figure A.6: 0.8 power factor failure condition

B

ESS & PMS integration

The section on ESS consists of the vessels discrimination diagrams, and FMEA tests proving the fault tolerance capability of the Solitaire in the event of a single engine failure and battery datasheet characteristics. The PMS section consists of the ESS management algorithm descriptions and rule based system PMS responses as test cases for different days.

FMEA tests- thruster phaseback

EQUIPMENT SUB-SYSTEM:	THRUSTER LOAD LIMITING
Test No 47: Thruster Phase back – Power Plant Stability Part 1	
FMEA Reference:	Performance
Objective:	To demonstrate that standby generators are able to connect during thruster phase back – no problem with synchronization during thrust reduction. To demonstrate that the thrust reduction measures are able to cope with a generator which has not yet been able to share load.
Method:	With the vessel under DP control all thrusters online. Make sure all offline generators are assigned as not standby but be ready to make a standby generator available. Use thrusters in opposition such that the generators are loaded to about 55-60%. <ol style="list-style-type: none"> Open Bus - With two generators connected to subject Bus - when stable at high load, trip one generator and observe that thrust is immediately phased back to prevent the single generator overloading and vessel continues using the remaining power. Put all thruster levers to full thrust during this time (No Blackout). Carry out for both switchboards. Closed Bus - With three generators connected to subject Bus - when stable at high load, trip one generator and observe that thrust is immediately phased back to prevent the single generator overloading and vessel continues using the remaining power. Put all thruster levers to full thrust during this time (No Blackout).
Results Expected:	<ol style="list-style-type: none"> Thrust reduced to prevent overload of surviving generator. Unable to apply further thrust. Thrust reduced to prevent overload of surviving generator. Unable to apply further thrust.
Results:	<ol style="list-style-type: none"> As expected Not performed
Comments:	Performed with 55%
Witnessed by:	Rainier Verra
Date:	20-01-2018

Figure B.2: MDG trip at 55% load



EQUIPMENT SUB-SYSTEM:	THRUSTER LOAD LIMITING
Test No 48: Thruster Phase back – Power Plant Stability Part 2	
FMEA Reference:	Performance
Objective:	To demonstrate that standby generators are able to connect during thruster phase back – no problem with synchronization during thrust reduction. To demonstrate that the thrust reduction measures are able to cope with a generator which has not yet been able to share load.
Method:	With the vessel under DP control all thrusters online. Make sure all offline generators are assigned as not standby but be ready to make a standby generator available. Use thrusters in opposition such that the generators are loaded to about 85%. <ol style="list-style-type: none"> Open Bus - With two generators connected to subject Bus - when stable at high load, trip one generator. Observe that thrust reduction operates. Make a stand-by set available as soon as the standby set connects, but before it has a chance to load-share, trip the generator which is in parallel with it. Observe that thrust reduction operates again to prevent over-load and allows the generator to follow its load-up ramp. Make another standby set available and observe that it connects – thrust demand can be reduced after connection. Carry out for both switchboards. Closed Bus - With three generators connected to subject Bus - when stable at high load, trip one generator. Observe that thrust reduction operates. Make a stand-by set available as soon as the standby set connects, but before it has a chance to load-share, trip the generator which is in parallel with it. Observe that thrust reduction operates again to prevent over-load and allows the generator to follow its load-up ramp. Make another standby set available and observe that it connects – thrust demand can be reduced after connection.
Results Expected:	<ol style="list-style-type: none"> Thrust reduced to prevent overload of surviving generator, stand-by generator connects. As soon as stand-by connect, loaded generator trips and immediately thrust is reduced to prevent blackout, connected generator will load up to maximum. Stand-by generator connects and loads up, thrust increases back to DP set points.
Results:	<ol style="list-style-type: none"> As expected Not performed
Comments:	
Witnessed by:	Rainier Verra
Date:	20-01-2018

Figure B.3: MDG trip at 85% load

FMEA tests-Heading change overshoot

EQUIPMENT SUBSYSTEM	DP CONTROL SYSTEM																																						
Test No. 101 Heading Change																																							
Objective: To prove position keeping and heading control during DP Operations.																																							
Method: From DP Console, with Turn Rate of 20° / minute: <ol style="list-style-type: none"> 1. Adjust heading 90° to starboard. 2. Adjust heading 90° to starboard. 3. Adjust heading 90° to starboard. 4. Adjust heading 90° to starboard. 																																							
Results Expected: <ol style="list-style-type: none"> 1. Controlled heading change with minimum position excursion. 2. Controlled heading change with minimum position excursion. 3. Controlled heading change with minimum position excursion. 4. Controlled heading change with minimum position excursion. 																																							
Results: <table border="1" style="margin: 10px auto;"> <thead> <tr> <th colspan="6">Settings and Environment</th> </tr> </thead> <tbody> <tr> <td>Start Hdg:</td> <td>326°</td> <td>Wind Speed:</td> <td>8.9m/s</td> <td>DP Current:</td> <td>0.5m/s</td> </tr> <tr> <td>Gain:</td> <td>Medium</td> <td>Rot Speed:</td> <td>15°/min / 20°/min</td> <td>Wave Height:</td> <td>2m</td> </tr> </tbody> </table> <table border="1" style="margin: 10px auto;"> <thead> <tr> <th>Part</th> <th>Lat</th> <th>Long</th> <th>Overshoot</th> </tr> </thead> <tbody> <tr> <td>1.</td> <td>028° 05' 34.6'N</td> <td>015° 22' 09.2'W</td> <td>+0.6°</td> </tr> <tr> <td>2.</td> <td></td> <td></td> <td>+1.1°</td> </tr> <tr> <td>3.</td> <td></td> <td></td> <td></td> </tr> <tr> <td>4.</td> <td></td> <td></td> <td>+1.1°</td> </tr> </tbody> </table>		Settings and Environment						Start Hdg:	326°	Wind Speed:	8.9m/s	DP Current:	0.5m/s	Gain:	Medium	Rot Speed:	15°/min / 20°/min	Wave Height:	2m	Part	Lat	Long	Overshoot	1.	028° 05' 34.6'N	015° 22' 09.2'W	+0.6°	2.			+1.1°	3.				4.			+1.1°
Settings and Environment																																							
Start Hdg:	326°	Wind Speed:	8.9m/s	DP Current:	0.5m/s																																		
Gain:	Medium	Rot Speed:	15°/min / 20°/min	Wave Height:	2m																																		
Part	Lat	Long	Overshoot																																				
1.	028° 05' 34.6'N	015° 22' 09.2'W	+0.6°																																				
2.			+1.1°																																				
3.																																							
4.			+1.1°																																				
Comments: Note: Rotation speed increased for steps 3 and 4 and single heading change of 180° carried out. Maximum position excursion ±3m.																																							
Witnessed by: R. Purser	Date: 13 Oct 2016																																						



Figure B.4: Overshoot during heading changes

Battery datasheet



SLPB 80Ah HIGH POWER SUPERIOR LITHIUM POLYMER CELL



Kokam's patented manufacturing process produces battery cells for applications that require:

- Excellent energy density(140 – 200 Wh/kg)
- Excellent power-to-energy balance
- High cycle life
- Longer battery life
- Low impedance and heat generation provide improved safety
- Light weight

Advantages of SLPB

Lower Cost/Consistent Quality/Greater Reliability

Innovative SLPB manufacturing technology: Simple and fast manufacturing process with Z-Folding technology

Applications

- Transportation
 - Fully electric vehicles
 - Plug-in electric vehicles
- Military
- Aviation
- UPS(uninterrupted power supply)
- Industrial Machinery
- Marine
- Grid Storage
- Telecom

1.1 Typical Properties

Items	Unit	Specification		Remarks
Rated Capacity	Ah	100.0		Charge@0.2C, 23 °C Discharge@0.2C, 23 °C
Energy Density	Wh/kg	151		
Energy Density ⁽¹⁾	Wh/L	297		
AC Impedance	mΩ	Max. 0.55		@ 1kHz, AC
Weight	g	2,450 ± 50		
Cell Dimension [Maximum]	mm	Thickness^(C)	8.2	0.5kgf/cm ² , 3.7 ± 0.1V
	mm	Width^(A)	464	Unfolded
	mm	Length^(B)	327	Except for tab length
Voltage	V	Average	3.7	
	V	Lower limited	3.0	
	V	Upper Limited	4.2	
Current [Maximum]	A	Charge	Cont. 300 (3C)	@ 23 ± 3 °C
	A	Discharge	Cont. 500 (5C)	@ 23 ± 3 °C
	A		Peak 600 (6C)	<10sec , > SOC 50%
Available Operating Temperature	°C	Charge	0 ~ 10 °C	<0.3C
			10 ~ 35 °C	≤ 2C
			35 ~ 45 °C	< 1C
Available Storage Condition	-	Discharge	-20 ~ 25 °C	1 year
			25 ~ 40 °C	3 months
			40 ~ 60 °C	1 week
Cycle Life	Times	23 ± 3 °C	> 4,000	Cycles @1C/1C to 80% of Capacity 80% DOD or 3.4-4.1V
Self Discharge	%	23 ± 3 °C / Year	< 2%	50% SOC
Certification	UL1642			

⁽¹⁾Volume calculated using core cell dimensions, excluding tabs and seals

The information contained herein is provided solely for the purposes of general explanation and illustration, and is subject to modification without notice. No warranty or guarantee is given in regards to the information contained herein or the referenced products. Please contact Kokam for the most current and relevant product information for your particular application.

Kokam™ is a trademark of Kokam Co., Ltd

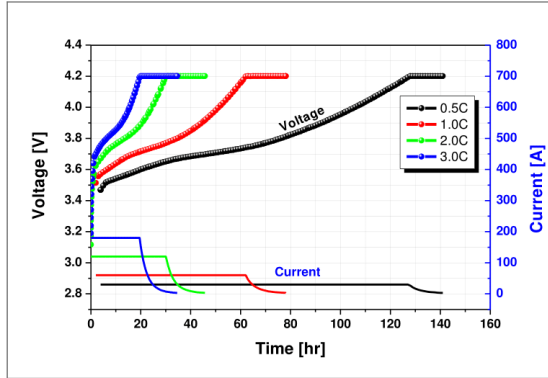
Figure B.5: Cell characteristics

MODEL SLPB80460330H

SUPERIOR LITHIUM POLYMER CELL

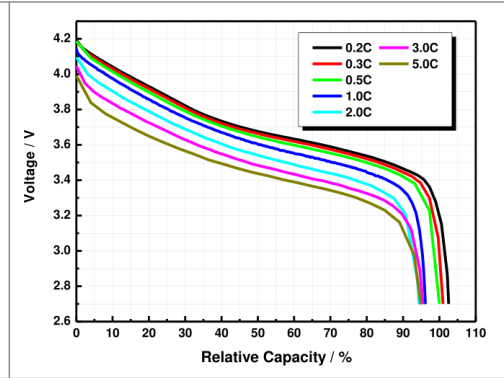
2. Technical Information

2.1 Charge Characteristics



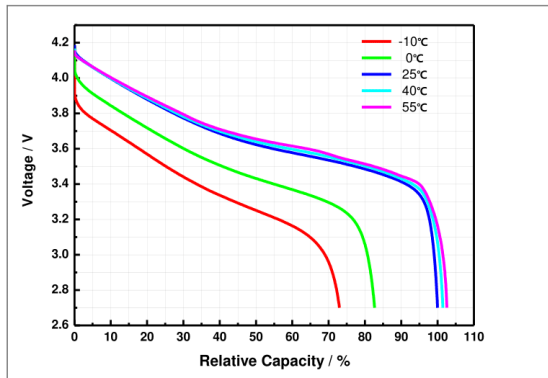
Charge	0.5C	< 150 min	CC-CV, 0.5C ~ 3.0C, 4.2V, 0.05C cut off @23 °C ± 2 °C
	1.0C	< 90 min	
	3.0C	< 40 min	

2.2 Discharge Characteristics



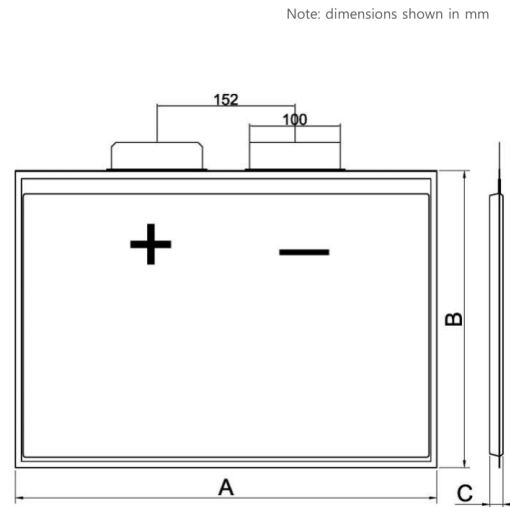
Discharge	0.5C	< 100 %	Charge : CC-CV, 1.0C, 4.2V, 0.05C cut off @23 °C ± 2 °C Discharge : CC, 0.5~8.0C, 3.0V cut-off @23 °C ± 2 °C
	1.0C	< 95 %	
	3.0C	< 93 %	
	5.0C	< 90 %	

2.3 Temperature Characteristics



Discharge	-10 °C	< 60 %	Charge : CC-CV, 1.0C, 4.2V, 0.05C cut off @23 °C ± 2 °C Discharge : CC, 0.5C, 3.0V cut-off @Each temp.
	0 °C	< 80 %	
	25 °C	100 %	
	55 °C	> 100%	

2.4 Mechanical Characteristics



The information contained herein is provided solely for the purposes of general explanation and illustration, and is subject to modification without notice. No warranty or guarantee is given in regards to the information contained herein or the referenced products. Please contact Kokam for the most current and relevant product information for your particular application.

Kokam™ is a trademark of Kokam Co., Ltd

Figure B.6: Charge, discharge & temperature characteristics

Voltage drop chart

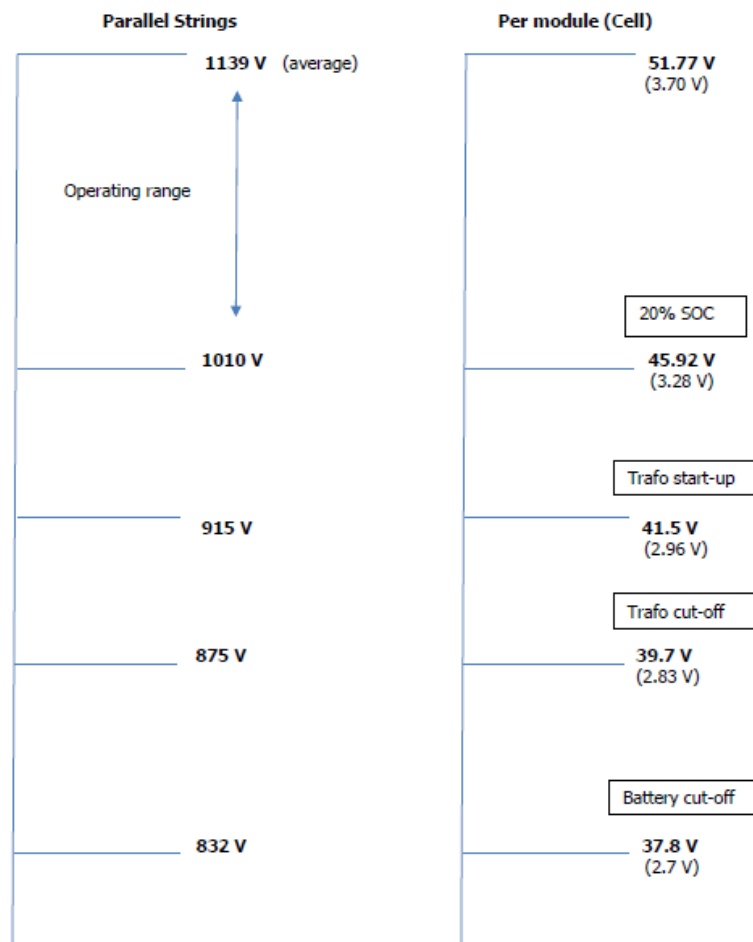


Figure B.7: Voltage drop chart

In the voltage drop chart, it can be seen that both, in the spinning reserve and power surge mode, the battery is appropriately protected. The BMS (Battery management system) must enable the battery system cutoff if the SoC has reached a value of 20%. An added level of protection is the transformers and inverters which have a minimum input voltage for it to be able to produce the 3-phase voltages and currents. So if the battery SoC drops below 20% the conversion capability will fail to ensure which protects the battery from reaching an under-voltage situation. The minimum possible voltage that the cells can safely operate at is 2.7 V, the BMS automatically enables a complete cut-off at this point preventing the battery from over-discharging. The transformer start-up & cut off is specific to manufacturers and is dependent on the inverter voltage output. From the voltage drop chart, it is possible to calculate the currents in the battery power generation system. The currents developed in the network have been outlined in Section 4.4: System Layout.

B.2. PMS

B.2.1. Stateflow @Rule based system model (per generator)

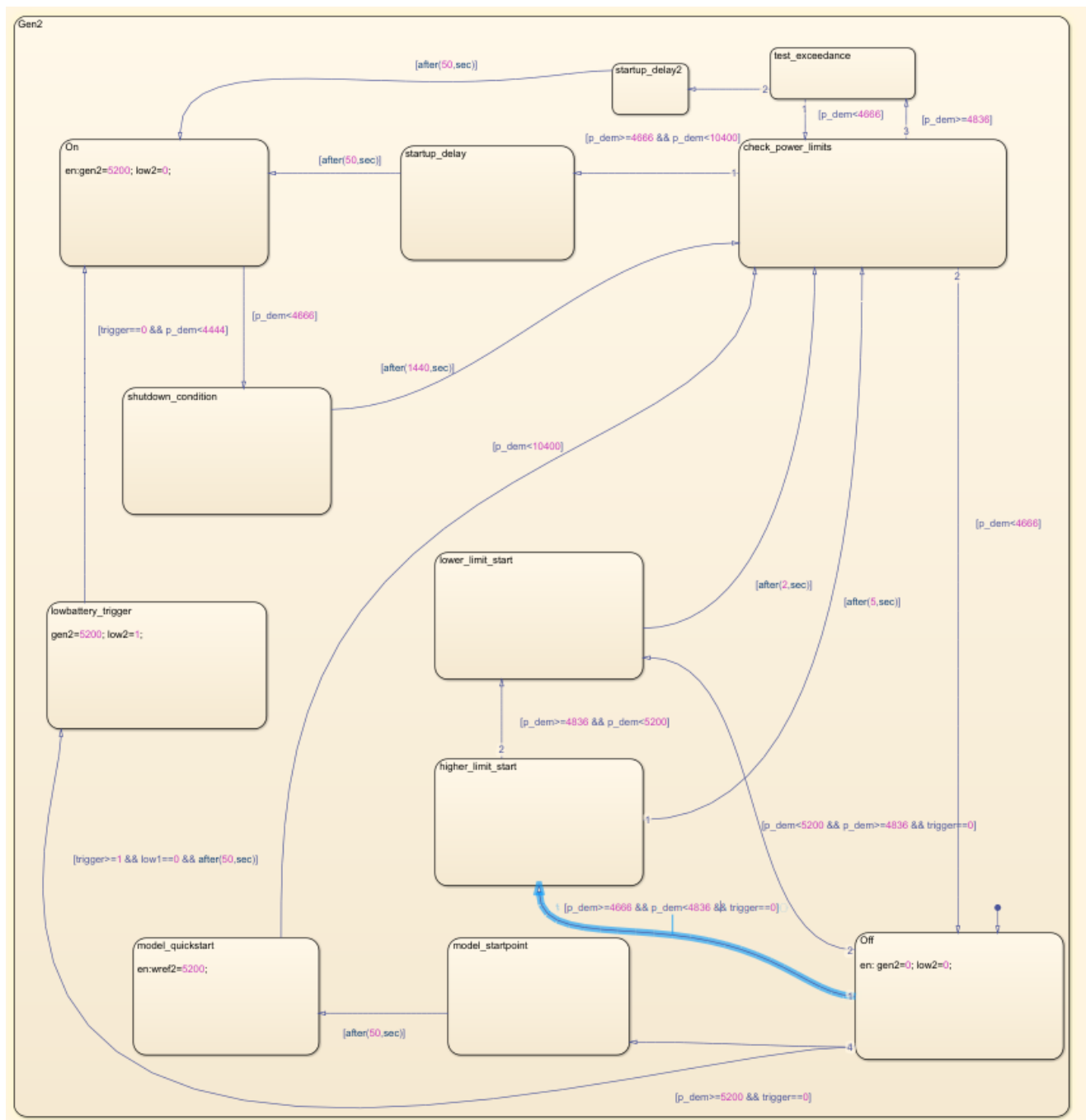


Figure B.8: Stateflow@Generator online capacity

Figure B.8 is a representation of the Stateflow @generator decision making model which determines how many generators must stay online in order to satisfy the load demand. The decision making model is essentially a programmed version of Table 5.1 & 5.3 in the old and new PMS case for the rule-based system.

B.2.2. ESS management algorithms

Algorithm A: Peak frequency

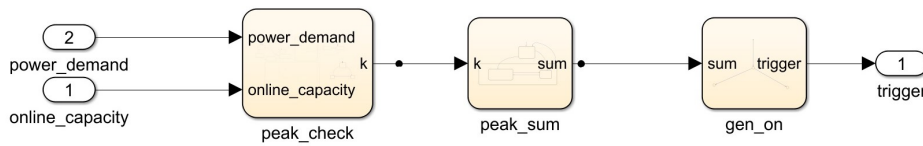


Figure B.9: Peak frequency monitor (Stateflow®)

Figure B.9 is the stateflow blocks used to determine if the number of peaks within a time window exceeds a threshold before setting the trigger value to '1'. The way it works is that the total power demand is fed into the block along with the total available capacity from the generator decision making model (Figure B.8), i.e., 5200 kW, 10,400 kW, 15,600 kW or 20,800 kW depending on the number of online generators. Any power demand exceeding this results in the variable 'k' to increase to 1 at every event of a power surge. The variable 'sum' counts the instances of 'k' within a 900 second window and then refreshes to reset to '0'. If the value 'sum' exceeds a pre-defined limit (for example 5 peaks), then the trigger variable is set to '1' in the last block, else it remains '0'. Note: Section 5.4.5 contains a notice about the differences between the model & reality.

Algorithm B: Peak magnitude

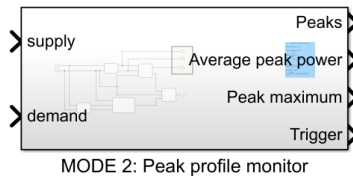


Figure B.10: Peak profile/magnitude monitor

Figure B.10 shows the Simulink block for the peak magnitude monitor. The inputs are the total power demand and the available online capacity from the generator decision making model (Figure B.8). From Figure B.11, it can be seen that 3 data ports are used for diagnostic information while the only variable used is the 'trigger' variable. The input signals branch out into two distinct blocks, i.e., the upperbound and lowerbound monitoring blocks. The goal of the upperbound monitoring is to quantify the magnitude of the power peaks and make decisions on whether to **turn on** a new generator. This is done by monitoring the peak value of the power peak i.e., if a power peak lasts 20 seconds above the online capacity of the engines (which means that it is drawn from the battery), the peak value of that power demand is noted- for example for a 2 MW peak, the value 2000 kW is noted as the maximum peak value 'p_max'. Similar to the peak frequency monitoring algorithm from Figure 5.14, this block also counts every instance of a peak using a variable 'k1'. Using the peak value and the number of peaks within a time window (1800s, 3600s,...), we can quantify the average value of the power peaks to see if it crosses a threshold value set within the block as 2298kW (1.5C battery discharge limit for continuous charge-discharge).

The lowerbound monitoring blocks are used to determine when it is appropriate to **turn off** a generator. The same strategy as the upperbound monitoring is used except that peak magnitude monitoring is continued by maintaining the 'online capacity (supply)-5200 kW', so in this way the measured load is used to determine what would happen if a generator were to be turned off- if it proves that the trigger variable would be set to '1' again then the algorithm will not initiate a generator shutdown instead it will continue to keep the generator running by maintaining 'trigger' at '1' until it reaches a point wherein it can initiate a shutdown by setting the variable to '0'.

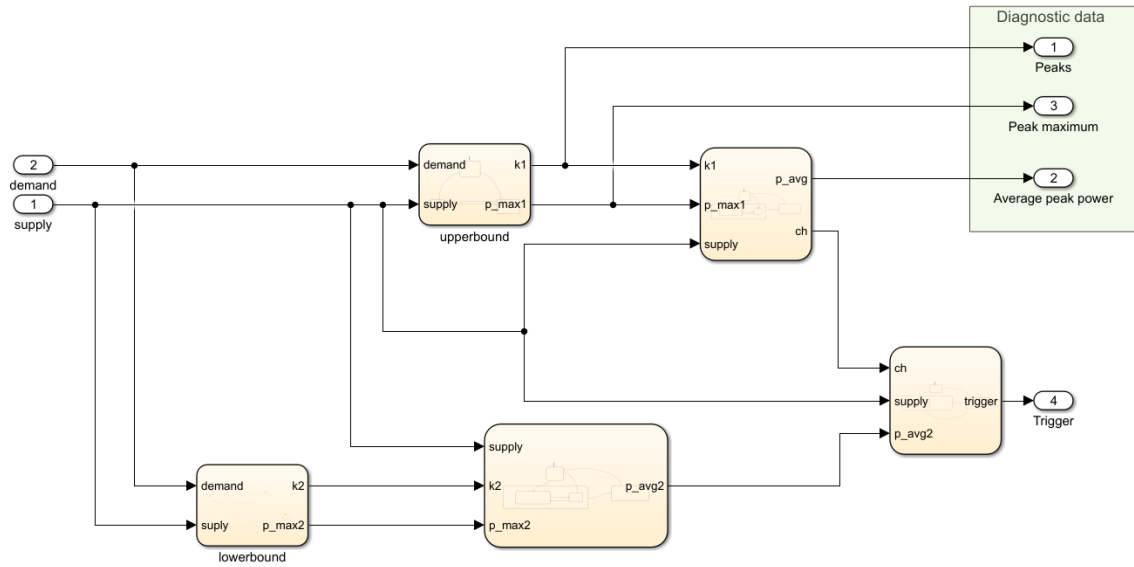


Figure B.11: Peak profile/magnitude monitor (Stateflow®)

Algorithm C: SoC Control

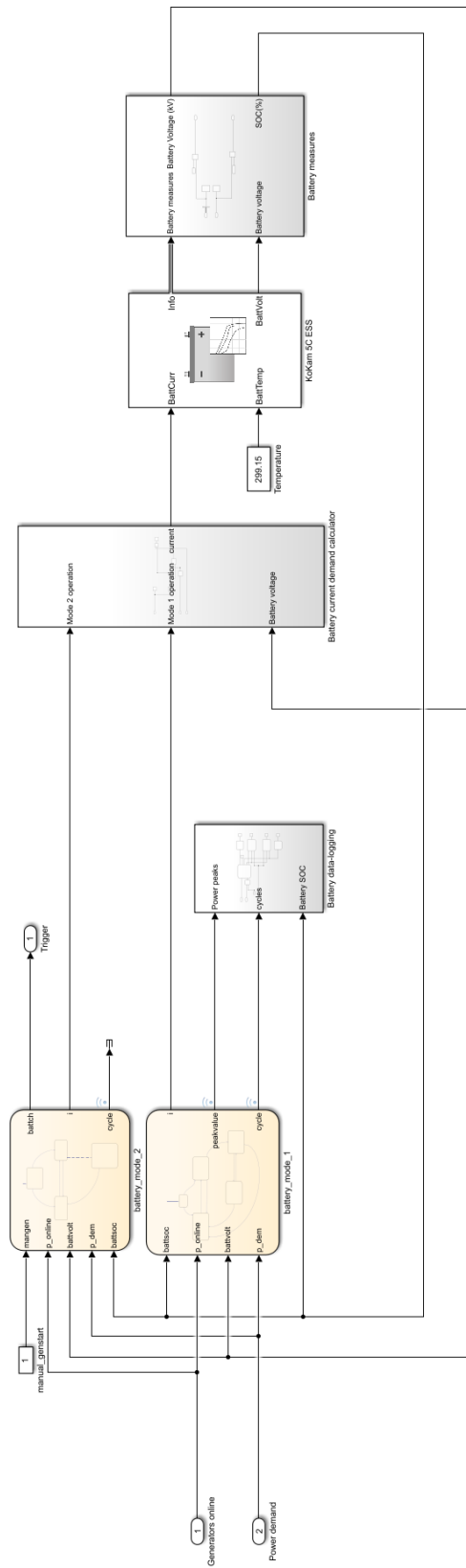


Figure B.12: SOC based battery control units

The battery SoC control unit consists of the charging methods that could be applied to the ESS followed by a datalogging block & the battery model itself. Depending on the charging procedure desired (pulse or limit), the algorithm receives the online capacity available and total power demand. Any power demand that surpasses the engines online capacity is drawn from the battery. Since the battery input requires the discharge current, the excess power demand is divided by the battery voltage to obtain the amperes required from the battery. The discharge is not controlled in any fashion i.e., the power demand will be drawn from the battery without any intervention. Every-time the battery discharges and re-charges- both the charging controller modes count the number of cycles the battery experiences. In addition to this the power drawn from the battery is divided by the battery sizing to determine the C-rates induced. The SoC is measured from the battery 'Info' output of the battery model. The DoD is noted once the battery discharged to a new SoC (For example, if the setpoint charge is 85% and a power peak occurs, the new SoC would be 82% after the discharge, this value is noted to calculate a DoD of 3%). Following this, the pulse mode or limit mode of charging are employed to re-charge the battery to its original setpoint of 85%.

Pulse mode

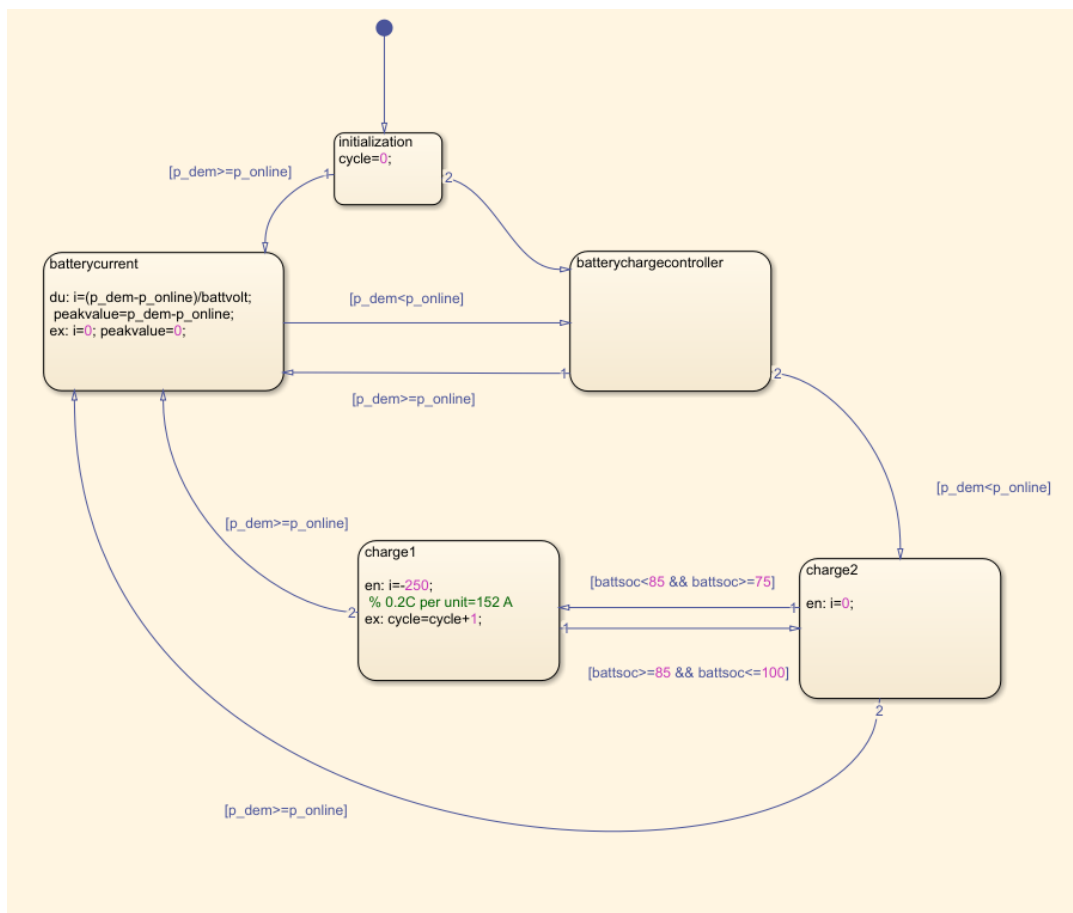


Figure B.13: Battery mode 1 flowchart (Stateflow®)

In Figure B.13, the Stateflow diagram shows the determination of the 'batterycurrent' when the power demand is greater than the online capacity. The difference is divided by the battery voltage (obtained from the output of the battery model). In 'charge1' condition, if the SoC is less than 85% and greater than 75%- a charge current will be sent to the battery model. This is only done when the power demand is lower than the online available capacity i.e., when the vessel is not experiencing a power peak. This results in a scenario wherein the battery discharges from 85% when a power peak is experienced and after the power peak is completed, the SoC drops to below 85% which means that the 'batterycurrent' will be 250A (in this example), until the 85% setpoint is reached. Once 85% is reached, the current goes to '0' ('charge2' block). During each such an event, the cycles are counted using a counter 'cycle'.

Limit mode

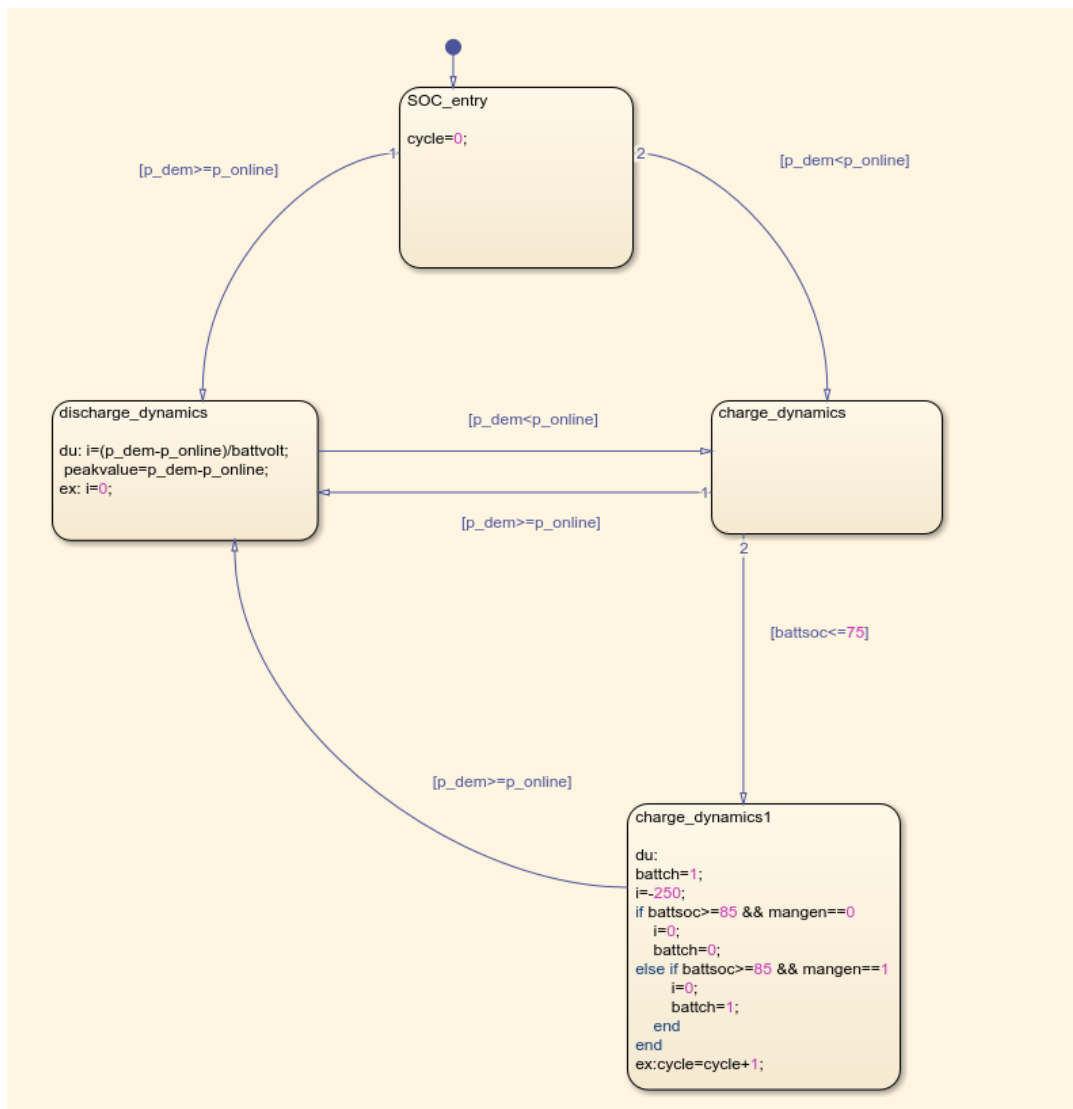


Figure B.14: Battery mode 2 flowchart (Stateflow®)

In the limit mode of operation (not used in analysis), the higher SoC limit of 85% is used and the battery is allowed to discharge until it reaches an SoC of 75%. Once the 75% SoC has been reached, the battery is re-charged to 85% SoC. Once cycle hence is a 10% DoD. To maximise cycle life with many smaller charges, the pulse mode was used instead for the analysis as the cycle life is better in that case. Similar to the pulse case, the battery current is determined by dividing the excess power demand by the battery voltage that is obtained from the physical battery model.

B.2.3. New PMS response

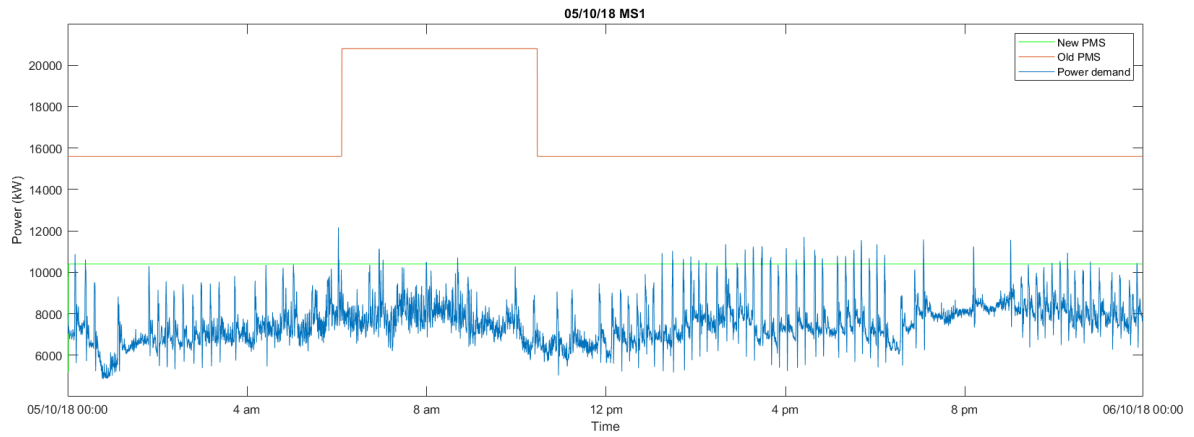


Figure B.15: 05/10/18 MS1 response

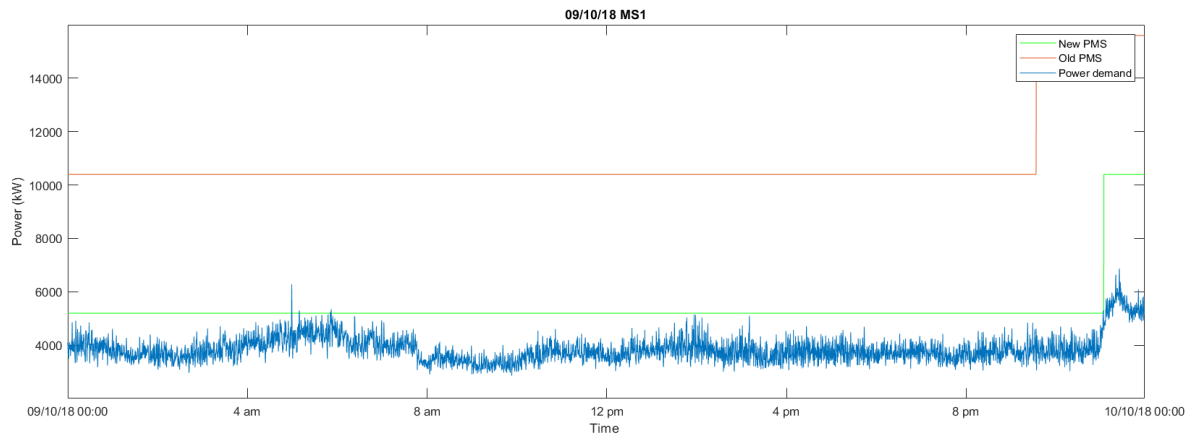


Figure B.16: 09/10/18 MS1 response

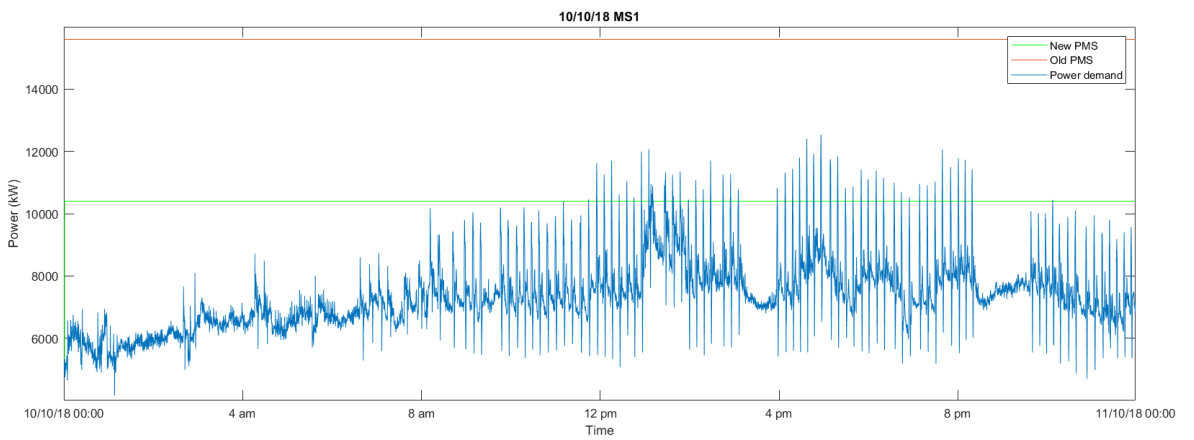


Figure B.17: 10/10/18 MS1 response

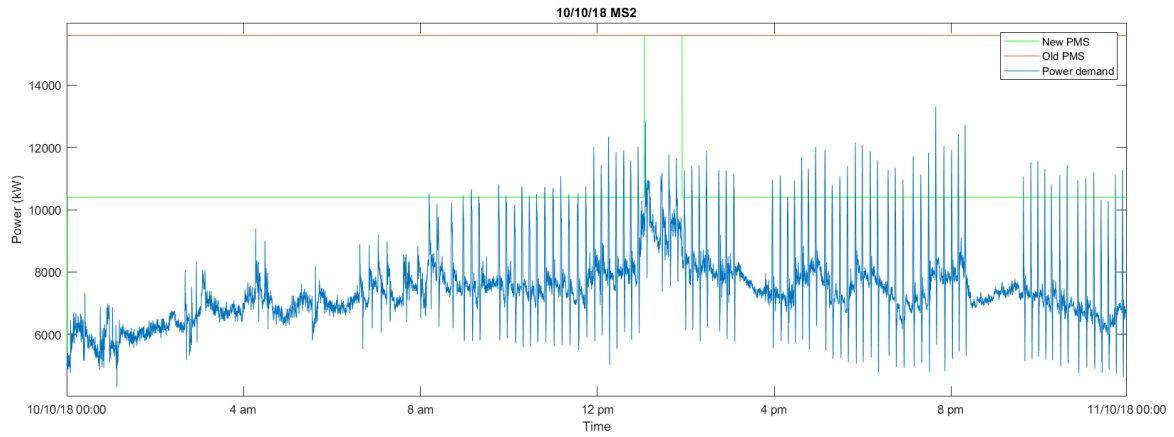


Figure B.18: 10/10/18 MS2 response

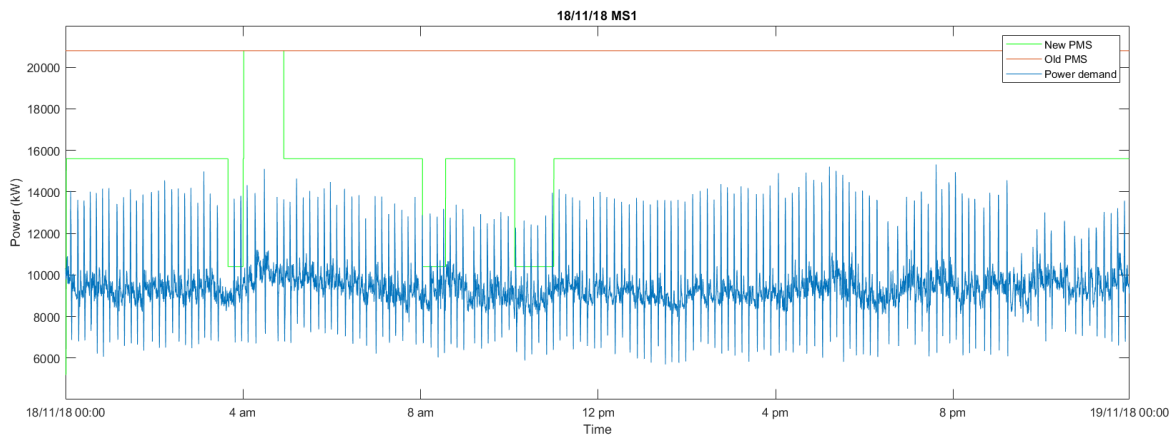


Figure B.19: 18/11/18 MS1 response

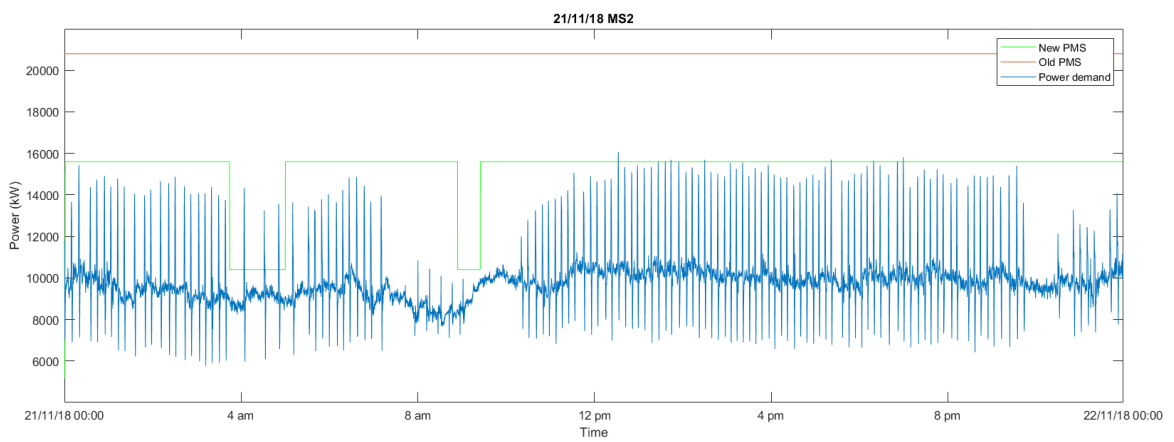


Figure B.20: 21/11/18 MS2 response

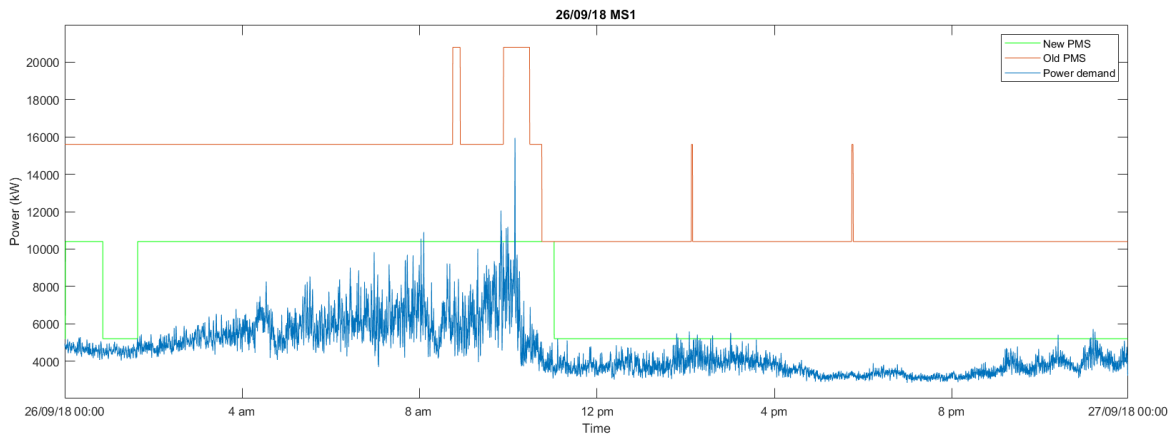


Figure B.21: 26/09/18 MS1 response

C

Artificial neural network

C.1. Commonly used terms

Seasonality, cyclical patterns and trends

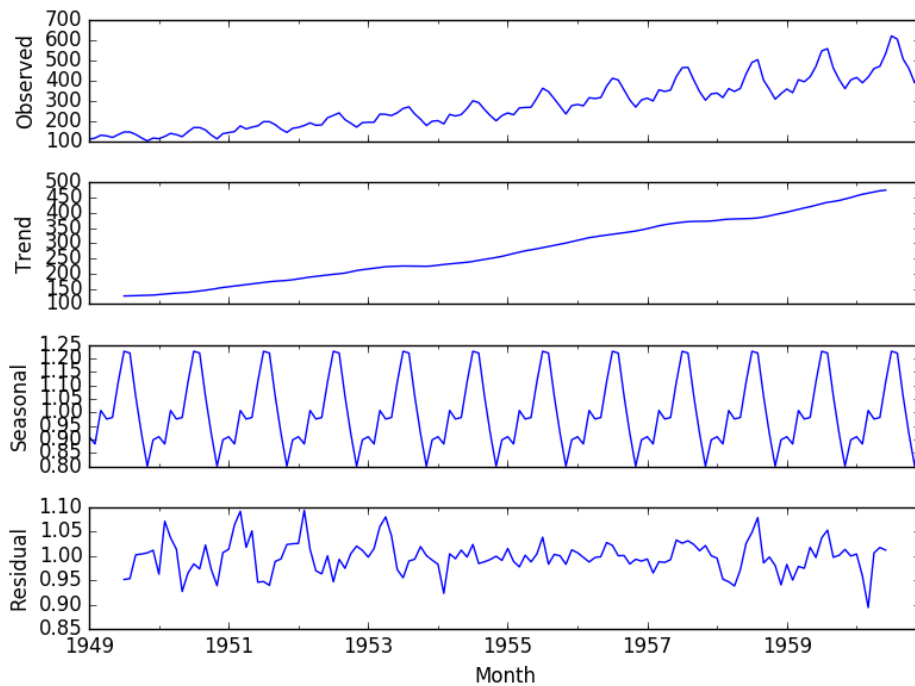


Figure C.1: Seasonality in data [13]

Figure C.1 shows the decomposition of the observed data that consists of a trend and cyclical patterns that are a function of seasonal fluctuations caused in the data. To be able to make predictions, the way forward would be to use a linear trend estimation and a statistical prediction approach applied to the stationarised data i.e., the seasonal component. Due to this requirement for statistical forecasting, the limitation of the forecasts are that it can only be done for short term forecasts as the trend of DP load is rarely ever increasing—they may only ever be considered to be increasing over a short forecast horizon. To be able to capture more complex trend variations due to the weather and heading changes—more advanced models based on machine learning are to be used as they have the capability to capture these effects given enough training data.

Stationary

A stationary time-series is one whose properties do not depend on the time at which the series is observed. Thus, time series with trends, or with seasonality, are not stationary — the trend and seasonality will affect

the value of the time series at different times. On the other hand, a white noise series is stationary — it does not matter when you observe it, it should look much the same at any point in time [29].

In the case of the load profiles of the *Solitaire*, the profiles are not stationary as several seasonal and cyclic patterns are commonly seen. As weather conditions change throughout the day, the load profile changes significantly. Statistical methods cannot be used for long term forecasting due to this problem. Using a machine learning approach, it could, in theory, be possible to capture the effects of the input parameters on the vessels load profiles given enough data to train the neural network model.

Over-fitting

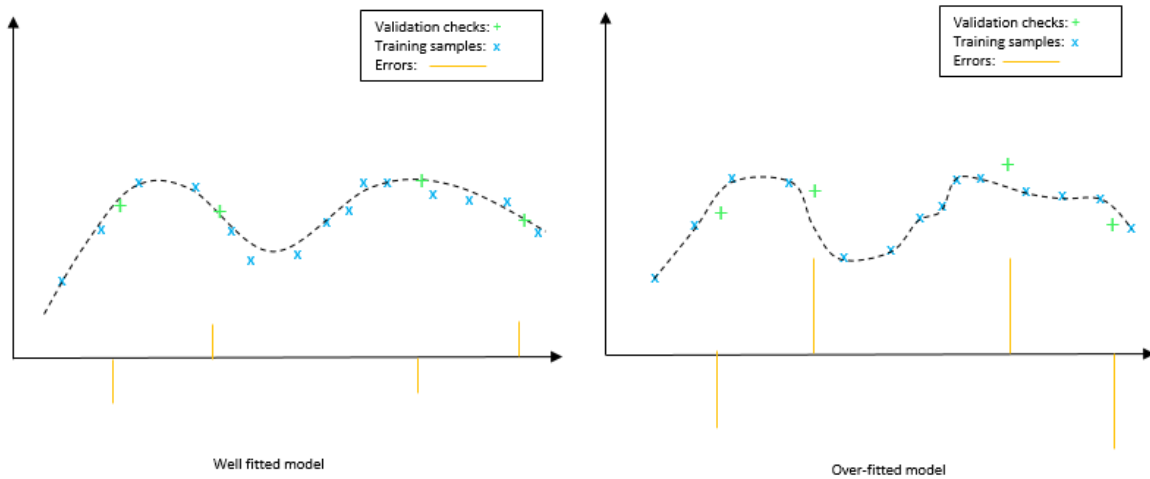


Figure C.2: Neural network validation check

Figure C.2 shows the effect of overfitting the model. As the goal of the neural network is to represent the non-linearity's of the ships model as a 'black-box' it is supposed to be able to generalise and fit a smooth curve to the input output relationships. However, if the model is overfitted- it will attempt to satisfy all these input output relationships with minimal training error. The overfitting is tested by introducing new inputs into the neural network that it has never seen before- if the model is overfitted- it will produce erroneous outputs while a well fitted model will give an error, however the solution will be generalised well.

Bias

The bias is a term analogous to the y-intercept of linear systems. The sigmoid activation function would attempt to fit the data with its crossover point on the x-axis at 0 if there was no bias value Figure C.3). The bias term allow the sigmoid to move more freely to the right or left as shown in Figure C.4 which allow it to fit data better.

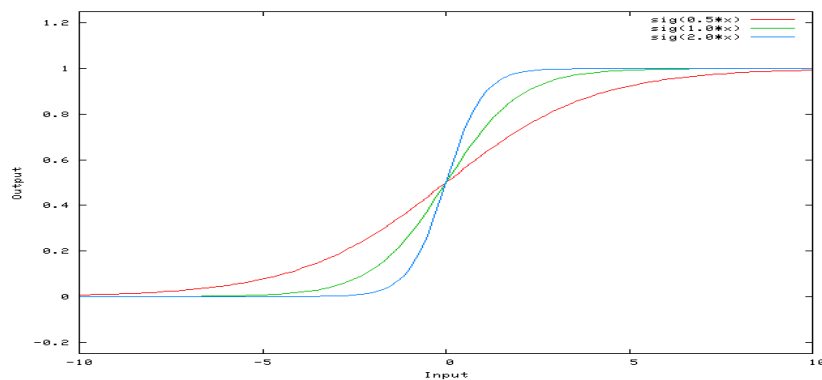


Figure C.3: Activation function with '0' bias

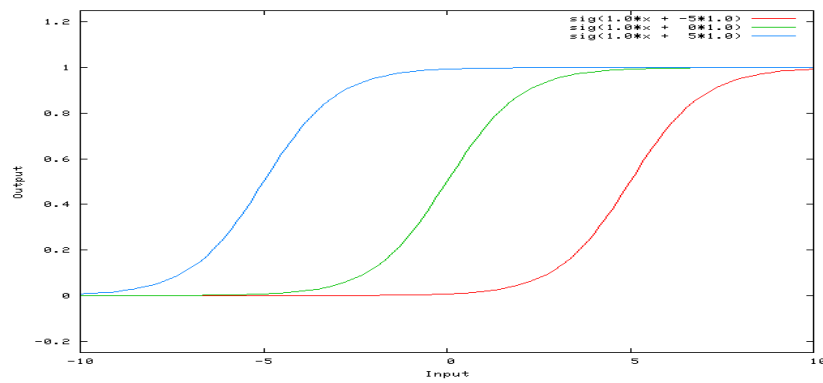


Figure C.4: Effects of different bias values

Momentum

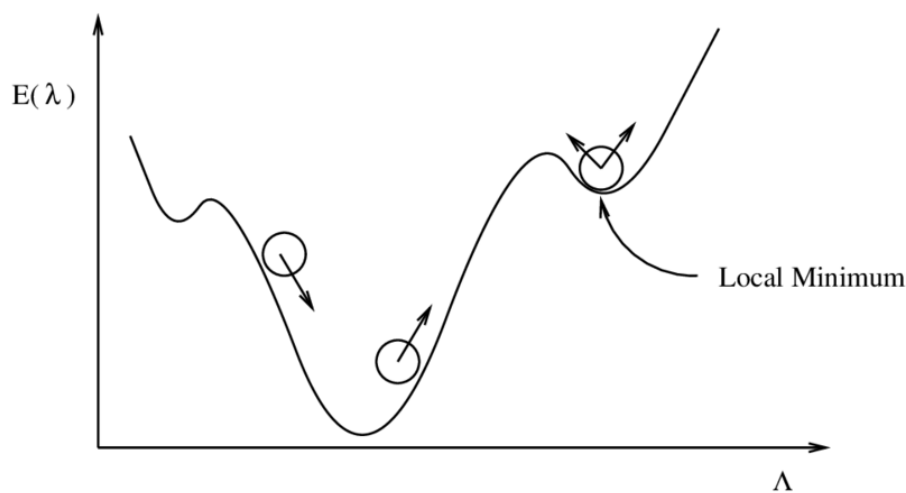


Figure C.5: Momentum term in optimisation

Figure C.5 is a representation of a local and global minima. A typical back-propagation type optimisation algorithm would converge at the local minima, however by adding a momentum term- an adhoc attempt is made to escape the local minima and continue the optimisation process until it reaches the global minima. This approach is rather inefficient as the momentum constant is typically manually chosen and the effectiveness of the momentum constant is dependent on the unknown search space. If the constant is chosen to be too high, there could be a situation that the search exits the global minima altogether.

Hessian matrix

The hessian matrix is a matrix consistent of second order partial derivatives. The matrix is used to conduct the second order partial derivative test in optimisation. The tests helps us verify whether a point (x_0, y_0) is a local maximum, minimum or a saddle point. Specifically it is computed as:

$$H = f_{xx}(x_0, y_0)f_{yy}(x_0, y_0) - f_{xy}(x_0, y_0)^2 \quad (C.1)$$

If $H > 0$, then the function definitely has a local maximum/minimum at the point (x_0, y_0) , if $H < 0$, then the function has a saddle point at (x_0, y_0) and if $H = 0$, then it is indeterminate.

C.2. Literature on hybrid models

Khashei et al mentions that the model formulation can include the strengths of multiple models combined into one i.e., to use the strengths of the statistical models and to combine that with neural networks in order to produce a 'hybrid' neural network. The aim is to reduce the risk of failure and obtain more accurate results for time series forecasting [28]. Kankal et al used a neural network with a teaching-learning based optimisation [38] for modelling the long term electric energy demand in Turkey. This forecast was based on the GDP, population, imports and exports. However, this was done to forecast only the trends for the next five years [27]. Another example of a hybrid model is that made by Chunshien Li [30] which is a neuro-fuzzy ARIMA model. The neuro-fuzzy component is a synergy of a neural network combined with a fuzzy inference system (FIS). FIS's can extract a human operators' experience and knowledge in the form of 'if-then' rules and such a setup has been shown to be useful in time series forecasting.

One of the problems associated with statistical methodologies of forecasting is that the time-series must be stationary. In the case of forecasting the DP load of a ship, this is not the case as the weather conditions during a day are variant and so is the orientation of the vessel. Wong et al gets around the requirement for a stationary data set by using a fuzzy set which is based on linguistic inputs. One of the drawbacks of this type of model that must take into account 'if-then' based rules is that these models require a large amount of computation time as the max-min operations are used for reasoning [48].

Taskaya et al argues that hybrid models- as they are a function of all the smaller models used to supplement it, are not necessarily better than using a standalone mode. Based on the tests conducted on nine time series datasets on an ARIMA neural network (ARIMA-NN) & an autoregressive (AR) model and time delay neural network (TDNN), it was found that the standalone models (AR & TDNN) outperformed the hybrid models and that it can be sufficient to use a single model. The reasoning for this is that the relationship between the linear and non-linear components may not necessarily be additive.

C.3. Optimisation algorithms

Conjugate gradient methods

To handle large datasets, the applicability of the gradient descent method of back-propagation is not recommended and it is generally accepted that a class of optimisation method called the ‘Conjugate gradient methods’ are well suited. The Conjugate gradient method is also based on the same optimisation strategy, however the selection of the search direction and step size are done more carefully by using information from the Hessian matrix (second order information i.e., $E''(\hat{w})$). In this method the $E(\hat{w} + \hat{y})$ term is estimated as $E(\hat{w}) + E(\hat{w})^T \hat{y} + \frac{1}{2} \hat{y}^T E''(\hat{w}) \hat{y}$ using a Taylor expansion [36]. The advantage of this method is that one can make use of the second order information in order to determine whether the computed point of minimum error is a local minima (saddle points) or a global minima. This is done with the help of the second order matrix $E''(\hat{w})$ called the Hessian matrix. If the Hessian matrix is positive definite ¹, then it can be said that there exists a unique global minimum[36].

Algorithm 6 Standard Conjugate gradient algorithm [36]

- 1: Choose initial weight vector \hat{w}_1 and set $k=1$.
Set $\hat{p}_1 = \hat{r}_1 = -E'(\hat{w}_1)$
 - 2: Calculate second order information:
 $\hat{s}_k = E''(\hat{w}_k) \hat{p}_k$,
 $\hat{\delta}_k = \hat{p}_k^T \hat{s}_k$
 - 3: Calculate step size:
 $\mu_k = \hat{p}_k^T \hat{r}_k$,
 $\alpha_k = \mu_k / \hat{\delta}_k$
 - 4: Update weight vector:
 $\hat{w}_{k+1} = \hat{w}_k + \alpha_k \hat{p}_k$,
 $\hat{r}_{k+1} = -E'(\hat{w}_{k+1})$
 - 5: If $k \bmod N=0$ then restart algorithm: $\hat{p}_{k+1} = \hat{r}_{k+1}$
else create new conjugate direction:
 $\beta_k = (|\hat{r}_{k+1}|^2 - \hat{r}_{k+1}^T \hat{r}_k) / \mu_k$,
 $\hat{p}_{k+1} = \hat{r}_{k+1} + \beta_k \hat{p}_k$
 - 6: If the steepest descent direction $\hat{r}_k \neq \hat{0}$ the set $k = k + 1$ and go to (2).
else terminate and return \hat{w}_{k+1} as the desired minimum.
-

Example

To demonstrate the working of the Conjugate gradient method of optimisation, a simple numerical example is shown for a linear set of equations ²:

$$\begin{bmatrix} 2 & 1 \\ 1 & 2 \end{bmatrix} \cdot \begin{bmatrix} x_1 \\ x_2 \end{bmatrix} = \begin{bmatrix} 2 \\ 1 \end{bmatrix}$$

Assume a starting vector (i.e., initial guessed solution) as $x_0^T = [0, 0]$, we have:

$$r_0^T = (b - Ax_0)^T = [2, 1] \tag{C.2}$$

We now have to compute α

$$\alpha_0 = \frac{r_0^T W_0}{W_0^T A W_0} = \frac{5}{14} \tag{C.3}$$

The new estimate of x is given as:

$$x_1^T = (x_0 + \alpha_0 W_0^T) = \frac{5}{14} [2, 1] \tag{C.4}$$

¹A positive definite matrix is a symmetric matrix whose eigenvalues are all positive. The multiplication of such a matrix with a vector will ensure that the transformed vector points in the same ‘general direction’.

²Due to the complexity of calculating the non-linear set of equations i.e., with second order information, an example is shown with a linear set of equations. The more complex non-linear systems are solved more easily on a computer.

The new residual is calculated as r_1 :

$$r_1^T = (b - Ax_1)^T = \frac{3}{14} [1, -2] \quad (C.5)$$

$$\beta_0 = \frac{r_1^T A_0 W_0}{W_0^T A W_0} = \frac{9}{14^2} \quad (C.6)$$

The new weights are found as:

$$W_1^T = (r_1 + \beta_0 W_0)^T = \frac{15}{14^2} [4, -5] \quad (C.7)$$

This process is repeated until the solution converges (in this case until $k=2$). When $k=2$, the calculated 'x' value is the missing matrix from the initial problem which has been solved. The same process is used for larger non-linear problems albeit with the use of second order information.

Table C.1: Numerical example results [15]

k	x	r	α	β	W	Remarks
0	$\begin{bmatrix} 0 \\ 0 \end{bmatrix}$	$\begin{bmatrix} 2 \\ 1 \end{bmatrix}$	$\frac{5}{14}$	-	$\begin{bmatrix} 2 \\ 1 \end{bmatrix}$	Initial solution
1	$\frac{5}{14} \begin{bmatrix} 2 \\ 1 \end{bmatrix}$	$\frac{3}{14} \begin{bmatrix} 1 \\ -2 \end{bmatrix}$	$\frac{14}{15}$	$\frac{9}{14^2}$	$\frac{15}{14^2} \begin{bmatrix} 4 \\ -5 \end{bmatrix}$	-
2	$\begin{bmatrix} 1 \\ 0 \end{bmatrix}$	$\begin{bmatrix} 0 \\ 0 \end{bmatrix}$	0	0	$\begin{bmatrix} 0 \\ 0 \end{bmatrix}$	Converged solution

Scaled-conjugate gradient algorithm³

One of the drawbacks of the Conjugate gradient method is that it relies on the computation of the Hessian matrix which is computationally more intensive. The second order information in the CGD (Conjugate Gradient method) is stored in a term ' \hat{s}_k ' as $E''(\hat{w}_k) \hat{p}_k$. Møller (1993), developed a scaled conjugate gradient method to be used for fast supervised learning. In this method the second order information is estimated as:

$$\hat{s}_k = \frac{E'(\hat{w}_k + \sigma_k \hat{p}_k) - E'(\hat{w}_k)}{\sigma_k} + \lambda_k \hat{p}_k \quad (C.8)$$

Where: λ_k : Scaling parameter
 σ_k : Scalar i.e., $0 < \sigma_k \ll 1$

The parameter λ_k in each iteration looks at the value of $\delta_k = \hat{p}_k^T \hat{s}_k$ after scaling as:

$$\delta_k = \delta_k + (\lambda_k - \bar{\lambda}_k) |\hat{p}_k|^2 \quad (C.9)$$

If $\delta_k \leq 0$, then the Hessian is not positive definite and λ_k is raised and \hat{s}_k is re-estimated. The full description of the algorithm⁴ can be found in Møller (1993) [36]. For this research study, the scaled conjugate gradient method was employed during the training phase as it was capable of handling a large dataset and reaching convergence within a few hours.

³The scaled conjugate gradient algorithm was used for training purposes of the neural network model. The implementation was done with the Matlab®Neural Network Toolbox®

⁴The Pseudo-code for the algorithm is available in Appendix C

Algorithm 7 Scaled Conjugate gradient algorithm [36]

-
- 1: Choose weight vector \hat{w}_1 and scalars $0 < \sigma \leq 10^{-4}$,
 $0 < \lambda_1 \leq 10^{-6}, \lambda_1 = 0$
 Set $\hat{p}_1 = \hat{r}_1 = -E'(\hat{w}_1), k = 1$ and success = true.
 - 2: If success = true, then calculate second order information:
 $\sigma_k = \sigma / |\hat{p}_k|,$
 $\hat{s}_k = (E'(\hat{w}_k) - E'(\hat{w}_k)) / \sigma_k,$
 $\delta_k = \hat{p}_k^T \hat{s}_k$
 - 3: Scale $\delta_k : \delta_k + (\lambda_k - \bar{\lambda}_k) |\hat{p}_k|^2$
 - 4: If $\delta_k \leq 0$ then make the Hessian matrix positive definite:
 $\bar{\lambda}_k = 2(\lambda_k - \delta_k / |\hat{p}_k|^2),$
 $\delta_k = -\delta_k + \lambda_k |\hat{p}_k|^2$
 $\lambda_k = \bar{\lambda}_k$
 - 5: Calculate step size:
 $\mu_k = \hat{p}_k^T \hat{r}_k,$
 $\alpha_k = \mu_k / \delta_k$
 - 6: Calculate the comparison parameter:
 $\Delta_k = 2\delta_k [E(\hat{w}_k) - E(\hat{w}_k + \alpha_k \hat{p}_k)] / \mu_k^2$
 - 7: If $\Delta_k \geq 0$ then a successful reduction in error can be made:
 $\hat{w}_{k+1} = \hat{w}_k + \alpha_k \hat{p}_k,$
 $\hat{r}_{k+1} = -E'(\hat{w}_{k+1}),$
 $\bar{\lambda}_k = 0, \text{ success} = \text{true}.$
 If $k \bmod N = 0$ then restart algorithm:
 $\hat{p}_{k+1} = \hat{r}_{k+1}$
 else:
 $\beta_k = (|\hat{r}_{k+1}|^2 - \hat{r}_{k+1}^T \hat{r}_k) / \mu_k,$
 $\hat{p}_{k+1} = \hat{r}_{k+1} + \beta_k \hat{p}_k$
 - If $\Delta_k \geq 0.75$, then reduce the scale parameter:
 $\lambda_k = \frac{1}{4} \lambda_k.$ else:
 $\bar{\lambda}_k = \lambda_k, \quad \text{success} = \text{false}.$
 - 8: If $\Delta_k < 0.25$, then increase the scale parameter:
 $\lambda_k = \lambda_k + (\delta_k (1 - \Delta_k) / |\hat{p}_k|^2)$
 - 9: If the steepest descent direction $\hat{r}_k \neq 0$, then set $k = k + 1$ and go to (2)
 else:
 Terminate and return \hat{w}_{k+1} as the desired minimum
-

C.4. Effects of varying number of neurons

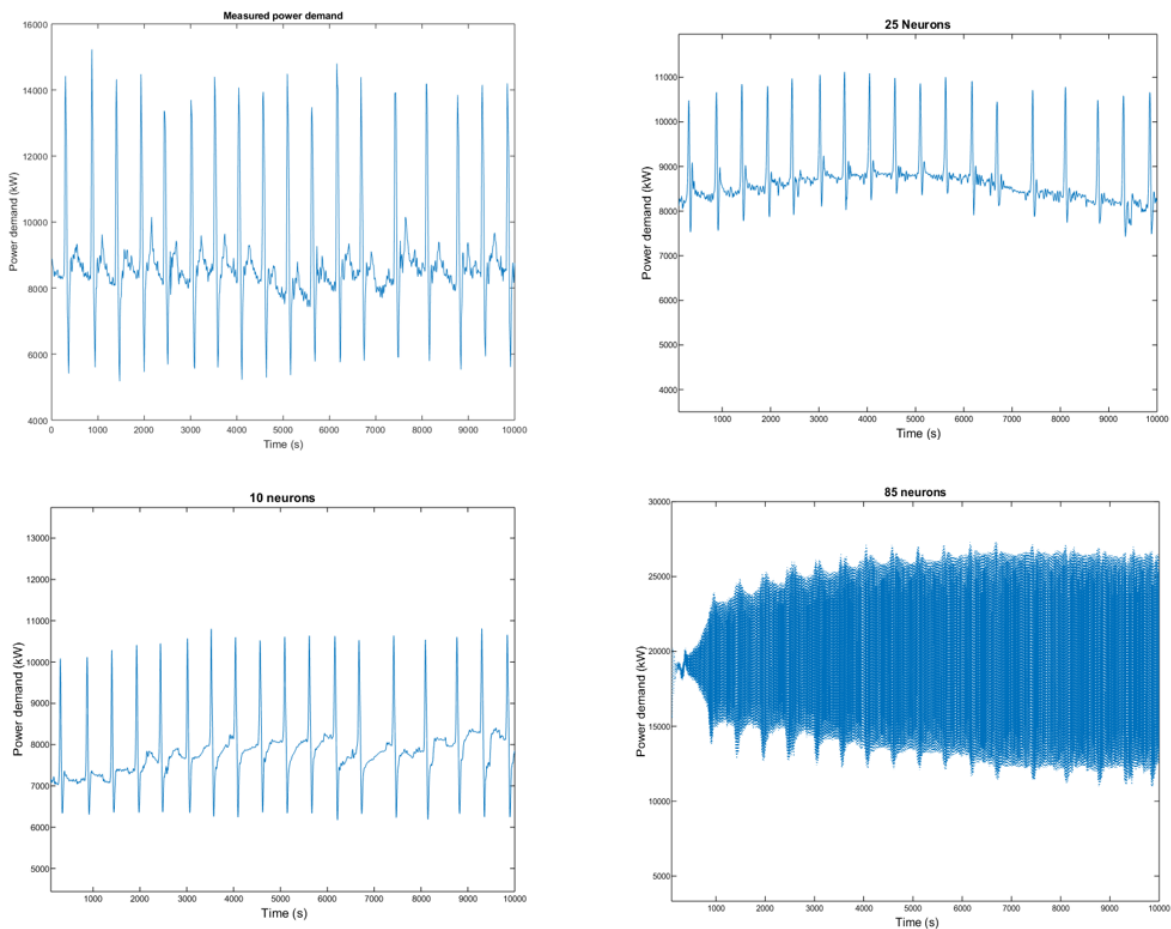


Figure C.6: Comparison of response from different neuron settings in the hidden layer

Figure C.6 shows the variations in results obtained from a small training set. In the event of using 10 neurons, the forecasting model captures the power peaks reasonably well however, the moving average load is misrepresented around the 7-8 MW range when in reality, based on the measured values, it is around 8-8.5MW. In the case of 85 neurons in the hidden layer, the output obtained has not yielded any fruitful results meaning that the number of neurons must be reduced or the dataset must be expanded. The same problem persisted on expanding the dataset and it is assumed that a much larger dataset than the one available for training is required to test the effects of large number of neurons in the hidden layer. Based on further trial and error methods of testing the response, 25 neurons produced the most promising results across the small and large dataset. It appears to capture the moving average DP load reasonably well (within the 8-8.5MW range), however, in this case as a small training set was used, the power peaks have not yet been accurately captured. But at this stage of the network design, it can be gauged that the appropriate number of neurons, preceding training on larger datasets, is to be set to 25 neurons. This conclusion is based on the fact that adding the more than necessary neurons to the hidden layer will allow the network to identify more complex patterns and give the network enough complexity to overfit (which is the reason for the aberrations seen in the 85 neuron model case) [40].

C.5. Load forecast scenarios

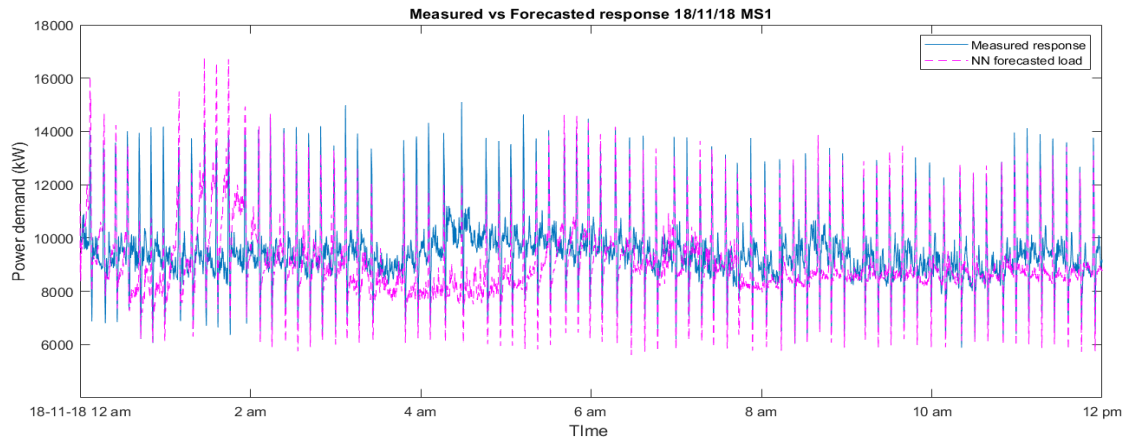


Figure C.7: 18/11/18 MS1 response

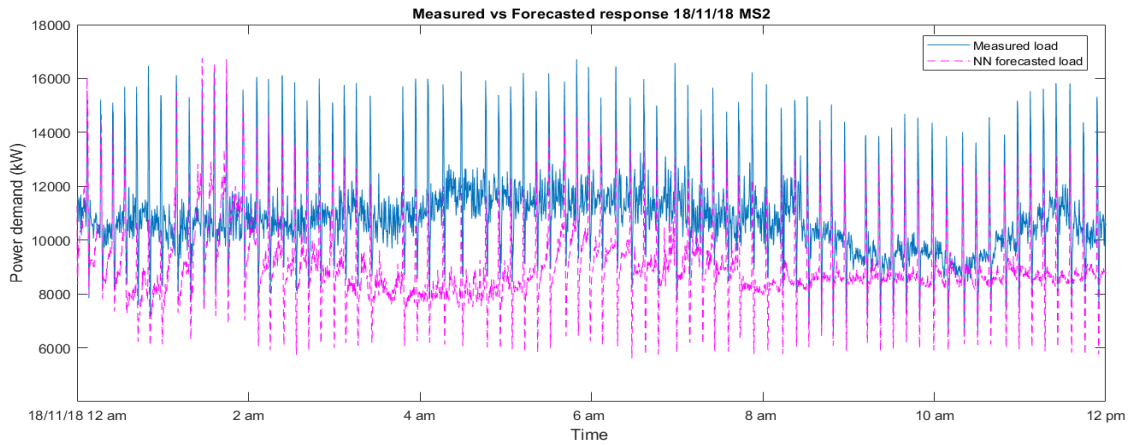


Figure C.8: 18/11/18 MS2 response

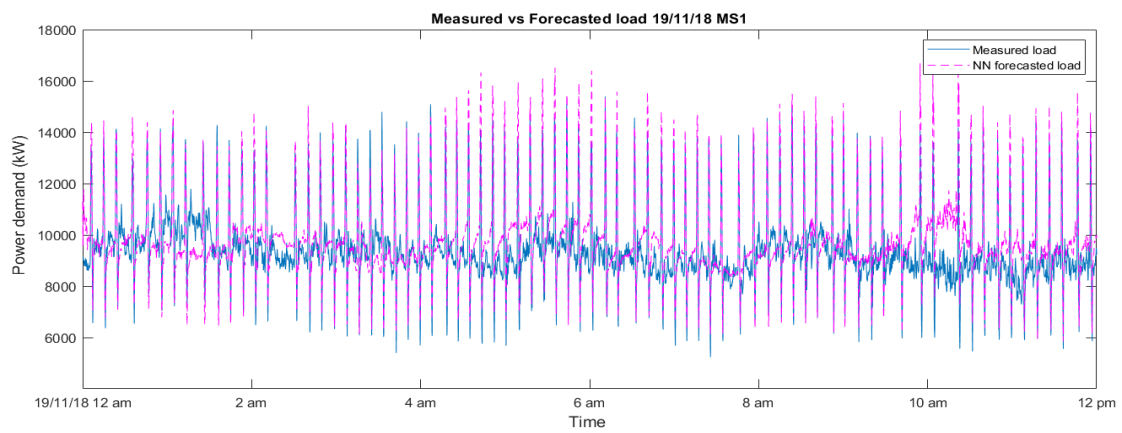


Figure C.9: 19/11/18 MS1 response

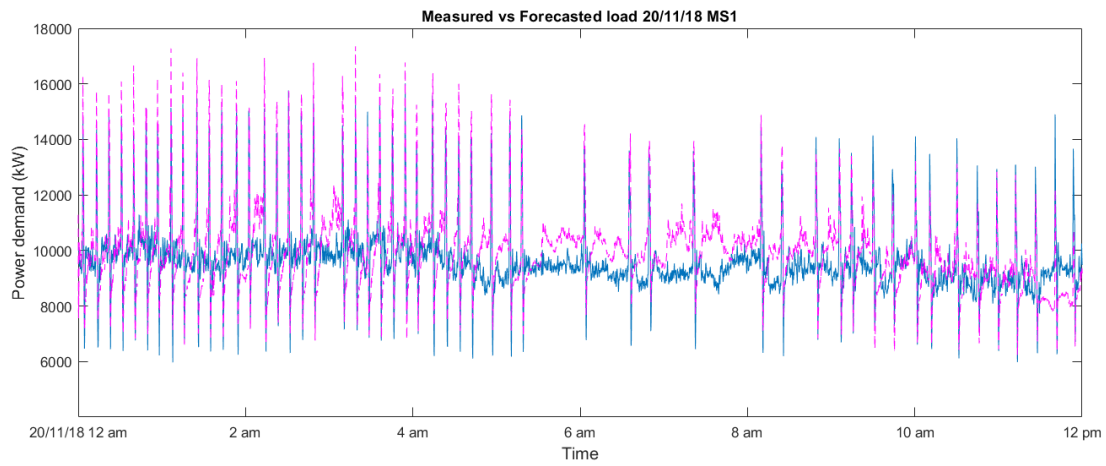


Figure C.10: 20/11/18 MS1 response

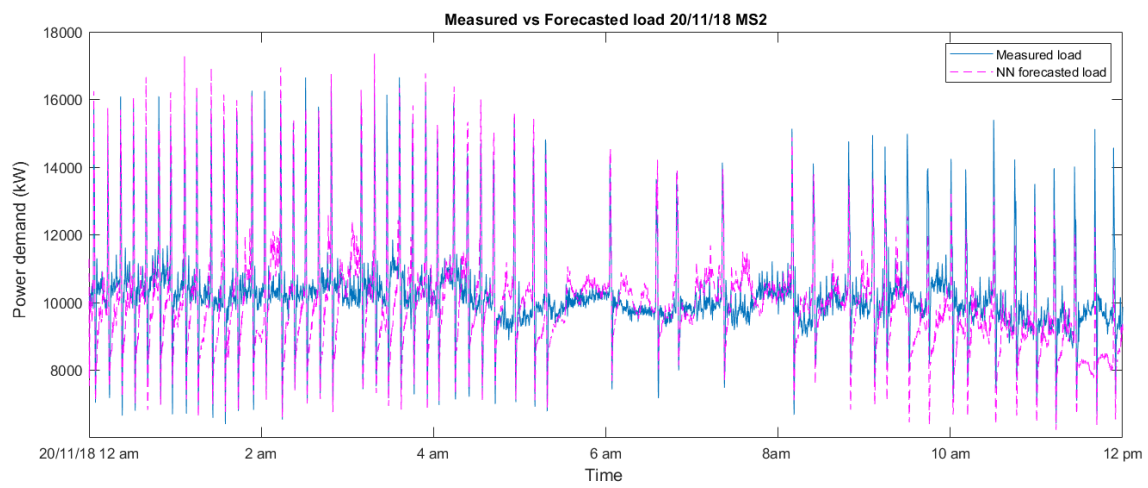


Figure C.11: 20/11/18 MS2 response

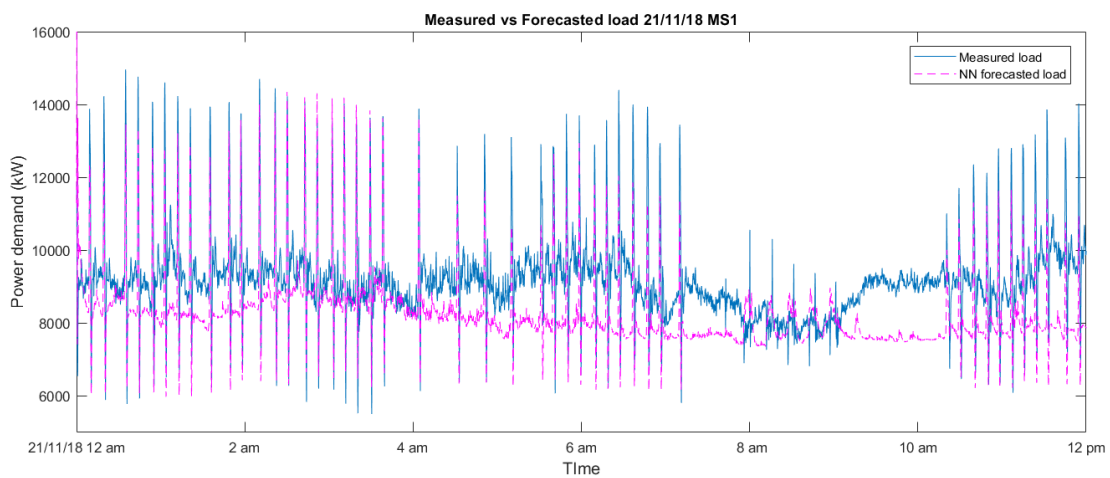


Figure C.12: 21/11/18 MS1 response

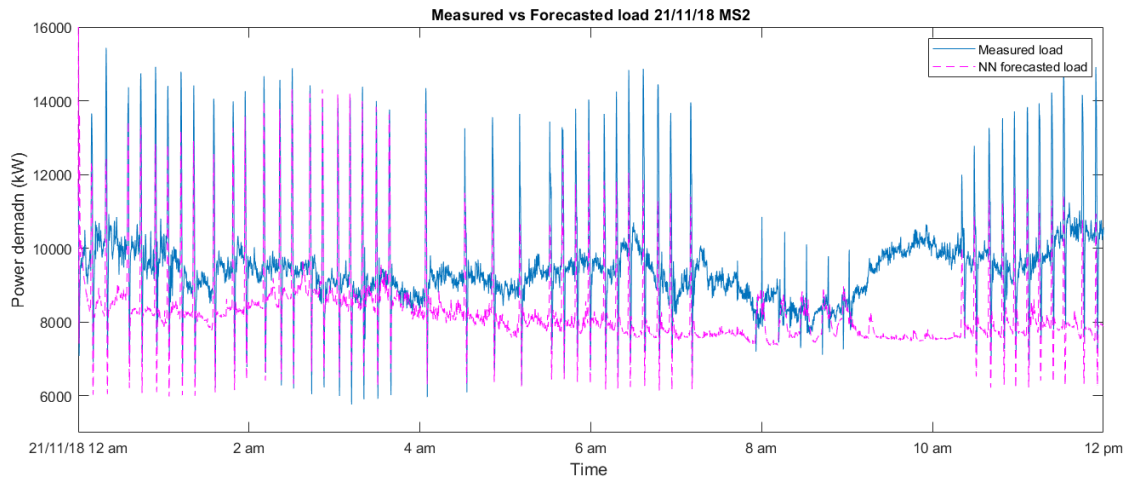


Figure C.13: 21/11/18 MS2 response

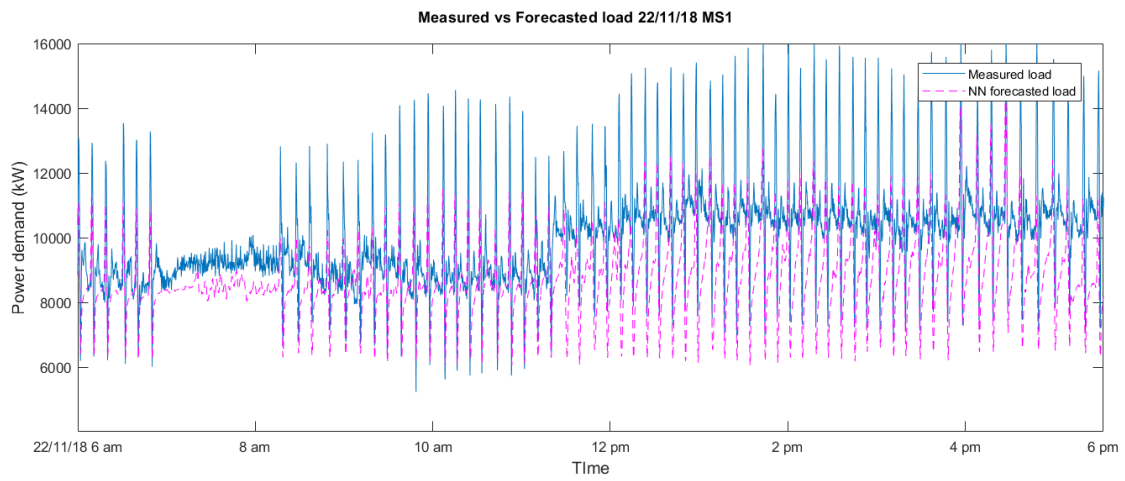


Figure C.14: 22/11/18 MS1 response

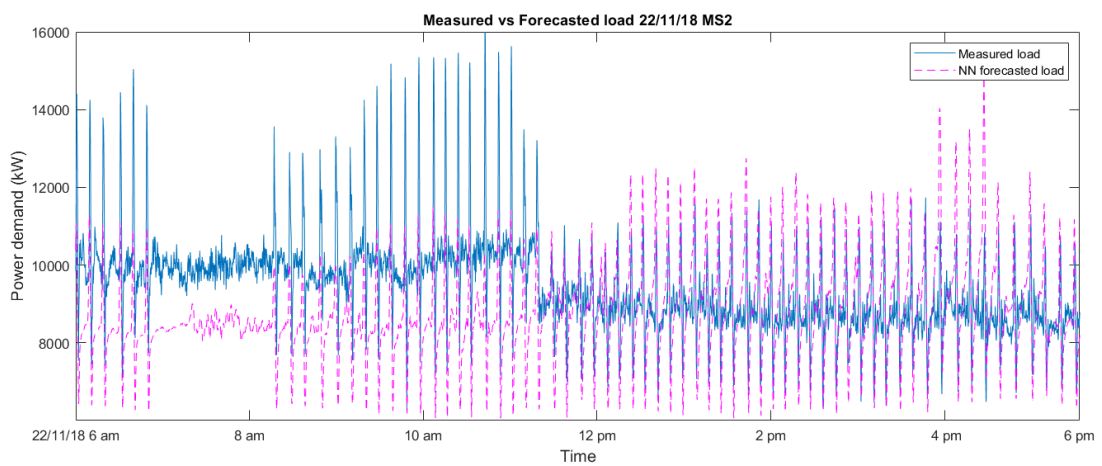


Figure C.15: 22/11/18 MS2 response

C.6. Power peak forecasting

Using only the groundspeed as the correlation, the power peaks can be forecasted with a high accuracy. Note that from Section C.4, the load forecasts of 18/11/18 MS1 and 18/11/18 MS2 were not deemed to be accurate enough to be used for PMS applications, however the power peak forecasts have shown very good agreement.

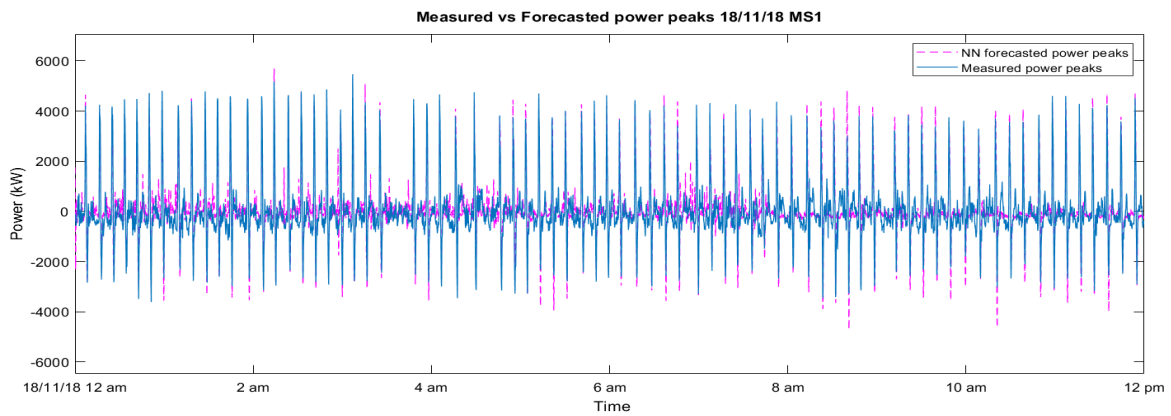


Figure C.16: 18/11/18 MS1 response

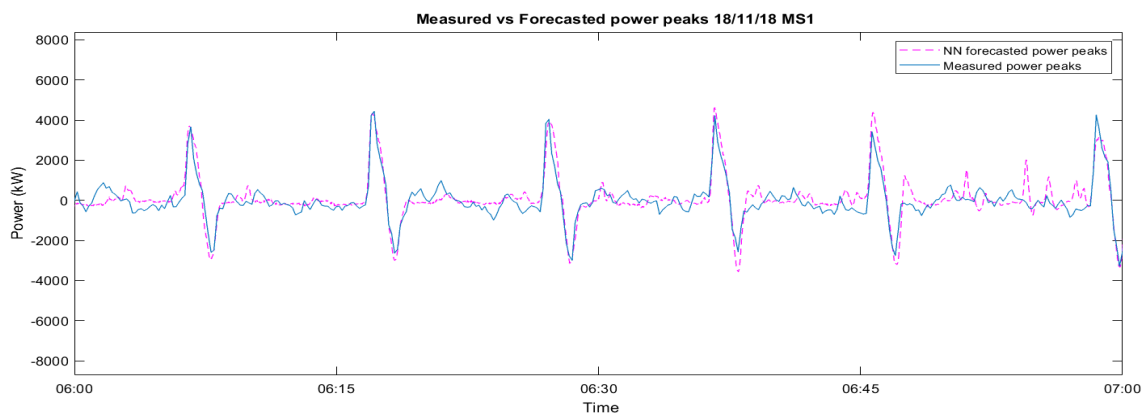


Figure C.17: 18/11/18 MS1 response

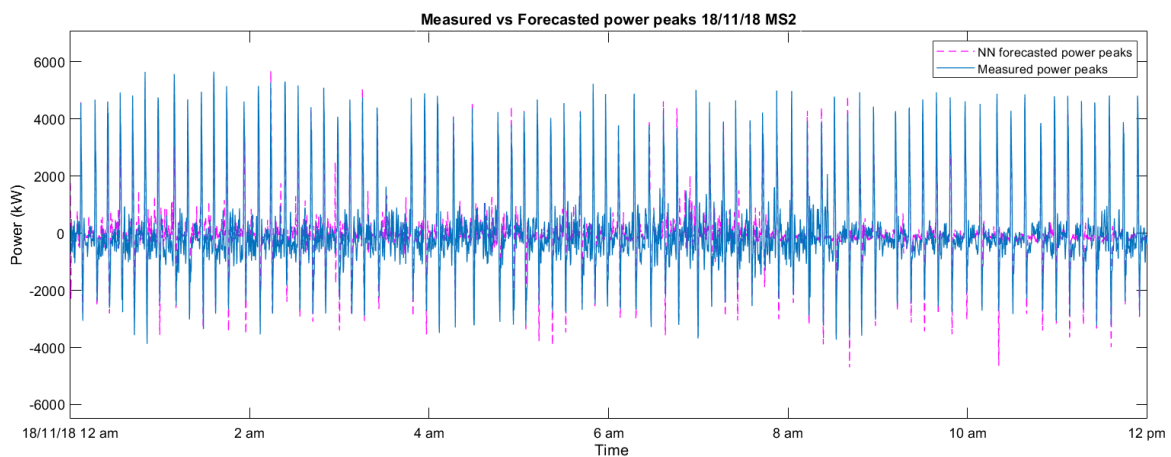


Figure C.18: 18/11/18 MS2 response

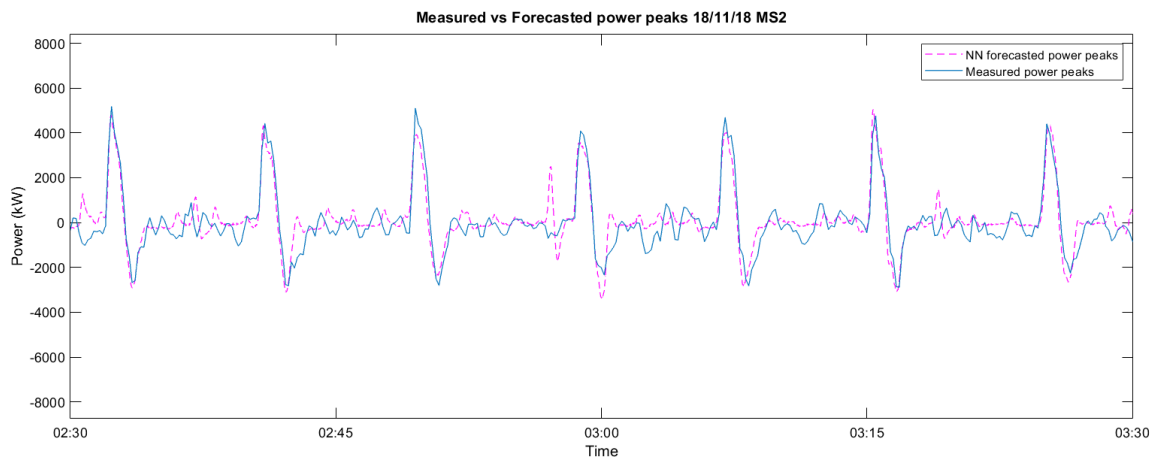


Figure C.19: 18/11/18 MS2 response

C.7. Neural network Matlab @code

```

1 %% Artificial neural network code
2 % Requires Neural network toolbox
3 % Author: Akash Menon
4 % Supporting files available via USB
5
6 %% Inputs and Target definitions
7 X = train_input_nn(1:end);
8 T = train_target_nn_MS1(1:end);
9
10 %% ANN design
11 trainFcn = 'trainscg';
12 inputDelays = 1:25;
13 feedbackDelays = 1:25;
14 hiddenLayerSize = 25;
15
16 %% Open-loop training mode (-o)
17 neto = narxnet(inputDelays, feedbackDelays, hiddenLayerSize, 'open', trainFcn);
18 neto.layers{1}.transferFcn = 'logsig';
19 neto.inputs{1}.processFcns = {'removeconstantrows', 'mapminmax'};
20 neto.inputs{2}.processFcns = {'removeconstantrows', 'mapminmax'};
21
22 %% Prepare neural net
23 [Xo, Xoi, Aoi, To] = preparets(neto, X, {}, T);
24
25 %% Data division
26 neto.divideFcn = 'dividerand'; % Divide data randomly
27 neto.divideMode = 'time'; % Divide up every sample
28 neto.divideParam.trainRatio = 70/100;
29 neto.divideParam.valRatio = 15/100;
30 neto.divideParam.testRatio = 15/100;
31
32 %% Performance
33 neto.performFcn = 'mse'; % Mean Squared Error
34 % Plot performance parameters
35 neto.plotFcns = {'plotperform', 'plottrainstate', 'ploterrhist', ...
36 'plotregression', 'plotresponse', 'ploterrcorr', 'plotinerrcorr'};
37

```

```

38 %% Training parameters and train neural net
39 neto.trainParam.epochs=5000;
40 neto.trainParam.goal=1e-6;
41 [neto, tr] = train(neto, Xo, To, Xoi, Aoi);
42
43 %% Parallel computing notice:
44 % If parallel computing is to be used- a parallel pool must first be
45 % created before the code is run.
46 % (... , 'useparallel', 'yes')-> add for parallel computing option (multi-core
47 % devices) to train(neto, Xo, To, Xoi, Aoi, 'useparallel', 'yes');
48
49 %% Test the Network
50 Yo = neto(Xo, Xoi, Aoi);
51 Eo = gsubtract(To, Yo);
52 performance = perform(neto, To, Yo)
53
54 % View the network structure
55 view(neto)
56
57 % Plots
58 figure, plotperform(tr)
59 figure, plottrainstate(tr)
60 figure, ploterrhist(e)
61 figure, plotregression(t, y)
62 figure, plotresponse(t, y)
63 figure, ploterrcorr(e)
64 figure, plotinerrcorr(x, e)
65
66 %% Closed Loop Network for multi-step prediction
67 netc = closeloop(neto);
68 netc.name = [neto.name ' - Closed Loop'];
69 view(netc)
70
71 [Xc, Xic, Aic, Tc] = preparets(netc, X, {}, T);
72 Yc = netc(Xc, Xic, Aic);
73 closedLoopPerformance = perform(neto, Tc, Yc)
74
75 %% Simulink model of the neural network
76 gensim(netc)

```

